UNIVERSITY OF SOUTHAMPTON

FACULTY OF ENGINEERING AND PHYSICAL SCIENCES

SCHOOL OF ELECTRONIC AND COMPUTER SCIENCE

Tailored Polydimethylsiloxane Circuit Encapsulation for Washable and Mechanically-Deformable Proximity and Touch Sensing Electronic Textiles for Wearables and Beyond

Olivia Olamide Ojuroye

Thesis for the degree of Doctor of Philosophy

May 2019

"*My brain is only the receiver, in the Universe there is a core from which we obtain knowledge, strength, and inspiration*."

- Nikola Tesla (1856-1943)

  Serbian-American engineer, inventor, physicist, and futurist

University of Southampton

Abstract

Faculty of Engineering and Physical Sciences
Electronics and Computer Science

Thesis for the degree of Doctor of Philosophy

Tailored Polydimethylsiloxane Circuit Encapsulation for Washable and Mechanically-Deformable Proximity and Touch Sensing Electronic Textiles for Wearables and Beyond

Olivia Olamide Ojuroye

An ambition exists in literature for electronic textiles (e-textiles) to resemble traditional textiles in their usability, wearability, washability, and deformable attributes. To be worn and/or used frequently in other means, their benefits can be experienced. For this, a literature review concluded that flexible electronic circuits need to be packaged so they do not disturb the functionality, mechanical deformity, and usability of traditional textiles. Hence, they need to be hidden, unobtrusive, and protected from aqueous solutions. Therefore, by encapsulating sensing embedded circuits and integrating them among textile fibres to produce sensing textile yarns or sensing woven textiles, the electronics can be disguised. By selecting a flexible circuit substrate, electronics can retain their undetected state as the resulting electronic textile is folded, bent, or twisted whilst in use. This approach was taken as part of the EPSRC-funded project 'Novel manufacturing methods for functional electronic textiles'. To add to the existing work, this Ph.D thesis describes the development of an e-textile system with a high level of electronic integration whereby a capacitive touch and proximity sensing circuit is integrated into the core of a knitted yarn sleeve and woven to form a channel within a fabric swatch – using today's textile construction techniques. Consequently, the novelty of this work is the system of a proximity and touch sensing washable electronic textile which retains functionality after being submerged underwater for 6 months, can survive being washed in consumer washing machines with detergent and fabric conditioner; can survive over 10,000 cyclic twists and 50 cyclic bends. The system has off-the-shelf components, uses industrially available resources, materials, and processes to ensure industrial feasibility. The result is an experiment-verified washable, mechanically deformable flexible capacitive circuit that is compatible with the textile integration process to create novel e-textile demonstrators. Additionally, novelty includes tailoring polydimethylsiloxane (PDMS) to increase its hydrophobicity to water, detergent, and fabric conditioner for e-textile applications.

Table of Contents

List of Figures

List of Tables

Research Thesis: Declaration of Authorship

I, Olivia Ojuroye, declare that this thesis and the work presented in it are my own and have been generated by me as the result of my own original research.

Thesis title - **Tailored Polydimethylsiloxane Circuit Encapsulation for Washable and Mechanically-Deformable Proximity and Touch Sensing Electronic Textiles for Wearables and Beyond.**

I confirm that:

1. This work was done wholly or mainly while in candidature for a research degree at this University;

2. Where any part of this thesis has previously been submitted for a degree or any other qualification at this University or any other institution, this has been clearly stated;

3. Where I have consulted the published work of others, this is always clearly attributed;

4. Where I have quoted from the work of others, the source is always given. With the exception of such quotations, this thesis is entirely my own work;

5. I have acknowledged all main sources of help;

6. Where the thesis is based on work done by myself jointly with others, I have made clear exactly what was done by others and what I have contributed myself;

7. Either none of this work has been published before submission, or parts of this work have been published as:
   - Ojuroye, Olivia, Torah, Russel, Beeby, Steve and Wilde, Adriana (2016), 'Autonomy is the key: from smart towards intelligent textiles.' In, *Workshop on Autonomous Everyday Objects: Exploring Actuation in Ubiquitous Devices (within UBICOMP/ISWC 2016)*, Heidelberg, DE, *12 - 16 Sep 2016*. New York, US, ACM, 678-681. (doi:10.1145/2968219.2968558).
   - Ojuroye, Olivia, Torah, Russel, Beeby, Steve and Wilde, Adriana (2016), 'Autonomy is the key: from smart towards intelligent textiles.' In *WomENcourage Computer Science* Conference 2016; Poster Presentation, Linz, Austria, 12-14 Sep 2016.

- Ojuroye, Olivia., Torah, Russel., Beeby, Stephen., and Wilde, Adriana. (2016), 'Smart textiles for smart home control and enriching future wireless sensor network data.' *Sensors for Everyday Life: Healthcare Settings.* Cham, CH, Springer, 159-183. (Smart Sensors, Measurement and Instrumentation, 22). (doi:10.1007/978-3-319-47319-2_9).
- Torah, Russel., Komolafe, Abiodun., Li, Menlong., Ojuroye, Olivia., and Beeby, Steve. (2017), 'Novel Manufacturing Methods for Functional Electronic Textiles'. *Printed and Stretchable Congress*, Poster Presentation, London, UK, 25 Feb 2017.
- Ojuroye, Olivia, Torah, Russel, and Beeby, Steve (2017), 'Levels of Electronic Integration within Textiles' Chart. *WomENcourage Computer Science Conference* 2017; Poster Presentation, Barcelona, Spain, 06-08 Sep 2017.

  Ojuroye, O., & Wilde, A.G.; (2018), 'On the feasibility of using electronic textiles to support embodied learning', in *Perspectives on Wearable Enhanced Learning (WELL): Current Trends, Research, and Practice*, Buchem, I., Klamma R., & Wild, F., (eds), Springer.
- Wilde, A.G & Ojuroye, O. (2018), 'Ubiquitous Embodied Learning with E-Textiles Electronic Textiles', *in Mobile, Wearable, Ubiquitous Systems Research Symposium*, University of Cambridge
- Ojuroye, O., Torah, R., & Beeby, S., (2018, May), 'Improving the integration of e-textile microsystems' encapsulation by modifying PDMS formulation.' In *2018 Symposium on Design, Test, Integration & Packaging of MEMS and MOEMS (DTIP)* (pp. 1-6). IEEE.
- Ojuroye, O., Torah, R., & Beeby, S., (2019), 'Modified PDMS packaging of sensory e-textile circuit microsystems for improved robustness with washing. *Journal of Microsystem Technologies* , Springer Berlin Heidelberg, (https://doi.org/10.1007/s00542-019-04455-7)
- Ojuroye, O., Torah, R., Komolafe, A.O., & Beeby, S., (2019), 'Embedded capacitive proximity and touch sensing flexible circuit system for Electronic Textile and Wearable Systems', IEEE Sensors (pp. 1-11). IEEE.
- Torah, R., Komolafe, A., Li, M., Ojuroye, O., Wei, Y., Nunes-Matos, H., Hardy, D., Anastasopoulos, I., Kumar, V., Nour Nashed, M., Dias, T., Tudor, J., Beeby, S., (2018) 'FETT: Novel Manufacturing Methods for Functional Electronic Textiles', Large-Area Organic Printed Electronics Conference (LOPEC) 2018, Munich Germany.

Acknowledgements

This research was funded in the UK by the *Engineering and Physical Sciences Research Council* (EPSRC) via the project: Novel manufacturing methods for Functional Electronic TexTiles (FETT). Grant number: EP/M015149/1. This Ph.D would not have been possible without securing the funding of this work. Thanks to supervisors Professor Steve Beeby and Dr. Russel Torah; also, project partners at the University of Nottingham Trent and Helga Nunes who helped create e-textile demonstrators using circuits produced through this research. Furthermore, this Ph.D benefited from equipment in the Life Sciences department to conduct material science experiments, and those more knowledgeable on bioengineering concepts who taught me new and helpful concepts. Additionally, I would like to acknowledge Adriana Wilde who presented me with the idea of applying to this Ph.D and Professor Mark Nixon who has guided me as my personal tutor from my first day at the University of Southampton until the last. The close friendships I have made whilst completing this Ph.D are ones I will cherish and nurture in my future. Lastly, I would like to acknowledge and thank my family who have been a strong support system whilst completing this work.

Definitions and Abbreviations

ATRG – Advanced Textile Research Group

EPSRC – Engineering and Physical Science Research Council

FETT – Novel Manufacturing Methods for Functional Electronic TexTiles Project

IC – Integrated Chip

HAS – Hand Surface Area

HCI – Human Computer Interaction

MEMS – Micro-electro-Mechanical Systems

NTU – Nottingham Trent University

PCB – Printed circuit board

PDMS – Polydimethylsiloxane

SEM - Scanning electron microscope

SMD – Surface Mount Device

SOIC - Small Outline Integrated Circuit

WLCSP – Wafer Level Chip Scale Package

Chapter 1: Introduction

This chapter outlines background knowledge on electronic textiles, the contribution to the field which is further explained through this research's aims, objectives, and novelty statement. This chapter also details publications to date and outlines the structure of this thesis.

1.1 Electronic Textiles Background

Textiles are materials constructed by interlacing or interloping artificial or natural individual yarns (Horrocks & Anand, 2000). Fabrics are fibrous, planar structures which form a porous material due to the density of fibres woven together. They are typically permeable, flexible, and mechanically deformable. Yarns are made from raw fibre bundles such as hemp, cotton, and wool and are spun, woven, felted, crocheted, knotted, or knitted together to make fabrics and textiles (Horrocks & Anand, 2000). Overall, their softness and being lightweight allow them to deform due to exerted forces or their own weight which cause them to drape (Zeng, Shu, Li, Chen, Wang, & Tao, 2014). Their structures can be maintained after numerous washing tests with different solvents, temperatures, and durations. Fibre-based textiles can be stretchable, twisted, bendable, flexible, soft, breathable, washable, and durable. As electronics have smaller dimensions, driven by the miniaturisation pushed by the mobile phone and tablet industry, it becomes more possible to integrate electronics and conductive elements into fibre-based textiles to produce textile electronics – wearable or as technical textiles (Horrocks & Anand, 2000) which are manufactured for performance more than aesthetics such as in medicine, furniture, and construction.

Textiles are gradually considered to becoming 'smart' or reacting to their environment (SAPICH, 2013). Smart textiles are textiles which feature technological enhancements (Cherenack & van Pieterson, Smart textiles: challenges and opportunities, 2012) such as conductive and/or electronic elements that allow them to sense, respond, and adapt to their environment. This creates passive, active, and intelligent smart textile types respectively (Xingxiang & Xiaoming, 2001). This description of level of intelligence such textiles have (Schwarz, Van Langenhove, Guermonprez, & Deguillemont, 2010) in turn describe the order of increased interaction with its environment and ability to give context about its environment. Whereas passive smart textiles sense, active smart textiles have an actuating function, and intelligent smart textiles have ability to learn from its environment via artificial intelligence and control its functionality based on context and its own judgements. Additionally, smart textiles could be capable of storing and supplying power (Normann, Kyosev, Ehrmann, & Schwarz-Pfeiffer, 2016), wirelessly communicating, and generating power based upon these circuits part of its functional system when worn or part of a textile product (Lymberis & Paradiso, 2008).

Smart textiles and electronics textiles are terms used interchangeably (Berzowska, 2005) but electronic textiles seem to have a stronger emphasis on the evidence of hardware with textiles –

compared to categorising based on behaviour for smart textiles. The definition and scope of electronic textiles has been addressed by Andreas Köhler (Köhler, 2013). Köhler defines electronic textiles (e-textiles) as those with "*seamless integration of textiles with electronics and other high-end materials*." Literature has explored e-textiles with energy harvesting (Pan, et al., 2016), antenna (Salvado, Loss, Gonçalves, & Pinho, 2012), and sensor (Pang, et al., 2012) applications. As textiles are a composite structure of bonded yarns which themselves are comprised of fibres within them, this electronic textile definition implies that electronics featured at yarn-level could be described as an electronic textile if bonded together.

On the macro-scale, yarns have a cylindrical structure that is a composite of woven, spun, or knitted individual yarns. On the micro-scale, these yarns are made from fibre bundles (Matveev, Long, & Jones, 2012). To increase the level of conductivity and electronic integration into textiles - from having printed circuit boards (PCBs) attached on the textile surfaces by conductive thread (Park, Mackenzie, & Jayaraman, 2002), to acting as the woven yarns themselves if metallically coated (Paradiso & De Rossi, 2006), to at best being integrated within woven yarns – packaging challenges need to be overcome. These challenges are unique when at yarn-level. When electronics and conductive elements interface on the textile surface, they have the greatest exposure to mechanical forces, dirt, and moisture. The level of exposure decreases as the level of electronic integration into the textile increases. Therefore, although at fibre bundles located within the yarn gives the lowest level of exposure and one of the highest levels of electronic integration into textiles it introduces a unique set of challenges.

One challenge is protection over mechanical deformation. At yarn level, the conductive and electronic elements would be amongst fibres which nest side-by-side and feature voids between fibres (Matveev, Long, & Jones, 2012). When the yarn is flexed, the electronics could experience mechanical abrasion. This could detach electronic components from their position on circuits, or provide friction to degrade the quality of conductive tracks. If the conductive elements and electronics featured at yarn level, mechanical abrasion due to the highly-scattered forces exerted by the distribution of fibres would cause highly-scattered friction against the hardware (Pickering & Murray, 1999). Furthermore, if the electronic and conductive elements are not flexible this would increase the Young's modulus of the yarn which would affect the textile's overall flexibility (Matveev, Long, & Jones, 2012). Another challenge is when textiles are washed or submerged in water. When this occurs, water penetrates through the hierarchical structure of the textile, causing the textile fibres to expand due to water absorption. The expansion increases as duration with moisture increases. Electronics and conductive elements can suffer from water damage – corrosion due to solvents in washing cycle, water causing electronic functionality to fail.

A solution to overcome such challenges is by having an encapsulation film that acts as a protective barrier for the electronics and conductive elements against mechanical abrasions and moisture. Furthermore, it is important to ensure this encapsulation film is hydrophobic to counteract water damage, chemical-resistant to prevent degradation of the protective layer, and elastomeric to

absorb mechanical shocks. Such could increase the lifespan of electronics at yarn-level and allow electronics to function at the greatest level of electronics integration in textiles.

1.2 This Thesis' Novel Contribution to the Functional Electronic TexTiles (FETT) Project and its Research Scope

1.2.1 FETT Project Background

This thesis' content is funded by and expands the work of the EPSRC-funded '*Novel manufacturing methods to achieve Functional Electronic TexTiles*' (FETT) (Torah, Komolafe, Li, Ojuroye, & Beeby, 2017). This project is a collaboration of the University of Southampton, Nottingham Trent University and 10 commercial partners. The FETT Project began with an idea in 2007 to integrate electronics into the core of textile yarns, specifically for wearable applications. Its aims are to produce new manufacturing and packaging methods that would allow advanced electronics, such as microcontrollers and sensors, to function within the core of a textile yarn – as seen in Figure 1.

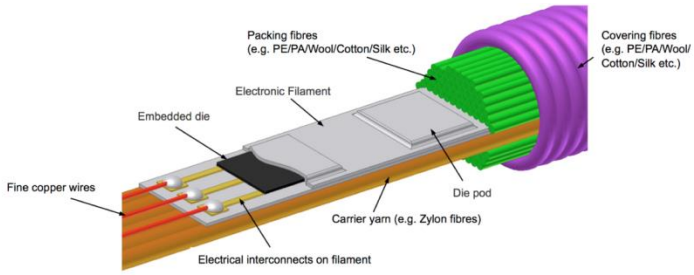

Figure 1 Image of original FETT project electronic yarn concept with ultra-thin die on a thin flexible plastic film, surrounded by yarn fibres and contained in covering fibres to form a yarn sleeve *(Torah, Komolafe, Li, Ojuroye, & Beeby, 2017)*.

In addition to the idealised system design of this e-yarn in figure 1, another iteration where semiconductor chips were integrated into the core of yarns using SMDs were pursued. However, the topography of the chips beneath the textile caused visible bumps, revealing the hardware's location and therefore not offering an unobtrusive packaging of electronics in textiles. Integrating electronic circuits, instead of single SMD chips, was attempted in the FETT Project. In 2015, a research project concluded the use of a flexible copper-polyimide film to act as the circuit substrate to ensure the resultant e-textile could still bend, flex, and twist. Research and circuit design rules to make this flexible copper-polyimide circuit in L-Edit had already been conducted in the FETT project prior to this thesis. The circuit fabrication method of the copper-polyimide circuit to be integrated into a yarn was established before the work in this thesis began. This is outlined in Appendix D.

1.2.2 This Thesis' Novel Contribution to the FETT Project and E-Textile Field

The FETT project had already established the fabrication process turning copper-polyimide into strip-shaped functional circuits for microcontrollers, accelerometers, and light emitting diodes (LEDs) – Appendix D. The use of copper and silk copper litz wires were also pre-requisites for this research. However, capacitive proximity and touch sensing circuits had not been pursued in the FETT project, with intention to be a switch to control existing FETT circuits and to control other systems. Prior to this thesis, rigid encapsulation had been applied to protect semiconductor chips from aqueous and mechanical abrasions. However, applying this rigid resin on a circuit size of 3.0 cm and longer – like the copper-polyimide circuits developed – would result in rigid areas of the textile and preventing it to be wearable. Hence this Ph.D thesis applies of the fabrication processes developed in the FETT project to investigate the feasibility and performance of proximity and touch sensing circuits designed to operate in the core of a yarn and in textiles. Doing so allowed a connected circuit, such as an LED for visible feedback, to be operated with at a distance and tactile interaction. Also, it provides a switching mechanism to textiles via touch or presence with indication of how close a trigger object is to the sensor. Although touch and proximity sensors are not novel, their operation embedded within a textile when encapsulated in a hydrophobic material and the evaluation of the effect of textile integration and use on the performance of the circuits is novel.

Furthermore, prior to this thesis the flexible copper-polyimide circuits produced in the FETT project was not waterproof or tested for its survival for consumer washing. Therefore, the work produced in this thesis was to introduce a flexible, hydrophobic, and aqueous-resistant conformal layer to the existing FETT circuit fabrication method for e-textile applications. Such a layer would help disguise the topography of the SMDs on the flexible copper-polyimide circuit substrate. This is because the layer will be conformal (adding minimal thickness to the circuit) and flexible (allowing the resultant e-textile to mechanically deform). The resultant e-textile also had to be constructed with machinery using today's textile construction machinery, packing materials, electronic circuit bonding equipment to ensure its methodology could be scaled for commercial development.

With the addition of this flexible, hydrophobic, and aqueous-resistant conformal layer - onto a capacitive proximity and touch sensing circuit - and integrating this into textiles would not only extend the FETT project but fulfil its last two work packages – SMIT Demonstrators and Scalable Manufacturing.

1.3 Research Aims, Objectives and Questions

1.3.1 Aims

- Validate the FETT fabrication method by producing a human interactive touch/proximity sensing strip-shaped circuit suitable for use in an e-textile;

- Enable electronic circuit at the core of yarns to be protected from mechanical abrasion and strain during and post textile weaving when located at the core of a yarn;
- Enable electronic circuit at the core of yarns to be protected from water, detergent, and fabric conditioner during washing cycles when located at the core of a yarn;
- Contribute to the categorisation of e-textiles in the field, as a result of the e-textile system from this thesis research which expands the state-of-the-art.

1.3.2 Objectives

- Validate Functional Electronic TexTiles (FETT) circuit fabrication method with a touch/proximity sensing use-case, whilst showing its commerciality and textile compatibility;
- Show that touch/proximity sensing circuit, made from FETT fabrication methodology, could survive consumer water, detergent, and fabric conditioner washing machine process with new protective layer added to system;
- Show that touch/proximity sensing circuit, made from FETT fabrication methodology and added aqueous protective layer, could survive mechanical abrasions experienced by traditional textiles in the washing process;

1.3.3 Questions

This research aims to exemplify this body-textile-environment communication by developing an 'electronic textile switch' mechanism. Whereby supplying an input to the electronic textile circuit will trigger an output in a different form. These research questions were developed from the research and aims and objectives in the anticipation the research challenges needed to be overcome to create the proximity and touch sensing e-textile that is still washable and mechanically robust. These questions will be consulted throughout the research presented in this thesis and answered in the Conclusion.

- Question 1: How can IC-based sensors function and be interacted with when integrated into a textile among fibres?
- Question 2: Can the proximity and touch sensing circuits still function with an encapsulation layer when integrated into a textile?
- Question 3: Can the circuits still survive and function after being integrated into fabric using industrial weaving and knitting machinery?
- Question 4: Can the proximity and touch sensing circuit still display functionality after being washed with a commercial washing machine?
- Question 5: Can the proximity and touch sensing circuit still display functionality after being mechanically deformed like a traditional textile?

1.4 Statement of Novelty

The novelty of this work is the systematic tailoring of polydimethylsiloxane (PDMS) as an aqueous-resistant and flexible circuit packaging for e-textile applications, by creating a 40.3 µm conformal PDMS-encapsulated 3 mm-wide capacitive touch/proximity sensing circuit - that can operate underwater and when integrated into textiles for machine washing.

This research has fulfilled this statement of novelty by these achievements:

1. Demonstrated a working capacitive proximity and touch sensing circuit integrated into the core of a knitted yarn and channel of a woven textile using an automated knitting machine and a hand- loom for weaving;
2. Identified an appropriate PDMS formulation for conformal encapsulation of such circuits to be integrated and washed for e-textile applications;
3. Demonstrated the encapsulated sensory circuit can still function 6 months underwater;
4. Identified washing settings to improve the functional longevity of the encapsulated circuit when washed with water, detergent, and fabric conditioner complied to textile standards;
5. Produced an encapsulated sensing circuit system which can survive 10,000 cyclic twists at 180° rotation and maximum 50 cyclic bends at 90° at 10 mm radius.
6. Created two e-textile demonstrators that can achieve self-capacitance proximity and touch sensing at yarn-level through knitted and yarn-formats;
7. Published 11 peer-reviewed publications, from time of this thesis hand-in, covering experimental findings and applications of the e-textile system in commercial settings;

Therefore, this work demonstrates for the first time unobtrusive and robust textile proximity/touch switching and indicator circuits for wearable and other textile applications. Also, it helps others in the field determine what type of technologically enhanced textile they have and whether it can be made into a commercial product.

1.5 Publications to Date

1. Ojuroye, Olivia, Torah, Russel, Beeby, Steve and Wilde, Adriana (2016) Autonomy is the key: from smart towards intelligent textiles. In, *Workshop on Autonomous Everyday Objects: Exploring Actuation in Ubiquitous Devices (within UBICOMP/ISWC 2016),* Heidelberg, DE, *12 - 16 Sep 2016.* New York, US, ACM4pp, 678-681. (doi:10.1145/2968219.2968558).

2. Ojuroye, Olivia, Torah, Russel, Beeby, Steve and Wilde, Adriana (2016) Autonomy is the key: from smart towards intelligent textiles. In *WomENcourage Computer Science* Conference 2016; Poster Presentation, Linz, Austria, 12-14 Sep 2016.
3. Ojuroye, Olivia, Torah, Russel, Beeby, Stephen and Wilde, Adriana (2016) Smart textiles for smart home control and enriching future wireless sensor network data. *Sensors for Everyday Life: Healthcare Settings*. Cham, CH, Springer, 159-183. (Smart Sensors, Measurement and Instrumentation, 22). (doi:10.1007/978-3-319-47319-2_9).
4. Torah, Russel, Komolafe, Abiodun, Li, Menlong, Ojuroye, Olivia and Beeby, Steve (2017) Novel Manufacturing Methods for Functional Electronic Textiles. *Printed and Stretchable Congress*, Poster Presentation, London, UK, 25 Feb 2017.
5. Ojuroye, Olivia, Torah, Russel, and Beeby, Steve (2017) 'Levels of Electronic Integration within Textiles' Chart. *WomENcourage Computer Science Conference* 2017; Poster Presentation, Barcelona, Spain, 06-08 Sep 2017.
6. Ojuroye, O. & Wilde, A.G. (2018), 'On the feasibility of using electronic textiles to support embodied learning', in *Perspectives on Wearable Enhanced Learning (WELL): Current Trends, Research, and Practice*, I Buchem, R Klamma & F Wild (eds), Springer.
7. Wilde, A.G. & Ojuroye, O (2018), 'Ubiquitous Embodied Learning with E-Textiles Electronic Textiles', *in Mobile, Wearable, Ubiquitous Systems Research Symposium*, University of Cambridge
8. Ojuroye, O., Torah, R., & Beeby, S. (2018, May). Improving the integration of e-textile microsystems' encapsulation by modifying PDMS formulation. In *2018 Symposium on Design, Test, Integration & Packaging of MEMS and MOEMS (DTIP)* (pp. 1-6). IEEE.
9. Ojuroye, O. O., Torah, R., & Beeby, S. Modified PDMS packaging of sensory e-textile circuit microsystems for improved robustness with washing. *Journal of Microsystem Technologies* (pp. 1-16). Springer Berlin Heidelberg, (https://doi.org/10.1007/s00542-019-04455-7)
10. Ojuroye, O. O., Torah, R., Komolafe, A.O., & Beeby, S. Embedded capacitive proximity and touch sensing flexible circuit system for Electronic Textile and Wearable Systems, IEEE Sensors Journal (pp. 1-11). IEEE. (https://doi.org/10.1109/JSEN.2019.2911561)
11. Torah, R., Komolafe, A., Li, M., Ojuroye, O., Wei, Y., Nunes-Matos, H., Hardy, D., Anastasopoulos, I., Kumar, V., Nour Nashed, M., Dias, T., Tudor, J., Beeby, S., (2018) 'FETT: Novel Manufacturing Methods for Functional Electronic Textiles', Large-Area Organic Printed Electronics Conference (LOPEC) 2018, Munich Germany.

1.6 Thesis Content and Organisation

This thesis is organised into 9 chapters.

- Chapter 1 focuses on the thesis's aims, research questions, and objectives whilst highlighting the FETT project that it is part of.
- Chapter 2 is the literature review which evaluates the state-of-the-art research on integration of electronics into textiles with commercial viability/using industrial practices, and how the capacitive means of proximity and touch sensing was decided.
- Chapter 3 outlines the system design for the resultant self-capacitance proximity and touch sensing textile, with intended inclusion of a hydrophobic, flexible, polymer layer, and how this could be integrated into knitted yarn and woven formats.
- Chapter 4 details the fabrication of the self-capacitive proximity and touch sensing circuit by covering prototypes, utilisation of the FETT circuit fabrication method, the sensory IC selection, and the final circuit design which could be integrated into a textile.
- Chapter 5 discusses how the packaging substrate was chosen for this research and presents experiments from peer-reviewed published (Ojuroye, Torah, & Beeby, Improving the integration of e-textile microsystems' encapsulation by modifying PDMS formulation, 2018) tailoring the substrate for its hydrophobic e-textile applications. The experiments investigate how the robustness of the substrate when in water, detergent, and fabric conditioner solutions used in the machine washing and handwashing process.
- Chapter 6 presents how the self-capacitive proximity and touch sensing circuits were integrated into textiles using knitting and weaving methods, and how this resulted into the e-textile demonstrators.
- Chapter 7 details a series of experiments which cover how dual-functionality capacitive proximity and touch sensing performance was improved for detecting a human hand. It also includes the washing test experiment of the proposed e-textile system which includes the integrated capacitive circuit and conformal packaging. The results are undergoing peer review
- Chapters 8 examines how the packaged capacitive proximity and touch sensing circuit responds to cyclic mechanical motions experienced in washing machines and consumer usage. These experiments are compliant with international textile standards and evaluate the durability of the system.
- Chapter 9 ends the thesis with the conclusion, discussion, and recommended future work with research applications. The conclusions compare outcomes of this work with the aims, research questions and objectives in Chapter 1. The discussion evaluates the functionality of the novel system and whether it is feasible for use. Future work recommends areas of research that can follow this thesis.

The Appendices contain simulation design and construction, experimental tables, and comparison table of used packaging substrates.

Chapter 2: Literature Review

This literature review provides the reader background knowledge on capacitive touch and proximity sensing electronic textiles. This literature review covers why an interest in touch and proximity sensing electronic textiles exists, on the advantages and disadvantages of the different approaches touch and proximity detection can be achieved, clarification on why the field opts for capacitive sensing approaches as well as its suitability for this research. It also covers capacitive sensing theory and different configurations possible for electronic textiles. Detail is provided on the state-of-the-art work on integrating flexible electronic circuits into textiles, and resultant design considerations for this research to further the field. Some of this chapter has been peer-reviewed and published in (Ojuroye, Torah, & Beeby, 2018)

2.1 Suitability of Touch and Proximity Sensing Mechanisms for Electronic Textiles

Touch and proximity sensing human computer interfaces (HCIs) are now ubiquitous in how humans interact with technological devices from smartphones, automotive dashboards, and tablets (Vallett, Young, Knittel, Kim, & Dion, 2016). Advancements in the micro-electro-mechanical systems (MEMS) field have enabled technologically advanced sensors to become miniaturised allowing them to integrate into more compact regions (Arshad, et al., 2016). Examples of the potential ubiquity of touch and proximity sensing electronic textiles (e-textiles), resulting from MEMS advancement, are evident in the different industries they have proved feasible. Wearable technology, specifically those which are textile-based has had extensive research in featuring touch and proximity interaction which feature soft and flexible electronics for greater invisibility and usability. Touch and proximity sensing in wearable and non-wearable purposes have been explored for use for diverse applications. A state-of-the art commercial example is Google's collaboration with Levi Jeans in the Project Jacquard project (Poupyrev, Gong, Fukuhara, Karagozler, Schwesig, & Robinson, 2016). This collaboration created a denim jacket to control smartphone features by swiping above (proximity) or touching integrated sensors. To monitor smart environments, touch sensors were integrated in a carpet to detect walking and lying interactions in work by Aud et al. (Aud, et al., 2010). In automotive interiors, proximity detection was exhibited by a car steering wheel for identity recognition which was considered as more secure method than using biometric data (Frank & Kuijper, 2017); touch sensing has been explored in the automotive industry to identify who is controlling devices within the car for more personalised interaction (Wang, Garrison, Whitmire, Goel, & Patel, 2017). In this sense, touch and proximity sensing integrated into textiles can give passive surfaces some ambient intelligence as they are able to interact and react to their environment (Rus, Sahbaz, Braun, & Kuijper, 2015).

Proximity sensing detects the presence of a conductive or non-conductive body from a distance. Touch sensing detects the direct physical contact of a conductive or non-conductive body.

The mechanisms at which they are achieved are based on whether the detected body is conductive or non-conductive. To achieve proximity and touch detection when a sensor is integrated within or among textile fibres can increase the complexity, as such a system would also need to behave and be treated as fabric. To allow electronic textiles (e-textiles) to detect touch and/or proximity, designers of such systems have multiple mechanisms to choose from. However, although there are many mechanisms that can allow a textile to touch or sense presence, the hardware used would need to be integrated into a textile for it to become an e-textile. As a result, literature has explored different mechanisms to achieve touch and proximity sensing in a textile environment which has realised their advantages, disadvantages, and a consideration if they are truly textile compatible.

Inductive mechanisms to sense proximity has been pursued, which involves a sensor coil of primary transducer is excited by electronics that have a high-frequency current through them. This generates a magnetic field which induces an eddy-current in the detected object, and its proximity distance is measured in the difference of electrical parameters in the coil (Jagiella, Fericean, & Dorneich, 2006). However, challenges with textile integration include its need for coils of sufficient size to work and textile-based coils have unreliable functionality and reliability. Readings are influenced by temperature (Kan, Huang, Zeng, Guo, & Liu, 2018). Optical proximity sensing can be used in smartphone applications and it relies on the reflection and detection of a light source. The amount of light detected back into the receiver indicates relative distance. However, it is not suitable for textile environments because optical mechanisms require a bright environment for operation, so this limits the amount of textile integration feasible (Zimmerman, Smith, Paradiso, Allport, & Gershenfeld, 1995). Furthermore, line of sight is affected by surface topology, there can be false—negative detections due to shadows, and to operate accurately optical mechanisms require a bright environment (Zimmerman, Smith, Paradiso, Allport, & Gershenfeld, 1995). Microphone-based proximity sensing has been explored to work with audible systems, measures audible sounds to give a sense of relative object position (Dobbelstein, Winkler, Haas, & Rukzio, 2017). Though, it can be affected by dampers and environmental/ambient noise can distort readings making it prone to false positives. (Braun, Wichert, Kuijper, & Fellner, 2015). It would be unsuitable for this research, as the size of the electronics needed is not small enough to integrate into textiles using weaving and knitting machines - nor disguised amidst the textile fibres. The incompatibility of sensing mechanisms due to hardware sizes is comparable with camera-based proximity sensing. Proximity sensing using a camera can be based on visible light (RGB) or Infrared (Braun, Wichert, Kuijper, & Fellner, 2015) by either detecting markers on an object to track or by using image recognition to detect specific objects. However, this would require high processing to evaluate a 3D image compared to a 2D image, which does not fully represent the real complex environment it situates in. Processing this real-time data can cause high power consumption, draining the entire device (Davison, 2003). For it work, the camera would need to be external to the e-textile as the camera itself is too rigid, large, to not be detectable within fabric. However, how long it takes to detect an object is also worth considering on a sensor mechanism's suitability. Pyroelectric sensing utilises an electrical response in a dielectric material due

to temperature change. Therefore, by measuring infrared emitted from a human, the change in temperature can indicate an object touching or in proximity of the dielectric material (Zappi, Farella, & Benini, 2008). However, it is known to have a slow responsive interaction (Braun, Wichert, Kuijper, & Fellner, 2015) due to determining an accurate detection. For accurate measurement of proximity distance in a textile, would require at least two pyroelectric infrared (PIR) sensors facing each other within a fabric. It is unclear how to achieve this in a fabric setting. Therefore, this would be compatible with wall-based textiles (Zappi, Farella, & Benini, 2008) but not wearable textiles.

Touch sensing via resistance changes works by measuring the resistive difference between at least two electrodes due to an exerted force can indicate touch and/or pressure (Han, 2005). Disadvantages includes requires pressure of the finger or hand touch which is not reliable if speed or contamination prevention is preferred (Dobbelstein, Winkler, Haas, & Rukzio, 2017). Reliability of operation depends on quality of the textile themselves, if textile degrades sue to mechanical abrasion or washing, the functionality of the sensing is compromised. Additionally, requires a large number of resistive sensors for improved reliability, which if rigid can make the textile inflexible (Wimmer & Baudisch, 2011). Piezoelectric touch sensing operates like a strain gauge whereby materials generate charge proportional to the amount of touch/pressure exerted onto it (Bartolozzi, Natale, Nori, & Metta, 2016). However, an e-textile made with this technology could not be mechanically-deformed as premature aging of electrodes occur due to frequent wear (Bartolozzi, Natale, Nori, & Metta, 2016). Piezoelectric sensing requires use of thick wires for reliable and successful operation reported in literature (Orr & Abowd, 2000) which would be detectable through fabric. Alternative solution is textile fibre threads but this may be too fragile/lack robustness. Proximity using magnetic mechanisms is also not appropriate for this research. Here, a source generates magnetic waves when an object of sufficient proximity is detected. It also measures impedance changes through a coil due to detection of an object (Jamone, Natale, Metta, & Sandini, 2015). It is not compatible with textile integration to create electronic textiles as the presence of metallic components, fastenings, and/or metallic coated fibres may be featured. Presence of metallic objects can distort detected signal (Braun, Wichert, Kuijper, & Fellner, 2015).

Proximity and touch can be pursued by infrared, whereby a source emits infrared light and detector receives the infrared light after deflection from static or moving object (Ascari, Corradi, Beccai, & & Laschi, 2007). Yet, this requires large amounts of power to operate over wide surface areas (Brandstein & Silverman, 1997) which may be the case for textile fabric. Specific to this research, the electronics will be integrated beneath and among textile fibres. Therefore, as infrared cannot distinguish between conductive or non-conductive materials it will sense the textile layer and nothing beyond it. Light may diffuse when they travel through different media (Braun, Wichert, Kuijper, & Fellner, 2015), such as textile fibre layers above the sensors, which makes it unsuitable for this research.

For wearable technology and e-textile applications, capacitive sensing is reported to be the most used (Frank & Kuijper, 2017), most reliable (Wang, Garrison, Whitmire, Goel, & Patel, 2017),

one of the least complex (Rus, Sahbaz, Braun, & Kuijper, 2015), low cost (George, Zangl, Bretterklieber, & Brasseur, 2010) and textile compatible (Jagiella, Fericean, & Dorneich, 2006) mechanism to achieve touch and proximity sensing. Other advantages literature has used to justify capacitive sensing for proximity and touch sensing specific to textile settings include:

- Generated electric field travels through any non-conductive material, making it suitable to sense through and be integrated into fabric (Braun, Wichert, Kuijper, & Fellner, 2015);
- Has low energy consumption and can have low-power operation (Braun, Wichert, Kuijper, & Fellner, 2015);
- Is highly modifiable, as the electrodes can be made into a variety of sizes, shapes, or degree of flexibility dependent on the application (Braun, Wichert, Kuijper, & Fellner, 2015);
- Can detect and distinguish between different types of interactions, such as touching, movement presence, tapping, and swiping (Dobbelstein, Winkler, Haas, & Rukzio, 2017).
- Can sense through surface which may be bent, stretched, or flexed making it suitable for textile integration (Grosse-Puppendahl, et al., 2017);
- Wearability and long-term unobtrusive monitoring of dynamic environment (Cheng, Amft, & Lukowicz, 2010);

Hence, many of the mechanisms mentioned above are either too large or rigid to be integrated into a textile, would require large power consumption, have limitations on what types of objects it can detect, hardware would have reduced functionality due to the surface topology of the fibrous textile, and the cost of the hardware would be too expensive to justify when cheaper alternatives are available. By referring back to 1.3.1, this research's touch and proximity sensing textile will be used to detect human movement and touch. The electronics and circuity used in this project need to be small and lightweight enough to adhere to a flexible film circuit substrate which will be expected to function and survive when located at the core of a yarn (Figure 1). As a result of this preliminary literature study, to ensure the resulting electronic textile can sense only humans, is simple to implement, can sense through fabric, is low cost to operate, and features small components to make it undistinguishable within fabric, capacitive sensing will now be compared as a sensing mechanism to achieve proximity and touch sensing.

2.2 Capacitance-based Touch and Proximity sensing for E-Textiles

Table 1 summarises a comparison of different approaches reported in literature that have used capacitive proximity or touch sensing specific for wearable and non-wearable e-textiles. It also highlights the textile integration method compared to the FETT design considerations:

Literature reference	E-Textile system	Proximity/touch interface	FETT Compatibility	Possible solutions
(Wijesiriwardana, Mitcham, Hurley, & Dias, 2005)	Knitting and weaving conductive polymers and coated metallic fibres between fibrous yarns.	Electrode made from knitted and woven conductive textile yarns as part of a fabric.	Not compatible, there is no hardware integrated within the textile itself. All hardware used to interface with the electrodes are separate from the textile	To achieve and sensing and actuating textile that has all associated hardware integrated at yarn level. The computer needed to detect the proximity and/or touch will be integrated within the textile.
(Rus, Braun, & Kuijper, 2017)	A couch embedded with capacitive touch sensors in the seats and backrests.	Textile capacitive sensing electrodes and OpenCapSens Board.	Not compatible, features large rigid external computers to measure the detected objects that cannot be fitted into the core of a yarn nor woven as yarns into a fabric.	Have electrodes and sensing circuity integrated inside the core of the yarn or woven fabric that has dimensions small enough to be woven into fabric.
(Frank & Kuijper, 2017)	A locking and unlocking system based on a capacitive electrode arrays located around the inner and outer semi-circle of the steering wheel as a security feature of a vehicle.	Copper-based capacitive electrodes located in a semi-circle around the outer and inner areas of the steering wheel.	Not compatible, as electrodes used are too wide to fit inside the core of a yarn (2.5cm) and resulting system cannot be called an e-textile as the hardware is external to the textile.	Ensure that the hardware, circuitry, and sensing electrodes are all embedded into the textile to make it an e-textile. Make the width of the circuity and/or electrode thin enough to fit inside the core of a yarn (max 3.6mm) as an ideal s that it will be undetectable when woven into fabric.
(Saponas, Harrison, & Benko, 2011)	A capacitive sensing grid to allow touch/finger stroke detection through fabric, specifically the outer and inner sections of a trouser pocket. The touching/finger stroking through the fabric is used to control smartphone operation.	A re-calibrated capacitor array mounted on the back of a smartphone	Overall no; capacitive system can sense through fabric but the system is not bendable as it is a rigid PCB and thus the hardware cannot fit inside the core of the yarn. The sensor PCB also needs to connect to a host computer via USB to function.	Ensure the capacitive sensing circuit is flexible to enable textile integration and development into a textile. Also ensure the operation of the circuit does not require an external host computer for operation to increase comfort and make the circuit appear unobtrusive.
(Rekimoto, 2001)	GestureWrist – uses capacitive sensing to	GestureWrist is a wristband made by	No, although capacitive approach means sensing	Make sure circuit substrate is flexible and features

	detect change in wrist movement and shape and translate this into gestures. GesturePad - uses capacitive sensing to detect fingers and decipher gestures made by them. Has a shield layer between the human body and the array to block the wearer's capacitive influence.	modifying a wristwatch. GesturePad is a touch pad made from a copper wire.	is possible through fabric this literature does not use fabric as part of its GestureWrist system. Rigid PCB is mounted onto of a wrist-band for the prototype. GesturePad is used to be covered by textile, making it detachable and applicable to clothes that already exist, but is not integrated as part of a textile, nor feature any hardware.	hardware small enough to allow circuit to still drape, flex, and bend like fabric. Ensure the circuit still has a shielding electrode to minimise the wearer's body capacitance, if the e-textile is worn.
(Holleis, Schmidt, Paasovaara, Puikkonen, & Häkkilä, 2008)	Phonebag – touch sensitive areas on the bag exterior used to control a music player fitted inside the bag. Gloves – has control on the outer hand region and a device controller on the index fingertip to operate a music device. Apron – has buttons sewn onto and embroidered onto an existing fabric for use as a remote control for media devices via Bluetooth.	Phonebag – thin conductive wires as touch interfaces embroidered onto already existing phone bag. Gloves – Conductive yarn is sewn onto the fingertip to the textile sensor pads which are detachable from the existing glove via Velcro. Apron – conductive thread sewn and embroidered onto textile in visible and invisible approaches to investigate usability.	Computational hardware which gives the operation complexity is external to the textile. Although flexible version of the sensing circuit can be made, flexing is limited by use of wires that offer only a slight bend.	Make all hardware used to operate the circuit contained within the circuit substrate dimensions, making the only hardware external to the circuit be batteries – like other circuits developed in the FETT project. Experimentation on the final circuits' flexibility, such as measuring its ability to bend under its own weight (drape), flex, bend, and twist.

(Guo, Huang, Cai, Liu, & Liu, 2016)	Creation of a capacitive sensing textile system comprising of flexible electrodes with a carbon black (CB)/silicone rubber (SR) composite dielectric using screen printing.	Textiles are used to encapsulate the flexible substrate capacitive electrodes made from a conductive rubber with the carbon black (CB)/silicone rubber (SR) dielectric between. Since this is multi-layered, this forms a parallel-plate capacitor within the textile.	System does not include the circuity, which is still a rigid PCB which is strapped around a wearer's leg whilst also being connected to the electrodes which are positioned in a sole of a shoe.	Make all hardware used to operate the circuit contained within the circuit substrate dimensions, making the only hardware external to the circuit be batteries – like other circuits developed in the FETT project.
(Cheng, Amft, & Lukowicz, 2010)	On-body textile-based capacitive touch sensor to measure changing capacitance within the human body. Capacitance changed may relate to shape changes in muscle, skin, and other physiological attributes.	Capacitor is made from flexible textile electrodes and the human body is treated as the dielectric material. Relies on self-capacitance, whereby on capacitive plate is an electrode and the other plate is "earth". Literature states the advantage is to integrate multiple electrodes close to each other when integrated within the textile.	Presented system has hardware that does the input processing on industrially-sourced rigid PCBs that would not be small enough to fit inside the core of the yarn, nor can be adapted due to the number of components upon the surface/routing of the wires without compromising circuit width.	Make all hardware used to operate the circuit contained within the circuit substrate dimensions, making the only hardware external to the circuit be batteries – like other circuits developed in the FETT project.
(Hirai & Naraki, 2016)	Capacitive-based sensing electrode made from fabric that can switch between proximity sensing and tactile sensing, with a robotic skin application.	Each sensing region of the textile is comprised of multiple layers to enable multi-modal sensing capabilities (proximity and tactile). Each bottom layer of the electrode is externally connected to an integrated circuit (IC)-based capacitive sensing chip which is considered as the active electrode.	Would be compatible if the microprocessor used had smaller dimensions (currently 6.50 mm ~ 4.40 mm), to enable it to be integrated into a textile using the FETT project method. Other electronics featured are small enough to be featured.	Make all hardware used to operate the circuit contained within the circuit substrate dimensions, making the only hardware external to the circuit be batteries – like other circuits developed in the FETT project.
(Poupyrev, Gong, Fukuhara,	Conductive fibre yarns used as electrodes, that	Electrodes made from metallic alloys wrapped around polyester and	As electronic circuit is not integrated into the fibre yarns themselves,	Have conductive interconnects between the yarns with flexible copper-

Karagozler, Schwesig, & Robinson, 2016).	interfaces with a detachable electronic circuit via conductive interconnects.	cotton fibres. Its construction was motivated by giving existing objects technological functionality. It shows that conductive yarns can me made using commercial textile machinery.	this is not the same as this research or with FETT project objectives. However, as it demonstrates that conductive yarns can be manufactured using automated processes, the technology can be used with the FETT project.	polyimide at its core and the conductive yarns made by Project Jacquard. The resultant e-textile system would not have any external hardware as it would all be manufactured simultaneously as the traditional textile fibres are interlaced or interloped. The result would create a commercially-scalable and advanced e-textile demonstrator.

Table 1 Comparison of different capacitance-based proximity and touch sensing systems from literature and whether they meet FETT project design criteria

Table 1 supports the novelty of this work as the hardware systems show incapability of being integrated into a textile due to being too large, bulky, and rigid. Table 1 also lists possible solution to their failures, though a primary improvement would be to make the circuit substrate flexible to increase the likelihood of the resulting e-textile to drape, bend, twist, and flex. Overall, literature has stated that flexible capacitive sensors are ideal to wearable technology circuits and sensors for this Ph.D's objective, with some literature showing preference of capacitive sensing in textile and wearable applications (Wei, Torah, Li, & Tudor, 2015). The benefits of using flexible circuit substrates for e-textiles will be discussed in section 2.5 of this chapter, and this research utilises the idea of using flexible circuit substrates specifically for e-textiles as part of the FETT Project (Torah, Komolafe, Li, Ojuroye, & Beeby, 2017).

2.3 Capacitive Sensing Theory applied to E-Textiles

Capacitance (units in Farads (F)) is defined as the measure of a system to hold electrical charge as a result of an electric field generated between charged electrode plates. The formula for capacitance describes the ratio between the electrical charge (Q) between the plates and the electric potential (V) difference as a result of distribution of charges in the generated electric field.

$$Capacitance, C\ (Farads) = \frac{Charge, Q\ (Coulombs)}{Potential\ Difference, \Delta V\ (Volts)} \quad (1)$$

Equation 1 Equation for Capacitance

A capacitive sensor comprises of two electrodes separated by a deformable dielectric that can hold electric charge. The electrodes can be metal or other conductive materials, such as metal foils,

metal sheets, the human body, inks, paints, and textiles. When a battery is connected to this arrangement, current flows and electrons are transferred from one electrode plate to the other. Capacitive sensing can be used to sense touch, proximity, location, and deformation by measuring the resultant change in the ability to store charge between the electrodes. The capacitance measured is influenced by the type and topology of the object that it detects. Furthermore, as the electrodes can be decoupled it offers more adaptability and customisation on designing capacitive measurement. Such as, choice of the electrode size, material, shape, and curvature. Specifically, for e-textiles, it allows touch and proximity sensing to take place under an opaque layer – such as textiles – without the use of large, expensive circuitry, or external equipment for functionality.

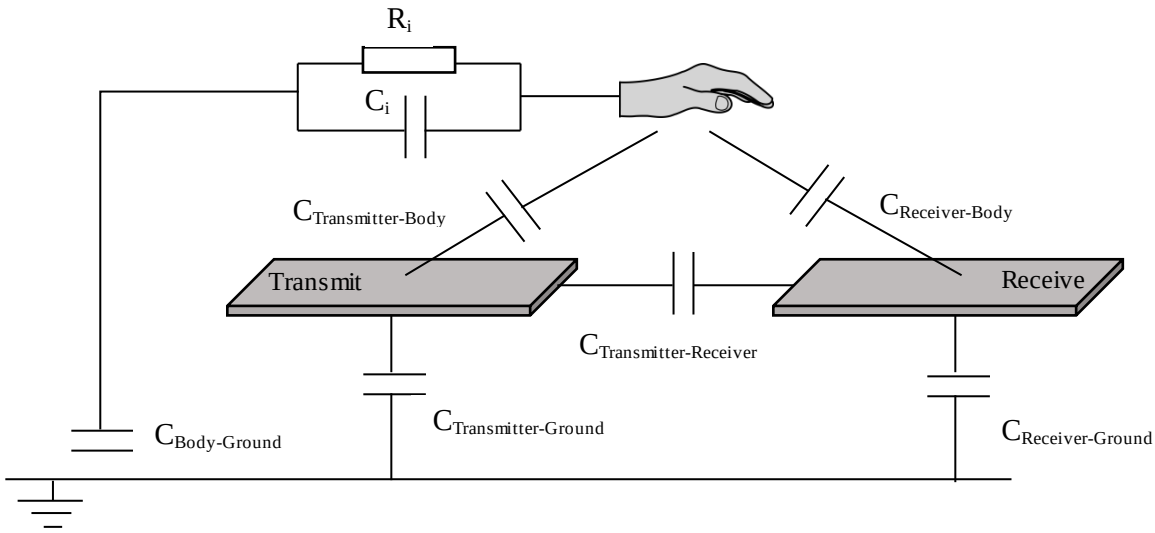

Figure 2 Circuit model diagram of different capacitive sensing models and different types of resultant capacitive-coupled measurements *(Smith, 1999)*.

Most capacitive touch and proximity sensing in e-textiles are based on measuring the capacitance between the human hand/detecting body and the electrodes. Ground allows all sensing capacitances to have a shared reference. This ground could be Earth, or the human body itself depending how the capacitive sensing is configured.

Capacitive sensing can either be passive or active:

- Passive capacitance Sensing: measures already generated electric fields that are ambient in the environment.
- Active capacitive Sensing: actively generates an electric field by generating a known signal upon the transmit electrode, to become capacitive-coupled with a trigger object (e.g. human hand) which may then be capacitive-coupled with a receiving electrode.

For e-textiles applications, the choice of which capacitive sensing mode is chosen can infer different information about the environment it operates in (see Figure 3). These four configurations are:

- *Loading Mode*: Also called 'self-capacitance'. The advantage of this setup is that the capacitor can have one electrode and the other is external like a detecting object e.g. human hand. This setup is common with touch screen, button, and panel operations. Due to the simple system, it is easier to shield (Reverter, Li, & Meijer, 2006), this improves its resilience towards electrical noise (Grosse-Puppendahl, et al., 2017), and can provide large operating proximity ranges.
- *Shunt Mode*: There is no initial connection between the detecting body with either transmit or receive electrodes, and as the electrodes are clearly separated this enables capacitive coupling between them. When the system does not detect a body, a displacement current flows between the electrodes. When detection occurs, capacitance values between the electrodes and the detected body changes. The human body capacitively-couples to both electrodes simultaneously, at the same value as the capacitive coupling between the electrodes themselves. This increases the displacement current from body to ground whilst reducing the displacement current from receive to transmit electrodes (Arshad, et al., 2016). Proximity to detected by measuring the decrease of displacement current at the receive electrode to ground. This is common in proximity sensing using capacitive arrays in e-textiles (Singh, Nelson, Robucci, Patel, & Banerjee, 2015) to achieve more accuracy and even produce gesture recognition (Rekimoto, 2001).
- *Transmit Mode*: detected body is close to the transmit electrode relative to the receive electrode meaning that the capacitive-coupling between the body and the transmit electrode is greater. The detected body is treated as part of the transmit electrode. The measured signal when the body moves towards the receive electrode causes the displacement current of the capacitor between the body and receive electrode to increase (Arshad, et al., 2016)]. The value of the measured signal is also based on the body's distance from the receiver's ground. In active-sensing, this mode can distinguish between which electrode is being interacted with (Wang, Garrison, Whitmire, Goel, & Patel, 2017) for example and measure changes within the body if placed in between electrodes during passive capacitive sensing.
- *Receive Mode*: The opposite of Transmit Mode, whereby the detecting body is considered part of the receive electrode (Arshad, et al., 2016). Therefore, the opposite behaviour applies when the body moves closer to the transmit electrode.

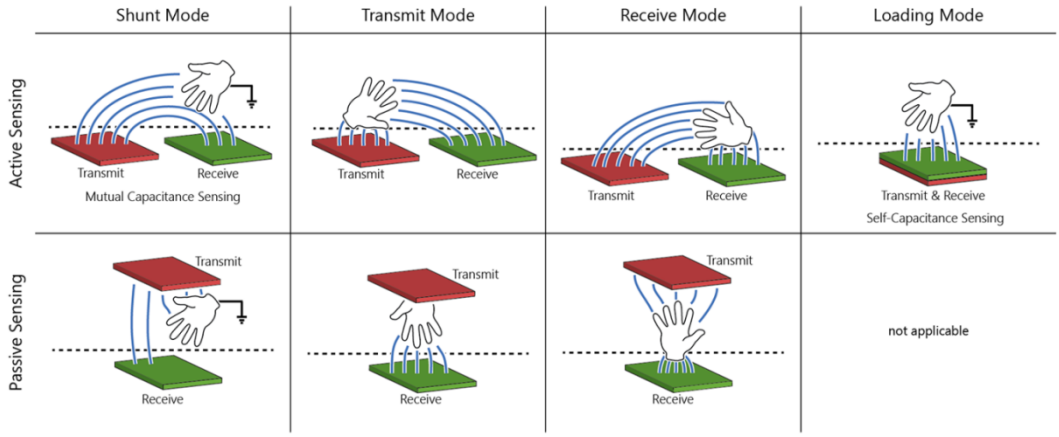

Figure 3 Different capacitive sensing types and associated operating modes for detecting objects. Dashed line represents boundary between the capacitive sensor and its environment *(Grosse-Puppendahl, et al., 2017)*.

Although there are research challenges associated with capacitive proximity and touch sensing, more consideration is needed when such operation occurs at the proposed core of a yarn. Out of the four approaches, loading mode (self-capacitance) would be most applicable to the e-textile system generated in this Ph.D. This is because one electrode can be part of the textile itself, while another electrode is formed of a virtual capacitor e.g. a human hand, to act as a trigger object to disturb the electric field generated when a voltage applied to the capacitive plate generates a charge. Hence, to ensure the circuit and sensing plate is unobtrusiveness within the textile, having the sensing of human interaction performed by one sensing plate instead of two would support this. The human hand acts as another sensing plate, which otherwise reduces the amount of circuitry in the textile that can make it heavy, rigid, or bulky. For usability, as this sensing type is familiar with touch screen it would make interacting with the resulting e-textile and intuitive experience.

2.4 State-of-the-Art Integration of Flexible Sensor and Actuator Circuits into Textiles

The idea of using film-based flexible circuit substrates as yarns for electronic textile applications has already been explored in literature. A novel manufacturing technique that used industrial weaving machines was developed to deploy electronic circuit strips to replace conventional natural fibrous yarns in a woven textile in work by Zysset et al (Zysset C. , Kinkeldei, Cherenack, & Tröster, 2010). Continuing work whereby circuits made from polyimide film as a substrate were woven using the warp and weft technique like conventional yarns (Zysset C. , Kinkeldei, Munzenrieder, Cherenack, & Troster, 2012), a new fabric was developed which evidenced a flexible fabric with LEDs woven into it. A hybrid fabric consisting of natural fibrous yarns, conductive yarns in the warp direction and flexible polyimide film in the weft direction was developed using this novel production line technique. The orthogonal arrangement of conductive warp yarns and electronic polyimide film circuit weft yarns was purposely chosen to allow electrical conductivity – to allow conductivity to cover the entire fabric. Similarly, the concept of utilising a strip-shaped circuit expressed by

Dementyev et al. (Dementyev, Kao, & Paradiso, 2015) has offered advantages to Zysset et al. (Zysset C. , Kinkeldei, Munzenrieder, Cherenack, & Troster, 2012) methodology to localise electronic activity. Some benefits of controlling the location of strip-shaped circuits using industrial textile weaving machines, to be used for fabric production include:

- Choosing the location of the electronic components and the distance between electronic components in the textile;
- Flexible plastic fibres with attached electronics in the weft direction allow the textile to drape;
- Flexible plastic fibres can be substrates for different kinds of electronic components e.g. thin-film devices and sensors - even in SMD chip form.

However, in both papers the flexible circuit strips were not fully integrated into the textile. Although the resultant e-textile was woven using a commercial weaving machine the flexible circuits were exposed which reduces its unobtrusiveness. Furthermore, the lack of packaging of the flexible circuit strips and the conductive thread caused functionality issues during mechanical testing. When bending rigidity was evaluated for a 0.75 mm radius, sensor signal errors occurred during their measurement due to ground yarn and power signals touching. This therefore presents a need to cover the conductive parts of the circuit – wires, circuit, conductive regions – with an insulation material to prevent short-circuiting and increase mechanical robustness. This could be done with an external textile layer or isolating conductive threads to the warp direction.

Similarly, the concept of utilising strip-shaped flexible circuit for e-textile applications was demonstrated by Dementyev et al.. They created a sensory tape called 'SensorTape' comprised of a dense sensor network that is can be cut and still function afterwards. SensorTape is a modular flexible circuit that has localised electronics allowing for the sections cut away from it to be functioning, miniature circuits. SensorTape could sense proximity of external objects but also to sense its own twisting and bending. The resultant prototype was double-sided polyimide with conductive solder pads for the SMDs and to mark cut lines. However, its dimensions were 2.3 m long but with a 25.4 mm width. This width supersedes that desired by the FETT project, which is less than 5 mm so that the circuitry can be handled by commercial weaving and knitting machines. Therefore, the sensor tape prototype is not applicable to e-textile applications and would need to rely on microtechnology or nanotechnology to reduce its width if the density of network and same functionality is to be achieved. Furthermore, the sensor tape could not be integrated into a textile due to its incompatible sensors. The ambient light sensor (TEMT6000 (Vishay)) and infrared sensor (VL6180 (ST Microelectronics)) used for detecting light and proximity respectively but both cannot sense through fabric. Both ambient light and infrared sensors underneath a textile will sense the textile first and not sense the presence of an object above the textile. This would lead to false readings and an unusable sensory e-textile. To mitigate this, the textile would need to have exposed regions for the infrared sensor but this would reduce unobtrusiveness and protection. This was why work by Zysset et al. has exposed the sensors integrated in their e-textile even in their latest research. Likewise, the concept of using strip-shaped

circuits was experimented for industrial applications by ETH Zurich (Zurich E.) to weave electronic sensor fibres into fabric and received funding from the Nano-tera TecInTex (Nano-Tera) and TWIGS project (Nano-Tera).

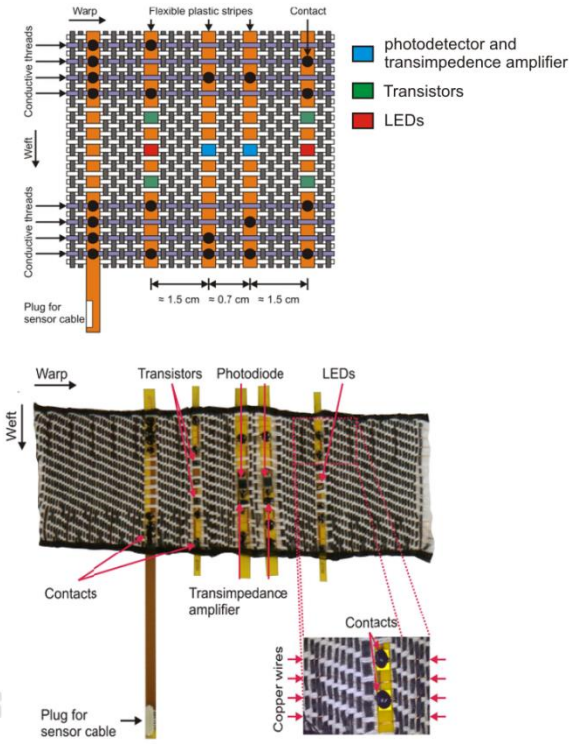

Figure 4 State-of-the-art for integrating flexible electronic circuits within textiles *(Zysset C. , Kinkeldei, Münzenrieder, Petti, Salvatore, & Tröster, 2013)*.

Furthermore, Takamatsu et al. (Takamatsu, Yamashita, Murakami, Masuda, & Itoh, 2015) used SMDs and polyimide to develop 5.0 mm x 20.0 mm LED flexible circuit. Takamatsu et al. (Takamatsu, Yamashita, & Itoh, Meter-Scale LED-embedded light fabric for the application of fabric ceilings in rooms, 2014) improved their technique, resulting in a product potentially used as a fabric ceiling cover or illuminated curtains. The LEDs SMD chips were still 5.0 mm in width but, using a newly developed automated weaving machine allowed for the LEDs to be woven into the fabric more precisely in the weft directions.

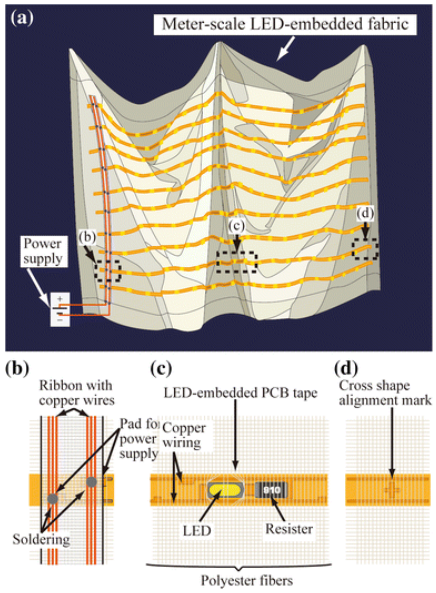

Figure 5 Diagram of flexible LED circuits stitched onto fabric *(Takamatsu, Yamashita, & Itoh, 2014)*

By expanding this technology by not focusing only on LEDs, but sensory circuits, the idea of sensory electronic textile circuit strips could become more prevalent. However, such circuits will not have self-awareness without some machine learning contribution (Dementyev A. , 2016). Still, a sophisticated novel system comprising of a densely compact circuit that can bend due being upon a flexible substrate and can be intuitively treated and handled like conventional textile yarns opens the opportunity to introduce novel electronic textile yarn circuits into the academic and industrial industries of smart textiles for wearable applications and other textile fields. Such a progression of wearable electronics will transition from examples featuring rigid yet small electronic circuits – like the LilyPad Arduino (Buechley, Eisenberg, Catchen, & Crockett, 2008) – and instead demonstrate the concept of flexible electronic circuits being interchangeable with fibrous yarns in dimensions, handling, and treatment.

In recent years, few publications have specialised in integrating flexible circuits into textiles. Those most similar to work completed in this Ph.D research is that from the FETT project. For example, work by Satharasinghe et al. (Satharasinghe, Hughes-Riley, & Dias, 2018) in 2018 presents work using textile construction methods that is part of the FETT project; however this work focused on integrating photodiode chips – not circuits – into the core of a yarn. Hence, it utilised the e-yarn technology the FETT project has contributed to the field, and motivated to make components undetectable once integrated within fabric whilst also being washable. In contrast to the literature reported in this subchapter, the SMDs were soldered onto copper wires to form electrical interconnects that interfaced with the photodiode semiconductor chips. Resin micropods encapsulated the chip to protect it from aqueous and mechanical impacts before being enwrapped in textile filler yarns via industrial knitting techniques.

Figure 6 Photodiode in rigid resin micropod to be integrated into core of a yarn *(Satharasinghe, Hughes-Riley, & Dias, 2018)*

As the resin micropod is rigid, this is not compatible with the system produced in this thesis research as the circuit would be centimetres in length rather than millimetres. Having a rigid resin on a longer, film circuit substrate would turn the circuit into a rigid tubular form that would prevent the textile to flex, drape, and bend once integrated. Therefore, this research was to extend this limitation by having a flexible circuit conformal layer that would allow the flexible circuit substrate it protects to still flex and bend. The result would enable the resultant e-textile to have similar degrees of freedom of movement as traditional textiles. Furthermore, by having smaller components on the circuit this would increase the feature size of the circuit once knitted or woven to become a textile. The result would have the same benefits of integrating the photodiode into the core of a yarn – the volume occupied by the electronics would be negligible compared to the total volume of the textile which would allow the textile to drape, flex, bend, and twist. Hence, this recent literature shows the importance of electronic integration within textiles and how it can affect the final design of the e-textile it creates. How the electronics are incorporated into the textile construction process has significant influence on whether the e-textile is practical to use, comfortable to wear, and can be intuitively treated like traditional textiles. This is fundamental to the desired acceptance of e-textiles by consumers if commercialised.

2.5 Flexible, Chemical Resistant, and Hydrophobic, Electronic Packaging for E-Textile Washability

Electronic packaging in addition to electronic circuit functionality contributes to the overall systems' durability, effectiveness, and performance. Electronic packaging describes the encapsulation substrate used to protect SMDs, integrated circuits, or even entire circuits including interconnections to ensure mechanical and aqueous resistance. Encapsulation technology has been researched in the textile industry to increase its durability and protection against chemicals, water, and mechanical abrasions. For washing e-textiles, water-resistance (hydrophobicity) and chemical inertness is needed to protect the circuits during the washing process which would include detergent and fabric conditioner. Microencapsulation for textiles has been actively studied in literature to act as moisture and mechanical barriers and increase the durability of the e-textiles system (Nelson, 2002). Microencapsulation is a packaging technique whereby a thin polymeric film is deposited on

microparticles (Nelson, 2001). Encapsulating electronic circuits that could be irreversibly integrated into textiles would need to be flexible, washable, and be resistant to the chemicals typically subjected to textiles to be durable and feasible to use.

To increase the mechanical robustness of electronic circuits, having an encapsulation layer has been proposed using spin-coating and thermal curing techniques (Christiaens, Loeher, Pahl, Feil, Vandevelde, & Vanfleteren, 2008). Flexible circuits with improved shielding from moisture and abrasion is needed (Zysset C. , Kinkeldei, Münzenrieder, Petti, Salvatore, & Tröster, 2013). Polyimide that can encapsulate electronic circuits and components using a sandwiching structure can retain mechanical robustness against strain due to bending and flexing. However, polyimide alone does not offer stretching capabilities, which is needed by some textile weaving machinery. Therefore, by further encapsulating a polyimide structure with an elastomeric substrate that has stretching capabilities, it may be possible to provide mechanical relief to create a flexible, and potentially twistable electronic circuit that can be used in conjunction with textile fibres to create a new kind of electronic textile. The result furthers efforts in integrating electronic circuits at yarn level, whilst also providing a multi-layered barrier against water and abrasion (Zysset C. , Kinkeldei, Cherenack, & Tröster, 2010).

Figure 7 Polydimethylsiloxane (PDMS) encapsulation of SMD transistor chips to create stretchable, elastomeric circuit matrix *(Matsuhisa, et al., 2015)*

Polydimethylsiloxane (PDMS) has been explored as a SMD encapsulation substrate to make resultant circuits mechanically deformable. Work by Matsuhisa et al. fabricated PDMS sheets in a 10:1 mixing ratio to form a large-area array of stretchable transistor arrays. The transistor was formed from DNTT (dinaphtho[2,3-b:2′,3′-f]thieno[3,2-b]thiophene)34 upon a kapton/polyimide flexible substrate, figure 8. This created a 12.0 x 12.0 cm matrix of a soft, flexible, and stretchable circuit, with intention to become a wearable electromyogram sensor. The conductive tracks were made from silver (Ag) flakes, while fluorine rubber, fluorine surfactant mixture was stencil-printed into the 150 µm-thick PDMS. The system could stretch 110 % with unaffected functionality; however, the disadvantage of having solely PDMS as a device substrate is fragility. Matsuhisa et al. reported the PDMS rupturing and hence device failure when strains were 200 %. This mechanical robustness could be improved by having substrates with a higher Young's modulus, such as polyimide, and increasing its surface area within the PDMS. If stretch is not required, such as the case of this Ph.D, and flexibility and twist mechanical deformities are then this solution could be explored for polyimide circuits with a PDMS-packaged layer. Additionally, having openings in the encapsulation substrate can permit electrical

contact with electrodes that may be surrounding the encapsulation layer (Kinkeldei, Munzenrieder, Zysset, Cherenack, & Tröster, 2011). Therefore, an encapsulation substrate that can be etched to have openings or regions of varying thickness would perform as conductive gateway to enable conductivity to transmit between layers and as a protective layer against liquids and mechanical deformation.

Achieving flexible, stretchable, low-cost, and light-weight electronic circuits, compatible with industrial manufacturing processes, has been attempted through fabricating conductive elastomeric substrates. Such substrates feature conductive nano-materials (Yao & Zhu, 2015) which can demonstrate computational behaviour creating nano-devices (e.g. strain gauges (Pu, et al., 2015) self-charging batteries (Lu N. L., 2012), capacitors). It is worth considering whether flexible and stretchable substrates, to make electronic circuits, are feasible. Its methodology would make circuits within textiles withstand high deformation whilst still being electronically functional.

Electronics that are flexible and stretchable have better contact on the human body (Kim, et al., 2011) – necessary for wearable applications. Elastomeric substrates for nano-scale electronic circuits have been laminated onto skin surfaces. They conform to the curvature of the human body and display high resilience to high strain deformation. However, when removed from the skin these electronics crumple due to extreme deformation, even with passive electronics residing within its body (Kim, et al., 2011). By improving the mechanical structure of the elastomeric substrate and locating the electronics and wires *within* the substrate that improves robustness and support, it may be possible to create a flexible, stretchable electronic circuit that achieves high bending and stretching capabilities to create drape-able, lightweight, and computationally functional electronic textiles.

More evidence of using elastomeric substrates as packaging and encapsulation of electronics has been exemplified through photolithography. A patterning technique has been multi-layered to produce stretchable, electronic circuits with conductive nanocomposite tracks that can be used in elastomeric substrates. An elastomeric membrane made from PDMS is patterned with a ma-N 490 photoresist layer and the conductive aqueous AgNW nanocomposites fill the hollow regions of the resulting membranes via vacuum filtration (Park, et al., 2016).

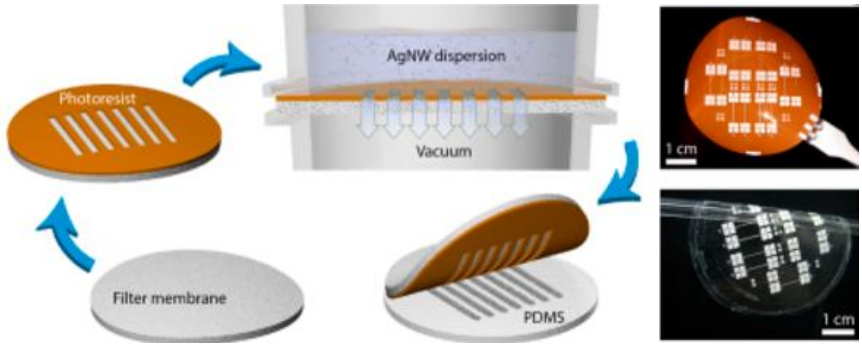

Figure 8 Photolithography fabrication of PDMS substrate and PDMS substrate with transferred nanowires (Tybrandt, Stauffer, & Vörös, 2016).

Nanowires were located within the flexible, stretchable, transparent, and light-weight membrane. An insulating layer of polydimethylsiloxane (PDMS) was placed on the nanocomposite regions leaving the conductive pads exposed yet it would be possible to insulate the whole structure to offer complete protection if needed. Conductive tracks are insulated by the surrounding PDMS regions, reducing short-circuit occurrences. Similarly, aqueous AgNW has been dispenser-printed to create nanowires for electronic circuits but have chosen to reside between two elastomeric substrates (Tybrandt, Stauffer, & Vörös, 2016). An LED matrix between two PDMS substrate layers was created with dispensed AgNW nanowires connecting the electronic components.

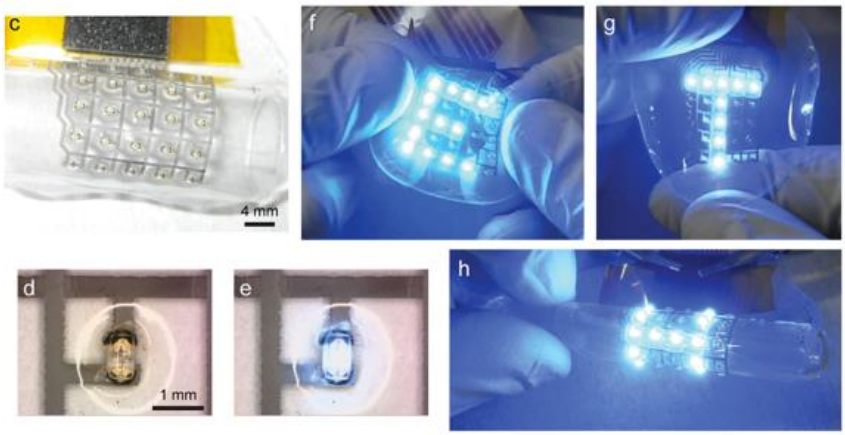

Figure 9 Stretchable LED Matrix, LEDs between two layers of elastomeric substrate sealed together *(Tybrandt & Vörös, 2016)*

Layers of PDMS are fabricated on top of each other by spin coating over laser-cut foil. Silver epoxy are stencil-printed onto the pads located on the AgNW tracks and the LEDs placed in a laser cut holder are simultaneously secured onto the pads when brought into contact. Contact between the LEDs and the silver epoxy sustained when strain was less than 20 %. For consumers, a basic requirement for wearable or non-wearable textiles is their washability or feasibility of being cleaned. If packaged electronic circuits within electronic textiles are to be considered functional, safe, and durable for use then electronic textiles need to be washable and sustain functionality after sufficient washing cycles to be considered robust (Wainwright, 2016). Recently, PDMS as a packaging

substrate for electronic textiles has been investigated to make integrated electronics withstand washing, (Ojuroye, Torah, & Beeby, 2018), (Ojuroye, Torah, & Beeby, 2019). PDMS, is characterised by its inorganic oxygen-silicon- long chain with are connected to organic groups of methyl moieties. Within the textile industry, the benefits PDMS offer to fabrics have been extensively used (Hénault & Elms, 2004). Benefits include aqueous repellence, abrasion resistance, strength retention, and reduced fabric shrinkage. In the e-textiles field, work by Tao et al. (Tao, Huang, Shen, Ko, Jou, & Koncar, 2018) report of a miniaturised, PDMS encapsulated, reliable, and fully washable Bluetooth activity monitoring system that can feature on wearable textiles. Other literature has reported washing cycle survival of less than 20 before failure (Linz, Kallmayer, Aschenbrenner, & Reichl, Embroidering electrical interconnects with conductive yarn for the integration of flexible electronic modules into fabric, 2005), (Merritt, Nagle, & Grant, 2009), (Varnaitė & Katunskis, 2009) which is not durable enough for long-time usage. Some literatures also report washing tests of circuits for e-textile applications that are not truly representative of how washing of textiles occurs. For example, conducting washing tests of circuits placing their circuits in wash/cloths bags during washing (Rantanen, et al., 2002) – such bags are used for washing delicates/underwear carefully. Nonetheless, the inclusion of this protective bag is not representative of how apparel and furnishing textiles are treated in a washing machine. Other literature report washing tests of circuits which include detergent but not fabric conditioner (Mattmann, Clemens, & Tröster, 2008), (Fu, et al., 2015) - and even complete washing tests with no other laundry in the washing cycle (Fu, et al., 2015). One of the greatest number of cycles recorded in literature for e-textile washing is 50 washing cycles (Kazani, Hertleer, De Mey, Schwarz, Guxho, & Van Langenhove, 2012), (Kaappa, Joutsen, Cömert, & Vanhala, 2017). However, these washing tests are not truly representative as some circuits under test were not integrated into a textile. Additionally, washing settings such as duration and spin speed were not investigated as a factor which would affect the survival of these circuits. Therefore, there is a need in the field for an inclusive and truly representative washing test of electronic textiles which can set new standards. Such an e-textile washing standard can be based on traditional textile washing standards but the e-textile under test features a fully integrated and fully functional circuit.

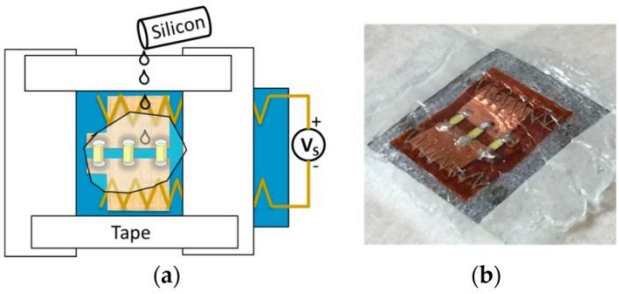

Figure 10 Encapsulation of the LEDs on the circuit only a) Scheme of encapsulation b) Encapsulation of LEDs on textile realised *(Tao, Koncar, Huang, Shen, Ko, & Jou, 2017)*

For washable electronic textiles to be reliable, usable, and commercially-viable it is imperative for the packaging used to enable it to survive the mechanical stresses imposed by the washing machine cyclic

process. This can cause points of failure whereby the circuit components could detach off the circuit and/or the conductive interconnects could tear off. As the field develops, it is hoped that the appearance of washable electronic textiles – which can sometimes be called washable 'textronics' – will feature a protective packaging that will cover the entire circuit and not just glob-topping the components on the circuit. Additionally, it is anticipated that the electronics would be completely embedded inside the textile and be undetectable. State-of-the-art literature that has almost achieved this has used silicone-based substrate to protect the electronic chips on a circuit that interfaces on a textile (Tao, Koncar, Huang, Shen, Ko, & Jou, 2017). Latex was dispensed onto a LED circuit whereby the circuit was a flexible conductive substrate and this circuit was attached via conductive thread to a planar, knitted fabric swatch.

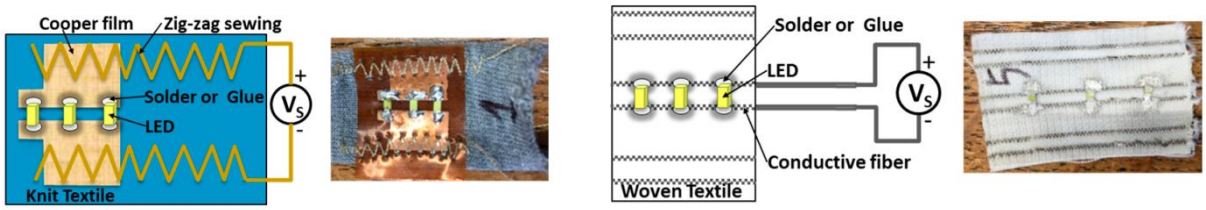

(a) (b)

Figure 11 Two types of circuit substrates for the 3-LED circuit a) flexible printed circuit board b) woven textile with conductive fibre *(Tao, Koncar, Huang, Shen, Ko, & Jou, 2017)*

The literature (Tao, Koncar, Huang, Shen, Ko, & Jou, 2017) does not state the reasoning behind encapsulating just the LEDs and not the entire circuit. For the woven-textile based circuit it is understandable, for encapsulating the entire fabric would affect its natural deformity which would influence its wearability. However, for the flexible substrate arguably an encapsulation over the entire surface could provide a greater surface area where water could not penetrate the components. This would provide more protection against water during the washing process. Tao, Koncar, Huang, Shen, Ko, & Jou, 2017 concluded that having a flexible printed circuit board circuit substrate with encapsulation was better than on a woven fabric due to withstanding more mechanical abrasion. More shedding on interconnects on the woven fabric was evident compared to that on the flexible PCB. Furthermore, it was suggested as future work that the combination of the silicone encapsulation on the components interfaced with conductive thread and flexible PCB should be combined for better washability – but this has not been researched further in literature.

Furthermore, the use of water-repellent silicone-based encapsulate to conductive fibres that are used as wires in electronic textiles has been investigated (Baribina, Baltina, & Oks, 2018). The existence of the hydrophobic encapsulate was found to protect the wires - minimising the electrical resistance change of the wires due to the washing process and to minimise the rate of change of electrical resistance due to the washing process. This is important, as conductive fibres increase in electrical resistance before becoming non-conductive, rendering the electronic textile as non-functioning.

Besides PDMS, other substrates have already been explored in literature to package electronic components on circuit substrates. However, these other substrates have been enhanced with PDMS to enable bio-compatibility and such examples have not been applied for use as washable e-textiles. Polyurethane (PU) has also been used to package SMDs for circuits integrated into textiles. However, to make PU a more effective barrier to moisture and chemicals, studies has reported modifying it with PDMS (Zhang, Song, Cui, & Qi, 2018). PDMS was also found to increase the flexibility and elasticity of PU in addition to providing a uniform hydrophobic layer. PU is not a suitable substrate for washing with detergent and fabric conditioner. As it is not chemically resistant to detergent, literature has reported completing washing tests with PU without detergents (Inoue, Tada, Itabashi, Kimura, & Taya, 2016).

Polyethylene terephthalate (PET) is a thermoplastic, recyclable polymer commonly used in manufacturing and clothing industries. It is used in many industries for its adaptability, transparency, and mechanical deformity. PET as a fabric is known as Polyester (Ramaratnam, Tsyalkovsky, Klep, & Luzinov, 2007). PET is known for its hydrophobicity (Pichal, Koller, Aubrecht, Vatuňa, Špatenka, & Wiener, 2004), low manufacturing costs, and chemical resistance. However, in plastic form PET can be toxic and cause adverse health effects due to the leakage of the antimony contaminant when in contact with water (Westerhoff, Prapaipong, Shock, & Hillaireau, 2008) making it unsuitable to be used as electronic packaging of circuits in textiles where it will be close to the human body. In plastic form, PET is not suitable for washing and therefore not appropriate for applications of circuit packaging to form e-textiles. Although PET is hydrophobic, other disadvantages when applied to e-textiles include its low heat resistance and its susceptibility to heat degradation (Matsuda, Kotani, Kogure, Tatsumisago, & Minami, 2000). Its chemical structure is weakened at 60 ºC, a washing temperature known to completely kill bacteria like methicillin-resistant Staphylococcus aureus (MRSA), when detergent is included (Lakdawala, Pham, Shah, & Holton, 2011). Therefore, it makes PET unsuitable for a wide washing temperature range to prevent the spread of germs or kill bacteria necessary to preserving health and textile usage. If PET supersedes this temperature, its chemical structure is irreversibly changed making the number of times it can be washed at high temperatures limited. PET is also not completely inert as it is susceptible to oxidation. This means that is has a low shelf-life and will eventually degrade structurally over time. Furthermore, due to PET's slow crystallization rate it has low mouldability when fabricated. It therefore becomes an expensive process to fabricate. Usage of PET introduces health concerns with continued contact. To mitigate the wash risks with PET as an electronic packaging material, literature has instead used PET as a circuit substrate in plastic/film form (Briand, Molina-Lopez, Quintero, Ataman, Courbat, & de Rooij, 2011) or featuring PET as its textile form as a circuit substrate (Wang, et al., 2017). For these reasons, it indicates why PET has not been pursued as a *washable* electronic packaging substrate in literature.

For e-textiles, substrates such as an epoxy resin Epo-Tek T7139 in work by Zysset (Zysset C. , Kinkeldei, Münzenrieder, Petti, Salvatore, & Tröster, 2013), and poly(3,4-ethylenedioxythiophene):poly(styrenesulfonate (PEDOT:PSS) was used by Hamedi et al. (Hamedi,

Forchheimer, & Inganäs, 2007). The Epo-Tek T7139 (Zysset C. , Kinkeldei, Münzenrieder, Petti, Salvatore, & Tröster, 2013) was used to glob-top passive components as mechanical support on flexible PCBs cut into strips and woven into fabrics by handling this strip circuits as yarns. The PEDOT:PSS (Hamedi, Forchheimer, & Inganäs, 2007) when fabricated and cured is rigid, and used to connect and protect bonded conductive yarns together to form transistors. Such substrates could protect the components from mechanical abrasions but washing tests were not investigated in these works. These two literatures did not evaluate the packaging's durability and robustness when washed. However, literature by Ankihili et al. (Ankhili, Tao, Cochrane, Coulon, & Koncar, 2018) investigated PEDOT:PSS in a washing test whereby the substrate encapsulating a cotton fabric would be tested against water and mechanical stresses. One detrimental factor was PEDOT:PSS and the capillary effect exhibited with the textile during the washing process. The capillary effect causes water to channel through the textile, with swelling causing fibre bonds to relatively weaken. The capillary effect describes the unaided movement of liquid through narrow spaces without external forces acting on it. This also caused the electrical resistances of the textiles to increase. This was due to the viscoelasticity of PEDOT:PSS, it can be absorbed by the textiles it interfaces with. Literature found that absorption of PEDOT:PSS by the textiles increases with subsequent washing cycles. For the applications of this specific paper, this was a good result - as coating the textiles in PEDOT:PSS would promote more absorption of sweat and thus advantageous in creating flexible electrodes suitable for ECG and would replace flexible, rigid, and uncomfortable metal-based ECG electrodes. However, for wearable applications whereby the electronic textile will feature an irreversibly integrated electronic circuit, it seems PEDOT:PSS is unsuitable substrate for this Ph.D thesis. Having an encapsulate substrate that would absorb into the textile over time and increase mechanical pressure onto the circuit could risk a cause of failure. Additionally, due to the capillary effect and that PEDOT:PSS is not permanently hydrophobic, water would reach the electronics that the substrate was aiming to protect. Therefore, another packing substrate is required by the field to make truly washable electronic textiles whereby the electronics is fully integrated into the textile and not detachable.

Moreover, different encapsulation techniques can affect its reliability to protect microchips and have varying production costs. Glob top has been used for its low cost (Kallmayer, Pisarek, Cichos, Neudeck, & Gimpel, 2003) but its protection is not reliable due to its low 60-70 % particle content. Transfer moulding is currently used to encapsulate microchips at high yield using epoxy resin and hardener and has a higher particle filler content of 70-90 % but highly expensive to implement (Linz, Kallmayer, Aschenbrenner, & Reichl, 2005). Hot melt is another technique that could melt polyimide sheets to form an encapsulation layer over microchips. It is one of the least expensive options (Braun, Becker, Koch, Bader, Aschenbrenner, & Reichl, 2005), and the material can be remoulded. However, materials used in this technique are not chemically resistant and furthermore become inflexible after undergoing hot melt. In addition, for –textile encapsulation substrates being elastomeric/flexible/bendable they need to be chemically resistant to withstand chemicals – detergent and fabric conditioner - used in the washing process.

2.6 Conclusions

To summarise the literature review, none of these projects utilised the idea of completely containing the strip-shaped circuit inside the core of a textile fibrous yarn. Though, an overlap is evident between electronic engineering and material science to create washable electronic textiles to create state-of-the art electronic textiles that can contribute novelty to the electronic textiles field.

Overall, the benefits to developing and having e-textiles with embedded flexible electronic circuits include:

- Flexibility;
- Large sensing surface area;
- Invisible electronics when integrated fully into the textile;
- Minimised wires that can be potential points of circuit failure;

The anticipated points of system failure when integrated electronics into textiles includes:

- Wires connected to circuit snapping due to bending
- Inelasticity of circuit and electronic components against the natural elasticity of the textile
- Losing circuit functionality after washing and/or coming in contact with aqueous solution
- Losing circuit functionality when encapsulated in hydrophobic packaging substrate
- Losing circuit functionality during the textile integration process
- Components coming off circuit due to mechanical abrasion
- Proximity and/or touch sensing not functional in the textile environment created for the circuit
- Electronic components or circuity detectable through fabric due to protrusion.

The FETT Project has already developed novel fabrication and assembly techniques for potential manufacture of e-textiles whereby the circuits are located at the core of the yarn. The objective is to use this FETT Project novel fabrication method and apply it to develop a touch/proximity switching mechanism that has the potential to control another sensor or actuator in future cases. Additionally, by furthering the assembly technique developed, it could expand the industries that this technology can impact. Expected industries for the FETT project e-textiles to impact are wearable technology, consumer electronics, and military for it enables the lightweight, undetectable, and flexible electronic system that can seamlessly be integrated into textiles using industrially-used weaving and knitting machinery. Therefore, in line of the development of the FETT project, this highlights the need for an e-textile capacitive touch and proximity sensing mechanism that fulfils technology-driven design considerations.

Chapter 3: System Design for Self-Capacitance Proximity and Touch Sensing E-Textile

This chapter will outline the design requirements needed to produce a functioning touch and proximity sensing electronic textile system that can be triggered through aqueous-resistant and textile outer layers.

3.1 System Design Requirements

To realise proximity and touch sensing electronic textiles that can trigger another circuit and be washable, the system has to be designed for private and public use if ubiquitous use is strived for. The approach used in this research to integrate electronics into textiles was governed by design requirements to avoid anticipated system failures. These system design requirements included:

A final circuit that is thin enough to fit inside the core of a knitted yarn ($\leq$ 3.0 mm) or woven channel ($\leq$ 5.0 mm), and this circuit to include all hardware and conductive tracks.

The circuit should operate at low power (3.0 – 4.0 V) to enable battery power operation. The touch/proximity sensing mechanism needs to operate in self-capacitance rather than mutual capacitance. This is because self-capacitance is more robust for changing environments e.g. dry, wet, bent, and flexed. Additionally, it allows for changing electrode size for yarn and fabric integrated demonstrators (Rus, Sahbaz, Braun, & Kuijper, 2015).

When the circuit is integrated into a textile, the method has to be such that it resembles a traditional textile e.g. lightweight, still drapes, has high wearability, and can withstand textile mechanical distortions. To ensure minimal false-positives the sensor has to have a near field detection range (max 2.0 cm) to minimise false triggers by neighbouring individuals, and primarily have the sensor controlled by humans. Therefore, it was worth considering a sensor that could auto-calibrate to different environments.

The final e-textile system should use materials that offer no health hazards when used by humans to ensure safe usage to different age groups. Its functionality should not be obstructed by textile itself e.g. can sense through textile fibres. Simple system architecture is needed with the component sizes used to be small and unobtrusive enough to be incorporated into the textile environment using weaving and knitting machinery. The circuit should have dual functionality if possible, to detect both touch and proximity to allow the e-textile to be multi-purpose depending on its application and environment;

Importantly, so that the resultant e-textile can survive realistic washing conditions, it needs to be chemical-resistant and waterproof. This will ensure it can survive aqueous environments and withstand detergent/fabric conditioners.

3.2 System Design Specifications

Therefore, the design specifications of the novel electronic circuit to be developed were:

- Can be mechanically deformed: expressed through some degree of flexibility e.g. bend, flex, twist. This is to enable its industrial compatibility of surviving through the textile weaving process when woven into the core of a yarn but additionally when the resultant electronic circuit textile yarn is woven into a fabric. Furthermore, this can enable the fabric that could be created from the electronic circuit yarns to flex, drape, in a behaviour that is akin to natural fibrous textile fabrics.
- Is 'thin': 'Thin' has been defined by the accepted width range that textile weaving machines at Nottingham Trent University can use to weave a strand of yarn. This width has been restricted to ≤ 3.0 mm. Whereas, the electronic circuit developed must be ≤ 5.0 mm to successfully be woven into textiles. The electronic textile's length will be based on the mask size used during the fabrication technique.
- Compatible with the FETT project circuit fabrication methodology: needs to feature on a thin and flexible copper-polyimide circuit substrate, using the fabrication method specific to the FETT project.
- Can be developed commercially: reliant upon using a combination of equipment and machinery that is used in industry in both the electronic and textile manufacturing industries, or if fabrication technologies are used in academia the techniques used can be adapted for industrial scalability. This specification will be fulfilled by the novel fabrication technique to produce these circuits, to be demonstrated through this research.
- Can survive textile washing usage and quality control: the encapsulation layer(s) developed and configured will determine the duration of the electronic circuit and its components survival. To be specific, the electronic circuit would have to survive the washing process and bending process. This research will aim to test the electrical and mechanical survival of the novel electronic textile circuits by having them experimentally tested through washing and cyclic quality control bending tests.

3.2 E-Textile System Design Concept Drawings

Consequently, this created an aim for the usability of this Ph.D research - to ensure the electronics were truly integrated and indistinguishable from the circuit whereby the circuitry would not need to be removed from the circuit to be washed, mechanical deformed and still sense proximity and touch afterwards.

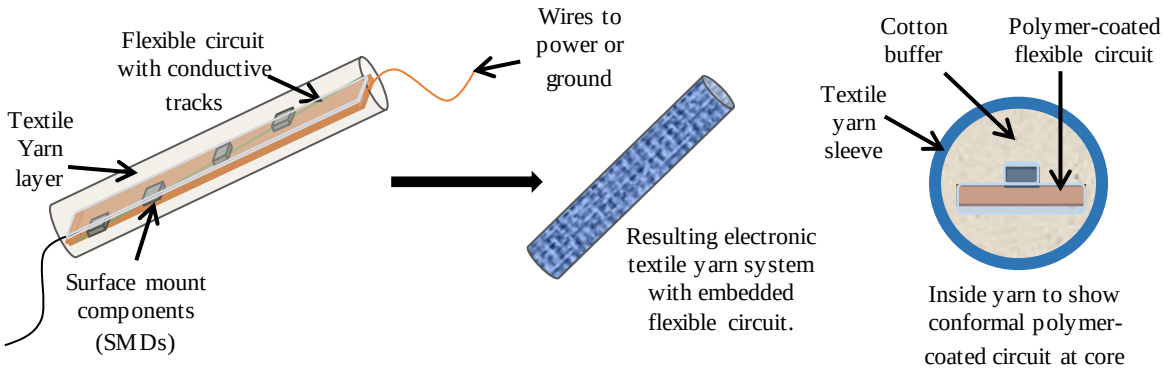

Figure 12 Viewpoints of planned location of a flexible circuit in conformal, aqueous-resistant, polymer-encapsulation into the core of a textile yarn

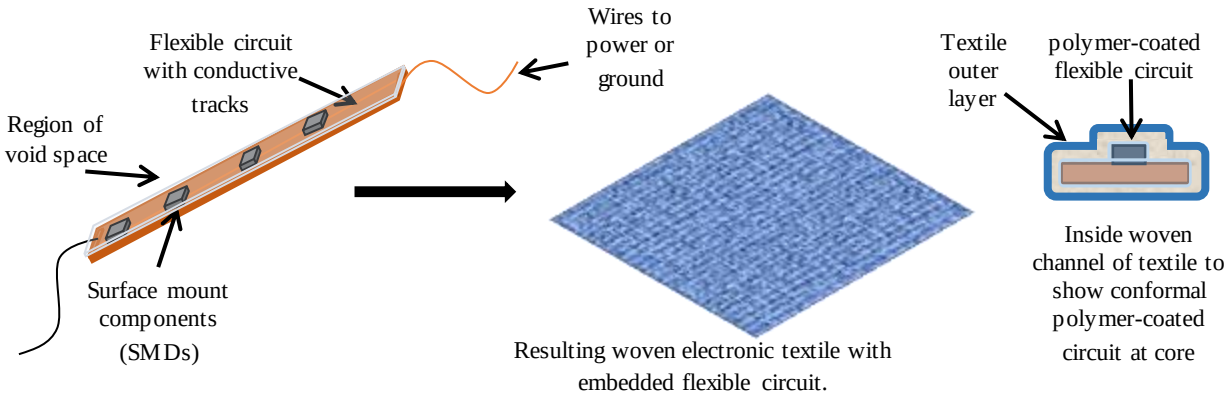

Figure 13 Viewpoints of planned location of a flexible circuit in conformal aqueous-resistant, polymer-encapsulation into a woven channel as part of a fabric.

As seen in the literature review, such an achievement would not have been achieved before and very little examples would be similar. Lab experiments and simulations would ensure the final system was tested before completion – these are detailed in Chapter 7 of this thesis.

Chapter 4: Design and Fabrication of Yarn-level Capacitive Touch and Proximity Circuit for E-Textile Applications

This chapter will outline the choice of capacitive proximity and touch sensing IC that will be made into a strip-shaped circuit, per FETT project specifications, to be integrated into textiles. It will also outline the development previous prototypes that led to the final system design of the e-textile system presented in this Ph.D thesis, including the circuit fabrication process used.

4.1 Considerations in Circuit Development

The final e-textile capacitive touch and proximity sensing system produced from this thesis is a concept application for integrating a proximity and touch sensor - for users to either touch, wave or hover their hand above a textile yarn to trigger the illumination of an LED on the integrated flexible circuit. To produce this result, the circuit would need to be calibrated to have high sensitivity to be able to detect a trigger object through the textile and hydrophobic packaging layer. Additionally, due to the strip-shape of the circuit and the small dimensions of the overall system, the self-capacitance sensing with an electrode dimension would be thin and rectangular shaped – both characteristics unadvised by the off-the-shelf commercial manufacturers of the evaluated touch/proximity chips.

Therefore, this Ph.D research had to experimentally determine the dimensions of the rectangular sensing electrode such that it is small as possible yet still functions as a capacitive sensing plate. Additionally, achieving this system required an understanding of the capabilities of the chip, the materials used to form the electrode, and the weaving technique used to encapsulate the metallic electrode inside the yarn. Interacting with the hybrid textile-electronics system marks the beginning of traditional textiles truly embedded with electronics to interact with hardware circuits.

4.2 Sensory IC Chip SMD Circuit Design for E-Textile Integration

Aforementioned, using capacitive MEMS was chosen for this project for its low-power, low-cost, and overall is component dimensions are smaller. Furthermore, its output signal is susceptible to less electrostatic noise (Kim, Cho, Shin, Lee, & Baek, 2013). Technical specifications for a capacitive proximity and detection were defined and used to influence the SOIC chip, also available in DFN SMD package form, considered to be used in this Ph.D thesis. The table of comparison can be found in Appendix C: Table of Comparison for Touch and Proximity Sensing Surface Mount Components for E-Textile Circuitry.

After evaluating technical specifications between all MEMS capacitive devices which can measure touch/proximity, the PCF8883 chip by NXP Semiconductor was used in this thesis research.

The PCF8883 circuit schematic used was sourced from the datasheet (Semiconductor, PCF8883 Capacitive touch/proximity switch with auto-calibration, large voltage operating range, and very low power consumption, 2014) and amended for increased sensitivity to detect external stimuli with a smaller than industrially advised electrode. The PCF8883 is an automatic self-calibrating single channel proximity and touch sensor which requires a conductive sensor plate e.g. metallic foil or sheet; in order to trigger an actuator circuit as its output pin. Comparing to chips listed in Appendix C, the PCF8883 was chosen for its:

- Customisable switching behaviour: the PCF8883 circuit can be re-wired to generate an output in three configurations; pulse, toggle, or momentary.
- Size: The PCF8883US specifically offered the smallest size capacitive proximity and touch sensing chip – with dimensions 1.16 mm (L) x 0.86 mm (W) x 0.44 mm (H)
- Adjustable sensitivity and response time: through a combination of resistor and capacitor values, it is possible to adjust the sensitivity of the PCF8883 to allow it to sense through variable sensor plate sizes, shapes, and trigger distances.
- Availability: the PCF8883 is continually in stock from a range of suppliers and at an affordable cost for repeated purchase throughout the research.
- Variable chip size: the PCF8883 technology has been created in SOIC8 package size and a size which is compatible to be on a circuit located at the core of a yarn, the wafer-level package chip size (WLPCS8). This meant prototyping a larger version of the circuit to establish reliable function was possible, but additionally that design can be scaled down for a smaller prototype without choosing a new chip.
- Diverse applications: the PCF8883 datasheet lists an array of applications covering diverse industries that its technology can be featured in. Examples include medical switches, security protection, transportation, proximity detection and sensing for (portable) electronic entertainment units.
- Automatic calibration: less susceptible to noise due to other nearby technology devices, contact with the body, or its changing orientation when put into the textile yarn or in fabric.
- Low power consumption: this means it could be battery-powered using affordable, off-the-shelf batteries which are purchasable to hobbyists/consumers and minimises the heat generated by the circuit once functioning and encapsulated.

The circuit used was sourced from the datasheet and amended for increased sensitivity to detect external stimuli with a smaller than industrially advised electrode and through fabric. A LED was connected to the R_{OUT} resistor on pin 5, and the co-axial cable was exchanged for a copper-plated polyimide electrode at pin 1. Part of the FETT project is to show that off-the-shelf components currently used and sourced from industry can be used for e-textile applications, and that existing circuit designs for the chip can be re-designed to feature on a strip-shaped flexible circuit that will be integrated into a textile. This research had to show that the PCF8883 chip could operate at yarn-level,

with a circuit width less than 5.0 mm and be handled by textile construction machinery to be made into an e-textile.

4.3 PCF8883 Capacitive Proximity and Touch Sensing of Human Hand Sensing Operation

The external sensing plate i.e. sensing electrode is connected at the chip pin IN, 1 where it is also connected to the internal resistance-capacitor (RC) timing circuit. The chip's logic output becomes either LOW or HIGH to represent non-detection or detection of a trigger object such as a human hand. This occurs when the discharge time of the internal RC timing circuit is compared to the second RC internal timing circuit that is used as a reference. Both timing circuits are periodically charged by the voltage from entering pin $V_{DD(NTREGD)}$, 8 and discharged by a resistor going to ground on pin V_{SS}, 4. If the voltage at one RC timing circuit falls below the internal reference voltage at the other RC timing circuit there is a logic output LOW, for vice-versa the logic goes HIGH and a pulse signal is sent to pin OUT, 6 to an actuator.

Component values that control the charge-discharge cycle are those which influence the detection efficiency of a trigger object i.e. human hand. These are:

- The capacitor at pin CLIN, 7 which controls the sampling rate (f_s): the sampling rate is half the frequency used in the RC timing circuit. By changing the capacitor value at CLIN, it is possible to adjust the sampling frequency between a specified range for functionality and hence make the chip suitable for its operational environment.
- The capacitor at pin CPC, 3 which controls sensitivity: Pulses control the charge on the external capacitor C_{CPC} on pin CPC. For every pulse produced, C_{CPC} is charged from $V_{DD(NTREGD)}$ for a fixed time causing the voltage on CCPC to rise.

If the capacitance on pin IN increases due to a human hand moving closer to the self-capacitance sensing electrode to increase the electric field or by the human hand touching the electrode – the discharge time also increases. It therefore takes longer for the voltage at $V_{DD(NTREGD)}$ to drop below the voltage reference V_{REF}. The output switching behaviour can be three forms. Push button was chosen as the resulting circuit design was compatible with the FETT project circuit design methodology and would avoid circuits crossing in order for other options to work. In push button mode, the output is active as long as the capacitive event exists (dynamic increase of capacitance at sensor input pin IN when a trigger object is interacting with it). The value of total capacitance at pin IN for the PCF8883US to operate at optimum functionality is 30 pF, where:

$$C_{TOTAL} = C_{SENS} + C_F \qquad (2)$$

Equation 2 Calculation of capacitance of sensing electrode for IC Capacitive Proximity and Touch sensing chip

- Where C_{TOTAL} is total capacitance at pin IN
- C_{SENS} is the capacitance generated from the sensor (sensing plate and trigger object)

  C_F is the capacitance from component C_F at pin IN which is a smoothing capacitor.

As C_F = 10 pF, C_{SENS} needs to be approximately 20 pF. Therefore, factors such as electrode dimensions, C_{CLN}, C_{CPC}, and dielectric layers such as the packaging substrate and the textile outer layer would be decided such the resultant C_{SENS} value would be approximately 20 pF.

4.4 Previous Prototypes

4.4.1. First Prototype

The first 9-month research created the first prototype of this thesis. It demonstrated that the commercially-sold and available PCF8883US SOIC chip could be triggered by a novel yarn electrode that featured a sensor plate at its core. This novel yarn electrode was designed and developed as part of this Research in collaboration with Advanced Textile Research Group (ATRG) at Nottingham Trent University. This novel yarn electrode was 0.1 cm width x 10.0 cm length strip made from 25 µm-thick polyimide film which had an 18 µm-thick copper layer. Multiple strips of the copper-plated polyimide film were connected with copper-enamelled wire to ensure conductivity throughout the whole length of the yarn.

The objective of the first prototype was fulfilled in demonstrating a capacitive touch and proximity electronic textile switch concept. This switching capability is comparable to a transistor or mechanical switch and can control more behaviours exhibited by the electronic textile or enable communication with connected devices if part of a larger internet of things (IoT) system.

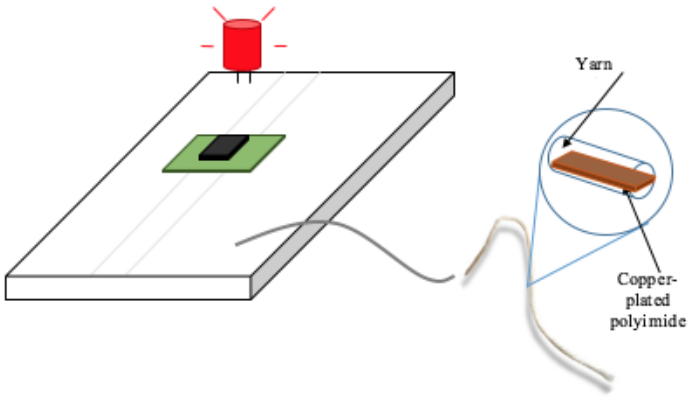

Figure 14 Concept diagram of first touch-sensing yarn prototype

The datasheet of the capacitive proximity/touch PCF8883 chip suggested an actuator circuit to trigger an output response. For textile embedment, the suggested circuit was adapted to a strip-shape by a careful selection of component sizes that would fit into the strip as well as within the textile weaving machinery. An LED was connected to the R_{OUT} resistor on pin 5, and the co-axial cable was

exchanged for a copper-plated polyimide electrode at pin 1. The SOIC chip were soldered onto SO8 adaptor boards and secured onto the circuit.

Overall, testing the circuit revealed it was possible to use the novel electronic yarn electrode to trigger the PCF8883 circuit detecting touch but not proximity. As a result, by touching outer yarn layer of the copper-polyimide yarn an LED illumination occurred as an output response. This validated the electronic textile switch at is basic form. Therefore, the circuit required a change of component values responsible for the sensitivity and response time of the PCF8883. This was completed later, detailed in 7.1 Experiments Modifying PCF8883US Component Values and Determining Electrode Dimensions for Improved Calibration to Textile Environments.

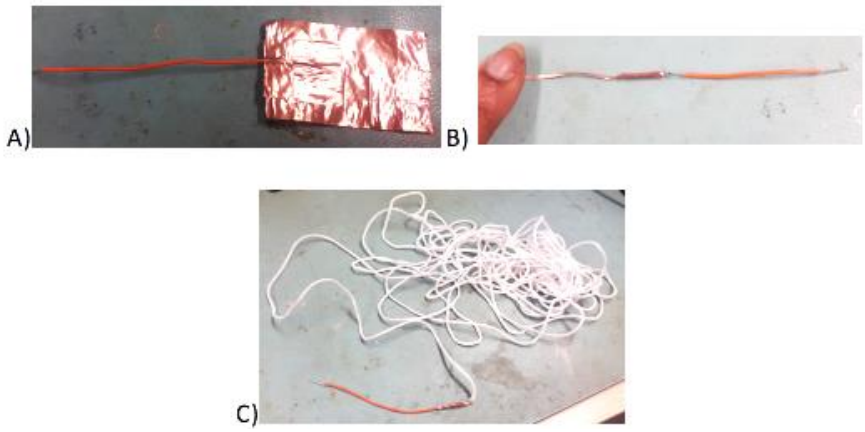

Figure 15 Timeline of sensing electrode development to trigger PCF8883 capacitive sensing output response

Figure 15 displays the iteration of the sensing electrode connected to the breadboard.
A) 6.0 cm x 4.0 cm copper tape sensing plate electrode attached to wire to connect to breadboard;
B) 5.0 cm x 0.1 cm copper-plated polyimide strip sensing plate electrode attached to wire;
C) Novel Electronic Textile Yarn with copper-plated polyimide strip/carrier yarn core, connected with wire.

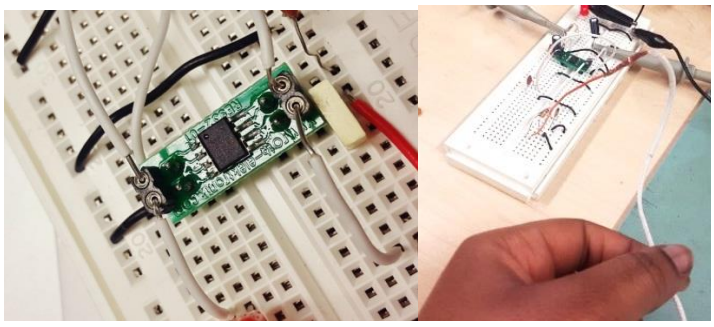

Figure 16 PCF8883 soldered onto SO8 Adaptor board for second prototype circuit (left), touch detection with a textile yarn electrode with copper-plated polyimide/carrier yarn core causing LED output response (right)

Proximity detection was not achieved during the first 9 months of research with the yarn electrode either due to breakage of the copper wires within the yarn or, the high resistance value of the copper wire materials used.

4.4.2. Second Prototype

The SOIC8-version of the PCF8883 chip (PCF8883T) used in the first prototype was exchanged for the WL-SCP version (PCF8883US) to be used in the second prototype. This changed the location of the pins which meant the circuit design of the second prototype would differ. The same chip technology is present in both the PCF8883T and PCF8883US, but the latter chip is smaller.
The PCF8883 can be purchased in SOIC8 form (PCF8883T) or WLCSP form (PCF8883US). THE PCF883T was used in the first prototype and was exchanged for the WLCSP version (PCF8883US) to be used in the second prototype.

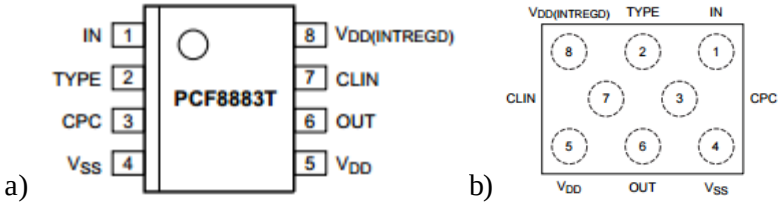

Figure 17 Comparison of top-view a) PCF8883T (SOIC8) and b) PCF8883US (WLCSP) chip pin layouts to denote change in circuit layout needed

This changed the location of the pins which meant the circuit design of the final prototype integrated into the yarn would differ from previous designs and the circuit design provided in the PCF8883 datasheet. The same chip technology is present in both the PCF8883T and PCF8883US, but the latter chip is smaller.

Symbol	Pin	Type	Description
IN	2	Analog input/output	sensor input
TYPE	3	input	pin OUT behaviour configuration input
CPC	4	Analog input/output	sensitivity setting
VSS	5	supply	ground supply voltage
VDD	6	supply	supply voltage
OUT	7	output	switch output
CLIN	8	Analog input/output	sampling rate setting
VDD(INTREGD)	8	supply	internal regulated supply voltage output

Table 2 Pin description of PCF8883T and PCF8883US

Consequently, the changed pin locations dictated the regions on the strip where the components would be placed on the copper-polyimide strip-shaped circuit. The datasheet of the capacitive proximity/touch PCF8883 chip suggested a sub-circuit to trigger an output response. For textile embedment, the suggested circuit was adapted to a strip-shape by a careful selection of component sizes that would fit into the strip as well as within the textile weaving machinery.

Previous literature had not featured the PCF8883US for e-textiles applications before, so it is indicated that a publication from this thesis (Ojuroye O. , Torah, Komolafe, & and Beeby, 2019) evidences the first time it is reported this use-case for this chip.

4.4.2.1 L-Edit Circuit Design Layout and Mask Creation

The imperative attribute of the novel capacitive proximity/touch circuit layouts presented in this thesis is its strip shape. Hence, the circuit must be of narrow shape with a uniform width whereby its length is always greater than its width. This is important so that the circuit can be woven into a textile yarn and fit within the insertion dimensions of an industrial textile weaving machine. Single-sided copper cladded polyimide film was used as the substrate of the novel sensory electronic circuit for textile yarn embedment. This was used in creating a single-sided flexible copper-plated circuit. The wires connecting the components to each other would be conductive copper tracks on the copper-polyimide film. Hence, the circuit design was influenced by the strip-shape of the circuit, the fact that tracks could not touch or cross over each other, and that track layout should be to minimise any stresses on the circuit when it would be bent, twisted, or flexed when integrated into a textile.

Compared to the first prototype, wires were replaced with copper tracks connected by the ends of solder pads which connect with terminals of surface-mounted electronic components. The only wires existing on the circuit would be at the two terminals either ends of the circuit to connect to a power supply. Additionally, ground and power rails common with rigid circuit boards were replaced with conductive solder pads either end of the strip for external battery connection.

The size of the solder pads for the PCF8883US was recommended by the data sheet, the solder pads for the passive components - capacitors, resistors, LEDs – were standard. They were drawn in L-Edit and saved as components in the software such that groups of components were positioned onto the circuit. As a result, the circuit was drawn in L-Edit in successive layers, the first layer being the size of the circuit represented as the pale grey background, then the conductive elements represented in blue, and the central PCF8883US chip had its size and solder pads grouped as separate entity to ensure it accurately aligned with the chip and fit on the circuit. The conductive tracks from the PCF8883US solder pads were positioned such that they were centred. This would ensure the strain upon the chip when the circuit was mechanically deformed was even. Furthermore, conductive tracks bend around the circuit at a 45° angle to counteract stress points otherwise occurring if the conductive track was at a 90° angle. Such rules were part of the FETT project methodology this research was to use and repeat. Multiple circuit designs could be implemented on the flexible circuit substrate but the component size and layout will determine the extent of mechanical deformation before functionality fails. In regard to the capacitive proximity/touch sensing circuit, three layouts were determined:

- Components were concentrated in the middle of the circuit;
- Components localised at one end of the circuit;

- Components evenly spread along the length of the circuit.

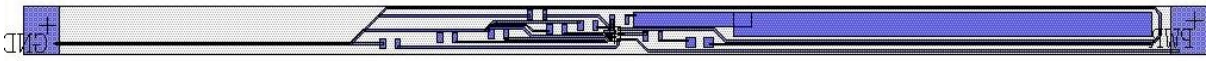

Figure 18 Components were concentrated in the middle of the circuit

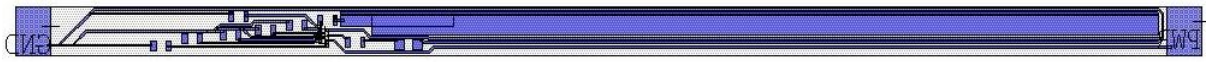

Figure 19 Components localised at one end of the circuit

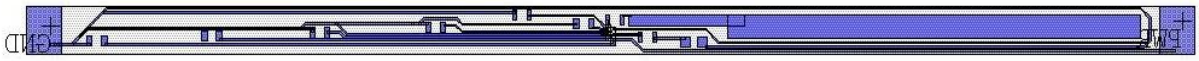

Figure 20 Components evenly spread along the length of the circuit.

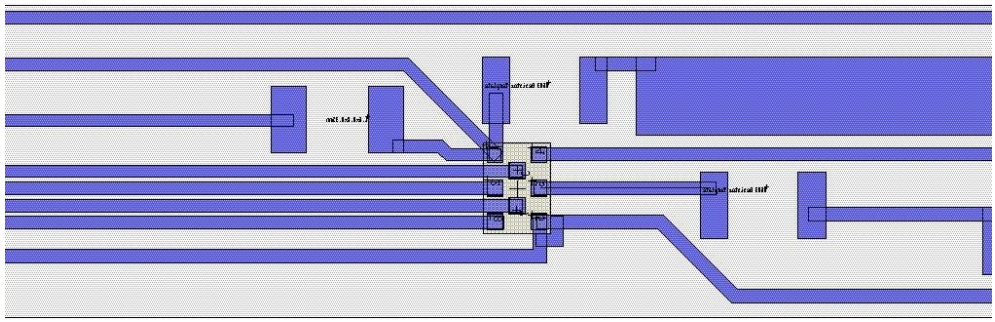

Figure 21 Close up of central PCF8883US solder pads and conductive tracks connected to other passive components, power, and ground

This produced the second prototype of a 4.0 mm (W) x 100.0 mm (L) dimension PCF8883US flexible copper-polyimide circuit - with conductive tracks and its 0603 metric package-sized components (i.e. 0.6 mm x 0.3 mm) fit within this size. Its circuit design was completed via L-Edit computer software such that the conductive elements include the dimensions of the surface-mount pads, the tracks, and the sensor plate/area. These elements have to fit within the dimensions of the strip-shaped circuit. Specific design guidelines resulted from this circuit layout development with intention of textile integration for wearable applications. Track widths ranged from 150 – 175 µm in order to fit the proximity/touch circuit design within a 4.0 mm x 100.0 mm strip-shaped circuit restriction. A minimum gap of 50 µm between the conductive tracks was featured in the circuit design layout.

These designs were duplicated and arranged in L-Edit, exported as a Gerber file to get the circuit design made. This circuit design was printed onto a positive, high-resolution acetate photomask by MCI Precision Screens Ltd. The acetate mask would be used in the photolithography part of the circuit fabrication process and was high-resolution to represent the 50 µm gap between the 150 - 175 µm-width tracks. The acetate mask acts as a stencil in the photolithography process, whereby the parts which are not black (Figure 22) will be where the copper is removed on the copper-polyimide sheet in a positive process.

.

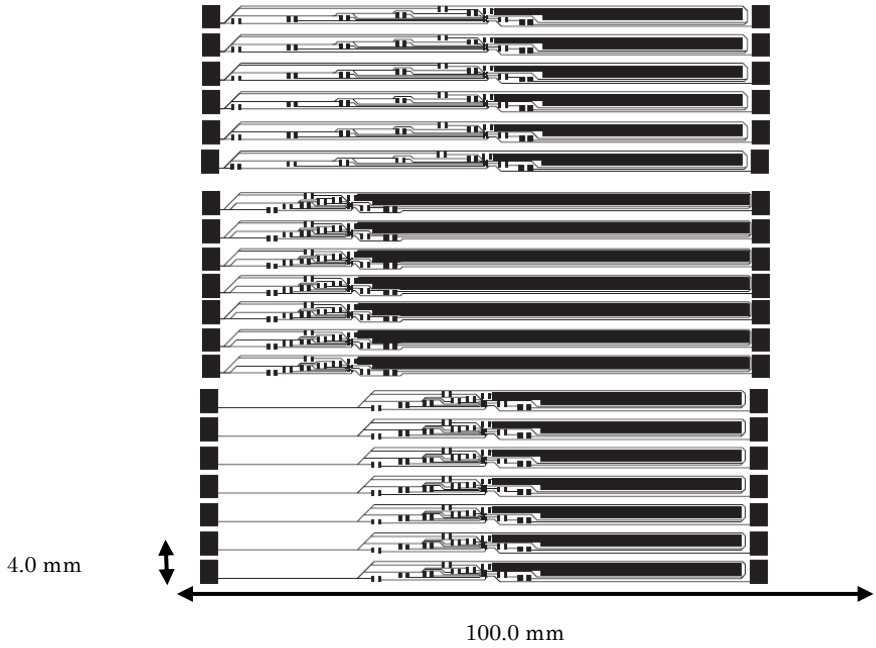

Figure 22 Picture of three circuit designs layouts for second prototype for the flexible circuit textile yarn embedment - resembles a strip shape.

The second circuit prototype of this circuit utilised the FETT fabrication process to make the first flexible copper-polyimide capacitive circuit. This methodology was used in consistency with how other circuits in the FETT project were developed. The full detail of the methodology used in this research is in Appendix D. A summary diagram of the methodology is below in Table 3.

Spin Coating	Thermal Curing	Photolithography	Photoresist Removal	Copper Etching	Dry and Chemical Treatment
Step 1) Silicon wafer deposited with even layer of with 81813 positive photoresist within Brewer Resist Spinner E4109.	Step 3) This silicon wafer structure undergoes a thermal cure for 3 minutes at 100ºC in the Thermo Scientific Heraeus Oven.	Step 4) Thermally cured silicon wafer structure with copper-polyimide is placed in EVG Photolithography aligner machine for UV exposure and operated using the EVG Mask Aligner software. The AK2070_AK recipe is used, with a 10 s UV exposure time.	Step 5) the UV -cured, copper-plated polyimide silicon wafer was placed into a 4:1 ratio of water to AZ 400K Developer solution in a flask for 20s.	Step 7) 1.1kg of Fine Etch Crystals, made by Universal Etch, were saturated with 4.5 L 20ºC water and mixed until all the crystals had dissolved.	Step 9) After the copper etch, the wafer is swirled in water and dried with nitrogen gas.
Step 2) Copper-polyimide sheet placed on spin-coated silicon wafer. Step 1 occurs again.			Step 6) Wafer was dried with nitrogen gas to remove the water and any residue.	Step 8) The solution and wafer were placed in a Mega Electronics PA104 etch tank for 8-15 mins copper-etching.	Step 10) Residue photoresist and crystal solution is removed with acetone.

Table 3 Summary of FETT Flexible Circuit Fabrication Methodology

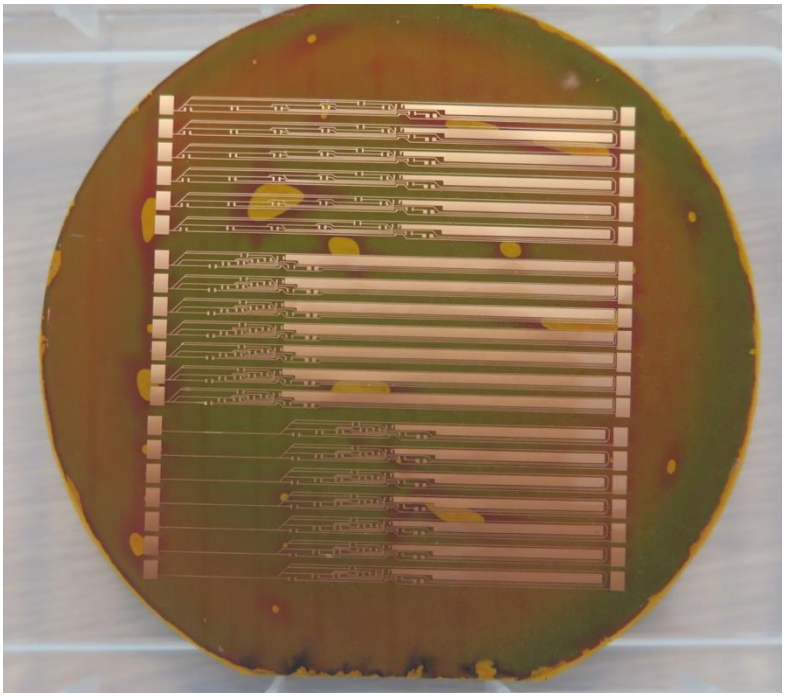

Figure 23 Photo of silicon wafer showing three circuit designs for the second circuit prototype. Circuit design has been transferred onto copper-plated polyimide silicon wafer through etching techniques – an industrially-used process.

All components but the PCF8883US were manually mounted by hand individually on all the designs. The PCF8883US was mounted onto the circuit using flip-chip bonding, and this is outlined in the next subchapter.

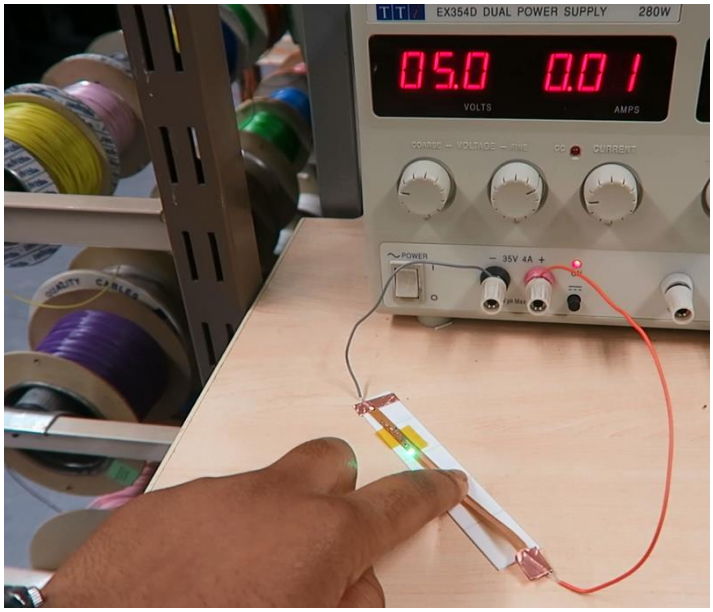

Figure 24 Photo of PCF8883US sensing circuit successfully detecting a touch trigger response

The following table summarises the component values of second prototype circuit to achieve touch detection[1]:

Pin	Symbol	Value
1	R_C	45 kΩ
1	R_F	6.8 kΩ
1	C_F	10 pF
2	-	GND
3	C_{CPC}	680 nF
4	-	GND
5	C_{VDD}	1 µF
6	R_{OUT}	14 7Ω
6	LED	3.8 V
7	C_{CLIN}	22 pF
8	$C_{VDD(INTREGD)}$	100 nF

Table 4 Table of component values of second circuit prototype with PCF8883US

4.5. Final Copper-Polyimide Self-Capacitance Proximity and Touch Sensing Circuit for E-Textile Integration

4.5.1 Component Values and Circuit Fabrication

The following table summarises the component values of the final prototype circuit to achieve proximity and touch detection through fabric[2]:

Pin	Symbol	Value
1	R_C	45.0 kΩ
1	R_F	6.8 kΩ
1	C_F	10.0 pF
2	-	-
3	C_{CPC}	2.2 µF
4	-	-

[1] Proximity detection was later enabled.

[2] Details on how these values are determined are in Chapter 7 of this thesis.

5	C_{VDD}	1.0 µF
6	R_{OUT}	147.0 Ω
6	Green LED	3.8 V
7	C_{CLIN}	82.0 pF
8	$C_{VDD(INTREGD)}$	100.0 nF

Table 5 Table of final component values of second circuit prototype with PCF8883US

Compared to the second prototype, the third and final prototype had 0402-sized components instead of 0603-size. Experiments detailed in 7.1.3.1 Experiment 1: External Electrode Length Influence on Proximity and Touch Detection Efficiency, 7.1.3.2 Experiment 2: External Electrode Width Influence on Proximity Detection Efficiency Experiment, and 7.1.3.3 Experiment 3: Maximising Electrode Sensing Area for Improved Proximity Detection resulted in the third and final prototype having:

- Thinner dimensions due to the smaller sized passive components and thinner tracks
- A shorter length as experiments revealed that the electrode that circuit did not have a large enough surface area to collect enough charge to trigger proximity and touch sensing.

As a result, the final prototype had its circuit design edited in L-Edit and fabricated in a method outlined in Appendix D. The result of those experiments presented the final circuit design. The circuit design was completed via L-Edit computer software such that the conductive elements include the dimensions of the surface-mount pads, the tracks, and the sensor plate/area. These elements have to fit within the dimensions of the strip-shaped circuit. The research produced a 3.0 mm (W) x 35.0 mm (L) size PCF8883US flexible copper-polyimide circuit - with conductive tracks and its 0402-metric package-sized components fit within this size. Specific design guidelines resulted from this circuit layout development with intention of textile integration for wearable applications.

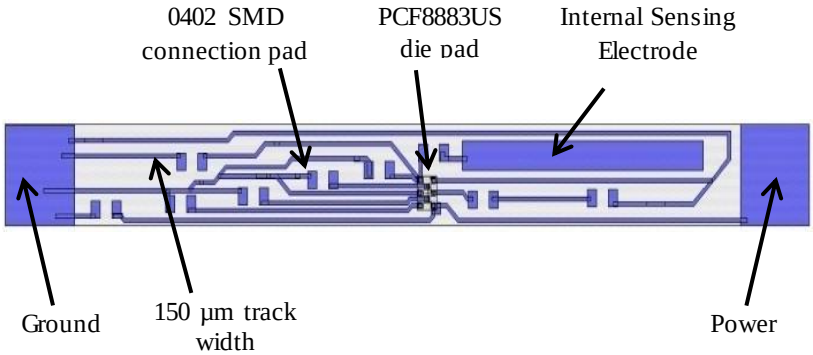

Figure 25 L-Edit circuit design of the final capacitive proximity and touch sensing circuit

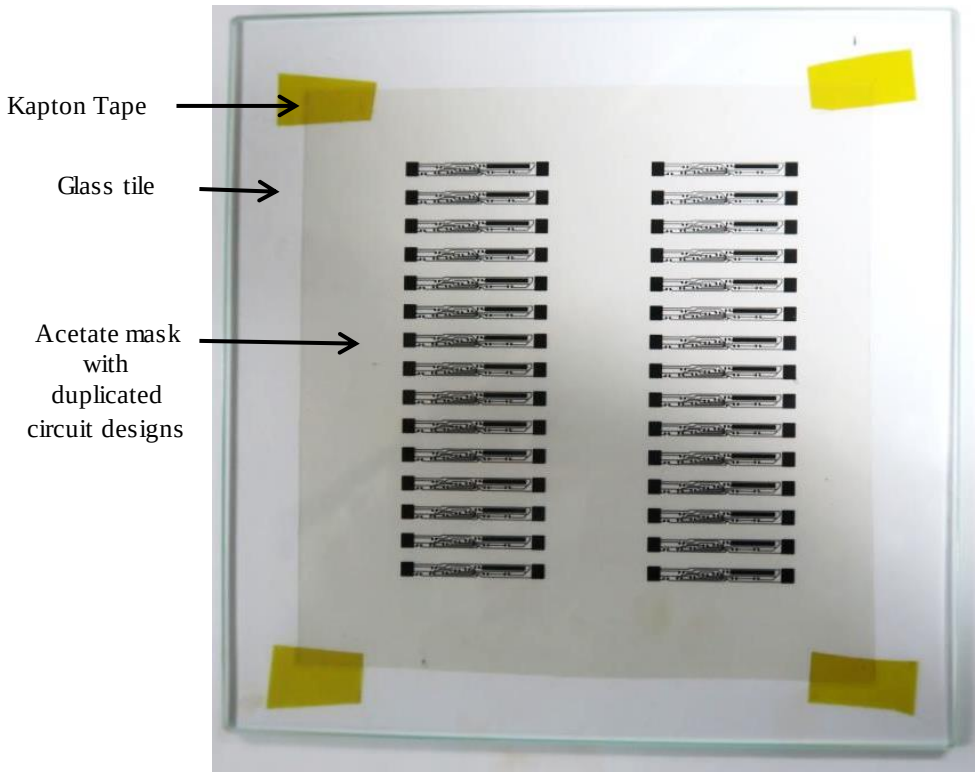

Figure 26 Updated Acetate mask for final circuit design for capacitive proximity and touch sensing circuit for e-textiles

The third and final prototype followed the same FETT project methodology as outlined in Table 3. The result of these steps created the copper-etched copper-polyimide film with the PCF8883US circuit design for textile integration, seen in Figure 27.

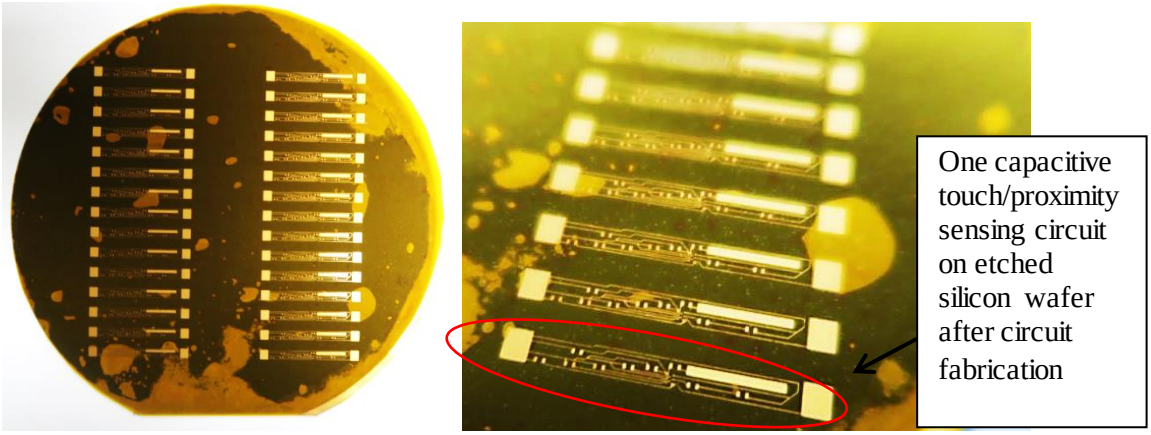

Figure 27 Etched copper-polyimide substrate on silicon wafer following FETT project fabrication methodology applied to capacitive proximity and touch sensing circuit design

The Flip Chip Bonding Machine "FINEPLACER® lambda", a Pick and Place machine, was used to handle the PCF8883US with a flip-chip bonding technique. This precise technique was chosen to accurately position its solder bumps onto the solder pads etched on the polyimide through the lithography and etching processes (Figure 28). Flip-chip assembly is one electrical interconnect method to place electronic components onto a circuit board. This technique places the electronic

component faced down on the substrate. The component would have conductive pads or solder bumps underneath it would make electrical contact with conductive regions on the circuit board. Just the PCF8883US was used with the pick and place machine presented in this thesis. The intention was to demonstrate the feasibility to using an industrially-used technique, commonly for PCB manufacturing, with the novel circuit process presented in this research.

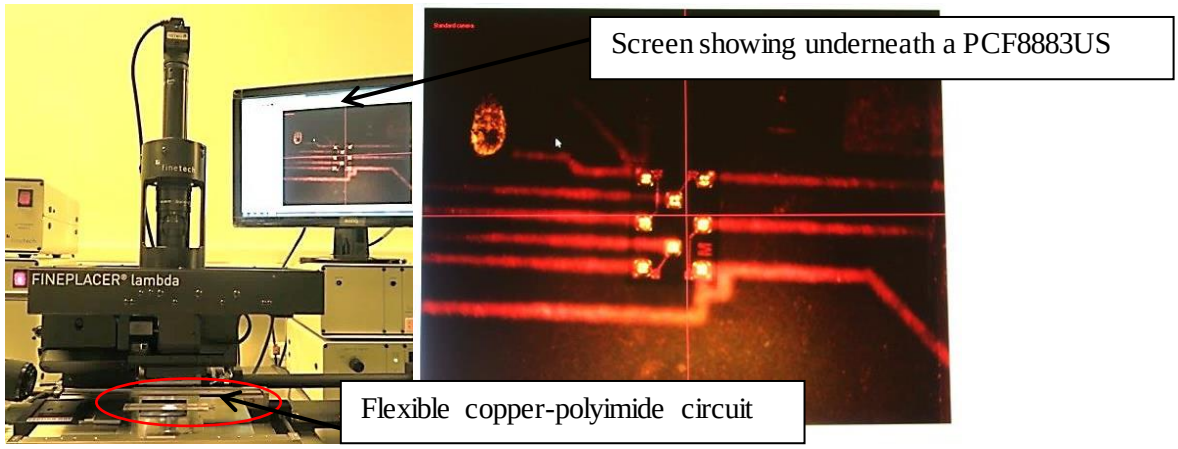

Figure 28 FINEPLACER (R) lambda Pick and Place machine displaying an underneath view of the PCF8883US capacitive proximity and touch sensing chip before mounting on to circuit (left) aligning it with copper etched solder pads on circuit (right)

The PCF8883US has 8 connections made from solder bumps unlike the other surface mount components on the second prototype circuit. Therefore, a flip chip bonding machine was used to position and secure the chip precisely onto the substrate. FineTech computer software was used to operate the pick and place machine. An unpopulated polyimide circuit strip was secured onto an alumina tile with polyimide tape along its length and width. This was to keep the circuit flat to provide an even surface to position and solder the PCF8883US chip and additionally to prevent the circuit from curling during the heating process. The taped copper-polyimide circuit was then placed on the pick and place handling plate. To ensure the alumina tile stayed in position throughout the pick and place process and bottom vacuum underneath the tile was activated. Furthermore, flux was applied on the solder pads for the PCF8883US to remove any oils or dirt from the surface and promote better adhesion during the solder stage.

The PCF8883US chip was positioned with tweezers on top of its solder pads on the etched circuit on the polyimide strip. Levers attached to the Fineplacer were used to lower and position the vacuum head, with a 1.0 mm diameter gap, on top of the PCF8883US. Then, the vacuum head is slowly raised for viewing inspection of the chip. The viewing angle of the camera was underneath the PCF8883US. Once the PCF8883US chip is picked up, alignment of its solder balls and the solder pads for the chip that reside on the polyimide circuit trace can occur using the FineTech software. A camera located above and to the side of the plate could be controlled to view the circuit and the chip at different focuses and resolutions to allow accurate solder balls and solder pad alignment. Manual

alignment using the flip chip bonding machinery can be completed to ensure the solder balls would be positioned on top of the solder pads when subsequently lowered back onto the substrate.

The vacuum holding plate was lowered such that the PCF8883US solder bumps underneath the chip lightly touched the solder pads; pressure upon the solder pads were to be minimised to prevent the solder balls spreading outwards during melting which could cause a short circuit. Adhesion of the aligned PCF8883US to the copper-polyimide circuit involves heating on the chip surface and underneath the polyimide substrate simultaneously. Another vacuum was activated underneath the alumina tile to hold its position in place one alignment with the PCF8883US solder balls were achieved. Then, the heating plate below the alumina tile was programmed via FineTech software to start heating from a 40 °C temperature at a 3.0 K/s rate to a temperature just below the solder balls' melting point. This was 240 °C, and this temperature was stabilised for 35 s. During these 35 s the plate holding the PCF8883US with a vacuum was gently raised and lowered to vary the bonding pressure of the PCF8883US to the polyimide solder pads as the solder balls melted. The temperature was lowered back to 40 °C at the same rate (3 K/s) to cool the solder down. Simultaneously, the CCH (holding plate) had a starting temperature of 40 °C, which was raised to and stabilised at 260 °C for 40 s, and lowered back to 40 °C. Once these processes were completed, the copper-polyimide substrate and PCF8883US made contact for 30 s without heat and cooling before the holding plate was raised to leave the PCF8883US chip soldered and secured onto the polyimide circuit surface. This process was repeated for all other circuits under development, and one circuit went through this process at any time.

Lead-free solder paste by BLT and reflow oven techniques was used to adhere the surface mount components on the remaining solder pads following the pick and place stage. The lead-free solder paste used was provided me as one of the FETT material resources. Therefore, for consistency among all the circuits created from this group, the same lead-free solder paste was used. Flux was applied to the associated solder pads for the eight surface mount components to be soldered to complete the circuit. This was the same flux used in the pick and place stage. A needle was used to apply the solder paste in the middle of solder pad with the intention that the weight of the surface mount components would cause the lead-free solder paste to spread to some degree. The surface mount components were then positioned, aligned, and straightened onto the solder pads with tweezers. On the last stage, lead-free solder paste was then applied to upper conductive region of the solder pads and around the sides to connect to the solder paste underneath the chips. This was to increase the bondage of the chip to the circuit to consequently increase the amount of lead-free solder paste interfacing with the chip to promote improve reflow soldering to the copper-polyimide circuit.

The FT05 batch reflow oven by C.I.F was used to heat and eventually melt the solder paste. The C.I.F FT05 reflow oven uses convection heating to solder electronics. In the pre-heating stage, the starting reflow oven temperature of 90 °C was set to rise to 100 °C. This 100 °C temperature was activated, risen, and stabilised at 250 °C for approximately 5 minutes. Once the polyimide circuit(s)

with solder paste and SMDs on its surface was placed in the middle of its oven tray and the tray was locked. In the reflow stage, 250 °C was applied to the polyimide circuit for an allotted time of 1 min until the temperature was decreased back to 100 °C. In this period, the solder paste melts forming solder joints between the SMDs and the copper-etched polyimide circuit substrate. When returned to 100 °C the extraction fan was turned on to cool down and solidify the molten lead-free solder paste. Finally, once the extraction fan has completed its cool down function, the polyimide circuit could be removed from the oven tray to now have SMD components secured onto its surface. With all components mounted, the third prototype of the capacitive proximity and touch sensing circuit was developed using the FETT project platform technology. This was 35.0 mm (length) x 3.0 mm (width) dimensions (Figure 29).

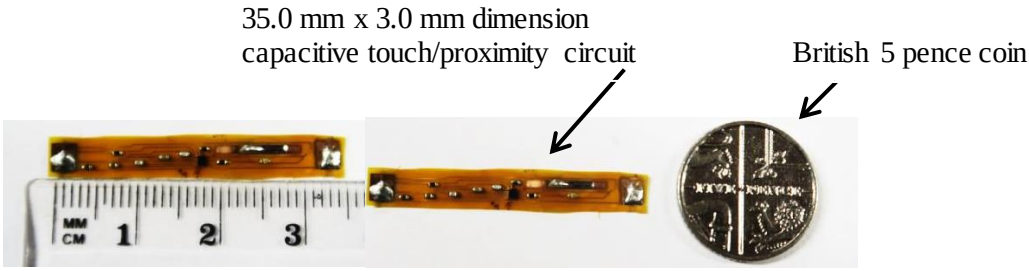

Figure 29 Photos of final capacitive proximity and touch sensing circuit for electronic textile applications for weaving and knitting showing its 35.0 mm length (left) and its 3.0 mm width with its size compared to a 5 pence British coin (right)

So that this circuit could still bend, flex, and twist when embedded into a textile, this research had established the need – through literature review – of a flexible, elastomeric conformal coating. This coating also had to be hydrophobic, and aqueous-resistant to solutions used in the textile washing process so the resultant e-textile could be used like a traditional textile. The additional of this conformal coating is part of this Ph. D novel research contribution and its addition to the FETT Circuit Fabrication methodology. How this hydrophobic conformal coating was chosen is reviewed in the next chapter.

4.5.2 Functionality Test

Using a DSO3062A digital storage oscilloscope, it is possible to get a time response curve (TRC) to confirm proximity and touch responsiveness of chip. This is possible due to the R_F resistor and C_F capacitor present on pin 1 of the circuit, and the capacitor formed from the sensing electrode and the human hand to form parallel plates. Each circuit under test was given a 4.5 V supply voltage and 3.0 mA supply current for operation via power supply. The oscilloscope was used to measure the self-capacitance of the electrode – comprised of the internal and external copper electrode. This was completed by using an X10 probe to hook onto a wire connected to the external electrode and attaching its clip to the circuit's ground connection. Operating the circuit produced a TRC curve as an oscilloscope trace. When a human hand or finger is moved above the self-capacitance electrode, this

changes the capacitance enough such that you can quantify how long it takes for the voltage to drop as it takes longer for the capacitor formed to discharge. The peak charging voltage, rise time (charging time), and fall time (discharging time) of the TRC curve – corresponding to C_F - was collected by the oscilloscope. The peak voltage of the TRC curve is the voltage the capacitor is charged to. As the circuit under test only had one metal electrode and the other electrode was the human hand, the capacitance of the sensor plate C_{SENS} from equation 2 could be written as:

$$\text{Time constant, } T = R_{Forward} \times C_{SENS} \qquad (3)$$

Equation 3 Time constant equation using capacitance of sensing electrode used by capacitive proximity and touch sensing chip

The oscilloscope was used to calculate C_F, connected to the sensing plate, full rising and falling time. The oscilloscope showed five time constants for C_{SENS} to fully charge (rise) and discharge (fall). The specific values can be selected and viewed by the oscilloscope when the TRC sawtooth waveform appears on the screen (Figure 30).

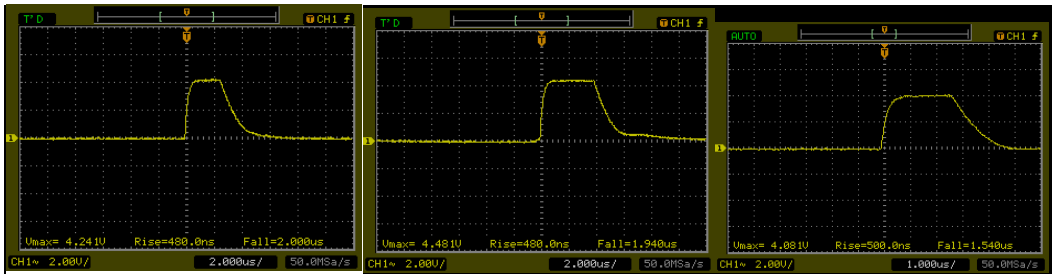

Figure 30 TRC sawtooth waveforms observed with oscilloscope to show functioning capacitive proximity and touch sensing circuit when is not triggered (left), senses proximity (middle), and touch (right) of a human hand is detected

Therefore, the time constants of the rise and fall times were retrieved as:

$$\text{Rise time} = T_R = 5T \qquad (4)$$

Equation 4 Total charge time of self-capacitance sensing electrode, also called rise time

$$\text{Fall Time} = T_F = 5T \qquad (5)$$

Equation 5 Total discharge time of self-capacitance sensing electrode, also called fall time

The circuit was tested for functionality by evaluating whether it could detect both 2.0 cm proximity distance and touch of a human finger. This functionality test is further detailed and demonstrated in subchapters 7.3 Underwater Experiment Evaluating Durability of PDMS Packaged Self-Capacitive Proximity and Touch Sensing Circuits, and 7.4 Washing Experiment Evaluating Robustness of Integrated Conformal PDMS Packaged Capacitive Proximity and Touch Sensing E-Textile Circuit .

4.6 Conclusions

This chapter has detailed the system design requirements, circuit design, fabrication, and testing of the capacitive proximity and touch sensing circuits. System design requirements were focused on developing a functional sensing circuit that can respond to a human hand when it is embedded into a textile. For this, the circuit had to be designed such that was thin (5 mm width or less) to fit inside the core of the yarn using the automated knitting machine and also to be handled by the manual looming weaving machine – the two e-textile demonstrator formats that would be made by this research. The selection of the IC chip that could perform capacitive and proximity section was then outlined in this thesis, comparing different IC chips available at the time for their technical specifications, dimensions, and sensing capabilities. The PCF8883 IC chip by NXP Semiconductor was chosen – primarily as it had the smallest dimensions, its customisable sensing ability, and dual functionality operation. Additionally, compared to other IC chips, it came in SO18 and SMD format, allowing for different prototypes to be developed and testing. The circuit in this research was made from a 25 µm thick polyimide film substrate that had an 18 µm copper-annealed layer, fabricated by GTS Flexible Ltd. The circuit design for the PCF8883US, SMD, was designed in L-Edit to fit within the smallest width possible without tracks touching and without the possibility of tracks crossing over each other. To make the circuit as thin as possible, track widths were limited to 175 µm maximum width, and components were 0402 sized. Design rules created in the FETT project were followed in the design of the circuit, such as reducing mechanical strain on the circuit by having 45° turns for the tracks, and aligning the bottom of the component solder pads to the tracks. The finished design was then duplicated and arranged in L-Edit to the width and length dimensions of a silicon wafer that would be used in the circuit fabrication process. Fabricating the circuit adhered to the rules outlined in the FETT project. Its methodology – spin coating, thermal cure, photolithography, resist removal, and copper etching – was applied to the capacitive proximity and touch sensing circuit. As this had not been done before, this would support the idea of the FETT Project e-textile circuit manufacturing methodology as a potential platform technology. The methodology successfully created the capacitive proximity and touch sensing circuit, verified by the functionality test conducted before and after textile integration. Components were mounted onto the circuit using semi-automated and manual process. Ideally, this step can be completed autonomously using an industrial pick and place machine. The FinePlacer pick and place machine was used to position and thermally cure the PCF8883US to accurately align its 8 solder bumps to its associated solder pads on the fabricated copper-polyimide circuit. It was realised that for the PCF8883US to be positioned flat onto the circuit, no neighbouring components must be present. If this occurred, the PCF8883US' solder bumps would thermally-cure unevenly creating a structural weak point. As a result, the PCF8883US SMD had to be secured onto the circuit first. This was to ensure the vacuum head of the pick and place machine would not be obstructed by surrounding components. By doing so, the PCF8883US was completely level when secured onto the substrate. Other components were successfully adhered onto the circuit using a

reflow oven. This step was originally part of the FETT manufacturing method but this research successfully showed reliability and consistent melting and curing of the solder to create the capacitive proximity and touch sensing circuits. These circuits were then to be encapsulated in PDMS, detailed in 5.1.1.1, and before integrating them into a textile via knitting and weaving techniques. The circuits still functioned after both processes, showing they can survive the knitting and weaving process using industrially-used machinery. Sources of failure for these textile integration processes were difficult to determine once the circuit had been embedded. This was because the circuit was irreversibly integrated into the textile, and to determine how it failed would require detaching the circuit for inspection. Nevertheless, this research did observe that during the knitting and weaving process causes of failure could be wires snapping or circuits experiencing compression.

Chapter 5: Systematically Tailoring Polydimethylsiloxane for an Electronic Packaging Substrate for E-Textile Applications

This chapter details how a hydrophobic packaging substrate was selected for the touch and proximity flexible circuits and experiments measuring the resulting robustness in underwater and washing machine circumstances. It consists of published and peer-reviewed results from IEEE (Ojuroye, Torah, & Beeby, 2018) and Journal of Microsystem Technologies (Ojuroye, Torah, & Beeby, 2019) in subchapters 5.2 and 5.3.

5.1 Selecting a Suitable Packaging Layer for Washable and Flexible Capacitive Proximity and Touch Sensing E-Textile Circuit

Electronic textiles (e-textiles) enhance traditional fabrics with electronic functionality. When embedded into textiles, flexible electronic circuits need to have reliable functionality but also survive within a textile once it has been integrated. For this, electronic microsystems would be expected by consumers and manufacturers to not alter the typical characteristics the textile inherently has – such as its washability, durability, and manufacturability. Therefore, the choice of packaging substrate for microsystems in a textile must also be hydrophobic and offer minimal expansion when washed; ensuring electronics are undetectable when the textile is handled or cleaned.
To select a packaging substrate, literature revealed that extensive work on comparing packaging substrates had already been conducted. However, a comparison for a packaging substrate for e-textile applications had not been conducted extensively. Yet, there was enough published material to not warrant an experimental comparison of substrates but instead comparing the characteristics of the packaging substrates and establishing the requirements of the packing substrate for the FETT project and the specific capacitive proximity and touch sensing circuit was completed.

As the FETT project is using a flexible circuit substrate, it is therefore important that the chosen packaging substrate had the following characteristics for e-textile applications and to be useful to the FETT project:

- Be flexible to still allow the copper-polyimide circuit to contort – bend, flex, twist
- to be hydrophobic and chemical resistant to survive the washing process that will likely include detergent and fabric conditioner
- to have a low dielectric constant to have minimal detrimental effects on the chip as it senses with capacitance
- to be transparent to enable the LED on the circuit to shine through the packaging and for the light to be visible through the fabric for visual feedback of functionality

- to withstand high temperatures to allow the resulting e-textile to be washed at high temperatures
- to be elastomeric for the circuit to be protected from mechanical deformations further, to allow the packaging substrate to act as a buffer
- to be compatible with the human skin i.e. non-toxic if the circuit had to be removed
- to be low cost to manufacture for industrial feasibility
- to be manufactured that it is industrially scalable

Following this, an extensive table was created covering all the packaging materials that could be used to protect the flexible circuit developed in this Ph.D and be suitable for e-textile applications. This table is in Appendix A: Table Comparison of Circuit Packaging Substrates for Ph.D System Design Specifications. Each packaging material was compared for the characteristics listed above and more criterions to make a decision. As a result of this table, it was decided that Parylene and Polydimethylsiloxane (PDMS) were the most suitable packaging substrates choices to be directly compared for this thesis.

5.1.1 Polydimethylsiloxane vs Parylene

Achieving low-cost fabrication of elastomeric circuits appears to be challenging but freeform manufacturing could be a solution. An interest in these flexible, stretchable, soft circuits has begun to affect the development of flexible circuits for textile applications in the pursuit of electronic textiles - that can survive mechanical deformations such as strain, crimpling, bending, and stretching (Hu, et al., 2016). However, an elastomeric substrate containing a circuit *within it* - that can reside in the core of a yarn – has yet to be achieved.

5.1.1.1 Polydimethylsiloxane (PDMS) Circuit Packaging Methodology

Polydimethylsiloxane (PDMS) can be applied as an elastomeric substrate to create flexible and stretchable electronics – see Literature Review. PDMS is a polymer used in several areas of bioengineering such as microfluidics (Fujii, 2002) and in-situ microelectronics (Mark & Pan, 1982). It is fabricated as a 2-part silicone elastomer where its chemical and mechanical properties are altered via the mixing ratio of base agent to curing agent. Sylgard 184 Silicone Elastomer, from Dow Corning, recommends a 10:1 (base to curing agent) mixing ratio to be well-suited to electrical/electronic applications (Jeong, et al., 2015). 10:1 is the most commonly used mixing ratio in electronics and bioelectronic applications (Jeong, et al., 2015). Sylgard 184 was evaluated for its suitability before selecting it in this Ph. D thesis – see Appendix B: Table Comparison of Polydimethylsiloxane Products for Ph.D System Design Specifications. Changing the cross-linking density of the repeating methyl -CH_3- groups (Figure 31) can control the extent of PDMS' surface hydrophobicity (Armani, Liu, & Aluru, 1999). Literature reports microsystems integrated into textiles but not packaging the entire system. Instead, only MEMS and silicon chips are glob-topped and not the entire circuit

(Cherenack, Zysset, Kinkeldei, Münzenrieder, & Tröster, 2010), microsystems are external to the textile due to circuit size and rigidity (Zysset C. , Kinkeldei, Munzenrieder, Cherenack, & Troster, 2012), and the packaging substrates used are at times inflexible and offer insufficient encapsulation to protect the electronics from water and solvents. PDMS is porous and permeable to different micromolecules found in solvents (Toepke & Beebe, 2006). Hence, PDMS swelling can occur due to aqueous or gaseous environments permeating the substrate and/or chemical attacks of organic alkaline or acidic solvents (Dam, 2006) which could be the case during washing conditions.

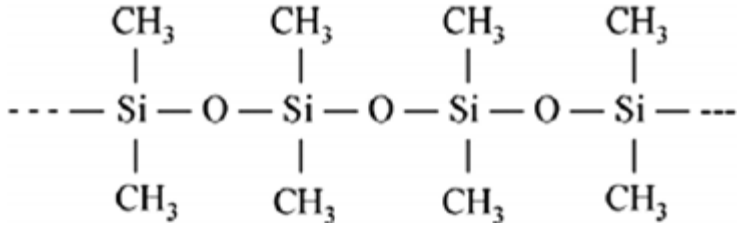

Figure 31 Chemical molecular structure of Polydimethylsiloxane (PDMS) *(Morent, et al., 2007)*

By changing the PDMS fabrication, it is possible to select the mixing ratio to offer best waterproof and swell-limiting properties. Thus, this research preliminarily explored the use of PDMS as a hydrophobic encapsulate for embedding flexible electronic sensors into a woven textile. The concept of using PDMS to package the copper-polyimide circuit originated with a cylindrical shape. The shape was intended to mimic the shape inside the core of the yarn (Figure 12) such that no sharp edges of the circuit would be detectable through the yarn. This was later changed to a conformal coating of PDMS, allowing the same circuit to be integrated into a fabric swatch via weaving (Figure 13). Instead, filler yarns would surround the encapsulated circuit in the core of a yarn to give the characteristic cylindrical shape. The criteria of this PDMS and its fabrication were:

- Transparent to allow optical light to pass through (LED);
- Encapsulate entire on the circuit before textile fibre outer layer;
- Provide hydrophobic layer to enable washing;
- Be flexible, twistable, and bendable

The conformal PDMS packaging substrate was formed by fabricating the PDMS in a 3D printed TangoBlack Plus material mould. The Object Connex 3000 3D printer was used to make this mould. TangoBlack Plus material is malleable, bendable, and is non-stick with PDMS meaning that when cured the PDMS can be easily removed from the mould. The benefits of PDMS on the circuit would be exemplified, but with a conformal coating the circuit and packaging would use less space compared to the textile and filler yarns in the channel/pockets it resides in during the textile integration process. Hence, making the textile soft, lighter, and make the circuit even more undetectable. The elasticity of PDMS makes it possible to apply as a conformal layer on a copper-polyimide circuit with components already soldered upon it. Additionally, as PDMS is homogenous and self-levelling it enables for an even coat around the circuit when curing.

Glass beakers acting as containers for the circuits were first put in a vacuum chamber for 30 minutes that was filled with a vaporised Trichlorosilane (C2H,2H perfluro-) solution that would deposit a hydrophobic conformal layer on all exposed areas. This made the moulds non-stick and allows for easier removal of the PDMS cylindrical structures once cured. Aforementioned, the PDMS substance is commonly developed by a 10:1 ratio of monomer (solid granules form of PDMS) and its curing agent. These two chemicals were mixed together in a beaker until a transparent, viscous substance was formed. This would then be layered into the channel of the moulds using a pipette. Parafilm was used to tape the silk-encapsulated copper wires connected to the populated copper-polyimide circuit together. The 3D-printed TangoBlack Plus mould was then placed on top of this parafilm to act as a weight during this dip-coat-suspension method (Figure 32).

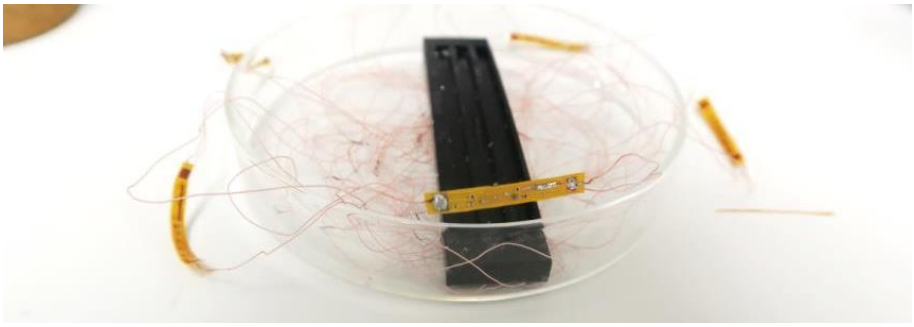

Figure 32 3D printed TangoBlack Plus mould used as weight to suspend copper-polyimide capacitive circuit strips before PDMS conformal coating

The following method used to complete the conformal coating is a form of dip-coating but this research took an additional suspension step to this technique. To start, a pipette was used to deposit a coat uncured PDMS at the bottom of a 3.7 mm width channel, part of the of the 3D-printed TangoBlack Plus mould which would contain the circuit. Then, tweezers were used to lower the flexible and populated copper-polyimide circuit onto this 3D-printed TangoBlack Plus channel. This immersed the entire circuit in the PDMS to produce a thin conformal layer. The tweezers were then used to flatten the copper-polyimide circuit that would otherwise bend due to being positioned within the channel or due to the viscous layer of PDMS underneath it. A pipette was then used again to apply PDMS on top of the circuit (Figure 33) – this includes the central PCF8883US, the surface mount passive components and the solder pads to power and ground with silk-encapsulated copper wires attached.

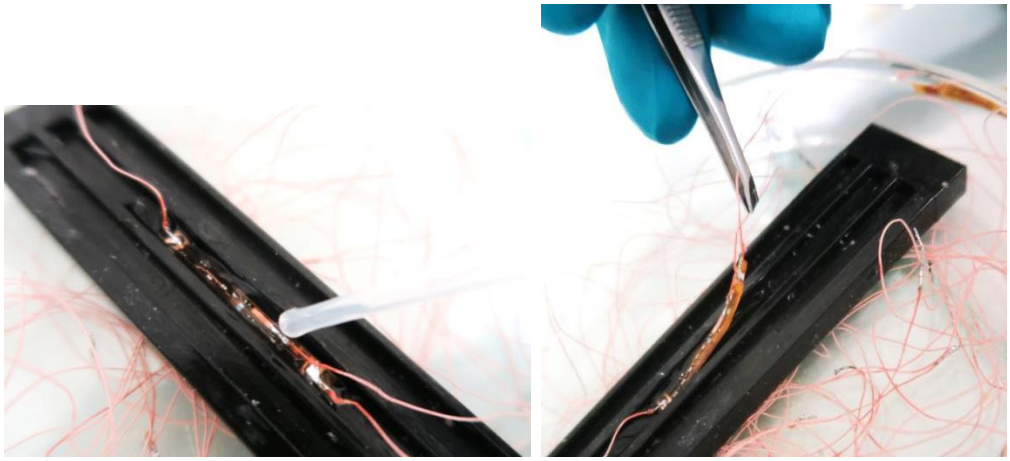

Figure 33 Pipette used to apply a layer of uncured PDMS on the circuit ensuring all surfaces are covered before using tweezers to lift the PDMS-coated circuit out for suspension

Once the circuit was completely immersed in PDMS, tweezers was used to lift the circuit from the PDMS-filled channel in the 3D-printed TangoBlack Plus mould. It was then suspended in the air due to the tautness of the Parafilm tape and the slight rigidity of the silk-encapsulated wires. The suspended circuit could be suspended above the 3D printed mould but still within the diameter of the glass petri dish which would be used as a surface during the thermal curing process. Lastly, the moulds with PDMS and the circuits were placed in a thermal oven at 70 ^{O}C for 1 hour 30 minutes, or its 140 ^{O}C for 10 minute fabrication equivalent - according to the manufacture datasheet. This created a thin, conformal coating of 20:1 PDMS packaging the entire circuit (Figure 34). Its thickness was determined as a 40.3 µm average, as shown in subchapter 7.3.1.

.

Figure 34 Cured PDMS conformal packaging on capacitive proximity and touch sensing circuit

The circuits had silk-copper wires soldered onto the power, ground, and electrode pads before they were to be given a hydrophobic conformal coating. This produced a hydrophobic, flexible, 40.3 µm averaged-thick packaging tailored for electronic textile applications. This produced the packaged circuit before they were able to be integrated into a textile via weaving or knitting.

Figure 35 Photo of lifted, thin, and translucent PDMS-conformal packaged proximity and touch sensing circuit with silk-encapsulated wires

5.1.1.2 Parylene-C Circuit Packaging Methodology

Parylene is a part of the semi-crystalline thermoplastic polymer group called poly(para-xyxylenes) and three forms of Parylene - N, C, and D – are used commercially (Rodger, Li, Weiland, Humayun, & Tai, 2013). Parylene is used for mechanical and moisture barriers for electronic devices both in academia and industry (Kang, Matsuki, & Tai, 2015). Its pore-sealing abilities offer impenetrable resistance against liquids, corrosive etchants, and chemicals which this research believes makes the possibility of making the resulting fabric made from electronic circuit yarns machine-washable. Whereas Parylene is commonly used to provide coatings of electronic devices in-situ of biological bodies (Chang, Liu, Kang, & Tai, 2013), this thesis research suggests another application. That Parylene could be suitable undetectable and thin packaging layer for electronic circuits embedded into textiles.

Conventionally, Parylene is a polymer used in biomedical and bioengineering industries (Lu, Liu, & Tai, Ultrathin parylene-C semipermeable membranes for biomedical applications, 2011) to ensure chemically-inert and hydrophobic encapsulation for electronic implantation within the body. It provides a flexible coating layer for microimplants (Feili, Schuettler, Doerge, Kammer, Hoffmann, & Stieglitz, 2006) , (Stieglitz, Kammer, Koch, Wien, & Robitzki, 2002). Bioelectronic devices such as neural prostheses (Hassler, von Metzen, Ruther, & Stieglitz, 2010) and cochlear implants (Johnson & Wise, 2015), have been encapsulated with Parylene to enable functionality when in-situ without contaminating the body. In addition to benefiting medical devices, Parylene is considered as a suitable conformal substrate for electronic circuity and sensors to provide environmental and dielectric insulation (Noordegraaf, 1996). Although silicone can be used to encapsulate biomedical devices or to coat electronic circuits, they are usually given subsequent parylene layers to reduce friction and increase the strain tolerance of the device over a period of time (Salem, Wilson, Neeb, Delk, & Cleves, 2009). Parylene's barrier effects against oxygen and water (Yoon, et al., 2006) on flexible substrates and flexible circuits have been explored at micron level in literature. Literature has reported Parylene to be a suitable substance to seal electronic devices - as an underlying layer, overlying layer, or both in a sandwich structure (Rodger, Li, Weiland, Humayun, & Tai, 2013). In order to reduce performance degradation and increase packaging reliability, Parylene has been a polymer of choice to provide buffer electronic packaging whilst retaining the lightness and small dimensions of microelectronics such as microelectronic mechanical systems (MEMS) (Lee & Cho, 2005). Of the

three forms of Parylene - Parylene N and Parylene D, Parylene C – Parylene C is the most hydrophobic, had the best pin-hole free conformability, and can survive elongation without breaking compared to all other Parylene types, polyimide (Stieglitz, Haberer, Lau, & Goertz, 2004), and silicone (Hoogerwerf & Wise, 1994) encapsulation options. This was important for package properties needed for the flexible circuits that would be integrated into a textile and subsequently washed. Furthermore, Parylene C is the most commonly used Parylene polymer to be used in hybrid manufacturing (Karnfelt, Tegnander, Rudnicki, Starski, & Emrich, 2006) for the reasons outlined thus far. Therefore, so that this research is compatible with commercial manufacturing processes, applying Parylene C as an encapsulation layer could be an industrially scalable process (Rodger, Weiland, Humayun, & Tai, 2005). Hence, preliminary explorations began in this research to evaluate whether Parylene-C would be an effective encapsulation layer for textile yarn- embedded circuits. As this polymer is transparent (Lu, Lin, Liu, Lee, & Tai, 2011), with a low dielectric value (1.63) relative to air (1.0059), it has minimal detrimental effects to the optical luminosity of the LED featured on the circuit to show proximity/touch detection (Lu, Lin, Liu, Lee, & Tai, 2011).

This research used a vapour deposition process of Parylene C on the copper-polyimide flexible circuits developed by William F. Gorham. The process was completed using the PDS Labcoater 2010 machine to deposit a conformal layer of Parylene C on the capacitive sensory copper-polyimide circuit. Proximity/touch sensing circuits were placed in a Parylene vaporisation chamber for even single-sided conformal coating over the entire circuit surfaces.

To produce the Parylene C conformal coating, 0.5 g of Parylene-C dimer, pure solid granules, was placed in the furnace of the PDS Labcoater 2010 machine where it was evaporated once 150ºC was reached. 0.5 g of dimer corresponds to a 500 nm thickness of deposited Parylene C. This thickness is the minimum quantity to provide sufficient barrier against humidity, chemicals, and other liquids to make the circuit hydrophobic yet still lightweight. The evaporated dimer takes part in a pyrolysis process when the furnace temperature lowers to -650-700 ^{O}C causing the Parylene C dimer compound to split into monomers. The residue monomers to be used in the deposition process are collected in the cold trap. At room temperature, the monomers deposit on the flexible copper-polyimide circuit within the vacuum chamber as part of the polymerisation process of the Gorham method. The polymerisation process is the pinhole-free conformal coating stage. The granules were then heated in a furnace at a 690 ºC temperature before the sublimation process occurs at 135ºC to give a permanent, waterproof, and chemically resistance layer to all exposed surfaces within the chamber.

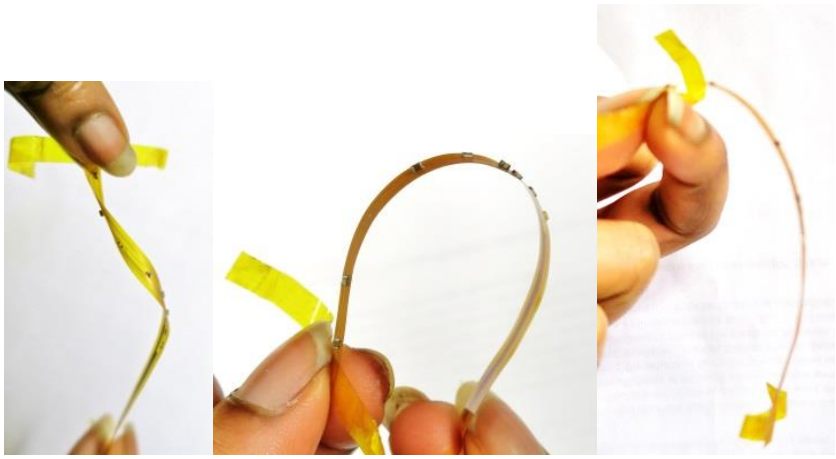

Figure 36 Photos of Parylene C encapsulated circuit that has mechanical deformative properties. Polyimide tape, attached to the circuit for temporary handling, has been highlighted. Left: twisting; middle: flexing/bending right: draping.

Polyimide tape covered the conductive solder pads either end of the circuit so they were not insulated and to enable power to be applied post-vaporisation. The thickness was of Parylene C was confirmed with the Veeco Dektak-8 profilometer that measured using a sensory stylus the Parylene C thickness deposited on a glass tile put in the chamber whilst the encapsulation process occurred. The glass tile was used as a reference, a method recommended by manufacturers of the machine. The profiolmeter stylus was autonomously dragged once over the layer with a 3 mg force, travelling 20 µm/s over a length of 277 µm. A 600 nm thick layer of Parylene was deposited via vaporisation on the capacitive proximity/touch sensing circuit over a 5-hour application process.

In summary, comparing Parylene C and Polydimethylsiloxane (PDMS), PDMS was the only substrate found that met all the criteria. Or, it superseded the requirements to enable the resulting e-textile to have more applications in different industries. Furthermore, Parylene C is a more expensive process than PDMS both in academia and industry, the fabrication time is greater than PDMS, and the amount of yield is significantly less than with PDMS. Importantly, PDMS' properties are tuneable (Matsuhisa, et al., 2015) which enables further investigation to make the polymer suitable for the system produced in this research. For these reasons, PDMS was the substrate chosen to encapsulate the capacitive proximity and touch sensing circuit for e-textile applications.

5.2 Experiments Tailoring PDMS for Robust and Aqueous-resistant Electronic Packaging for E- Textile Applications

5.2.1 PDMS Fabrication Process for Experiments

Aforementioned, Sylgard 184 2-part Polydimethylsiloxane was used in the fabrication process. The 2-part product formed of the curing agent and base agent mixture can be mixed in different ratios to

provided mechanical and hydrophobic variability. To make the moulds that would shape the different PDMS mixing ratios and make them non-stick, they were put in a vacuum chamber for 30 minutes with a glass sheet which had 1 drop of Trichlorosilane was deposited on its surface.

Meanwhile, the Sylgard 184 PDMS two-part product were mixed at 5:1, 7:1, 10:1, 15:1, and 20:1 base-curing agent ratios with 20 g of base agent for each mixture. These mixing ratios were chosen as they are most extensively evaluated for hydrophobic and mechanical properties in literature (Park, Yoo, Lee, Lee, Kim, & Lee, 2010), (Jeong & Konishi, 2006), (Yu & Han, 2006), (Seghir & Arscott, 2015). Each was mixed in a beaker for 1 minute and degassed in a vacuum chamber for 20 minutes with to remove any bubbles. For the contact angle tests, each degassed mixture was poured into separate 8 cm-diameter glass Petri dishes and cured at 140 °C for 10 mins. For the swelling tests, five strip-shaped PDMS per mixing ratio were made with the same fabrication method. They were cut into dimensions 5.0 cm x 0.3 cm x 0.3 cm, similar in dimensions to the flexible electronic sensory circuit developed in this thesis.

5.2.2 Selecting Consumer Detergent and Fabric Conditioner for Experiments

The Eppendorf pipette used in the PDMS hydrophobicity experiments dictated the choice of detergent and fabric conditioner used. The Eppendorf pipette was used in these experiments to comply with the laboratory environment these experiments were completed in and with the machinery used to complete these experiments. Specifically, the Eppendorf pipette can accurately and scientifically extract and dispense droplets of aqueous solution for the contact angle experiment. For consistency and to make a scientifically fair investigation, the detergent and fabric conditioner used in the contact angle experiments would also be used in the other aqueous-based experiments. Eppendorf pipette's interior is chemically incompatible with solutions that are too acidic, too alkaline, and highly volatile. Its manufacturers have a list of accepted chemicals (Corporation E. R.) that can safely be dispensed by its pipettes to prevent permanent damage.

For the washing test completed in this Ph.D, it was important for it to be truly representative of how traditional textiles are being cleaned. This meant, using detergent and fabric conditioner in the wash. Detergent and fabric conditioner are commonly used in households to maintain the quality of textiles and remove stains. From 2015 to 2017, 2.5 million people used fabric conditioner once a day or more (Frequency of fabric conditioner usage in the United Kingdom (UK) 2015-2017) and 2.2 million used liquid detergent once a day or more (Frequency of liquid detergents for fabrics usage in the United Kingdom (2015-2017)) to wash their textiles. To select the detergent and fabric conditioner under test, firstly the list of incompatible chemicals was collected from Eppendorf Research and this was compared with the most used and popular detergent and fabric conditioner products available in the UK. The UK consumer market was chosen for this research had prime access to UK-based stock. Detergent and Fabric Conditioner were compared by:

- Most popular brands bought by consumers in the UK from 2013-2016 and 2017 (Statistica), (Leading fabric conditioners in the United Kingdom (UK) 2017, by number of users);
- Most popular products belonging to those brands; (Leading liquid detergent brands of Ariel in the UK 2013-2017, by number of users), (Leading fabric conditioner brands of Comfort in the UK 2014-2017, by number of users)

Combining these results together provided the most used detergent and fabric conditioner product used by UK consumers, and it was anticipated that the selection would be most representative of that used in consumer households. UK consumers were focused as this Ph.D was completed in the UK and the detergent and fabric conditioner used were to be purchased in the UK. Consequently, the most popular brand for detergent was Ariel and most popular fabric conditioner brand was Comfort. Although the list of all the ingredients of these detergent and fabric conditioner is trade secret, the manufacturer of these products provides a key list of the chemicals for health and safety purposes. These key chemical lists for the detergent and fabric conditioner products were then compared to the Eppendorf Research chemical list. As a result, these specific products were chosen for the experiments:

- Detergent: Ariel's Excel Colour Wash
- Fabric Conditioner: Comfort Pure

5.2.3 Contact Angle Experiment for Measuring Surface Hydrophobicity

Due to PDMS' inherent hydrophobicity and its feasibility to have its hydrophobicity altered by increasing its cross-linking, literature exists on which mixing ratios are most hydrophobic to water. However, what is missing in literature is PDMS' hydrophobicity to detergent and fabric conditioner as the applications for these tests were not known. However, to consider PDMS as an encapsulating film for electronic circuits to be washed as part of a textile, the application exists for PDMS to evaluate its suitability to textile wet cleaning processes as a protector for electronic circuits. As a result, this chapter presents experiments evaluating different cross-linking amounts of PDMS and their hydrophobicity to water, water and detergent, and water and fabric conditioner to represent three kinds of wet cleaning processes used on textiles.

5.2.3.1 Contact Angle Theory

The contact angle of a liquid on a material can be quantitatively measured by measuring the angle an aqueous droplet makes when it interfaces with a surface. The greater the contact angle, the more hydrophobic the surface as the height of the droplet would be higher.

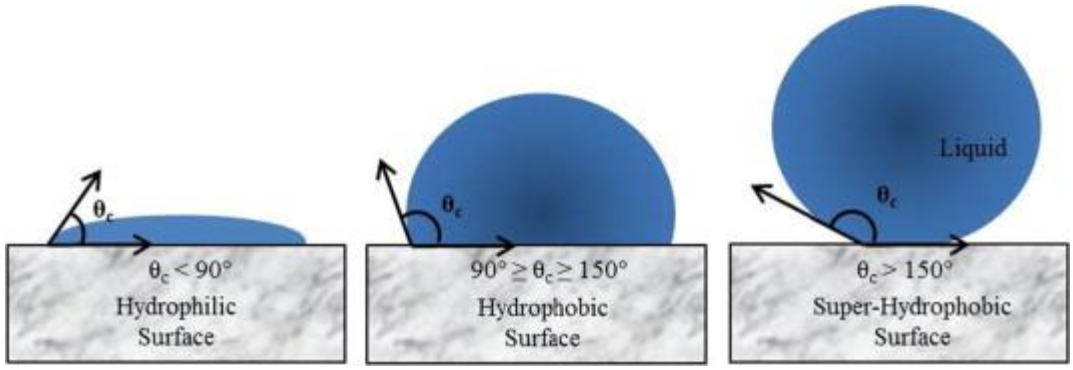

Figure 37 Contact Angle of droplet on hydrophilic, hydrophobic, and super-hydrophobic surfaces *(Gomes, de Souza, & Silva, 2013)*

Surface tension measures the resistance of an external force that causes liquids to otherwise have a contractive behaviour and prevents spreading on a surface. Water, for example, spreads on hydrophilic surfaces and forms droplets- akin to beads - on hydrophobic surfaces. Consequently, the contact angle value measures the degree of spreading of a liquid across a surface. The contact angle of a droplet on a surface is dependent on the surface tension of the investigated liquid. The surface that interfaces with the liquid may have characteristics that would influence the measured contact angle e.g. topography, chemical composition, and roughness. Furthermore, the surface tension of the net solution of a liquid droplet decreases due to impurities, such as detergent and fabric conditioner. This is because detergent and fabric conditioner are surfactants. Surfactants are compounds that reduce the surface tension of a liquid when added. As they are amphiphilic, the surfactants contain hydrophobic and hydrophilic group regions on opposite ends of the molecule. They change the intermolecular forces of the net attraction of adjacent molecules in most liquids, causing water for example to spread on a surface. Due to this, we would expect the contact angles for aqueous solutions containing detergent and fabric conditioner to be less than water, due to the impurities, and this experiment was to investigate the extent with different PDMS mixing ratios.

5.2.3.2. Experiment Methodology for measuring Contact Angle of PDMS

These tests were performed using the DSA30 Krüss Contact Angle Machine. Three washing aqueous environments were evaluated: distilled water, distilled water mixed with a commercial anionic-based detergent, and distilled water mixed with a commercial cationic-based fabric conditioner. Distilled water dispensed by the Millipore Q-POD® was used to ensure no contaminants would damage the pipettes used, or negatively influence experimental results and the PDMS under test. A commercial washing machine, the Bosch Exxcel Serie 4 Washing Machine WVD24520GB, based on this work states that 58 L of distilled water is used in a washer-dryer cycle and 25 L of distilled water in a wash only cycle per day. For 4-5 kg load it states 37 ml of detergent and 35 ml of fabric conditioner is needed. The experimental solutions are show in Table 5.

Aqueous Solution	Aqueous Conversions		
	Ratio Content	***Commercially-Recommended Ratio***	***Experimental Ratio***
DetergentA	Detergent:Water	37 ml:58 L	0.32 ml:500 ml
DetergentB	Detergent: Water	37 ml:25 L	0.74 ml:500 ml
FabricCondA	Fabric Conditioner: : Water	35 ml:58 L	0.3 ml:500 ml
FabricCondB	Fabric Conditioner : Water	35 ml:25 L	0.7 ml:500 ml

Table 6 Aqueous Ratio Conversion for Contact Angle Test

An Eppendorf Research® plus pipette was used to dispense five 10 µl droplets of distilled water, detergent, and fabric conditioner solutions upon each PDMS sample surface. Each contact angle was measured via the DropShape software five times to get an average, standard deviation, and error calculation.

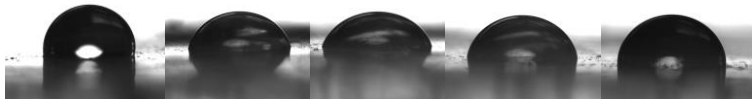

A B C D E

Figure 38 Droplets upon 20:1 PDMS surface for distilled water (A), DetergentA (B), DetergentB (C), FabricCondA (D), and FabricCondB (E), captured via DropShape software.

5.2.3.3. Results

Results showed decreasing the cross-linking of PDMS has an effect on how the water, detergent, and fabric conditioner droplets behave upon its surface (Figure 39). Overall, the contact angle increases when cross-linking reduces despite the concentration of surfactants increasing.

Aqueous Solution	Contact Angle (degrees)				
	5:1	***7:1***	***10:1***	***15:1***	***20:1***
Water	98.87	98.09	98.08	100.97	106.98
DetergentA	64.84	71.61	72.07	72.60	77.95
DetergentB	66.42	66.52	67.14	70.35	71.46
FabricCondA	99.41	97.73	101.15	99.22	102.12
FabricCondB	99.03	97.25	94.07	97.92	102.40

Table 7 Average Contact angle measurements

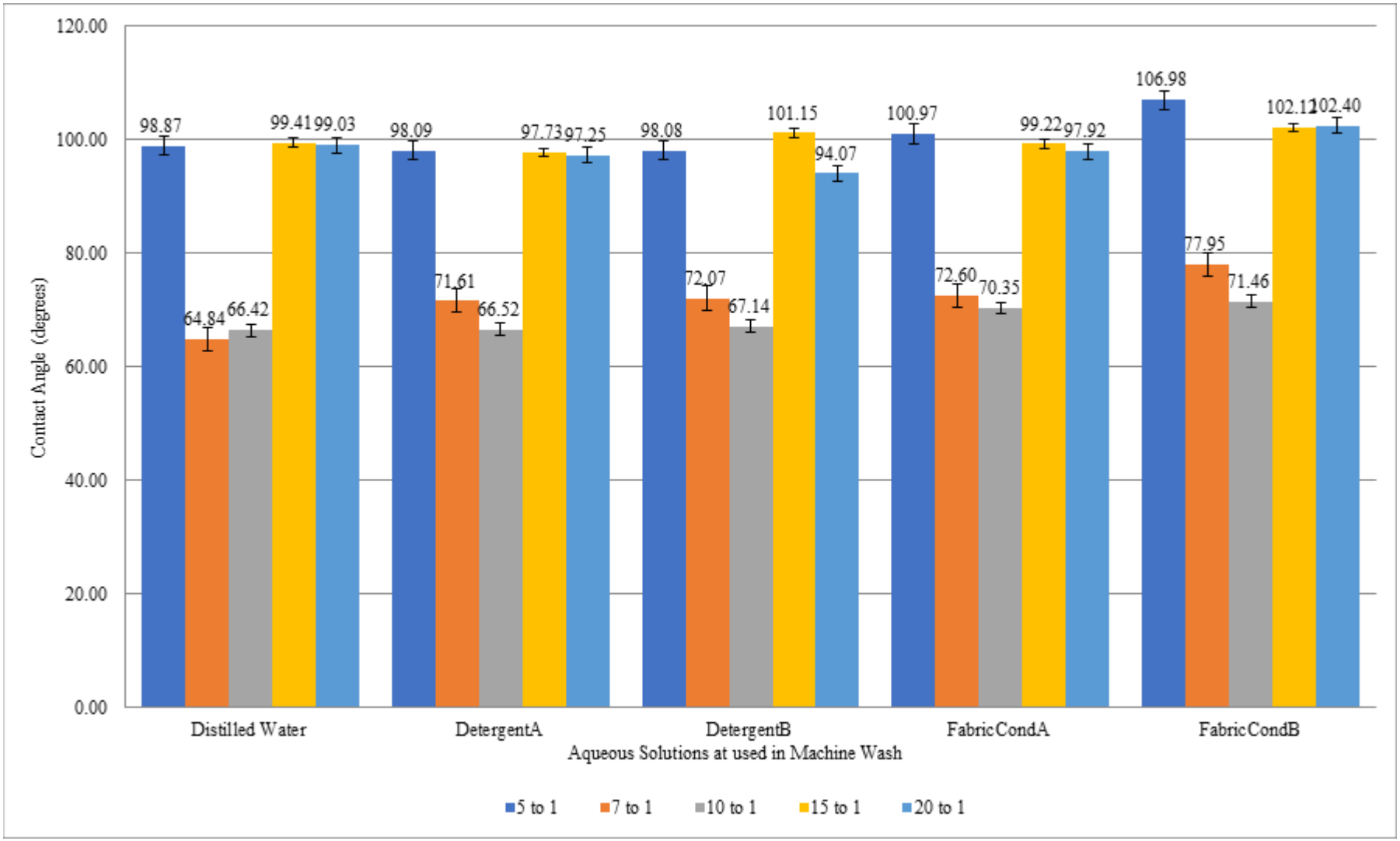

Figure 39 Graph showing comparison of the hydrophobicity of different PDMS mixing ratios and their contact angle with aqueous solutions used in machine washing

5.2.3.4 Analysis

Despite the changing surface tension of the solutions due to the concentration of surfactants, a PDMS mixing ratio of 20:1 overall gives the greatest contact angle values compared to other mixing ratios. This is expected, as increasing the cross-linking increases the number of excess silicon-hydride groups which prevents charged hydroxide ions to the surface as confirmed in literature (Kim & Jeong, 2011).

Additionally, detergent has a greater concentration of surfactants compared to fabric conditioner which encourages aqueous solutions to adsorb onto interfacing surfaces (Essö, 2007). This explains why the contact angles for detergent are lower as surfactants reduce the surface tension of the aqueous solution as it interfaces with surfaces during the washing process. Expectedly, detergent and fabric conditioner display lower contact angles compared to water. This shows that PDMS is compatible to these chemicals as it does not disrupt the desired functionality of detergent and fabric conditioner upon textiles - still allowing the adsorbing onto textiles whilst still protecting the electronics that would be encapsulated within it. For all aqueous solutions tested, 20:1 was the most hydrophobic with an 8.3 %, 7.5 %, 6.0 %, 1.0 %, and 8.1 % improvement compared to 10:1 for distilled water, DetergentA, DetergentB, FabricCondA, and FabricCondB respectively. Although measurements were similar – indicating similar surface energy between mixtures – they suggest that decreasing the crosslinking of the PDMS structure increases hydrophobicity to water, which is supported by literature (Palchesko, Zhang, Sun, & Feinberg, 2012). However, this thesis expands the literature by showing this trend is the same when using detergent and fabric conditioner solutions, not just water. Furthermore, measured contact angle values were within 10.0 % of those reported in literature (Palchesko, Zhang, Sun, & Feinberg, 2012) increasing confidence in the findings.

5.2.4 Aqueous Permeation Experiment

This test was designed to simulate textile handwashing by submerging the PDMS strips in various washing aqueous solutions for set washing times. The detergent used was not designed for handwashing by the product manufacturer. However, it was still evaluated to establish its behaviour with PDMS.

5.2.4.1 Swelling Theory

Polymers are permeable to gas and liquids due to their porosity and low density. Permeability occurs in three stages:

1) Adsorption – fluid molecules collect on the polymer surface
2) Diffusion – fluid molecules transport thorough the polymer medium
3) Desorption – fluid molecules secrete through polymer interface

Polymers swell in aqueous environments due to insertion of fluid molecules as they interact with the porous regions of the polymer. The diameters of the pores increase as they are packed with the fluid molecules, causing the net dimensions of the polymer to increase and its weight to increase. Depending on the chemical composition of the polymer, the pores can relax back to their original size as they reach a state of equilibrium. This will also depend on whether the polymer is elastomeric, with the ability to stretch and withstand strain at a molecular level to enable the polymer to return back to its original size or weight.

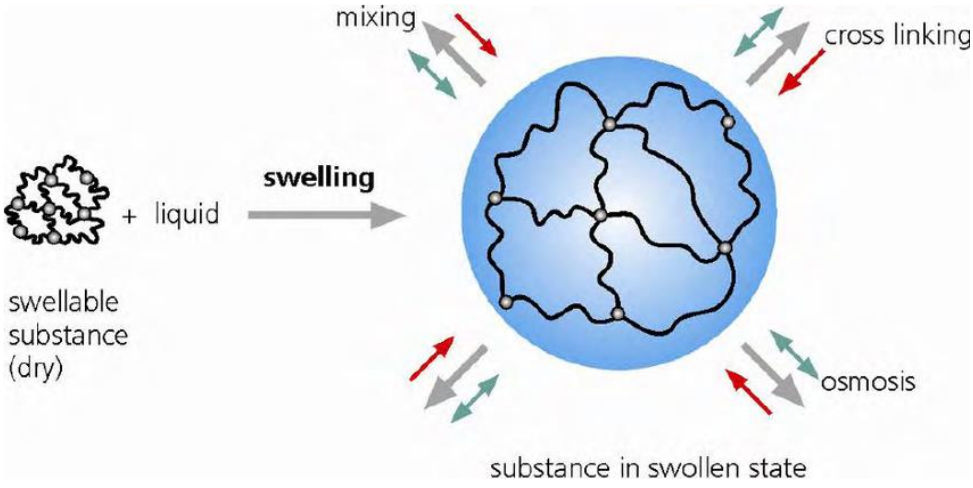

Figure 40 Swelling of polymeric substance due to a liquid permeating its surface *(Wack & Bertling, 2007)*

When the polymer is hydrophilic, it will attract liquid molecules to its surface to encourage swelling. However, PDMS is hydrophobic and therefore we would expect the degree of swelling to be negligible. However, porosity of a polymer is related to how tightly-packed the polymer molecules are – and this is related to the intermolecular forces between molecules. The intermolecular forces between molecules in PDMS decreases as the cross-linking density decreases - resulting with the Young's modulus of the lower cross-linked PDMS to decrease. The experiment in this chapter was to investigate PDMS' hydrophobic recovery as a result of being submerged in aqueous environments. These aqueous environments had different degrees of surfactants, which would influence the permeability of the fluid molecules into the PDMS of different cross-linking density.

5.2.4.2 Experiment Methodology for Measuring PDMS Degree of Swelling

Aqueous Solution	**Aqueous Conversions**		
	Ratio Content	***Commercially-Recommended Ratio***	***Experimental Ratio***
FabricCondC	Fabric Conditioner : Water	18 ml:10 L	1.8 ml: 1 L
DetergentC	Detergent : Water	N/A	1.8 ml: 1 L

Table 8 Aqueous Ratio Conversion for Swelling Test

As before, five 0.4 g strip-shaped PDMS samples for each mixing ratio were used. For each experimental trial, a 1.2 L capacity glass container was filled with either 1 L of distilled water, a mix of 1.8 ml: 1 L of fabric conditioner to water (FabricCondC), or a mix of 1.8 ml: 1 L of detergent to water (FabricCondC). Furthermore, a trial with 1 L tap water was investigated for further comparison. Each container had five PDMS strips which were spread out when submerged within the aqueous solutions to ensure permeation regions were not obstructed. The weight of each strip was measured before and after aqueous submerging using the KERN EMB 500-1. Any change in weight would be due to aqueous permeation into the PDMS. Aqueous submerging time of the strips for the swelling test reflected typical handwashing durations – 15, 30, 45 and 60 mins.

5.2.4.3 Results

Change in weight of the PDMS strips when submerged in distilled water, tap water, FabricCondC, and DetergentC is evident by calculating the degree of swelling (Lee, Park, & Whitesides, 2003) as in (Equation 6) from (Honda, Miyazaki, Nakamura, & Maeda, 2005),

$$\text{Degree of swelling } (\%) = \frac{\text{increased weight (g)} - \text{initial weight (g))} \times 100)}{\text{initial weight (g)}} \qquad (6)$$

Equation 6 Degree of Swelling Calculation

Swelling tests conducted in distilled water showed a significant improvement in reducing aqueous permeation of PDMS as the cross-linking decreased. Similar results show that mixing ratio has an influential factor regarding swelling in FabricCondC and DetergentC.

PDMS Mixing Ratio	**Degree of Swelling (%) 1 d.p.**			
	15mins	***30mins***	***45mins***	***60mins***
5:1	70.0	16.7	18.2	13.0
7:1	60.0	8.7	14.3	4.2
10:1	47.4	15.8	0.0	15.8
15:1	35.0	4.8	10.0	15.0
20:1	22.7	4.8	4.2	0.0

Table 9 Average Swelling Test Results for Distilled Water

By using 20:1 instead of 10:1, experiment recorded that the degree of swelling in water can reduce by (1- ((47.4-22.7)/47.4)) x 100 = 47.9 % ~ 48 % (Table 9). Additionally, as the duration of swelling increases, the degrees of swelling decrease until negligible or zero (Figure 41).

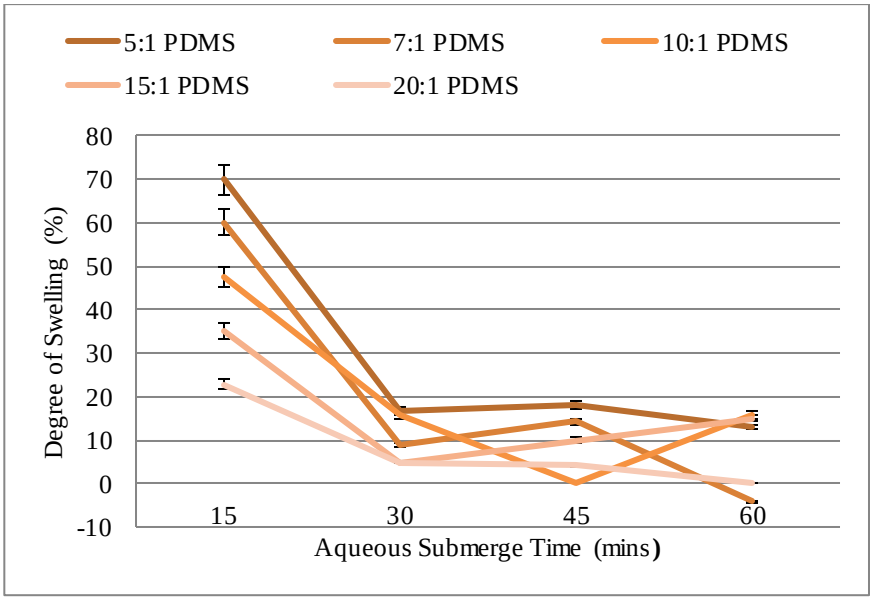

Figure 41 Average degree of swelling (%) reduces with time overall for five PDMS mixing ratios submerged in distilled water.

PDMS Mixing Ratio	**Degree of Swelling (%) 1 d.p.**			
	15mins	***30mins***	***45mins***	***60mins***
5:1	14.3	0.0	13.6	4.3
7:1	0.0	20.0	0.0	8.67
10:1	0.0	-5.0	10.0	0.0
15:1	4.6	0.0	14.3	0.0
20:1	13.0	9.1	4.3	13.0

Table 10 Average Swelling Test Results for FabricCondC

Degree of swelling in FabricCondC, are comparably less compared to the distilled water experiment (Table 10), whereby the behaviour crosslinking affecting aqueous permeability is overall inconclusive (Figure 42). Instead, it appears swelling increases for every 15 min cycle for all mixing ratios except 20:1 which alternates every 30 mins. This irregularity is possibly due to the surfactants encouraging more surface than permeability reaction.

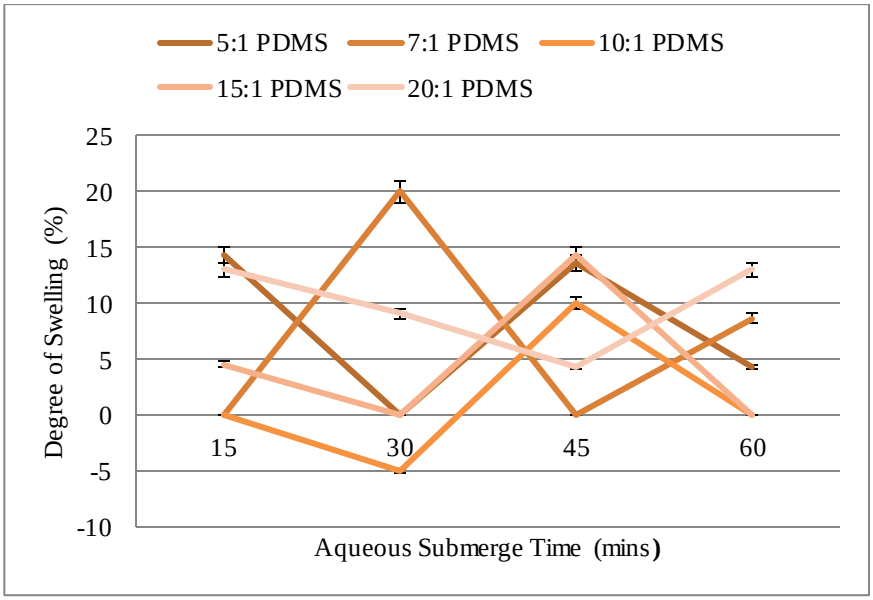

Figure 42 Average degree of swelling (%) reduces with time with 20:1, and reduces every 15min alternate with 5:1, 7:1 and 15:1 PDMS strips in FabricCondC solution.

Similarly, for DetergentC the degree of swelling reduces as the aqueous submerge time increases overall (Figure 43) for 20:1 and 15:1. Although at duration times 20:1 has the greatest degree of swelling at 15mins as time increases it is least affected by aqueous solution compared to other cross-linked PDMS types (Table 11). Interestingly, a similar behaviour occurs whereby swelling increases ever 30 min cycle for 5:1, 7:1, and 20:1.

PDMS Mixing Ratio	**Degree of Swelling (%)**			
	15mins	***30mins***	***45mins***	***60mins***
5:1	17.4	12.0	4.2	8.3
7:1	4.2	8.7	4.0	10.0
10:1	25.0	10.0	0.0	0.0
15:1	10.0	9.1	4.8	4.3
20:1	35.0	8.7	4.3	8.3

Table 11 Average Swelling Test Results for DetergentC

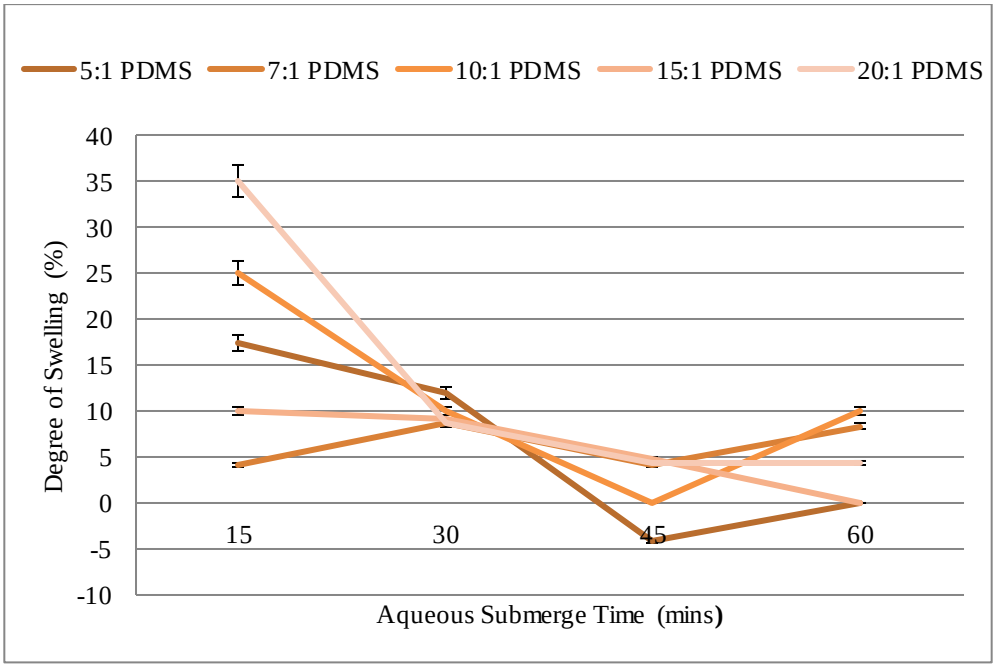

Figure 43 Average degree of swelling (%) reduces with time all PDMS fabrications under test in DetergentC solution

A further trial evaluating PDMS' reaction with tap water was also conducted – making results more representative of handwashing. Similarly to DetergentC and FabricCondC, tap water also shows that with increased aqueous submerge time the degree of swelling reduces for 30 min intervals (Table 12).

PDMS Mixing Ratio	**Degree of Swelling (%)**			
	15mins	***30mins***	***45mins***	***60mins***
5:1	26.1	21.7	17.4	17.4
7:1	29.2	8.3	22.7	26.1
10:1	20.0	10	15.0	25.0
15:1	9.1	9.1	0.0	25.0
20:1	9.1	0.0	4.3	0.0

Table 12 Average Swelling Test for Tap Water

Compared to 10:1, 20:1 PDMS has the largest reduction in swelling of (1-((20.0-9.1)/20.1)) x 100 = 45.7 % ~ 46 % after 15 minutes – similar to distilled water. As the time duration increases, the degree of swelling reduction of 20:1 compared to 10:1 becomes 10.0 %, 28.7 % and 25.0 %.

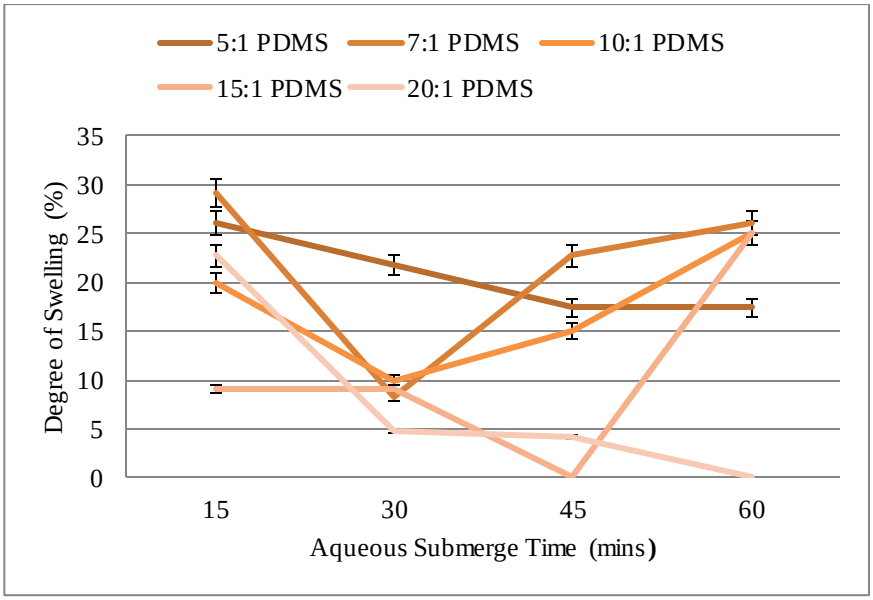

Figure 44 Average degree of swelling (%) reduces every 30 mins for PDMS fabrications under test in tap water

5.2.4.4 Analysis

The result that degree of swelling reduces with aqueous submerge time seemed counter-intuitive as it is expected to increase for typical porous materials. However, PDMS is hydrophobic which has a repellent effect on its interaction with aqueous solution at pore-level. PDMS can be synthesised to have specific mechanical or chemical characteristics enhanced for its application (Brook, 2000) by changing its cross-linking, fabrication method (Wei, et al., 2011), or thickness (Ren, Lu, Zhou, Chong, Yuan, & Noh, 2017) can control the porosity attributes of PDMS. Contact Angle tests suggested that reduced cross-linking increased PDMS' hydrophobicity. Consequently, experiments indicate that PDMS' degree of swelling reduces overall as cross-linking reduces when in water, hence as PDMS becomes more hydrophobic.

However, in detergent and fabric conditioner this degree of swelling alternates at set time intervals. As a result, this appears as PDMS having alternating degree of swelling and the set alternating time period depends on the aqueous solution the PDMS is submerged in. The reduced degree of swelling of PDMS in fabric conditioner and detergent solutions compared to water caused by *surface action*. Detergent (anionic surfactants) and fabric conditioner (cationic or anionic surfactants) used contains cleaning agents which reduce the surface tension of water, enabling water to penetrate the surface of oil, and stain particles into finer sizes as part of their removal process. Anionic surfactants have a negatively charged hydrophilic end whereas cationic surfactants have a positively charged hydrophilic end. The hydrophilic ends position themselves within the dirt, oil, and/or stain molecules on the surface, whilst the hydrophobic ends of the molecules break the hydrogen bonds on the water's surface, making them weaker. The hydrophobic surface of PDMS could prevent the degree of hydrophilic portions of the surfactant molecules that could reach the surface. As a result, fabric conditioner and detergent encourage more surface action that relatively

reduces permeation of aqueous solution which would theoretically explain the experimental results. Accordingly, when PDMS is submerged in an aqueous solution with a weaker surface tension, this reduces degree of aqueous solution that would otherwise be on its surface. Additionally, some fabric conditioners feature sodium silicates which produce a lubricating, protective layer over the tank and drum of the washing machine. This protective lubricating layer is also reported in literature (Brooks, Das, & Smith, 1989) to be present on the items in the wash. This is a type of chemical finish of surfactants, whereby fabric conditioners especially contain long chain fatty acids that soften fabrics to make them appear smoother and softer to touch. It is possible that the fatty acid layer (Kang & Kim, 2001) lubricates the PDMS whilst submerged in aqueous solution creating a buffer preventing aqueous permeation. Therefore, the phenomena described caused the minimised weight gain of the cured PDMS strips in FabricCondC and DetergentC – related to negligible degree of swelling.

Nonetheless, fabric conditioner and detergent only feature in machine washing towards the end of a washing cycle to be removed and replaced with water in the final spinning process (Using a washing machine: how to use detergent in your washing machine), (Where do I put fabric conditioner, washing powder, or liquid detergent in my washing machine?). Therefore, results for water should take more importance which means experiments suggest that 20:1 is the better mixing ratio choice rather than 10:1 to become a hydrophobic packaging for washable microsystems integrated into textiles. Importantly, all PDMS samples reverted back to their original mass 1-3 seconds after removal from the solution – supported by literature (Velderrain & Lipps, 2011) due to the aqueous solvents evaporating from the polymer. This suggests the PDMS will retain its initial flexibility and robustness after drying. Overall, results show PDMS' compatibility (Velderrain & Lipps, 2011) with these aqueous solutions allowing use in machine washing thus confirming its suitability as an electronic packaging choice for flexible electronic microsystems integrated into textiles.

5.3 Conclusions

This chapter has detailed how the packing substrate for the capacitive proximity and touch sensing circuit was chosen and how it was tailored for e-textile applications. Factors such as industrial feasibility and cost of manufacture were considered as a focus of this research is for it to be developed for commercial use. Furthermore, considerations such as transparency, dielectric constant, and responses to different use-case environments e.g. flammable, UV, and bio-compatibility were compared with possible substrates. This resulted with two materials, Parylene-C and PDMS, which were subsequently fabricated and evaluated to compare for suitability for this research. PDMS was finally chosen for its biocompatibility, lower cost of fabrication, shorter fabrication time, a high yield, and more resistant to environmental factors. To tailor the PDMS for e-textile applications, experiments were designed and executed to determine how PDMS can be fabricated for improved hydrophobicity to increase the likelihood of the capacitive proximity and touch sensing circuit survive

the textile washing process. The experiments explored the relationship between PDMS crosslinking and its hydrophobicity and permeability to aqueous solvent solutions specific to textile washing. Results showed that changing the amount of cross-linking can control the hydrophobicity of the PDMS to water, detergent, and fabric conditioner solutions. Furthermore, the Sylgard 184 standard 10:1 mixing ratio for electrical/electronic applications is not optimal for washable electronics integrated into textiles as it is not tailored to hydrophobicity to water, detergent, and fabric conditioner commonly used in consumer washing of textiles. Therefore, for PDMS to be used as a hydrophobic microsystem packaging layer for textile integration and survive washing, a mixture with lower cross-linking such as 20:1 should be used. Having 20:1 instead of 10:1 PDMS and the permeability of water can reduce by approximately 45 % - 48 %. The reduced degree of swelling with time behaviour holds for detergent (DetergentC) but is overall inconclusive with fabric conditioner (FabricCondC) as the solution discourages permeation; so, this therefore requires further investigation. Other factors such as temperature and PDMS dimensions are influential (Varnaitė & Katunskis, 2009) .This gives strong support for PDMS as a hydrophobic and durable packaging substrate for electronics, and if used in electronic textile applications can enable underwater sensory textiles for marine environments. The resultant 20:1 PDMS-conformal coated encapsulation layer, with a 40. 3 µm thickness, was applied to the circuit using a suspension method, to utilise PDMS' self-levelling characteristic and to package as many circuits as possible within a limited amount of space.

Chapter 6: E-Textile System Construction Featuring of PDMS-Packaged Flexible Capacitive Proximity and Touch Circuit

Collaboration with Nottingham Trent University (NTU) and Helga Nunes (a Textile Researcher from the Winchester Campus) with this thesis resulted with two types of e-textile system designs and hence two, novel, interactive e-textile demonstrators. Both included the conformal, hydrophobic, flexible, PDMS-encapsulated, copper-polyimide touch/proximity circuits. They were integrated into the core of yarns by a knitting technique and the second demonstrator type had the circuits woven into a fabric with a hand loom. For each textile integration technique, it was reflective of the textile construction methods used today. The consequent knitted and woven e-textile demonstrators evidences that the research from this thesis is compatible for scaling.

6.1 E-Textile Demonstrator System Designs

Increased integration in the textile has been achieved by embedding the flexible circuit strips within cylindrical textile yarn sleeves or weaving them within the fabric. In both cases an outer textile layer disguises the flexible circuit. In the case of the yarn approach, the circuits are conformably encapsulated with a flexible, thin, hydrophobic layer covering the entire circuit to make the system washable.

In this work, the system comprises of the capacitive proximity and touch sensing flexible circuit with a flexible, thin, hydrophobic polydimethylsiloxane (PDMS) layer used to protect the circuit from water, detergent, and fabric conditioner. As detailed in 5.1.1.1, the copper-polyimide PCF8883US proximity/touch sensing circuits were conformal-coated in a 20:1 mixing ratio previously identified as the most suitable blend for this e-textile application. This covered the SMDs and entire flexible circuit substrate. For each textile integration technique, the circuits had different treatments specific to type of machines that would handle them. The yarn approach requires the encapsulating layer to be cylindrical in shape which can be covered by the yarn fibres as shown in Figure 45.

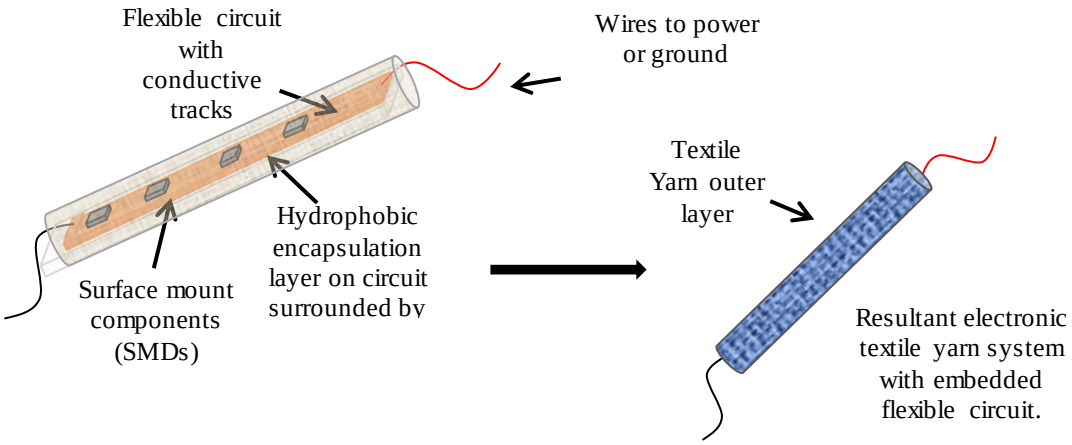

Figure 45 System design to embed a flexible sensing circuit into the core of a yarn

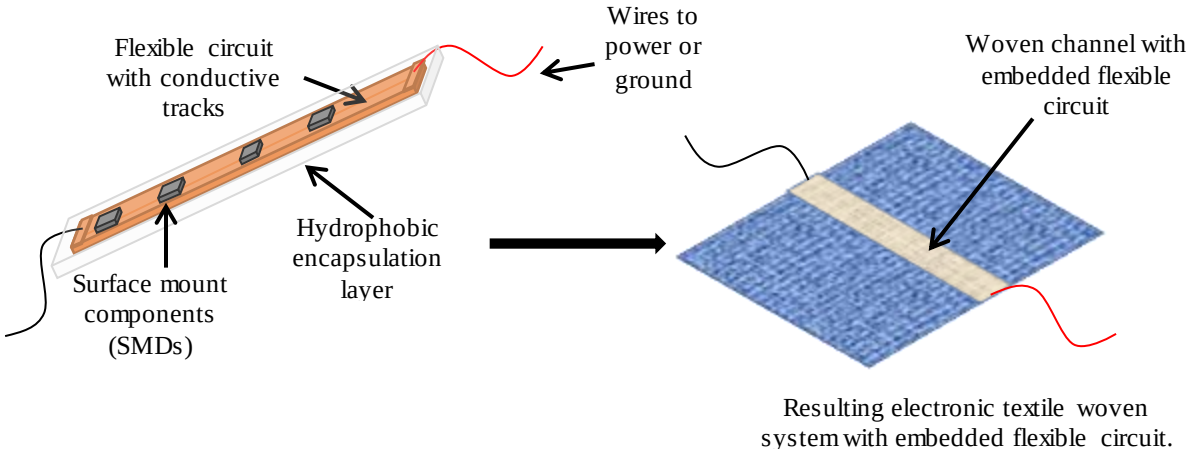

Figure 46 System design to embed a flexible sensing circuit into a woven channel in the fabric

The weaving approach involves a more planar encapsulation process that enables the circuit to be woven into a channel within the fabric as shown Figure 46. The motivation for these e-textile system designs were to ensure the electronics were truly integrated and hidden within the textile, would not need to be removed prior to the fabric being laundered and can withstand mechanical deformation without functionality being compromised. The flexible circuit with the PCF8883US has been coupled with capacitive sensing electrodes with a range of dimensions to identify the smallest electrode configuration that achieves the required performance.

6.2 Integrating PDMS-packaged Capacitive Proximity and Touch Sensing Copper-Polyimide circuits into the Core of a Knitted Yarn Sheath

The packaged circuits were integrated into the core of yarn as an example e-textile demonstrator for this research. This was done in collaboration with Nottingham Trent University's Advanced Textiles Research Group (ATRG). The industrially-used machine at ATRG was the Raschel warp knitting machine from RIUS Model (RIUS, Barcelona, Spain) make and model. This knitting machine had

been used by ATRG to make e-textile threads in a published methodology (Hardy, et al., 2018) In contrast, the research presented in this thesis was to use the same resources but instead feature the encapsulation of a circuit with a flexible packaging - as opposed to SMDs encapsulated in a rigid resin by ATRG. An important material used during the knitting creation of the capacitive proximity and touch sensing yarns was Vectran. Vectran is a light-sensitive fibre used by our partner team at Nottingham Trent University during the yarn knitting process. It is used to take a portion of the tension away from the circuit during the circuit integration process of the yarn knitting machine. It increases the tensile strength of the overall circuity when attached such that it is sufficient to travel through the knitting machine.

To prevent loose ends of wire of copper-polyimide, the circuit ends were trimmed and the Vectran was tied to the power, ground, and external electrode wires. The Vectran was first tied with the power and ground silk copper litz wires, and then the remaining Vectran was tied with a twisted cotton yarn that would be pulled through the knitting machine. It was essential that Vectran, cotton yarn, and silk copper wires were straight and parallel to prevent it hooking onto the knitting needles of the machine as the knitted tube is formed around the circuit. Additionally, the connected to the circuit had to be the same length so that they did not form a loop that could get caught in the knitting needles. The length of the silk copper litz wires on power and ground were 60.0 cm and the external electrode wire was 30.0 cm either end of the electrode.

To ensure the circuits survived the knitting process and could function afterwards, an additional packaging layer was added to the circuit. This is explained in detail in 8.1 Preparation of PDMS-packaged Self-Capacitive Proximity and Touch Sensing Circuits for Mechanical Cyclic Twisting and Bending Experiments.

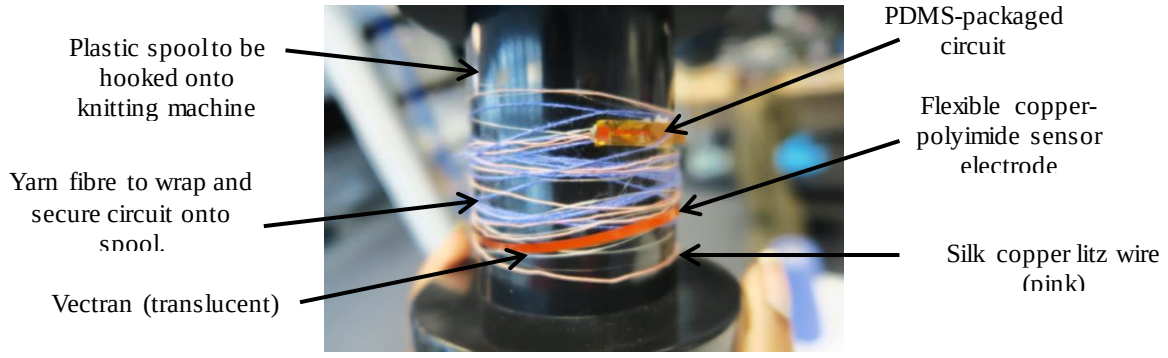

Figure 47 Photo of PDMS-conformal coated and UV-resin capacitive circuits tied with wool and Vectran fibres around a spool before the knitting process

The chain of PDMS-packaged proximity and touch sensing circuits were wrapped around spool with 60.0 cm cotton yarn between chains of circuits, Figure 47. Then, it was connected to the knitting machine and used an automated process to integrate into the core of a textile yarn. Packing yarns was incorporated into the knitting process to resemble the volume and weight of a traditional yarn of its diameter.

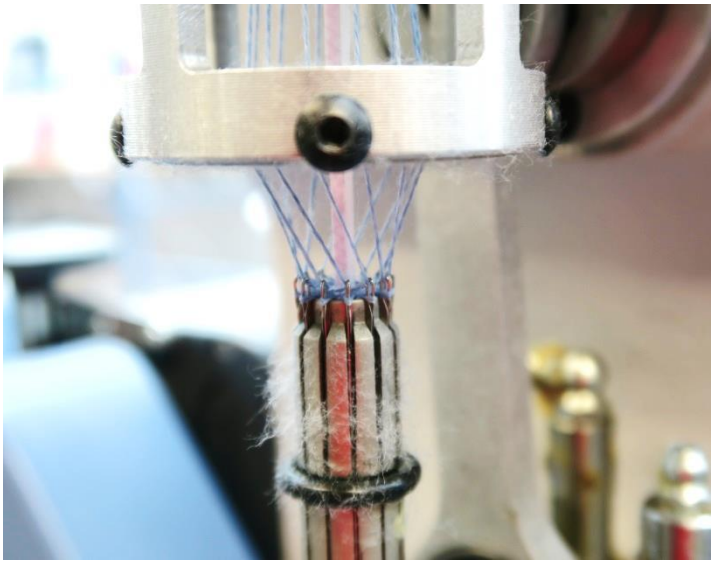

Figure 48 Photo of packing yarn fed through centre of knitting needles whilst it creates a hollow knitted tube

The automated process begins with multiple spools unwinding and feeding into a circular knitting machine, running at 50 rpm, single-entry point to the knitting process. The core yarn is positioned in the middle of the circular knitted needle cylinder and the PDMS-encapsulated sensory circuit would be combined with the raw cotton filler yarns at this point. The catching needles knit separate yarns around the circuit and filler yarn as the circuit travels down the entry tube, and this creates a tubular-shaped warp knitted sleeve with the circuit and filler yarns at its core (Figure 48).

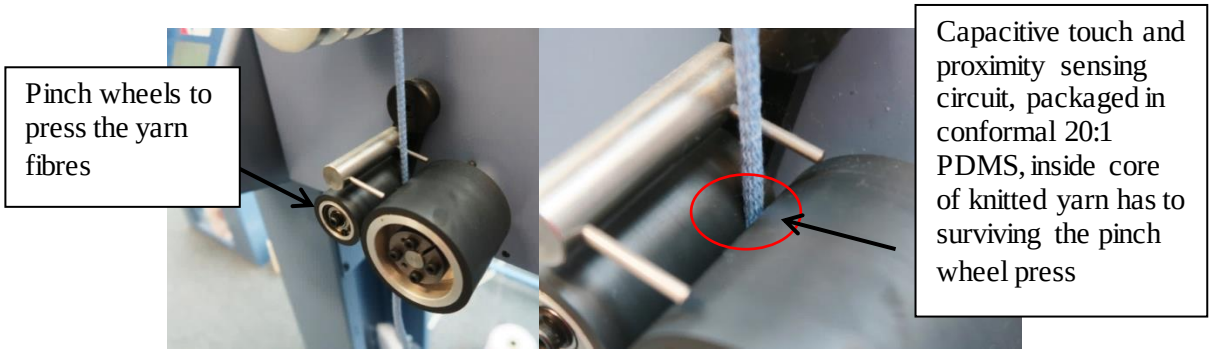

Figure 49 Final stage of the knitting process whereby rotating wheels compress the yarn to pull the packing yarn and circuit above

The resultant knitted circuit yarn is pulled though the machine automatically as it travels with the friction between two rotating rubber pinch wheels (Figure 49). The encapsulation had to be robust enough to survive this last stage. The result of this knitting process is a reel of knitted yarn with a chain of PDMS-conformal coated capacitive proximity and touch sensing circuits at its core (Figure 50).

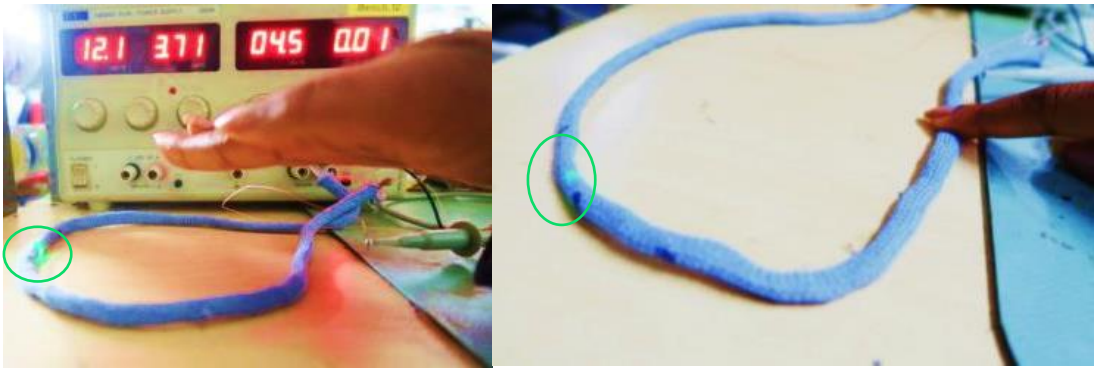

Figure 50 Photo of capacitive proximity and touch sensing electronic yarn connected to power to sense human hand proximity (left) and touch (right) with green LED illuminating for detection visual feedback

6.3 Integrating PDMS-packaged Capacitive Proximity and Touch Sensing Copper-Polyimide circuits into a Woven Fabric Swatch

To weave the circuits in to a fabric swatch, this was completed using an AVL studio folding loom 16 shafts with Computer Dobby IV, a non-automated process. The 20:1 PDMS-encapsulated copper-polyimide proximity and touch sensing circuits were given to textile researcher Helga Nunes to complete and the methodology she followed is in Appendix E: Woven Capacitive Touch and Proximity Sensing E–Textile Demonstrator Methodology . The result was the circuit being woven into channel that was being developed as the fabric was being created. The wires connected to ground, power, and a third connected to the electrode (for functionality testing and could be removed later), was the only part of the circuit visible from the fabric. They exited the woven pocket channel in the fabric. The woven fabric with the PDMS-packaged capacitive proximity and touch sensing circuit was then connected to an oscilloscope and checked for functionally as per subchapter 4.5.2 Functionality Test. They successfully could still function by detecting the proximity and touch of a human hand - after this weaving process.

Figure 51 Photo of illuminating woven capacitive proximity and touch sensing circuit detecting touch of a human hand

Figure 52 Photo of illuminating woven capacitive proximity and touch sensing circuit detecting proximity of a human hand

6.4 Conclusions

The integration of electronic circuits into textiles has been demonstrated in this chapter using scalable manufacturing methods. Copper-polyimide, self-capacitance proximity and touch sensing circuits were encapsulated in 20:1 PDMS, before integrating them into a textile via knitting and weaving techniques. The encapsulation layer was applied to the circuit using a suspension method, to utilise PDMS' self-levelling characteristic and to package as many circuits as possible within a limited amount of space. The circuits still functioned after both processes, showing they can survive the knitting and weaving process using industrially-used machinery. This chapter has shown that using today's industrial and hand textile machinery, it is possible to construct e-textiles without having to manipulate the manufacturing process. Also, this electronic integration into textiles method can be scaled. Sources of failure for these textile integration processes were difficult to determine once the circuit had been embedded. This was because the circuit was irreversibly integrated into the textile, and to determine how it failed would require detaching the circuit for inspection. Nevertheless, this research did observe that during the knitting and weaving process causes of failure could be wires snapping or circuits experiencing compression.

Chapter 7: Evaluating Self-Capacitance Proximity and Touch Sensing Circuit Suitability to Textile, Underwater, and Washing Environments

This chapter presents the experiments using the second circuit prototype which resulted in the final third circuit prototype which resulted with a dual-functionality capacitive proximity and touch sensing circuit of the smallest dimensions achieved in this work. Subchapters 7.1 and 7.4 have been published in the 2019 IEEE Sensors Journal (Ojuroye O. , Torah, Komolafe, & and Beeby, 2019) and Journal of Microsystem Technologies (Ojuroye, Torah, & Beeby, 2019). It also presents simulation work and aqueous experiments on the third circuit prototype with its conformal packaging.

7.1 Experiments Modifying PCF8883US Component Values and Determining Electrode Dimensions for Improved Calibration to Textile Environments

7.1.1 Motivation and Objectives

A main motivation for this thesis was to ensure the electronics were truly integrated and hidden within the textile, would not need to be removed prior to the fabric being laundered and can withstand mechanical deformation without functionality being compromised. The flexible circuit with the PCF8883US has been coupled with capacitive sensing electrodes with a range of dimensions to identify the smallest electrode configuration that achieves the required performance. The objectives of these experiments were to enable proximity and touch sensing functionalities of the PCF8883US flexible circuit using an external copper-polyimide electrode connected to input pin 1.

7.1.2 PCF8883 Proximity and Touch Sensing Considerations with Strip-Shaped Electrode for Textile Environments

The electrode geometry was restricted to rectangle/strip-shaped, due to constraints introduced by the textile integration approach. Referring to Figure 45 and Figure 46, the circuit and sensing electrode would be integrated into a textile using knitting and weaving machinery. These experiments were based on an earlier circuit prototype shown in subchapter 4.4.2. This first prototype had an internal sensing electrode size of 2.0 mm x 70.0 mm but could only sense touch and not proximity. In order to obtain operation at proximity, the internal sensing electrode was augmented by an additional external electrode connected in series. The circuit components influencing sensitivity and sampling frequency had to be optimised to achieve the required performance for the electrode geometries being evaluated. To keep the resulting knitted yarn and woven channel as narrow as possible, the electrode

had to be a thin as the circuit both of which should be minimised. This would make the circuit as unobtrusive as possible which was a key motivation of this research. The sampling frequency, sensitivity and sensing electrode size influence the time taken and maximum proximity detection distance of a trigger object for the PCF8883. The sampling frequency of the PCF8883 to a trigger object, such as a human hand, is controlled by capacitor C_{CLIN}. Increasing C_{CLIN} increases the circuit sampling rate and hence is important in reducing the detection response time of the circuit (Semiconductor, PCF8883 Capacitive touch/proximity switch with auto-calibration, large voltage operating range, and very low power consumption, 2014). Circuit sensitivity is defined as its ability to detect a given object. More sensitive circuits detect a given object at a greater distance and circuit sensitivity also affects response time. Sensitivity is governed by capacitor C_{CPC}. The PCF8883 has two internal RC timing circuits and its charge-discharge cycles are continually compared as part of its sensor logic (Semiconductor, 2014). The self-capacitive sensing electrode is connected pin 1 (input) of the PCF888 which connects to one of the internal resistor-capacitor (RC) timing circuits. The other internal RC timing circuit is used as a reference. Both RC timing circuits are originally synchronised, and change when a trigger object is detected. The discharge time of the internal RC timing circuit connected to pin 1 is compared to the reference internal RC timing circuit's discharge time (Semiconductor, 2014). Both timing circuits are periodically charged by the internal regulated supply voltage output at pin $V_{DD(INTREGD)}$ of the PCF8883 and discharged by a resistor going to ground on pin $V_{SS,}$ where V_{SS} is the ground supply voltage. Successful trigger object detection causes the capacitance of the sensing electrode to increase at pin 1. This causes the discharge time of the internal RC timing circuit at pin 1 to also increase. If the voltage at one RC timing circuit falls below the internal reference voltage at the other RC timing circuit there is a logic output LOW, for vice-versa the logic goes HIGH and a pulse signal is sent to pin OUT. Consequently, the chip's logic output becomes either LOW or HIGH to represent non-detection or detection of a trigger object such as a human hand. The charge-discharge cycle of this operation controls the time taken for the RC timing circuits' logic to switch from HIGH to LOW. This is importantly controlled by the sampling rate which is governed by C_{CLIN}. The auto-calibration feature of the PCF8883 continually functions to equalise the two internal RC timing circuits and compensate for changing static capacitances (Semiconductor, PCF8883 Capacitive touch/proximity switch with auto-calibration, large voltage operating range, and very low power consumption, 2014). The auto-calibration feature of the PCF8883 is controlled by a voltage-controlled current sink at pin 1. This voltage is the same that falls across $C_{CPC.}$ As a result, an increased C_{CPC} value speeds up the comparison of the two internal RC circuits by reducing the voltage needed for the two RC circuits to activate an output response. The compensation needed is lowered and the detection sensitivity is increased.

7.1.3 Electrode Dimension Experiments Methodology for Experiments 1 and 2

A human hand was used as the trigger object to enable touch and proximity detection of the PCF8883US circuit. The hand was moved to a given position to trigger the operating circuit and was held stationary for each reading and the gap between the hand and the electrode was varied during the measurements. The PCF8883US circuit was positioned on a grounded benchtop to minimise stray capacitances that would otherwise lead to false readings.

The strip-shaped, copper internal sensing electrode of length 7.0 cm on the circuit was extended by attaching an external electrode increasing the effective overall sensing electrode length in 3.5 cm increments with a fixed 2.0 mm width. The external electrode was made from the same material as the internal electrode. The influence of the electrode width was also investigated for a fixed electrode length of 7.0 cm and total widths of 3.0 mm, 6.0 mm, 9.0 mm, 12.0 mm, 15.0 mm, and 18.0 mm. A human hand was positioned directly above the internal and external electrode for each reading. Five readings were taken for each measurement and their average was used to create graphs. The circuit component values that would control the PCF8883 detection sensitivity and sampling frequency were C_{CPC} and C_{CLIN} respectively (Semiconductor, PCF8883 Capacitive touch/proximity switch with auto-calibration, large voltage operating range, and very low power consumption, 2014).

Detection takes 1.0 s or more to occur, whilst 0.0 s denotes a failed reading. The shortest acceptable detection time would be 1.0 s and the longest acceptable detection time would be 3.0 s. A human hand was positioned directly above the internal and external electrode for each reading. Five readings were taken for each measurement and their average was used to create graphs. Given the electrode constraints, C_{CPC} and C_{CLIN} require optimisation for operation within an e-textile and to minimise the electrode size. The default values suggested by the manufacturer are 22 pF for C_{CLIN} and 680 nF for C_{CPC}. Hence, for the experiments evaluating sampling frequency, C_{CPC} was fixed at 680 nF whilst C_{CLIN} was varied using values of 33 pF, 56 pF, and 82 pF. This was within the manufacturer's recommended range of 22 pF to 100 pF for C_{CLIN}. Experiments evaluating detection sensitivity used the optimum C_{CLIN} value as determined experimentally and C_{CPC} values were varied from 1.0 µF and 2.2 µF. This range was within the 470 nF to 2.5 µF recommended by the manufacturer. The circuits were powered by 4.5 V and 0.003 A.

7.1.3.1 Experiment 1: External Electrode Length Influence on Proximity and Touch Detection Efficiency

7.1.3.1.1 Results: Sampling frequency vs Increasing External Electrode Length

The experimental results are presented in Table 13 with the proximity distance table rows showing the gap between the sensing electrode and hand (0.0 cm being touch and 0.5 cm to 2.0 cm for nominal proximity detection distance) and the external electrode length column showing the length of the additional electrode added onto the internal electrode already on the circuit.

	33 pF				
External electrode length (cm)	Averaged detection time (s)				
17.5	1.0	0.0	0.0	0.0	0.0
14.0	3.0	0.0	0.0	0.0	0.0
10.5	9.7	0.0	0.0	0.0	0.0
7.0	12.0	0.0	0.0	0.0	0.0
3.5	19.0	0.0	0.0	0.0	0.0
Proximity distance (cm)	**0.0**	**0.5**	**1.0**	**1.5**	**2.0**
	56 pF				
External electrode length (cm)	Averaged detection time (s)				
17.5	1.0	30.0	11.3	11.0	6.0
14.0	5.3	36.0	66.7	37.7	0.0
10.5	15.0	6.3	19.0	42.7	1.0
7.0	14.3	0.0	0.0	0.0	0.0
3.5	13.3	0.0	0.0	0.0	0.0
Proximity distance (cm)	**0.0**	**0.5**	**1.0**	**1.5**	**2.0**
	82 pF				
External electrode length (cm)	Averaged detection time (s)				
17.5	1.0	1.0	2.3	2.0	2.0
14.0	4.7	34.7	36.0	24.0	2.0
10.5	16.7	15.0	1.0	17.7	11.7
7.0	8.0	0.0	0.0	0.0	0.0
3.5	9.7	0.0	0.0	0.0	0.0
Proximity distance (cm)	**0.0**	**0.5**	**1.0**	**1.5**	**2.0**

Table 13 Average detection time for sampling frequency vs increased electrode length for fixed C_{CPC} = 680 nF and 2.0 mm electrode width

7.1.3.1.2 Analysis: Sampling frequency vs Increasing External Electrode Length

It shows that for C_{CLIN} = 33 pF, the circuit does not detect proximity for proximity distance in excess of 0.0 cm. For C_{CLIN} = 56 pF, the circuit works as a touch and proximity sensor for electrodes 10.5 cm and longer. For longer electrode lengths, proximity detection occurs for electrode-hand gaps of 0.5cm and greater. As the sensitivity is kept constant, explanation of this occurrence are higher sampling rates caused by increased C_{CLIN} values. When C_{CLIN} is set to 56 pF and 82 pF, the reaction time of the circuit is lowered further due to increased sensor logic speed. Therefore, the PCF8883US is able to overcome the static capacitance at pin 1 more efficiently resulting in successful readings at external electrode lengths greater than 3.5 cm and proximity distances less than 1.0 cm – compared to when C_{CLIN} = 33 pF. Here, the average detection times become faster as the value for C_{CLIN} increases, with C_{CLIN} = 82 pF showing the fastest averaged proximity detection times. As the C_{CLIN} = 82 pF offered the fastest sampling frequency and more successful proximity detection readings. Therefore C_{CLIN} = 82 pF was used for the fixed, default value for the next experiment that evaluated detection sensitivity and varied C_{CPC}.

7.1.3.1.3 Results: Detection Sensitivity vs Increasing External Electrode Length

According to the PCF8883US datasheet, capacitor component C_{CPC} is the most important variable in enabling proximity detection. Results showed that with a fixed C_{CLIN} = 82 pF[4], a C_{CPC} = 1.0 µF gave 51 % detection readings across 0.0 cm to 2.0 cm range whereas 2.2 µF gave 15 %. From a 0.5 cm to 2.0 cm proximity detection range, C_{CPC} = 1.0 µF provided 36 % readings and C_{CPC} = 2.2 µF gave 20 %. Hence, a C_{CPC} = 1.0 µF, the second highest value, gives a more reliable circuit to detect proximity when the electrode width is fixed at 2.0 mm.

If electrode length was a primary influencer to proximity detection performance, when proximity was detected subsequent lengths would also enable proximity detection and the average time elapsed would be smaller. This is not the case when C_{CPC} = 2.2 µF. In Table 14, C_{CPC} = 1.0 µF shows minimal time taken to detect touch and proximity across all added electrode lengths. Proximity detection from 0.5 cm is not attained above a 3.5 cm and 7.0 cm additional electrode length but when increased to 10.5 cm. Yet, for C_{CPC} = 2.2 µF proximity detection is attained by adding 10.5 cm to existing copper electrode length but limited to 0.5 cm detection distance.

	1.0 µF				
External electrode length (cm)	Averaged detection time (s)				
17.5	4.7	1.0	3.0	1.7	7.3
14.0	3.7	1.7	2.0	1.7	7.3
10.5	3.0	1.7	2.7	6.0	46.0
7.0	12.0	0.0	0.0	0.0	0.0
3.5	6.0	0.0	0.0	0.0	0.0
Proximity distance (cm)	**0.0**	**0.5**	**1.0**	**1.5**	**2.0**
	2.2 µF				
External electrode length (cm)	Averaged detection time (s)				
17.5	2.7	0.0	0.0	0.0	0.0
14.0	2.0	32.7	0.0	0.0	0.0
10.5	45.7	19.3	0.0	0.0	0.0
7.0	34.3	0.0	0.0	0.0	0.0
3.5	62.3	0.0	0.0	0.0	0.0
Proximity distance (cm)	**0.0**	**0.5**	**1.0**	**1.5**	**2.0**

Table 14 Average detection time for detection sensitivity vs increased electrode length for fixed C_{CPC} = 680 nF and 2.0 mm electrode width

7.1.3.1.4 Analysis: Detection Sensitivity vs Increasing External Electrode Length

It is clear in Table 14, that C_{CPC} = 1.0 µF is the best option out of the two values to achieve proximity detection when the electrode width is fixed at 2.0 mm, with a varied electrode length. In

[4] In the frequency response vs electrode length experiment, C_{CLIN} = 82 pF was discovered to give the most efficient proximity sensing circuit. Therefore, it became the C_{CLIN} value for future experiments.

this case, the circuit was triggered by proximity approximately 33 % of the time in less than 3 s when a trigger object was 0.5 cm to 2.0 cm away from the sensing electrode. This compared to 0 % triggering for 2.2 µF. Comparing this to the 16 % when C_{CLIN} = 82 pF when C_{CPC} = 680 nF in the previous set of tables, it suggests that increasing sensitivity can make the proximity detection of the circuit more efficient than varying C_{CLIN} alone.

For increasing external electrode length, when C_{CPC} = 2.2 µF, this graph shows a limited ability to achieve proximity detection compared to when C_{CPC} = 1.0 µF. This can be logically explained by the circuit's increases sensitivity to interference which is a risk when increasing the C_{CPC} to its maximum setting. Experiments show that increasing sensing electrode length does not allow the circuit to operate at its highest sensitivity setting, however, the subsequent experiments investigated if increasing the sensing electrode width could enable an improved C_{CPC} value of 2.2 µF.

7.1.3.2 Experiment 2: External Electrode Width Influence on Proximity Detection Efficiency Experiment

7.1.3.2.1 Results: Sampling frequency vs Increasing External Electrode Width

As mentioned previously, the fixed electrode length for this experiment was 7.0 cm and the original 0.2 cm width was increased by 0.1 cm, 0.4 cm, 0.7 cm, 1.0 cm, 1.3 cm and 1.6 cm. Table 3, C_{CLIN} = 33 pF shows circuit operation as a touch sensor when 0.1 cm is added to the original 0.2 cm electrode width. When C_{CLIN} = 56 pF touch detection only functions with an added 0.1 cm width whereas for C_{CLIN} = 82 pF the circuit operates as a fast operating touch and proximity sensor as the electrode width increases. Compared to Table 13, when electrode length is 7.0 cm and electrode width is 2.0 mm, there were no readings for proximity detection when C_{CLIN} = 33 pF. In contrast, in Table 15 for a fixed electrode length of 7.0 cm proximity detection is enabled up to 2.0 cm when C_{CLIN} = 33 pF when the electrode width is increased by 1.0 mm. For C_{CLIN} = 56 pF, increased external electrode widths for a fixed 7.0 cm electrode length failed to function. This differs from results in Table 13 which showed the thinner width of 2.0 mm operating as a proximity sensor for the same C_{CLIN} value. As this result occurred repeatedly, an explanation could be the PCF8883US unable to adapt to changes in static capacitance at pin 1 with a wider sensing electrode. This suggests the geometry for the strip-shaped sensing electrode is more influential than C_{CLIN} and C_{CPC} to enable full functionality of the PCF8883US. Yet, strip-shaped electrodes are not an idealised sensing electrode shape for capacitive sensing, compared to those recommended in literature – which is one of the challenges to overcome in this research.

	33 pF				
External electrode width (cm)	Averaged detection time (s)				
1.6	0.0	0.0	0.0	0.0	0.0
1.3	0.0	0.0	0.0	0.0	0.0
1.0	0.0	0.0	0.0	0.0	0.0
0.7	1.0	0.0	0.0	0.0	0.0
0.4	1.0	0.0	0.0	0.0	0.0
0.1	2.7	12.7	12.7	12.7	13.0
Proximity distance (cm)	**0.0**	**0.5**	**1.0**	**1.5**	**2.0**
	56 pF				
External electrode width (cm)	Averaged detection time (s)				
1.6	0.0	0.0	0.0	0.0	0.0
1.3	0.0	0.0	0.0	0.0	0.0
1.0	0.0	0.0	0.0	0.0	0.0
0.7	0.0	0.0	0.0	0.0	0.0
0.4	0.0	0.0	0.0	0.0	0.0
0.1	5.3	0.0	0.0	0.0	0.0
Proximity distance (cm)	**0.0**	**0.5**	**1.0**	**1.5**	**2.0**
	82 pF				
External electrode width (cm)	Averaged detection time (s)				
1.6	7.3	1.0	1.0	1.0	44.7
1.3	1.0	1.0	1.0	7.7	1.0
1.0	15.0	10.7	29.3	6.0	28.7
0.7	5.7	1.0	1.0	18.0	1.3
0.4	5.3	22.7	41.0	49.0	0.0
0.1	9.0	33.7	1.0	0.0	0.0
Proximity distance (cm)	**0.0**	**0.5**	**1.0**	**1.5**	**2.0**

Table 15 Average detection time for sampling frequency vs increased electrode width for fixed C_{CPC} = 680 nF and 7.0 cm electrode length

7.1.3.2.2 Analysis: Sampling frequency vs Increasing External Electrode Width

Previous work has explored the different geometries of capacitive sensing regions and how reliable the touch and proximity detection become as a result. In contrast to strip-shaped sensing electrodes, round-shaped capacitive electrode sensing pads are favoured for touch detection as the geometry mimics the rounded fingertip (Schmitz, Maggiali, Natale, & Metta, 2010). Whilst the sharp-edged shapes such as squares and rectangles (strip-shaped) can cause localised electric field strength increase at the corners (Rao, Liu, & Qiu, 2013), which introduce electromagnetic interference (EMI) compliance issues due to field distortion (Baker, 1996). Although literature favours round-shaped sensing electrodes, the experimental result gives some indication that there is optimisable strip-shaped sensing electrode geometry for the PCF8883. The experiments suggest that this strip-shaped geometry is more influenced by having a greater width rather than a greater length in producing more reliable and quick-detection of short-range proximity and touch sensing.

Literature states that with proximity sensing the electric field is projected much further from the sensor into the air compared to with touch sensing (Semiconductor, AN12082 Capacitive Touch

Sensor Design, 2017). In an ideal case, the sensing area for proximity sensing would need to increase. However, the constraints on this e-textile circuit as to be a small and thin as possible. Therefore, in order to overcome the increased parasitic capacitance experienced during proximity detection C_{CLIN} can be increased to 82 pF. This is because C_{CLIN} = 82 pF appears to give fast response time to detect touch and proximity over a wide range of electrode widths. Only when the circuit has C_{CLIN} = 82 pF shows sufficient activity to argue that strip-shaped electrode width influences proximity detection.

7.1.3.2.3 Results: Detection Sensitivity vs Increasing External Electrode Width

Subchapter 7.1.3.1.3 Results: Detection Sensitivity vs Increasing External Electrode Length indicated that if C_{CLIN} = 82 pF, the electrode width was fixed at 2.0 mm and the electrode length was varied that C_{CPC} = 1.0 µF gives the best proximity and touch sensing response. However, by increasing the electrode width beyond 2.0 mm, increasing C_{CPC}, and keeping the internal electrode length as 7.0 cm the PCF8883US' performance is improved.

	1.0 µF				
External electrode width (cm)	Averaged detection time (s)				
1.8	9.7	1.0	14.3	1.3	1.0
1.5	10.0	1.0	12.3	0.0	0.0
1.2	23.3	14.3	9.3	5.3	10.3
0.9	8.0	1.0	25.6	1.7	0.0
0.6	3.0	36.0	18.0	1.0	0.0
0.3	1.0	2.0	37.0	4.3	43.7
Proximity distance (cm)	**0.0**	**0.5**	**1.0**	**1.5**	**2.0**
	2.2 µF				
External electrode width (cm)	Averaged detection time (s)				
1.8	1.3	1.0	2.7	1.0	1.3
1.5	1.0	1.7	36.3	3.0	2.0
1.2	1.0	1.0	1.0	1.0	1.0
0.9	1.0	1.0	33.7	0.0	0.0
0.6	1.0	2.0	0.0	1.0	1.0
0.3	1.3	1.0	7.3	1.0	1.0
Proximity distance (cm)	**0.0**	**0.5**	**1.0**	**1.5**	**2.0**

Table 16 Average detection time for detection sensitivity vs increased electrode length for fixed C_{CLIN} = 82 pF and 7.0 cm electrode length

7.1.3.2.4 Analysis: Detection Sensitivity vs Increasing External Electrode Width

Comparing C_{CPC} = 2.2 µF in Table 14 and Table 16, shows that the circuit can have its detection sensitivity increased beyond C_{CPC} = 1.0 µF if its electrode width is increased. When C_{CPC} = 2.2 µF and C_{CLIN} = 82 pF the circuit could accurately detect a trigger object in less than 10 s at a proximity range of 0.0 cm to 1.0 cm when the total external electrode width is no greater than 0.7 cm. However, greater proximity detection distances of 1.0 cm to 2.0 cm were achievable with external electrode widths of 1.0 cm to 1.3 cm. Table 16, C_{CPC} = 1.0 µF shows fast reaction time to touch and proximity

detection as proximity distance increases and electrode width increases. Performance is further improved for C_{CPC} = 2.2 µF which provides the shortest elapsed time to detect touch and proximity.

Switch sensitivity C_{CPC} has the highest influence compared to C_{CLIN} and total input capacitance of the (Semiconductor, 2009). A higher C_{CPC} value allows the sensing electrode area to be reduced. This enables proximity sensing and to sense more reliably at a greater distance (Semiconductor, 2009), (Semiconductor, 2014).

In summary, the results show optimum circuit performance can be achieved by increasing the external electrode width to 3.0 mm from the original 2.0 mm, and selecting capacitor values of C_{CLIN} = 82 pF and C_{CPC} = 2.2 µF. Experimental results showed that increasing electrode length was less influential than increasing width to produce a reliable and greatest nominal proximity distance. However, as the value of C_{SENS} for the PCF8883 had to be approximately 20 pF, further investigations were made. This was to determine the smallest electrode dimensions that would match the desired C_{SENS} for optimised PCF8883 circuit operation and be the least detectable within a textile.

7.1.3.3 Experiment 3: Maximising Electrode Sensing Area for Improved Proximity Detection Distance

Once the need for an external electrode was established further work was carried out to determine the influence of the layout of multiple electrodes on performance. Three factors were investigated in this section: number of touch and proximity detection, nominal proximity detection distance, and the capacitance value generated by the sensing plate and the human hand. This created two experiments, the first evaluated the layout of multiple electrodes to increase the proximity detection distance using the optimised C_{CLIN} and C_{CPC} values. The second experiment determined shortest electrode length to produce the desired C_{SENS} = 20 pF, to make the embedded hardware most unobtrusive within the textile.

7.1.3.3.1 Experiment Methodology

Although the width of the sensing electrode was previously found to be more influential than electrode length, increasing width is contrary to the objective of minimising the circuit width to aid seamless integration into a textile. The 3.0 mm width previously identified is the largest acceptable size and to increase the maximum proximity detection distance further, the surface area of the external sensing electrode could be increased by connecting multiple individual electrodes together. The woven textile structure enables electrodes to be located within woven channels. To connect the electrodes together with wires increases the surface area of the electrode which could increase the proximity detection distance of the PCF8883US circuit. In theory, the electrodes could be placed in parallel or series and located adjacent to the sensor circuit (Figure 53) which is also embedded into the textile. In the yarn form, this concept could be executed by having one electrode per yarn and

individual yarns placed in parallel in the weft direction. The result would be the multiple electrodes in the system designs for within the core of a yarn (Figure 45) or in a woven channel (Figure 46).

To connect the electrodes together, wires can extend through the yarns if in parallel and within the yarn if in series - Figure 53. In practice, the parallel electrode configuration for yarns was not feasible as it would require soldering wires during the automatic knitting process to create a seamless and robust yarn structure. Similarly, for the woven fabric channels created during the weaving process, the circuit and external electrodes can be placed in individual channels in a parallel arrangement and connected via wires. In practice it was feasible to create a single large channel/pocket that could contain a large electrode. However, but having multiple electrodes pre-wired together would get caught inside the roving machine used. Or, without the electrodes being permanently fixed in place, they would likely move inside the channel and would affect the PCF8883US sensing performance.

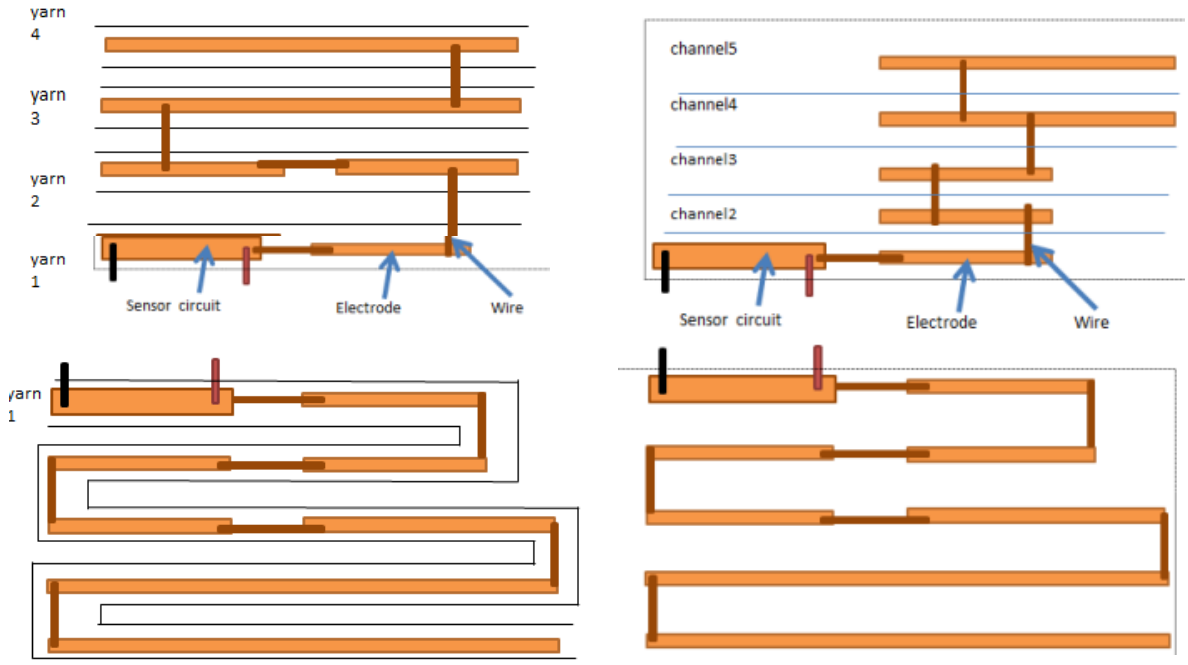

Figure 53 Concepts for integrating capacitive sensory circuit with external electrode in core of yarn and integrated into a woven textile in parallel and series configurations. The left-hand side shows the parallel (top) and series (bottom) internal electrode configuration when knitted into the core of a yarn. The right-hand side shows the parallel (top) and series (bottom) when woven as part of a channel opening to become fabric.

The values for C_{CLIN} and C_{CPC} were 82 pF and 2.2 µF respectively. In the first experiment, square surface area electrodes were evaluated for their nominal proximity detection distance. Their lengths 4 cm to 16.0 cm with 1.0 cm increments produced areas of 16.0 cm^2 to 256.0 cm^2. These electrode square-regions were connected to the internal electrode on the circuit using copper wires. This was compared to evenly-spaced multiple electrode strips. Each electrode was connected to each other with copper wires. They were arranged to fit into surface area that gave the greatest nominal proximity

detection distance for the single electrode. The purpose of this was to determine the electrode surface area needed to produce a particular proximity detection distances for the PCF8883US circuit – if electrode size was not restricted. It would be helpful to compare if thin, multiple electrodes arranged in the same area could offer the same nominal proximity detection distance – ideal in making the conductive elements within the textile minimised.

The circuit was connected to a DSO3062A digital storage oscilloscope to check the functionality of the circuit and supplied 4.5 V voltage and 3 mA current. A ruler was clamped to a stand perpendicular to the working desk as a reference to position a human hand at specified proximity distances. A stopwatch was used to measure the time taken for the pulse signal to be sent to pin OUT and turn the LED at pin OUT to illuminate due to proximity and touch detection. For each surface area, the proximity distance reading was collected five times and then averaged.

7.1.3.3.2 Results: Nominal Proximity Detection Distance with Tailored Electrode Surface Area and Strip-layout

As expected, increasing the surface area of the electrode increases the maximum proximity detection distance. The optimised PCF8883US circuit with improved detection sensitivity and sampling frequency was able to detect a human hand with multiple electrodes connected together with equivalent surface areas of 16.0 cm^2 to 256.0 cm^2. The proximity distance peaked at a 196.0 cm^2 electrode surface area, with an average proximity distance of 15.0 cm. The proximity distance then decreased back to 3.5 to 6.0 cm. This was due to larger electrodes being affected by interference, stray electric fields, and electrical noise. Appendix F, F.1 contains this experiment's numerical data.

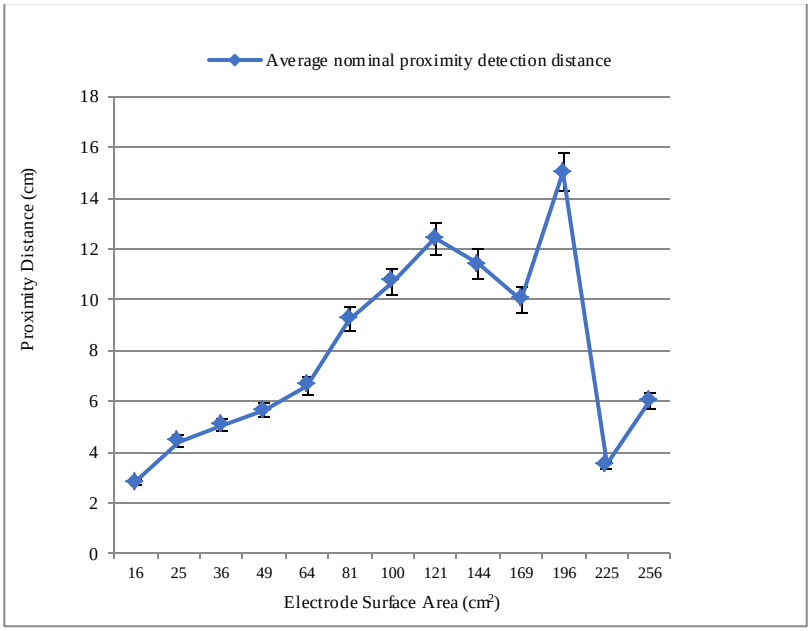

Figure 54 Graph of increasing surface area of external electrode (cm^2) and resulting average proximity detection distance (cm)

For the hand surface area (HAS) in this experiment, an electrode surface area of 121.0 cm^2 offered the greatest proximity detection distance of 12.0 cm. The overall trend of the collected data (Figure 54) shows a positive correlation between electrode surface area and the proximity detection distance. The nominal proximity detection distance initially peaks at 12.0 cm before declining for subsequent electrode areas at 144.0 cm^2 and 169.0 cm^2. The maximum electrode area of up to 121.0 cm^2 produces a proximity detection distance of 12.0 cm which is adequate for applications and increasing the surface area beyond this is not necessary. However, when placing multiple electrode strips within this 121.0 cm^2 area as the number of electrode strips forming the sensing electrode area increases, the nominal proximity detection distance increases. This is shown in Figure 55, whereby adding two 7.0 cm x 3.0 mm electrodes to the PCF8883US does not change the previously achieved 2.0 cm nominal proximity detection distance achieved in previous experiments. However, increasing the number of electrodes to 3 increases the nominal proximity detection distance to 4.0 cm with a 4.8 cm nominal proximity detection distance achieved for 7, 8, and 9 electrodes. The nominal proximity detection distance plateaus at these electrode numbers, and going beyond 9 electrodes would exceed the surface area limit of 121.0 cm^2. Nonetheless, using electrode strips compared to square-shaped electrodes decreased the average nominal proximity detection distance by 58.3 r%. This is due to the sensitivity of the circuit decreasing. With multiple electrodes, the electric field strength between the electrodes is relatively less than the field strength above the electrodes. This could be resolved by having wider electrodes or having smaller gaps between the electrodes. Widening the electrode is undesirable as the maximum was 3 mm. The gaps between the electrodes decreased as the number of electrodes added increases, and the proximity distance was maintained at 4.8 cm. Appendix F, F.2 contains this experiment's numerical data.

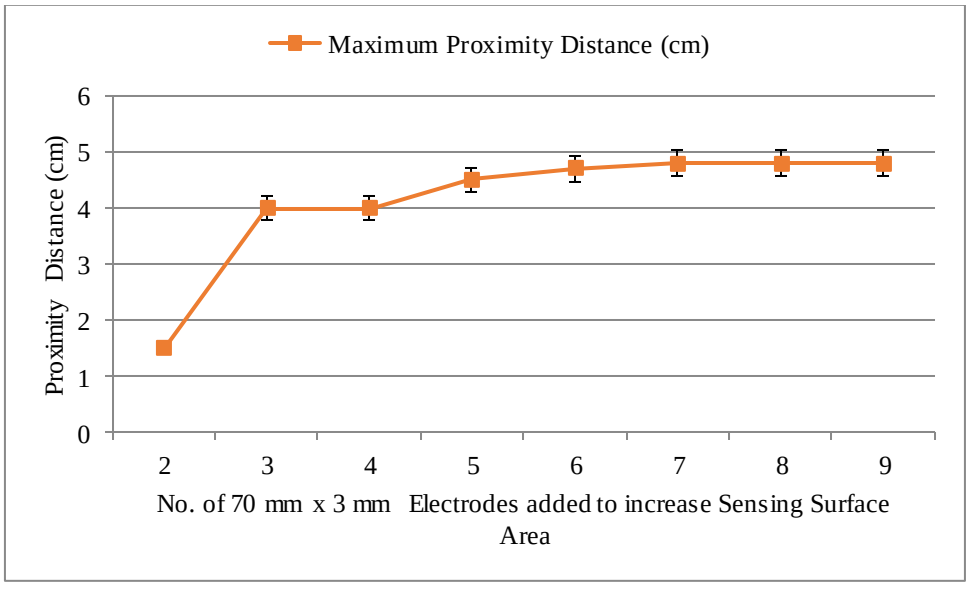

Figure 55 Graph of increasing number of strip-shaped external electrodes within a fixed 121cm^2 area and resulting average proximity detection distance (cm)

7.1.3.3.3 Analysis

Changing the sensing plate to one electrode to multiple electrodes changes the capacitance sensing from self-capacitance to mutual capacitance (Semiconductor, 2017). Unlike self-capacitance, mutual capacitance is influenced by the gap between the electrodes. Electrodes with a greater distance between them project the electric field upwards. However, the overall generated signal becomes significantly weaker in this circumstance. When a finger is in proximity of the electrodes, part of the electric field moves towards the finger instead of the neighbouring electrodes - causing the overall electric field to weaken (Semiconductor, 2017). As a result, the circuit requires more energy consumption to sense as efficiently. For this reason, proximity detection with mutual capacitance is not advised in literature (Semiconductor, 2017) despite it being more noise-resistant. However, as the configuration in this thesis does not have the typical external electrode and internal electrode arrangement, the effect is similar to increasing the area of a single electrode. This is would explain the similarity between Figure 54 and Figure 55.

Overall, experiments show that a square-shaped electrode rather than multiple electrode strips arranged to give the same surface area would offer the greater nominal proximity detection distance for e-textile applications. Based on this, a conductive textile demonstrator with multiple strip-shaped electrodes was created with an electrode surface area equivalent to 121.0 cm^2. This was formed by arranging seven identical copper-polyimide strips using the woven channel approach - of size 11.0 cm (L) x 3.0 mm (W) separated 1.5 cm apart. This gives a total surface area of 11.0 cm x 11.1 cm = 122.1 cm^2. The arrangement was one electrode per channel, and copper wire was made into a textile form using the woven technique. The electrodes were located into channels but the wires had to be soldered onto the electrodes after weaving, as seen in Figure 56. Integrating the electrodes into fabric reduced the proximity detection distance to approximately 5.0 cm on average (Figure 55). It seemed that, by separating the electrodes into channels, the resultant surface area of the electrode reduced**.** This can be explained by the analysis given for Figure 55. Therefore, a single electrode to enable proximity and touch sensing was pursued to be compatible with the knitting and weaving machinery used. The experimentally-verified electrode length to provide the 20 pF C_{SENS} value was investigated to determine the final sensing electrode dimensions.

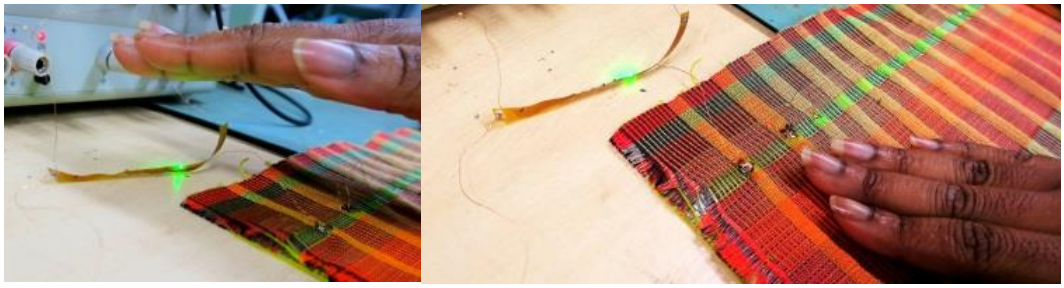

Figure 56 Textile electrode made from multiple electrodes woven into fabric and connected with copper wires to achieve approximately 5.0 cm nominal proximity detection distance (left) and successful touch detection (right).

7.1.3.4. Experiment 4: Evaluating the smallest external electrode dimensions for improved sensing plate capacitance C_{SENS}

This experiment was used to determine the smallest self-capacitance strip-shape electrode to be integrated into a textile and still enable proximity and touch detection. This was to keep the number of electronic components in the textile minimised to make the overall system unobtrusive as possible. Aforementioned, C_{SENS} is the capacitor formed of the self-capacitance copper-polyimide electrode connected at the input pin and the human hand. The value of total capacitance at pin IN for the PCF8883US (Electronics, 2014) to operate at optimum functionality is 30 pF, explained in subchapter 4.4. As C_F = 10 pF, C_{SENS} needs to be approximately 20 pF. Therefore, factors such as electrode dimensions, C_{CLIN}, C_{CPC}, and dielectric layers such as the packaging substrate and the textile outer layer would be decided such the resultant C_{SENS} value would be approximately 20 pF.

7.1.3.4.1 Experiment Methodology

The WK 6500B Impedance Analyser was used to measure capacitance of the sensing plate, C_{SENS} directly from the external electrode. The impedance analyser measures the capacitance of the electrode against a parametric sweep of frequencies. The chosen generated frequency for this experiment was 100 Hz as this was approximately the sampling frequency of the chip when the C_{CLIN} value is 82 pF according to the PCF8883US datasheet. One clip probe from the impedance analyser was connected to the external sensing electrode and the impedance analyser was triggered to generate a capacitance value at 100 Hz. This was completed five times for no trigger object detection, proximity detection at 2.0 cm distance, and touch detection with the tip of a human index finger. The graphs present the average result from those five data readings per electrode plate, per detection type. The lengths of the electrodes were 3.5 cm, 7.0 cm, 10.5 cm, 15.0 cm, and 17.5 cm. The electrode width was fixed at 3.0 mm. Compared to the last series of experiments, this experiment was to determine which electrode length produced the desired C_{SENS} = 20 pF necessary for optimised PCF8883 operation. The shortest length would make the final PCF8883US capacitive proximity and touch sensing circuit the most undetectable when embedded into the textile. The capacitance of the sensing electrodes, C_{SENS} measured at 100 Hz as this closely matches the sampling frequency when C_{CLIN} equals 82 pF (Semiconductor, PCF8883 Capacitive touch/proximity switch with auto-calibration, large voltage operating range, and very low power consumption, 2014). Five measurements were performed for no trigger object, proximity detection at 2.0 cm distance, and touch detection with the tip of a human index finger. The graphs present the average result from those five data readings per electrode arrangements, per detection type.

7.1.3.4.2 Results

When no human hand interacting with the external sensing electrode the capacitance value increases as the surface area (ultimately the length) of the sensing electrode increases. However, when sensing proximity and touch the capacitance value increases as the surface area decreases. The first result is expected, as more charge is present on larger capacitive plate and therefore the measured capacitance would increase. However, the presence of a human hand seems influential and therefore hints the relative sizes of the plates of a capacitor influence the generated capacitance. Ideally, the capacitor plates should be the same size to generate and even/uniform electric field between them (Zimmerman, Smith, Paradiso, Allport, & Gershenfeld, 1995).

Comparing the C_{SENS} values between no trigger object, proximity, and touch detection (Figure 57) the values are increasing and this is consistent with all electrode lengths under test. This is expected from self-capacitance as when supplied a charge the electrostatic capacitance of the electrode increases. When there is a greater sensing plate area, more charge can be collected and hence the electrostatic capacitance increases. Appendix F, F.3 contains this experiment's numerical data.

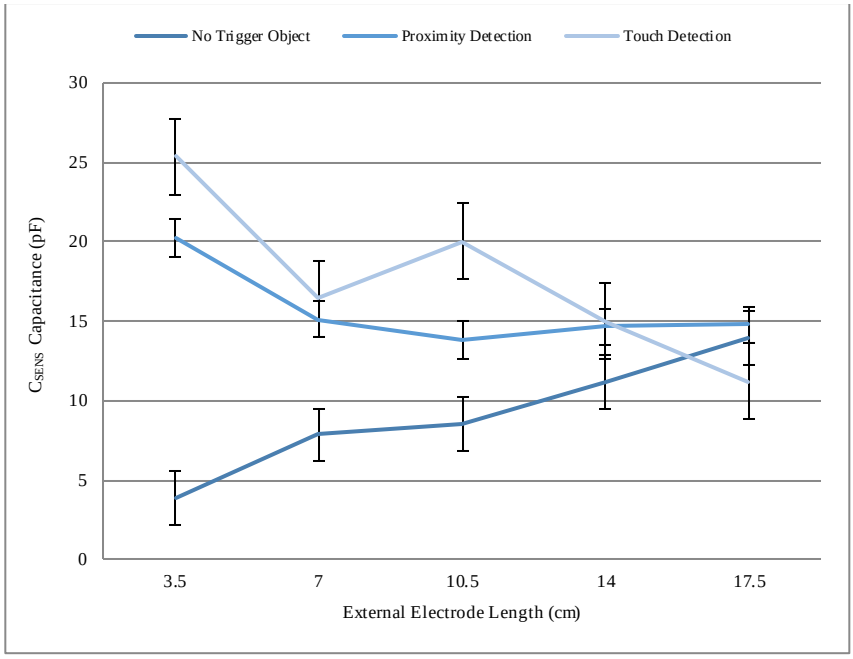

Figure 57 Graph of self-capacitance of External Electrode with increasing length with no Trigger Object Detection

7.1.3.4.3 Analysis

Figure 57 also shows that when proximity and touch sensing detection occurs, the capacitance overall decreases when the external electrode length increases. When a detection event occurs, the human hand capacitively-couples with the sensing electrode. This produces an additional electrostatic capacitance. The human hand has a dielectric constant is similar to water – 80 (Neumann, 1985) - which is greater than air - 1.00059 (Lowe & Rezkallah, 1999), and this causes an increased electric

field strength and hence greater capacitance. Additionally, the human skin has conductive properties and acts as the second capacitive plate – which has been explained previously. This explains why the capacitive value has increased for proximity and touch detection for all electrode lengths under test. A factor which could have caused this is the relative sizes of the capacitive plates – the human hand and the electrode plate. The distance from top of the middle finger to the bottom palm of the human hand used in these experiments was 17.0 cm and width was 10.0 cm. A larger plate area produces more charge collected on the plates (flux) for a given electric field force. However, when one capacitive plate is larger than the other, the electric field flux is more concentrated closest to the smaller electrode plate, which results with a larger overall capacitance. It appears that when the electrode plate connected to the circuit is smaller this generates a larger capacitance compared to when such electrode plate is relatively smaller to the human hand. Nonetheless, the C_{SENS} values when proximity and touch sensing occur are approximately 20 pF. Values are above 20 pF for 3.5 cm when detecting touch.

7.2 COMSOL Simulation of Generated Electric Field of Capacitive Circuit sensing through Textile Channel

A simulation representing the sensing electrode with a conformal layer of PDMS and encased in a textile layer was created to observe the electric flux distribution visually. Such electric flux behaviour was discussed in previous experiments, but simulation results could visually explain the behaviour seen in previous experiments. Furthermore, it would provide information on how the PDMS and textile dielectric would affect the electric field – if at all. The simulation was built in COMSOL software and its method is detailed in Appendix F: COMSOL Simulation Methodology.

7.2.1 Simulation Setup and Motivations

The model shows a copper-polyimide electrode strip in the centre, with an approximate 40 µm layer of PDMS on top, with a hollow textile cylinder to represent the textile yarn knitted sleeve and cotton woven channel (Figure 58). Overall, this represented the layers and structure of the e-textile system created in this Thesis but localised to the sensing plate only to see its electric field distribution. The objective of the experiment built in COMSOL was to determine how touch and varying max proximity distances would affect the electric field distribution. Furthermore, if a capacitive reaction at particular lengths of the electrode would change the electric field distribution in particular ways - which could provide instructions such as interfacing at the centre of the electrode or at the edges, for example. Perpendicular to this is a cylinder block made from human skin characteristics in COMSOL to represent a human finger. Individual parts of the model were encased in a cube of air so that the experiment occurs in similar conditions to the lab-based experiments presented in this thesis. Parametric sweep data collection was applied to the human finger to move it

vertically to perform touch detection and proximity detection of 0.5 cm to 5.0 cm at 0.5 cm intervals. Also, it was applied horizontally to move the finger along the length of the electrode also in 0.5 cm intervals. These parametric sweeps were performed simultaneously when the model was run.

7.2.2 Results

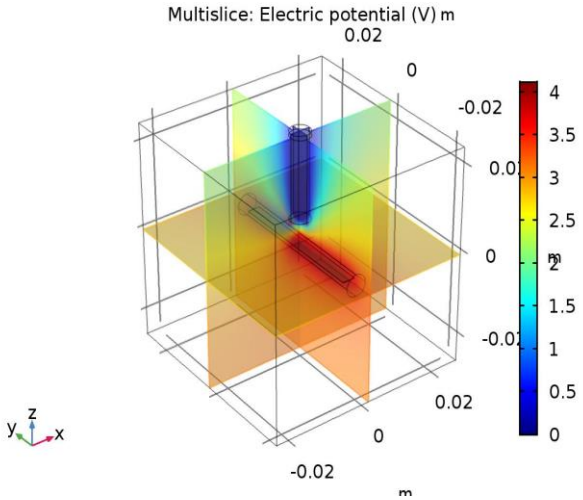

Figure 58 COMSOL Simulation result of sliced electric field distribution of capacitive external electrode with conformal PDMS packaging and textile layer

Simulation results suggested the generated electric field is strongest directly under the trigger object and radiantly reduced from the textile and the electric field is higher within the textile channel than external to it.

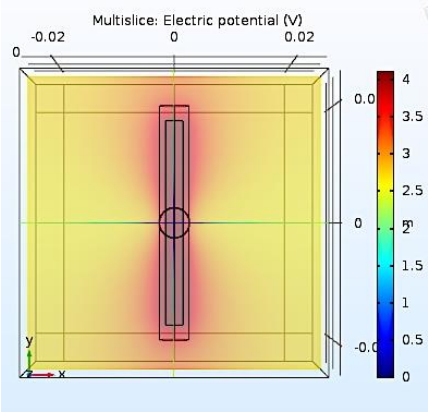

Figure 59 Above view of COMSOL simulation result showing electric potential strongest within the textile where the electrode is located and dissipates outwards

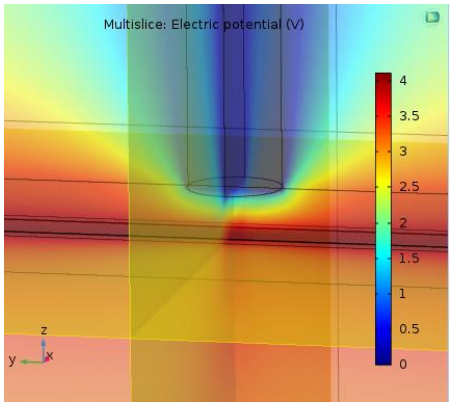

Figure 60 View of COMSOL simulation result showing human finger touching the e-textile electrode and the relative electric potentials

Overall, the COMSOL simulation results show that the electric potential increases as the finger gets closer to the e-textile electrode which agrees with electric field and triboelectric theory. Work is done by an external force against and electric field to move a unit charge to a point within the field. This increases the electric potential of that charge. Therefore, electric potential describes the work done in bringing an unit charge from infinity to a point in an electric field whilst keeping the charge in an equilibrium state. Simulation shows that the electric potential is strongest on the most conductive component which would be the copper on the electrode. It also indicates that the PDMS region also shows high electric potential readings. The variation of colours in the simulation indicates a non-uniform electric field in this experimental environment, indicating that the work done to bring a charge to a point in the field changes within the electric field. The behaviour of copper and PDMS can be explained by recent triboelectric theory (Mao, Geng, Liang, & Wang, 2015).

7.3.3 Analysis

The triboelectric effect is a form of contact electrification whereby two dissimilar materials generate a charge due to being pressed or brought into contact with each other. In recent years, a new mode of triboelectricity was introduced – single electrode mode. Here, one material acts as a triboelectric layer and the other material is not fixed - but acts as an electric potential reference within a region of space. With reference to this COMSOL simulation, the triboelectric single-electrode would be copper-PDMS combined and the reference electric potential material would be the human finger. The combination of PDMS and copper as a triboelectric single-electrode has been studied in literature (Li, et al., 2014) to form a triboelectrification layer. PDMS and copper are both negative-tendency charged materials compared to the human skin which is positive-tendency charged material. As more charge will be attracted to the copper-PDMS electrode, in addition to the combination of copper and PDMS, this increases the electric potential value near the electrode. The consequent non-uniform electric field, with the electric field strength increased nearer to the copper-PDMS electrode, indicates the improved ability for the sensor to detect the human finger trigger object. So, although the

simulation does not indicate that PDMS will act as a detriment to sensing the human hand – as PDMS is a greater negative-tendency charged material than copper – PDMS actually enhances the copper as a sensing electrode. This electrode would ultimately increase the sensitivity of the circuit it is connected to which will improve its ability to sense a trigger object.

Furthermore, when the human finger touches the e-textile, the location where this happens the electric field contour lines become more concentrated to signify field strength. Due to the COMSOL model's symmetry, it makes the electric field appear identical to other side of the human finger when it is directly in the centre. As the finger is towards one end of the electrode, the electric potential is still highest at the electrode the electric field strength becomes unevenly distributed and is greatest surrounding the finger. Although this COMSOL model is completed in ideal conditions, the results provide knowledge that irrespective of where the finger interfaces with the electrode it should not make a difference to the electrode's ability and efficiency to detect it and act as a capacitive sensor. The distance between the human hand and the electrode, along with factors such as electrode size and shape have greater influence than where the human hand is along the length of the electrode.

7.3 Underwater Experiment Evaluating Durability of PDMS Packaged Self-Capacitive Proximity and Touch Sensing Circuits

7.3.1 Background and Methodology

One method to test the durability of a packaging substrate for electronics that would need to function after aqueous contact is an aqueous immersion test. For electronic textiles that would be washed, an underwater test would be appropriate to observe how long the packaging substrate can preserve the functionality of the circuit whilst immersed and if it can still function whilst immersed. Hence, this can introduce underwater applications of wearable microsystems which have been explored in literature. Wearable systems that can operate underwater are needed in marine environments to monitor the physiological responses of divers (Gradl, et al., 2017), diver kinematics (Walker & Anderson, 2017), and its proximity to areas of aquatic life (Merchant, 2011). For example, underwater signal acquisition of cardiovascular behaviour of divers was the objective for Gradl et al. (Gradl, et al., 2017) who created a wearable current-based electrocardiogram (ECG) integrated into a fitness shirt. It was housed in plastic, and the circuit was a flat and rigid printed circuit board that could distort the underwater garment as its bends and flexes whilst in use. The circuits reported were only tested for 10 minutes, which does not imply it is suitable for longer underwater usage. Instead of rigid packaging, super-hydrophobic and flexible elastomer packaging has been considered more attractive (Sung, Cheng, & Fang, 2015) for better morphology whilst a diver is swimming and survival in aqueous environments. PDMS has been investigated as a micro-devices packaging substrate but it has yet to be tested for its durability in aqueous environments (Sung, Cheng, & Fang, 2015). Therefore, this presents a gap in literature that this thesis plans to cover through a variety of experiments.

Following these experiments, a 40.3 µm conformal 20:1 PDMS encapsulation was tested on five capacitive-based touch and proximity sensing circuits to test its functionality when immersed in water. This thickness of the PDMS conformal coating was confirmed by scanning electron microscope (SEM) image capture using the Zeiss EV0 50 XVP - *Figure 61*. This circuit has specifically been fabricated for electronic textile applications, made from a flexible substrate and 0402 packaged surface mounted components (SMDs). Based on previous experiments, component values on the circuit were chosen to enable touch and proximity for most reliable functionality within a textile environment. This revealed the need for an external electrode to the circuit, to enable dual touch and proximity detection. The underwater test did not feature the circuit integrated in the textile to observe the appearance of the circuit over the duration of the experiment.

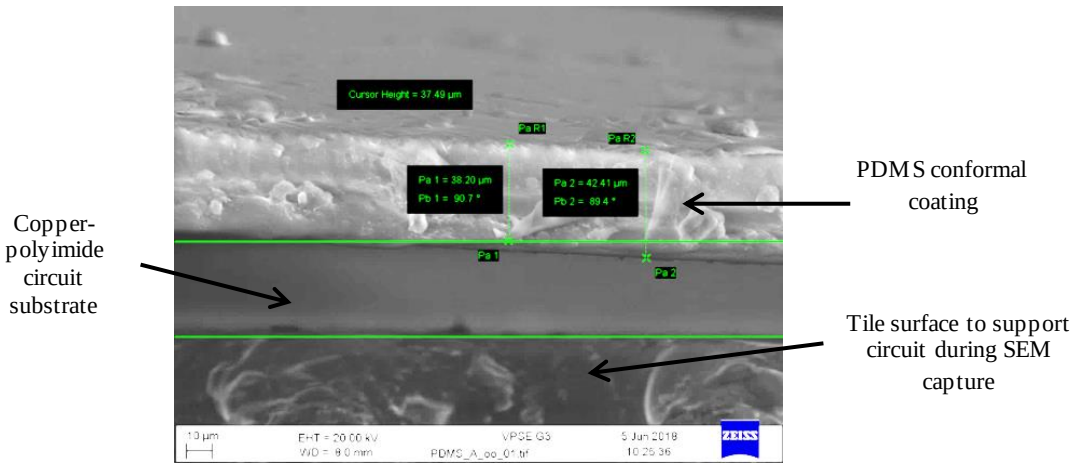

Figure 61 SEM image capture of averaged 40.3 µm conformal 20:1 PDMS averaged packaging of copper-polyimide flexible circuit substrate between two sections (Pa1 and Pa2)

Initially, three circuits were put into a plastic container with 300 ml volume of room temperature tap water and sealed in with an air-tight plastic lid. Each circuit could perform proximity and touch detection before being submerged underwater. To connect to power and ground, copper-enamelled wire was soldered onto the end pads and another cooper-enamelled wire was soldered onto the solder pad that would interface with the external electrode.

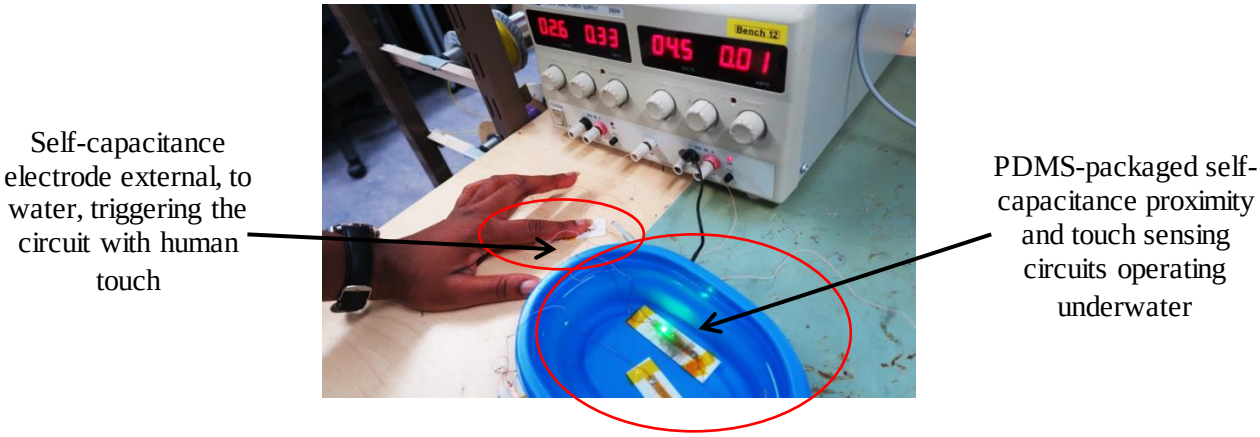

Figure 62 Photo of underwater experiment setup with PDMS-conformal coated circuit submerged in water container and external electrode

To check for functionality before immersion and for the remaining of the experiment, the same steps as in subchapter 4.5.2 Functionality Test were followed. Measurements were once per week for the first month, then subsequently once every month.

7.3.2 Results

The longest surviving proximity and touch sensing circuit with a 40.3 µm 20:1 encapsulation has demonstrated functionality after 6 months underwater. Not all circuits in the underwater tests have survived 6 months and results indicate that this is due to erosion and wear of the wires chosen to solder onto the circuit and not the PDMS encapsulation.

By the third month of experimentation there are no readings for Circuits A and B under test. This was because weak points in the wires were discovered on the copper wire connected to power on Circuit A when it snapped. This was likely due to weakness due to exposure to water and mechanical strain due to repeated bending whilst the circuit was connected to the oscilloscope per data collection. Due to the snapped wire, this prevented any readings from circuit A for the remainder of the experiment and future data for this circuit read zero. The same issue of weak copper-enamelled wire causing breakage occurred to circuit B on day 17. However, both power and ground wires have still survived on circuit C and has full functionality of the circuit sensing proximity and touch with an LED sub-circuit illuminating to add further visual confirmation of the circuit responding. This suggests that it is likely that the circuits still show functionality due to the PDMS, but their failure is more due to the weakness of the wires connected to power and ground – not the quality of encapsulation. By isolating Circuit C, the longest surviving circuit with the copper wire, result shows that over time the proximity sensing ability of the circuit declines as the duration of time underwater increases.

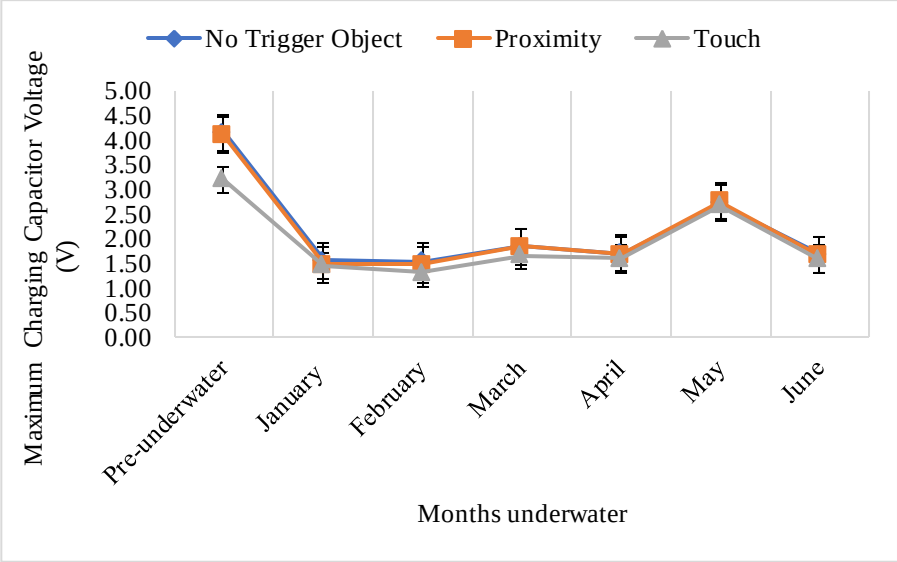

Figure 63 Underwater Test Graph showing maximum charging voltage of capacitive proximity and touch circuit C overall reducing as time underwater increases

As the number of months the circuit is submerged underwater increases, the difference in peak voltage for no trigger object, proximity, and touch detection decreases - with 1.56 % (2 d.p.) difference between no detection and proximity and 26.19 % (2 d.p.) difference between no detection and touch before going underwater, and 1.69 % (2 d.p.) and 5.92 % (2 d.p.) for the same criteria by 6 months. Ultimately, this result shows the circuits decline in differentiating between different detection types and therefore is a decline in functionality. Nonetheless, as the voltage for touch is lower for all months compared to no detection and proximity detection it is still functional as a touch sensor.

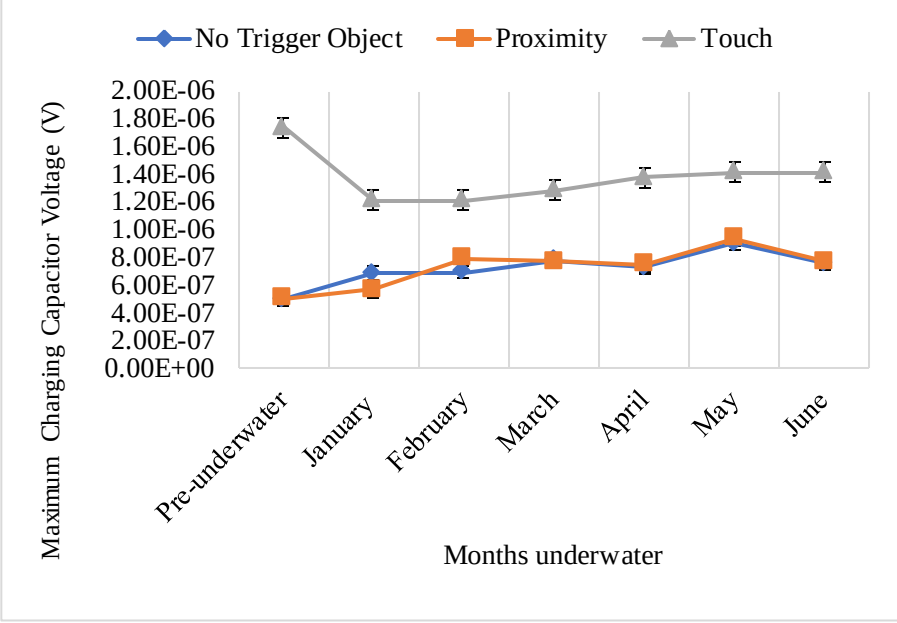

Figure 64 Graph showing comparison of total charging time of capacitive underwater circuit C with copper wires whereby touch is more distinctive than proximity sensing and detection of no trigger object (human hand)

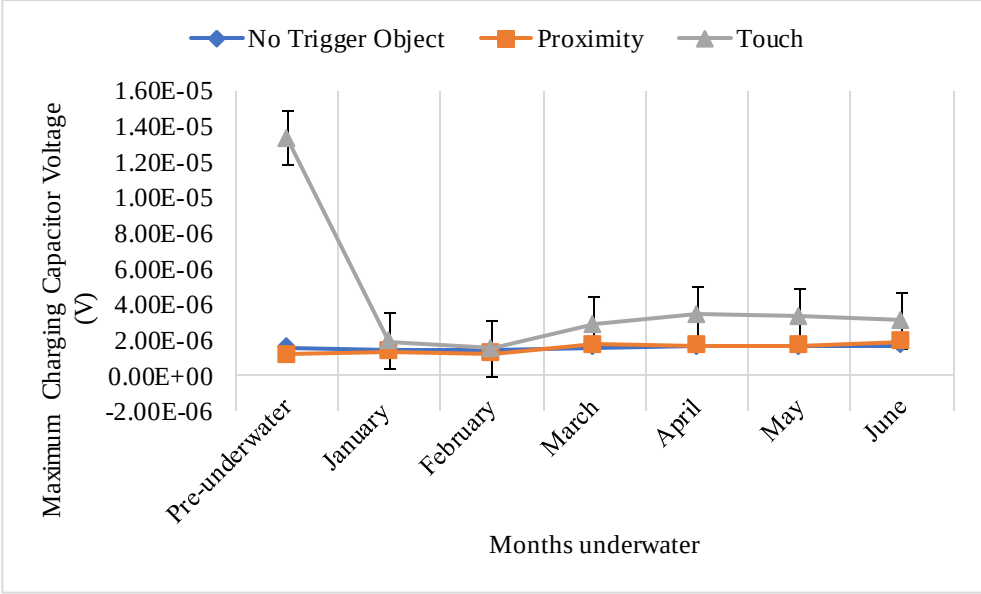

Figure 65 Graph showing comparison of total discharging time of capacitive underwater circuit C with copper wires whereby touch is more distinctive than proximity sensing and detection of no trigger object (human hand)

7.3.3 Analysis

Figure 64 and Figure 65 of the self-capacitance electrode at pin IN of the circuit overall show that as the duration of underwater submerge proximity detection ability of the circuit reduces. However, touch detection ability is still clearly observable, and this is shown graphically by the clear separation between data points for touch compared to no detection and proximity. Difference between 'no detection' and proximity detection is negligible from March for charging time whereas negligibility is observable for the complete 6-month duration for the discharge time. Despite the experimentally-validated choice of C_{CLIN} and C_{CPC} values, it seems that the PCF8883's chip ability to sense proximity is not optimally calibrated for underwater applications however seems capable for touch detection. The result that circuit can survive and still show detection ability after being in long contact with water, and being tested whilst underwater, shows promise for PDMS as an electronic packaging material for long-term underwater functionality. Reasons why the values in the graphs above did not remain steady over time is likely due to the chip's auto-calibration feature and being affected by being within a PDMS environment. PDMS' uneven porosity of the substrate creates an uneven dielectric and potentially varies how the chip can calibrate to its environment. With the additional electrode, a human hand can trigger the electrode that is outside of water but also the internal electrode that is on the circuit packaged in PDMS. Therefore, when the external electrode is interacted with, as it is joined by a conductive wire this causes charge to form on the internal electrode. Therefore, as the circuit is submerged underwater whilst being tested for functionality, consequently, water movement also affects auto-calibration as water becomes dielectric.

As a result, two more circuits were tested but with a silk-encapsulated multistring copper wire. The first circuit failed due to a tear in the PDMS prior to water immersion, which caused water

to reach the electronics. This ultimately meant this first circuit died upon water contact. However, the success of the second indicates the likely behaviour of the first if the PDMS packaging was not damaged and provides promising result that this change in wire is a better choice than the copper-enamelled wire. Out of the two, the longest surviving circuit is 2 weeks. The circuit with the silk-wires likely failed earlier than the longest-surviving circuit with the pure copper wire due to electrolysis. Electrolysis is the decomposition of a chemical compound into ions, within a solution due to an electric current passing through the solution (Rossmeisl, Qu, Zhu, Kroes, & Nørskov, 2007). Tap water can have traces of salt, which has ions in its solution. Although copper is a metal that does not react with water, it is highly conductive. When the circuit is powered underwater, the current travelling through the ground and power wires causes it act like an electrochemical cell in electrolysis conditions. It subsequently oxidises quickly and loses its conductivity over time – reducing the life of the copper.

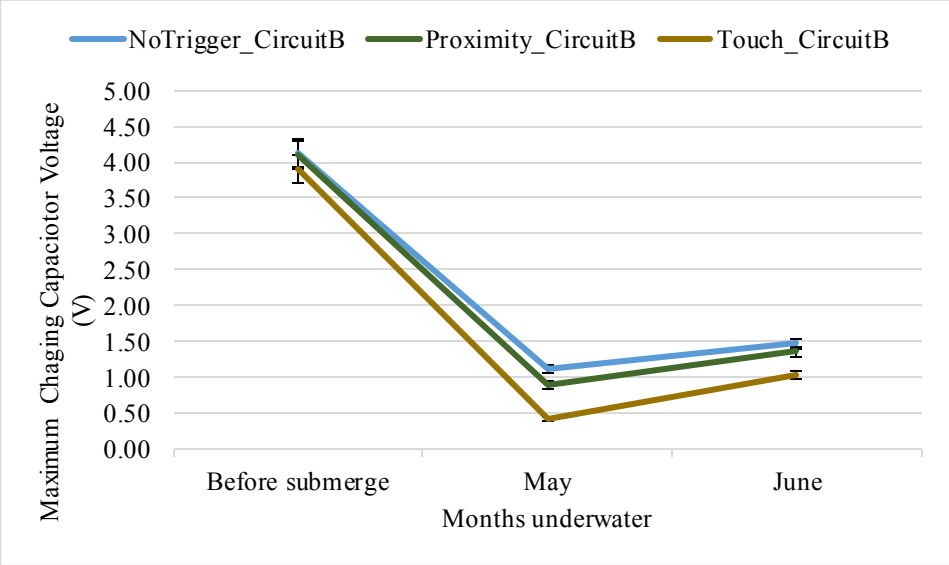

Figure 66 Graph showing comparison of peak charging voltage of capacitive underwater circuit B with silk-copper wires when interacting with a trigger object (human hand)

As seen in graphs Figure 66 to Figure 68, the values for max voltage, rising capacitance, and falling capacitance do not follow a clear trend. This was expected, as it would reveal the functionality of the calibration feature of the PCF8883US. The PCF8883US auto-calibrates to its environment in real-time to counter against parasitic capacitance.

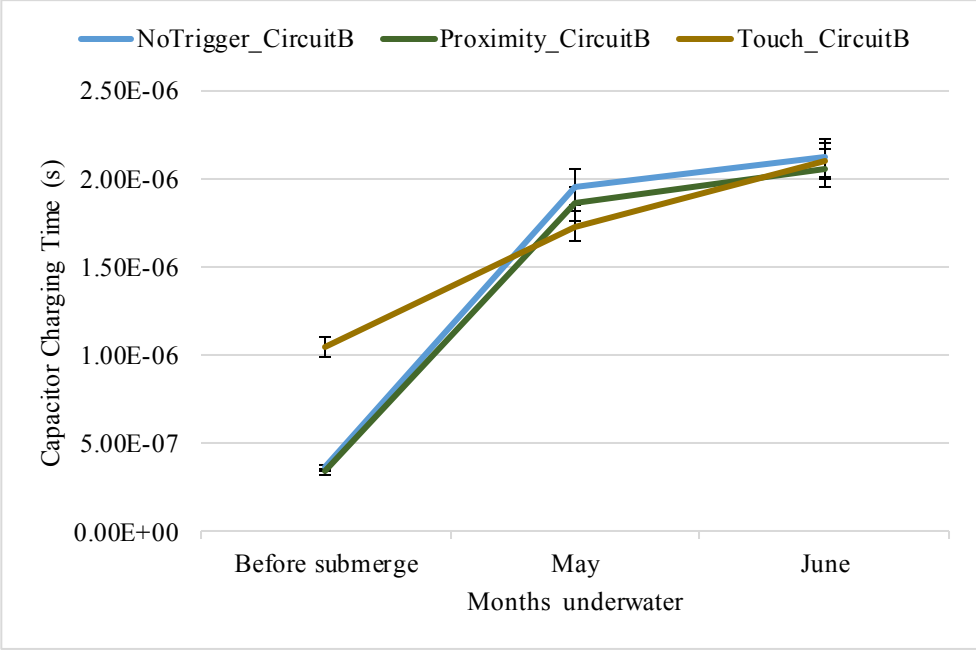

Figure 67 Graph showing comparison of total charging times of capacitive underwater circuit B with silk-copper wires when interacting with a trigger object (human hand)

Additionally, as the environment changes dynamically, and the quality of connection of the wires to the power supply is not guaranteed to be the same due to mechanical wear. Therefore, a fair judgement on the whether the circuit is still functioning is if there is any working operation of the IC chip and circuit or not when submerged underwater. Without encapsulation or a tear in the encapsulation, the circuits would fail due to a lack of protection from water. This is evident circuit A, with a likely instantaneous failure when submerged underwater.

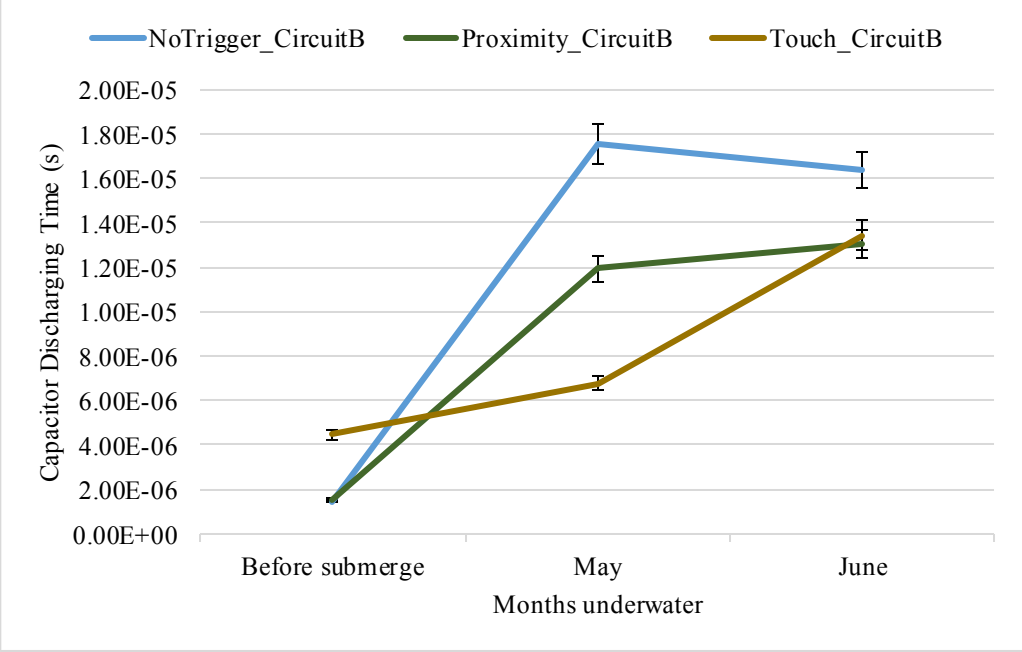

Figure 68 Graph showing comparison of total discharging times of capacitive underwater circuit B with silk-copper wires when interacting with a trigger object (human hand)

Overall, since experiment results show circuit operation surviving maximum 6 months, this is evidence of successful PDMS encapsulation of the circuit and that it is highly durable. Overall, results give promising evidence that a PDMS-based packaging substrate, certainly 20:1, can allow microsystems to operate and survive underwater.

7.4 Washing Experiment Evaluating Robustness of Integrated Conformal PDMS Packaged Capacitive Proximity and Touch Sensing E-Textile Circuit

7.4.1 Self-Capacitance Theory applied to Textile Environments

Following these experiments, an average 40.3 µm conformal 20:1 PDMS encapsulation was applied to four identical capacitive-based touch and proximity sensing circuits to test its functionality after multiple washing cycles. Proximity was defined as a stretched-out hand with a nominal detection distance of 2.0 cm and touch was defined as a finger pressing onto the sensing electrode portion of the circuit. The sensory circuit manufactured in this work is sensing through the conformal PDMS and through fabric layer. Aforementioned, it relies on human body capacitance via a hand to act as the second sensing plate. An electric field is created between the human hand and the sensing electrode, which is a flexible copper-film connected to the proximity sensor circuit via wire. The copper sensing plate when provided a voltage from the circuit becomes a self-capacitance sensing electrode and the human hand acts as a trigger object that the circuit can sense its proximity and touch.

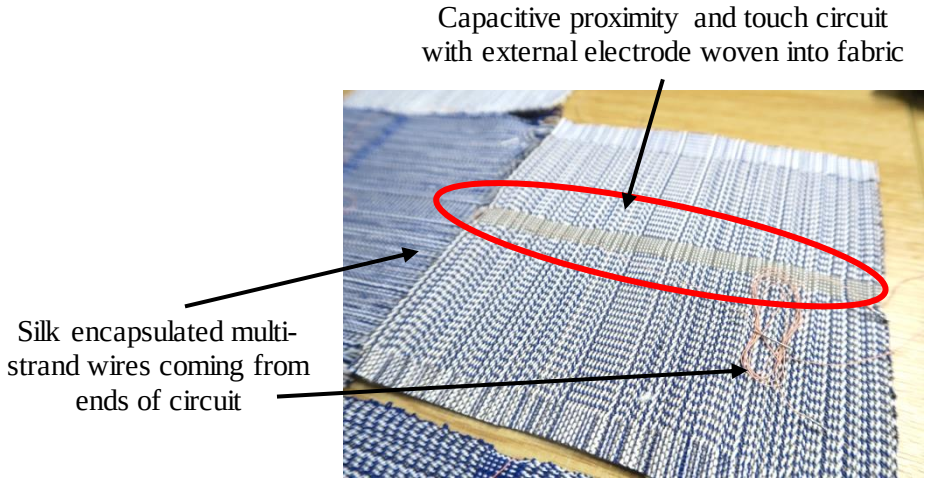

Figure 69 Photo of e-textile samples annotated with power, ground, and integrated circuit

The PCF8883US on the circuit has the external sensing electrode at its input connected to an internal RC timing circuit. The discharge time of the internal RC timing circuit is compared to a synchronized, second internal RC timing circuit that is used as a reference. Proximity and/or touch are registered by the IC chip when the discharge time is longer than the reference RC timing circuit.

Hence, the time delay for the IC chip when it responds to a proximity or touch equivalent signal is known as the time constant. It takes approximately five time constants during the transient response to fully charge or discharge a capacitor before reaching a steady state – called the rise time and fall time respectively. The voltage the capacitor charges to be is at a percentage change to the maximum supplied voltage. This means that as the capacitance on the input pin i.e. the copper sensing electrode integrated into the textile, increases then the discharge time also increases. This will cause an increase in rise time, fall time. Additionally, as the electric field strength between the copper electrode and the human hand increases as hand moves closer to the electrode it is expected that the rise time and fall time will increase. As a measure of the e-textile's sensing efficiency it is also anticipated that the amount of charging voltage will decrease as the number of washing cycles increases. These three factors –rise time, fall time, and charging voltage - of the self-capacitance copper electrode is obtained by the DSO3062A digital storage oscilloscope by an RC curve and indicated the sensing efficiency.

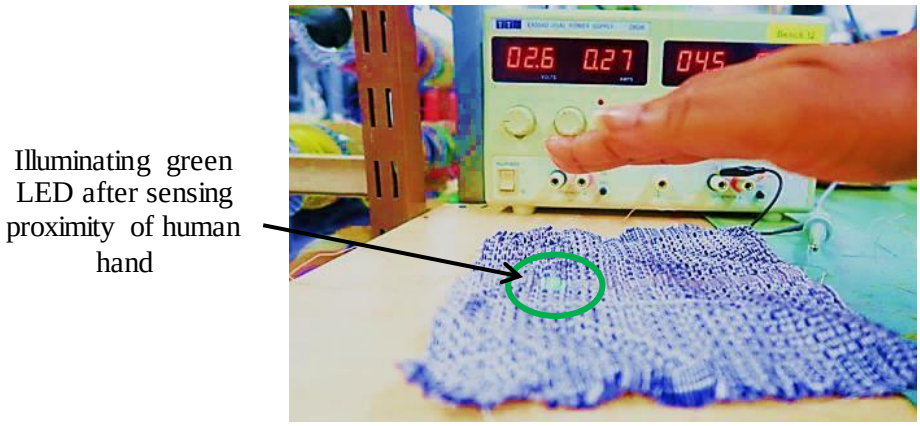

Figure 70 Photo of e-textile circuit green LED illuminating after being washed as visual feedback of functionality of proximity sensing

7.4.2 Experiment Methodology

Washing machine experiments were conducted in the same consumer washing machine used to calculate the detergent and fabric conditioner ratios. This commercial washing machine was the Bosch Exxcel Serie 4 Washing Machine WVD24520GB. Compliant with the textile washing standard ISO 6330:2012 ((ISO)), this was a type A washing machine i.e. a front-loading horizontal axis washing machine. The 40.3 µm-thick PDMS packaged sensory circuits were integrated into a textile via weaving and washed with 2 kg of cotton fabrics. This weight was compliant to ISO 6330:2012.

The e-textiles under test were subjected to three different commercial washing settings: SuperQuick (15 mins, 30 °C), Silk/Delicates (37 mins, 30 °C), and Wool/handwash (42 mins, 30 °C). These were chosen to represent typical washing settings for textiles (Kim & Jeong, 2011). 30 °C temperature is typically used for washing as most textiles are sensitive to heat. Each have different

spin time changes throughout the cycle making each washing cycle different in degree of mechanical abrasion.

Washing Setting	Explanation
SuperQuick	Short, 15 min cycle typically set at the highest washing speed of 1200 rpm. Typically used on cotton textiles
Silk/Delicates	Fabrics spun at the lowest speed of the washing machine (400 rpm), used to wash silk, viscose, and satin textiles.
Wool/Handwash	Fabrics spun at lowest speed at washing machine (400 rpm), to prevent woolens from matting due to moisture and heat the washing machine alternates from spinning and standing still.

Table 17 Washing Settings from Bosch Exxcel Serie 4 Washing Machine WVD24520GB

There was one circuit per each e-textile, and they were separated depending on the washing cycle setting they were examined against. The samples under test were put into the washing machine with approximately two-thirds of the 2 kg sample of cotton textiles/towels.

Figure 71 Annotated photo of e-textile samples in washing machine

The same detergent and fabric conditioner used in the Contact Angle and Aqueous Permeability experiments were used. For each experimental trial, 37 ml of detergent was poured into cap and placed inside the washing machine with the textiles as specified by the product manufacturer. The detergent was poured after the final third of the cotton textile/towels were placed on top of the e-textile samples in the washing machine. This was done so the e-textile samples would be in the middle of the drum and the concentrated detergent would not seep through the e-textile initially.
35 ml of fabric conditioner was put in the middle drawer of the washing machine – this amount is specified for a 4-5 kg wash but was appropriate also for the 2-3 kg wash occurring in this experiment.

The washing settings selected for this test was initially the super quick setting at an 800 rpm speed, 30 ^{O}C, for 15 minutes – equivalent to cycle type 3N. Due to the results of this washing cycle (see results section), other washing tests at the lowest possible washing spin speeds were chosen. These were 30 ^{O}C, 400 rpm for approximately 37 minutes which was equivalent to the silk/delicates washing machine setting and 30 ^{O}C, 400 rpm for 42 minutes which was equivalent to the wool/hand wash setting. After each wash, the circuits were flat dried on a stainless-steel drying rack – stated as drying method C in ISO 6330:2012 ((ISO)). Then, once dried for 1 hour and 30 minutes the circuits were tested for proximity and touch sensing functionality via an Agilent Technologies DSO3062A digital storage oscilloscope.

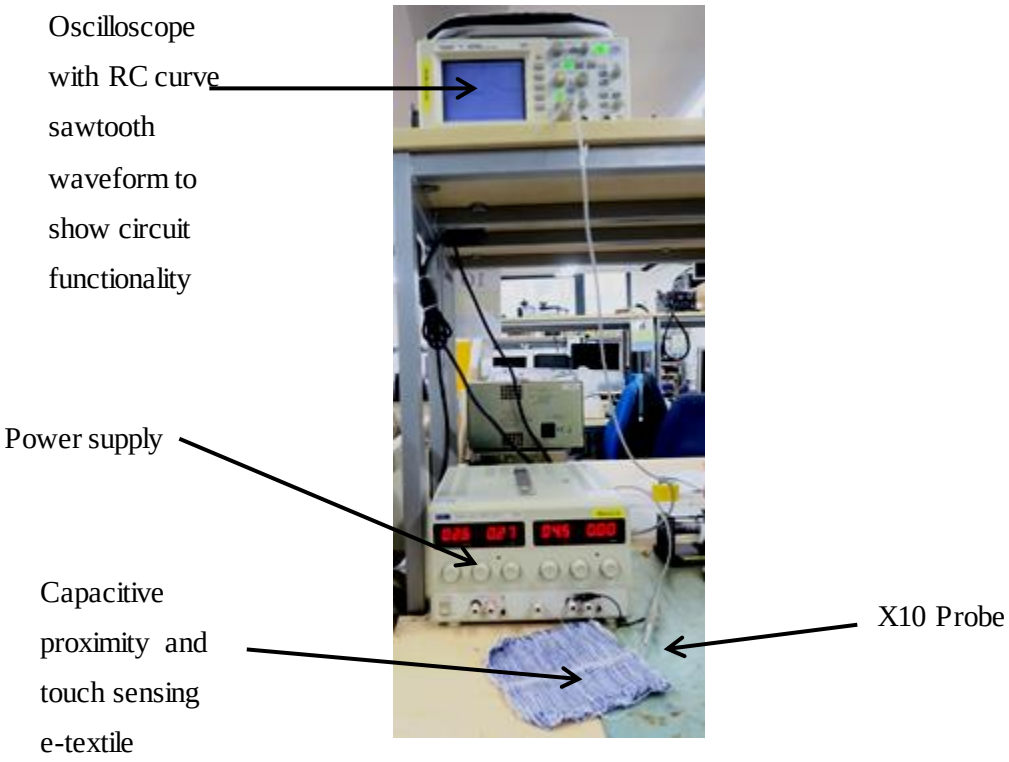

Figure 72 Photo of washing test functionality check setup of capacitive proximity and touch sensing woven electronic textile

Each e-textile circuit was powered via an EX354 Dual Power supply set to 4.5 V and maximum 0.03 A current. An X10 probe connected to the DSO3062A digital storage oscilloscope had its clip to circuit's ground and its hook to a wire soldered onto copper electrode before it was integrated into a textile, it is possible to acquire the RC characteristics of the copper self-capacitance sensing electrode. This RC characteristic is produced by the approximately 4.5 V source provided through the IC chip charging the self-capacitive copper electrode through a 6.8 kΩ resistor also at the input. The PCF8883US proximity chip used in the circuit has the external sensing electrode at its input connected to an internal RC timing circuit. The discharge time of the internal RC timing circuit is compared to a synchronized, second internal RC timing circuit that is used as a reference. Proximity and/or touch are registered by the chip when the discharge time is longer than the reference RC timing

circuit. Hence, the time delay for the proximity chip when it responds to a proximity or touch equivalent signal is known as the time constant. It takes approximately five time constants during the transient response to fully charge or discharge a capacitor before reaching a steady state.
These three factors –rise time, fall time, and charging voltage - of the self-capacitance copper electrode is obtained by the oscilloscope by measuring the RC curve and using this to determine the sensing efficiency. This functionality check was done after the first wash to check survival then with every fifth washing interval i.e. 5, 10, 15, 20 etc. This methodology was used in previous literature, (Merritt, Nagle, & Grant, 2009), (Varnaitė & Katunskis, 2009) , (Kazani, Hertleer, De Mey, Schwarz, Guxho, & Van Langenhove, 2012), (Kaappa, Joutsen, Cömert, & Vanhala, 2017) to test electronic textile functionality after multiple washing cycles to evaluate durability and robustness. Values for rise time, fall time, and max charging voltage were recorded five times per reading for each e-textile under test. These values were then averaged before put into graphs. The objective of this experiment was to reach or exceed 50 washing cycles, which is the most recorded in literature - at the time of writing.

7.4.3 Results

Looking at the difference between the e-textiles before they were subjected to washing tests (Figure 73) compared to after (Figure 74), we can visibly deduce that the integrated circuity has experienced bending, twisting, and levels of mechanical contortion. The e-textiles, once dried, did not return to a completely flat state and soft state. This is likely due washing the e-textile multiple times in a very short time period, causing the textile to contort. In comparison, whilst the circuits for the underwater tests which had copper wire snapped due to water damage and erosion, the silk-encapsulated multi-strand copper litz wire used in the washing test snapped due to mechanical abrasions of the washing machine. Experiment results suggest that the cause of failure of the circuits underwater was not the PDMS packaging but the weak-points of the copper wire.

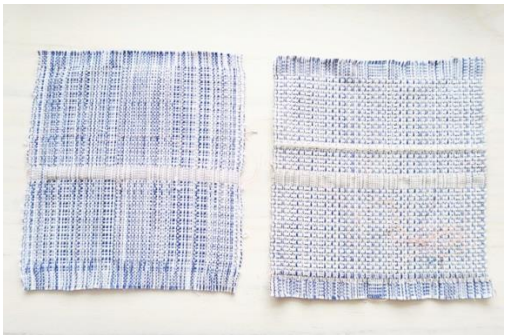

Figure 73 Photo of a selection of capacitive proximity and touch sensing e-textile samples before washing

Figure 74 Photo of capacitive proximity and touch sensing e-textile samples after washing showing the sample stretched out (left) and sample deformed shape after washing cycle (right)

Before subjected to washing in the washing machine, the functionality of all the e-textile samples under investigation were verified by the DSO3062A digital storage oscilloscope with the generation of the RC curve and measurements of its rise time, fall time, and charging voltage (V_C) - in accordance to theory and from subchapter 4.3 PCF8883 Capacitive Proximity and Touch Sensing of Human Hand Sensing Operation. Furthermore, it was anticipated that the maximum charging voltage (V_C) of the RC curve will not match the supply voltage (V_{SS}) value - which would occur in an ideal case. This is because some energy is stored in the capacitor at input pin of the circuit. This is due to lost energy from the capacitor used to function. This explains why the initial maximum charging voltage of all the e-textiles is less than the supply voltage of 4.5V.

With the experimental hypothesis and RC curve theory, as human hand gets closer to the copper sensing electrode the rise time and fall time increases whilst the peak capacitor charging voltage (V_{MAX}) decreases. However, Figure 75 to Figure *77* shows overall the maximum charging voltage decreasing as the number of washes increases. This occurs for non-detection and successful proximity and touch detection of a human hand. The likely reason for this is damage to the circuit as otherwise it is expected that the voltage difference to vary negligibly if not interfacing with water or not mechanically deformed. The potential cause of this decline could be damage to the encapsulation. For the first two circuits under test, which were washed together for 15 minutes at 800 rpm at 30°C, both circuits no longer functioned after the first wash. The fact that both circuits failed at the same time whilst being washed under the same conditions indicates that other e-textile samples would have failed. The washing speed of 800 rpm was perhaps too high and was presumed to impose detrimental mechanical abrasions and forces. Due to results from the contact angle and aqueous permeability tests, the failure was likely not due to the hydrophobicity of the packaging but the mechanical strain of the washing cycle process. Therefore, subsequent tests conducted washing tests at the lowest spin speed of the washing machine – 400 rpm. For washing tests completed at 400 rpm at 37 mins and 42 mins at 30°C these circuits survived between 10 to 15 washes. This is the same as that reported in recent literature for washing e-textiles, (Satharasinghe, Hughes-Riley, & Dias, 2018), with photodiode chips woven into textiles failing between 15 to 20 washes – another way of describing 10-15 wash survival. However, compared to work reported by Satharasinghe et al., the washing test reported in

this thesis had detergent and fabric conditioner in the wash, was compliant with ISO 6330:2012, and importantly did not use a wash bag. It was reported in this literature that a wash bag is a contributing factor that helped the e-textile survive in the wash due to structural support from the bag and reducing mechanical stresses on the e-textile within it. Therefore, it makes the washing test reported in this thesis more impressive as it agrees with the state-of-the-art but shows that the e-textile system produced in this thesis is more robust as it experienced more mechanical agitation. The touch and proximity sensing efficiencies of all the e-textiles under test were compared:

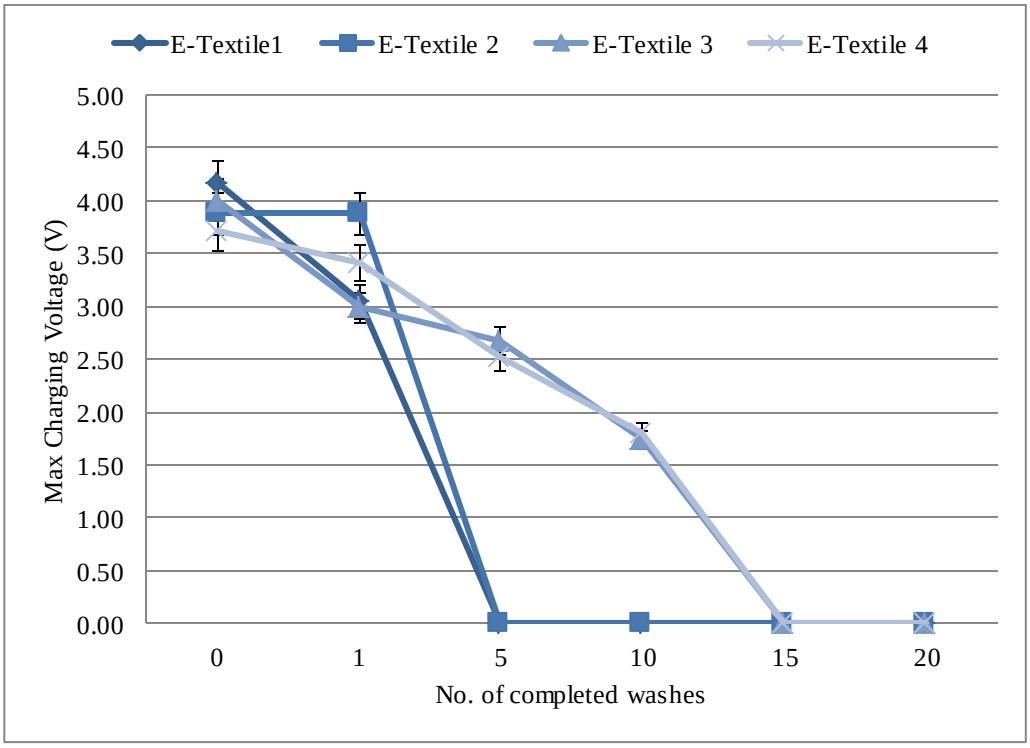

Figure 75 Graph comparing maximum charging voltages of e-textile circuits after being washed in successive cycles when there is no detection of a trigger object (human hand)

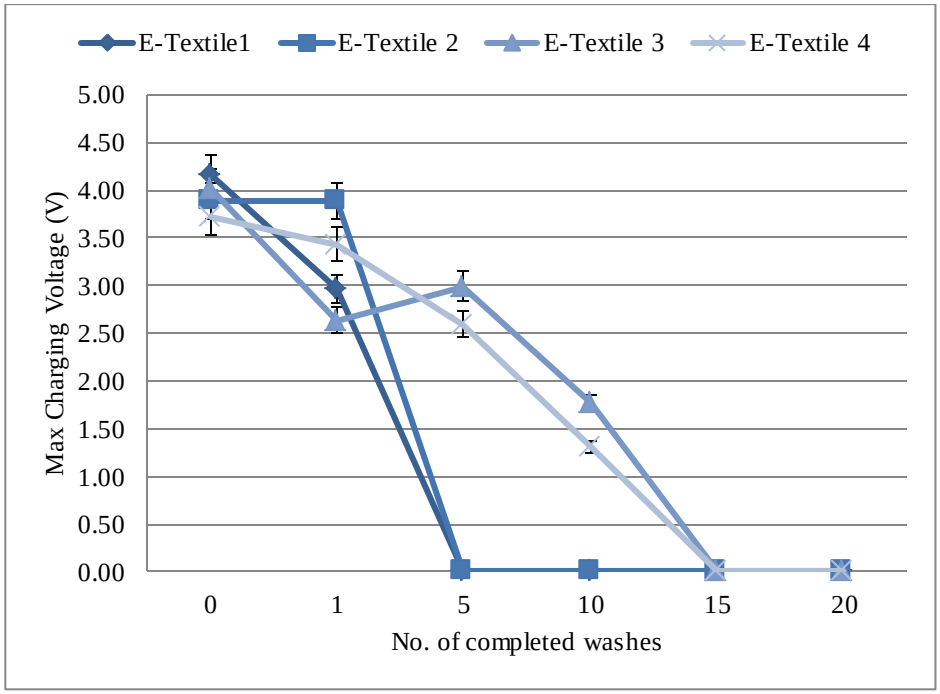

Figure 76 Graph comparing maximum charging voltages of e-textile circuits after being washed in successive cycles when there is proximity detection of a trigger object (human hand)

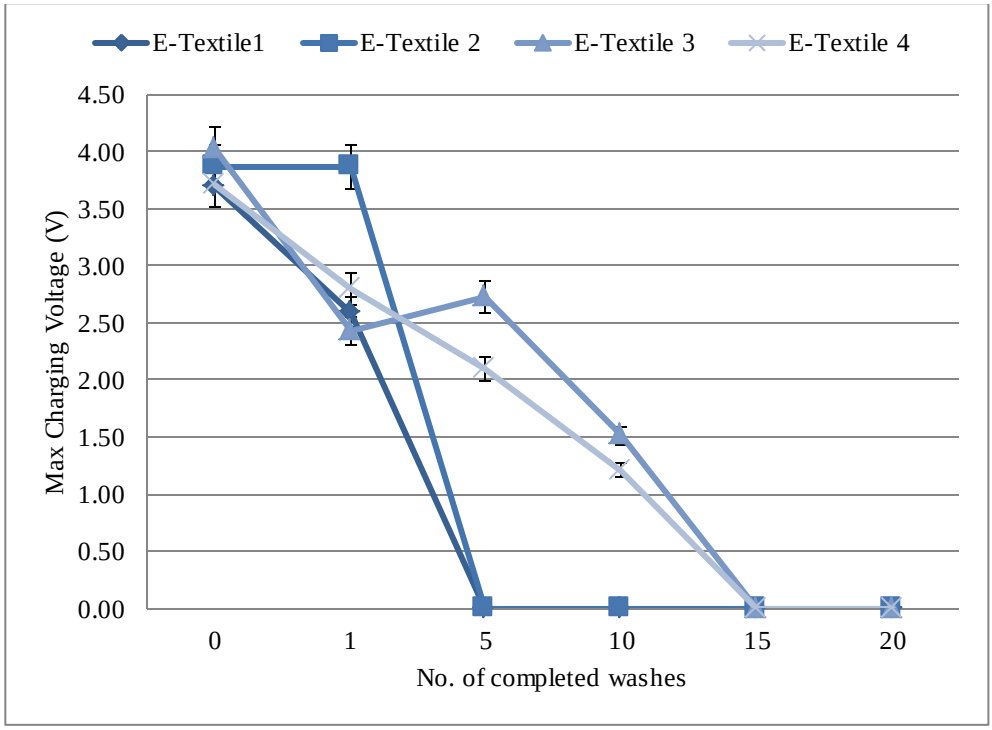

Figure 77 Graph comparing maximum charging voltages of e-textile circuits after being washed in successive cycles when there is touch detection of a trigger object (human hand)

The error bars on these graphs show the percentage error for each data point, which is an average of five readings. Examining the maximum charging voltage for proximity and touch detection (Figure 75 to Figure *77*) the graphs also reveal that some washing settings are more detrimental than others. With

the longest surviving textiles – E-textile 3 and 4 – their rate of change of difference suggests one washing setting is more detrimental than the other. Both e-textiles were washed at a lower washing spin speed at 400 rpm but at different washing settings. The washing machine manufacturer states the difference between silk/delicates (e-textile 3) and wool/handwash (e-textile 4) settings is alternate pause and spin motion, thus a difference in mechanical stress experienced by the e-textile under test. As the number of washing cycles increases, the difference between the e-textile 3 and e-textile 4 increases until the circuits stop functioning which is represented on the graphs as 0 V. Yet, as the rate of change for maximum charging voltage between the 1st and 5th wash is greater for e-textile 1 and 2 compared to 3 and 4 this suggests that the washing settings for e-textiles 1 and 2 contribute to a faster decline of circuit performance and functionality over time.

As expected, as the number of washing cycles increase, the rise and fall time of the generated RC curve increases. However, Figure 78 to Figure 81 also shows that as the e-textiles are washed for longer, the sensing functionality of the circuit becomes increasingly limited. In fact, one sensing functionality increasing declines with each wash – proximity. This is supported by the RC curve rise and fall time values in the washing test. The results show that 'touch' has a greater rise and fall time value compared to 'proximity' and 'no trigger object' values which appear negligible on the graphs. By isolating results for e-textile 3 and 4 which survived the greatest number of cycles and operated at the lowest washing cycle rotary spin speed of 400 rpm, it is observable that the circuit behaves better as a touch sensor rather than a proximity sensor due to the washing process.

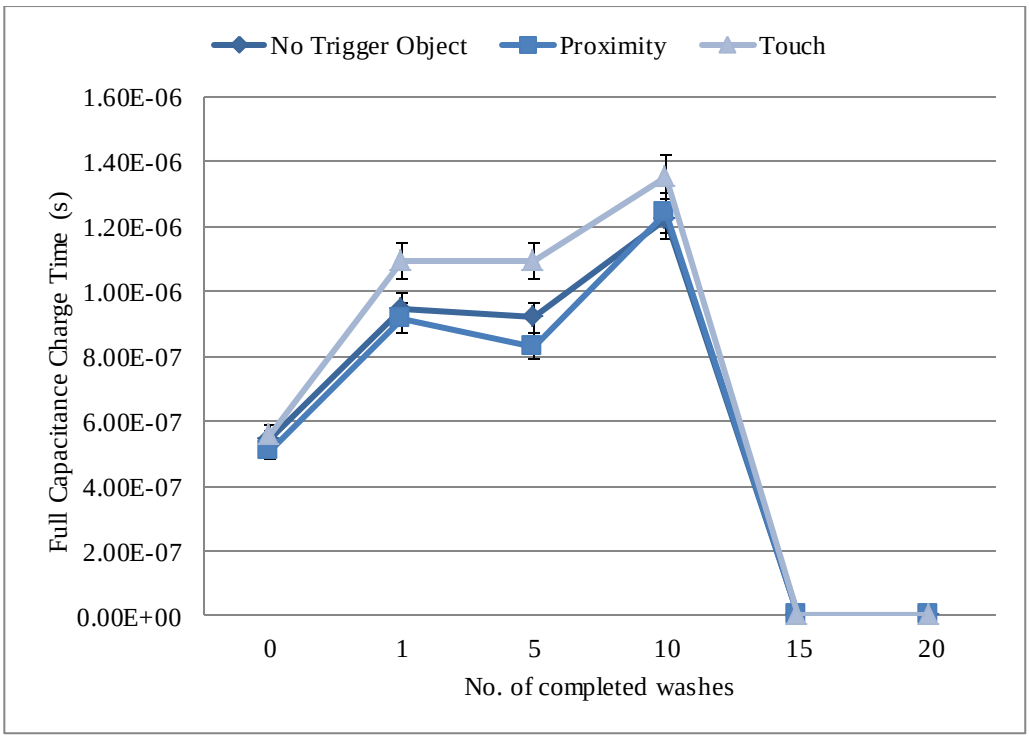

Figure 78 Graph comparing rise time (full charging time) of e-textile 3 capacitive circuit when there is no detection, proximity detection, and touch detection of a human hand after multiple washing cycles

Looking at the percentage change in rise time values in Figure 78, with e-textile 3's first wash the rise time proximity detection value increases by 81 % and on the tenth wash 145 % compared with before washing. Compare this to touch, whereby for the first wash the change is 95 % and on the tenth wash becomes 142 % compared with before washing. By looking at *Figure 79* the same behaviour shows that the capacitive copper sensor plate takes longer to discharge with more washing cycles - which is an indication of the speed at which it becomes able to sense a trigger object i.e. human hand.

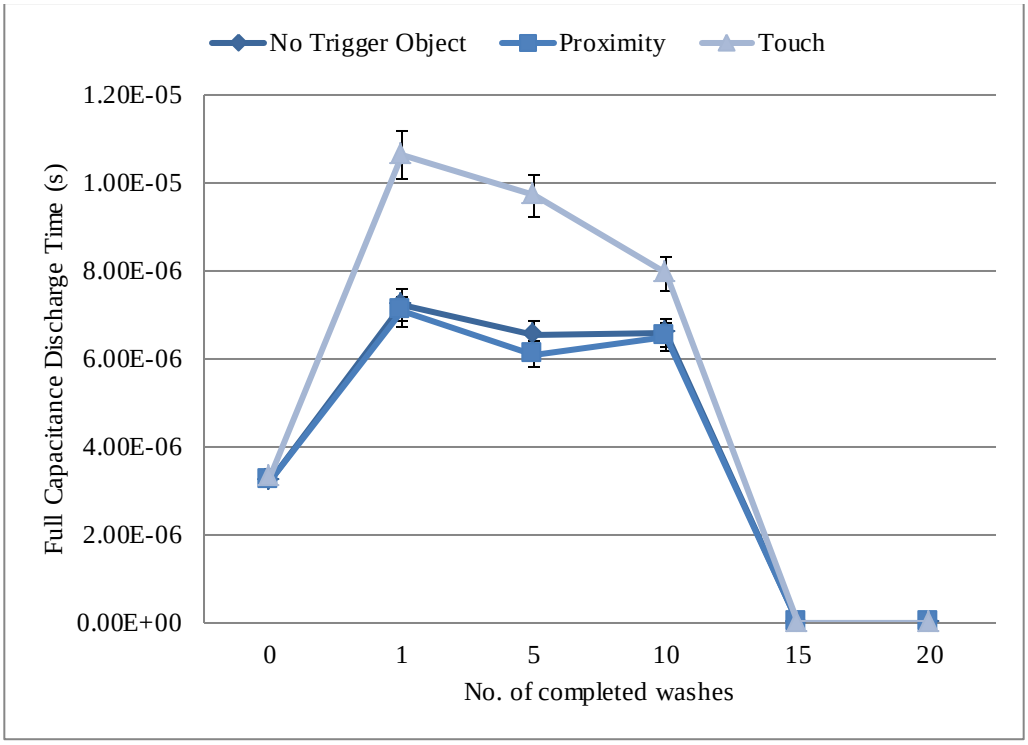

Figure 79 Graph comparing fall time (full discharging time) of e-textile 3 capacitive circuit when there is no detection, proximity detection, and touch detection of a human hand after multiple washing cycles

For fall time values in Figure 79, there is a 118 % change in fall time for proximity detection comparing the before washing value with the first wash and a 100 % change compared to the tenth wash. Compared to touch detection, whereby there is a 220 % change in fall time for proximity detection comparing the before washing value with the first wash and a 139 % change compared to the tenth wash. Regardless of these significant increases in rise time and times, the circuit is still functioning as expected. This is because capacitive theory suggests percentage change to be greater for touch as the electric field concentration is stronger. This is due to the zero distance between plates of the capacitor- the integrated copper electrode and human hand. The increase in rise time value means that the time taken for the internal capacitor connected to the copper sensor plate at the IC's input pin takes longer to charge. Therefore, the results could deduce that independent of the washing cycle duration but likely dependent on the washing machine spin speed and temperature - the process of washing reduces the ability of the circuit to sense a trigger object. Consequently, it becomes harder for the circuit to detect the proximity of a trigger object compared to touch.

The consistency of this result is also shown with e-textile 4 - whereby the rise and fall times of the circuits under test steadily increase with increased washing cycles. The circuit performs touch detection more efficiently than proximity sensing with increasing number of washes, as revealed by the percentage differences. Referring to Figure 80, e-textile 4's first wash the rise time proximity detection value increases from the before washing value by 64 % and on the tenth wash 216 %. Compare this to touch, whereby for the first wash the percentage changes from before washing is 202 % and on the tenth wash becomes 230 %. These values are much greater than that for proximity sensing. Apart from the data point on the fifth wash (Figure 80), touch produces a clear difference and hence longer discharge time compared to proximity and no trigger object trend lines. This touch data point on the fifth wash appears to be an anomaly, but appears again on the fourth e-textile shown in Figure 81.

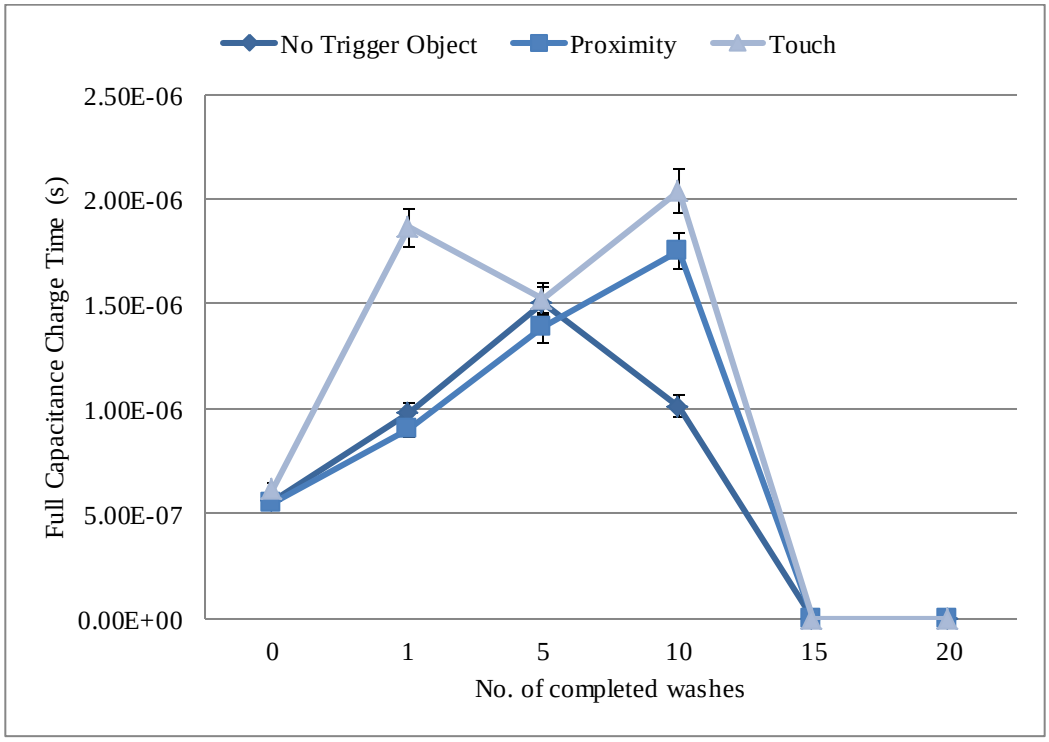

Figure 80 Graph comparing rise time (full charging time) of e-textile 4 capacitive circuit when there is no detection, proximity detection, and touch detection of a human hand after multiple washing cycles

The same restorative behaviour is noticeable on the fall time graph for e-textile 4. This anomaly could be due to a variable oxidized layer on the sensing electrode integrated into the textile during the drying process.

On Figure *81*, touch detection is even more distinguishable by the proximity chip compared to proximity detection. Nonetheless, this ability for the proximity chip to detect touch and proximity declines with successive washing cycles until it stops functioning which is shown through the general negative correlation trend lines for touch and proximity.

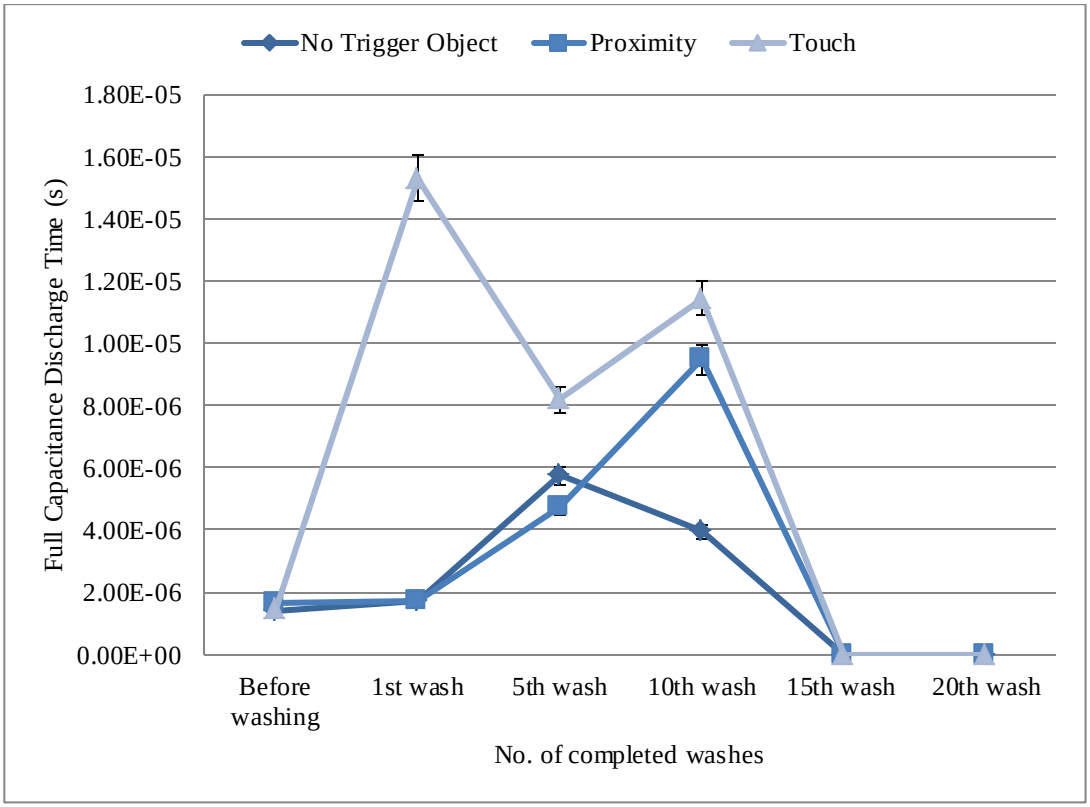

Figure 81 Graph comparing fall time (full discharging time) of e-textile 4 capacitive circuit when there is no detection, proximity detection, and touch detection of a human hand after multiple washing cycles

In comparison, for e-textile 4's first wash the rise time touch detection value increases from the before washing value by 3 % and on the tenth wash 47 8%. Compare this to touch, whereby for the first wash the percentage changes from before washing is 949 % and on the tenth wash becomes 684 %. Although the percentage change seems very high, this is actually a positive indicator at how successful the circuit is at detecting a trigger object compared to when there is no trigger object detected. An important observation from this experiment is the ability to predict when the e-textile would stop functioning when analysing the collected rise and fall time data. Agreeing with the experimental hypothesis and RC curve theory, as the human hand gets closer to the copper sensing electrode the rise time and fall time increases whilst the charging voltage (V_{MAX}) decreases. At the tenth wash, the fall and rise times for proximity and touch sensing appear to be similar before it fails. This observation appears to hold for all e-textiles under test and statistically supported by looking at percentage difference. Examining the data for Figure 78 and Figure 80, E-Textile 3 has a 17.7 % percentage difference between proximity and touch rise times after the first wash compared to an 8.6 % percentage difference after the tenth wash. Whilst E-Textile 4 has a 69.2 % percentage difference between proximity and touch rise times after the first wash compared to a 15.3 % percentage difference after the tenth wash.

7.4.4 Analysis

Consequently, experimental results provide an indication the e-textile is likely to fail when the difference between rise and fall times for proximity and touch detection becomes its smallest. This is an interesting result, as when this behaviour is observable it would suggest the e-textile circuit will not survive and hence no longer have functionality if subsequently washed. This behaviour is also indicated by the RC curve waveform captured by the oscilloscope.

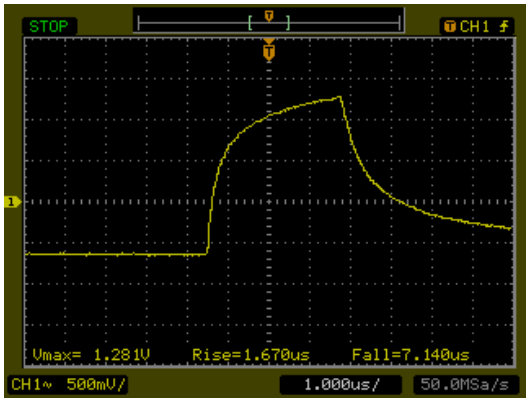

Figure 82 Example oscilloscope waveform of e-textile 4 after 10 washes with no trigger object detection

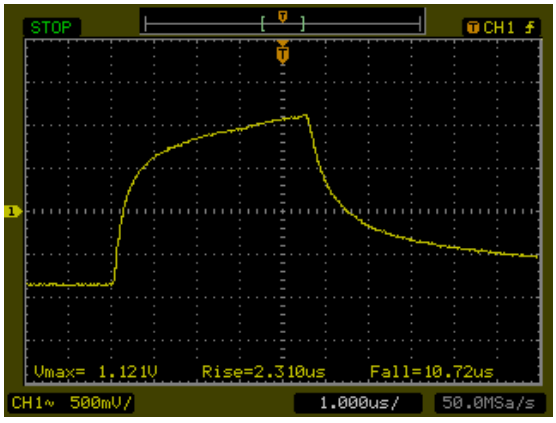

Figure 83 Example oscilloscope waveform of e-textile 4 after 10 washes with proximity detection of a human hand

The detrimental washing cycle effect on the e-textiles' functionalities is clear when compared the RC waveforms of an e-textile that has not been washed to that has been washed 10 times. The sawtooth waveform shapes in Figure 82 to Figure 84 show the capacitors' transient response ending prematurely and not appearing to reach a steady state response before the capacitor discharges. Nevertheless, the failure of the circuits in the washing test can also be due to bending and twisting of the circuit during the washing test. Figure 74 showed how the e-textile can be soaked and scrunched through the washing cycle process when washed with other textiles, rotary spin speed, and centrifugal force of the washing machine. This strain upon the wires is caused by the circuit being crushed and

wires caught in-between folds of the other textiles causes it to be pulled off the e-textile circuit in the washing machine during the cyclic motion.

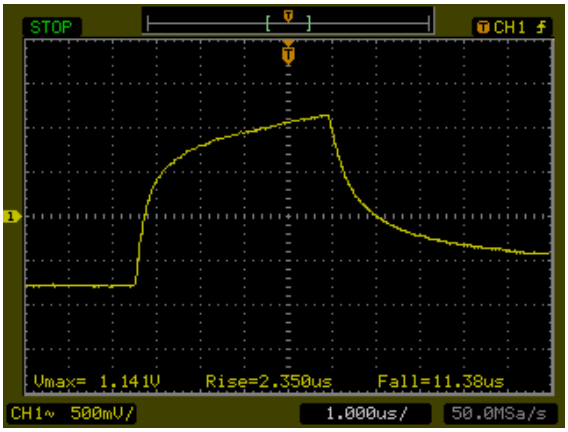

Figure 84 Example oscilloscope waveform of e-textile 4 after 10 washes with touch detection of a human hand

Additionally, the e-textile circuit was considered not functioning when wires were pulled from the solder joint connected to the circuit. When this occurred, readings could no longer be recorded from the circuit. This occurred for e-textile 2 and e-textile 4. Microscopic images were taken of extracted circuits from washed e-textiles to discover how mechanical abrasions of the washing cycle affected the PDMS hydrophobic layer. The failure of the circuits in the washing test could have also been due to bending and twisting of the circuit during the washing test. Figure 74 shows the extent e-textiles can be mechanically deformed from a washing cycle process which includes other textiles. The e-textile circuit was considered not functioning when wires were pulled from the solder joint connected to the circuit. When this occurred, readings could no longer be recorded from the circuit. This occurred for e-textile 2 and e-textile 4. This strain upon the wires is caused by the circuit being crushed and wires caught in-between folds of the other textiles causes it to be pulled off the e-textile circuit in the washing machine during the cyclic motion. It is likely that aqueous solution entered the packaging once a resulting tear in the PDMS occurred, reaching the components to cause failure. The microscope was used to investigate this hypothesis.

A Nikon Eclipse LV100 microscope was used to inspect the PDMS conformal layer of the circuits embedded into the e-textile after washing (Figure 85). They were extracted through the e-textile by irreversibly (as it was fully integrated) cutting through the textile.

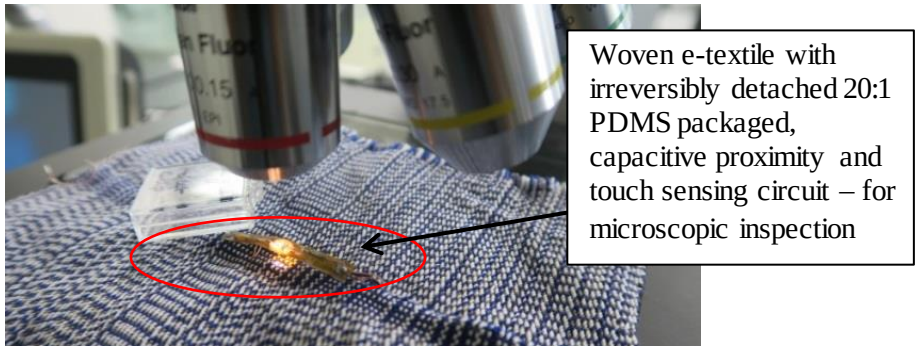

Figure 85 PDMS-packaged capacitive circuit removed from textile for damage inspection after consumer washing machine experiment

Microscopic analysis revealed that the PDMS had not torn or ruptured over the circuit where the chips were located. Instead, for the e-textile circuits where the spin speed was the highest at 800 rpm, the central capacitive sensing chip had detached from its solder pads. For this reason, the circuits no longer functioned. For the e-textile circuits that were washed at 400 rpm, the central capacitive chip was still attached to the circuit, along with all the other passive SMD chips. However, the cause of failure was friction with the PDMS underneath the circuit with the fabric causing it to detach on e-textile 3 and a wire being ripped through the PDMS conformal coating on e-textile 4. Both scenarios likely caused water to seep through the circuit causing instantaneous failure. Nonetheless, for all e-textiles the PDMS did not rip, rupture, or detach at the top surface of the circuit. Furthermore, the microscope revealed PDMS acting as a successful underfill for the PDMS circuit, providing a mechanical damping effect underneath the chip due to the rubber, elastomeric characteristic of the PDMS. Due to this feature, it is likely this characteristic helped to prevent high stress and strain points on the circuit whilst it was bent, flexed, and twisted in the washing machine.

7.4.4.1 SuperQuick, 15 mins, 800 rpm

E-textiles samples stopped functioning due to the PCF8883US detaching from circuit, Figure 86. Closer inspection to the circuit showed uneven soldering of solder bumps which is due to flip-chip bonding the chip, Figure 87. Therefore, the semi-automated process of using the pick and place machine could be replaced by a fully-automated mounting process to remove human error. Hence, reduce uneven soldering which could be a source of mechanical weakness. Also, closer analysis shows PDMS acting as a underfill, as evidence of the bottom of the chip imprinted/embossed onto the cured PDMS. This shows potential for PDMS being an elastomeric underfill for components. All other passive circuits were still attached onto circuit, Figure 88. However, better adherence between the PDMS and the polyimide is needed as the PC8883US chip detached from the solder pads and exited the conformal packaging through a rip/gap created due to the mechanical abrasions of the wash.

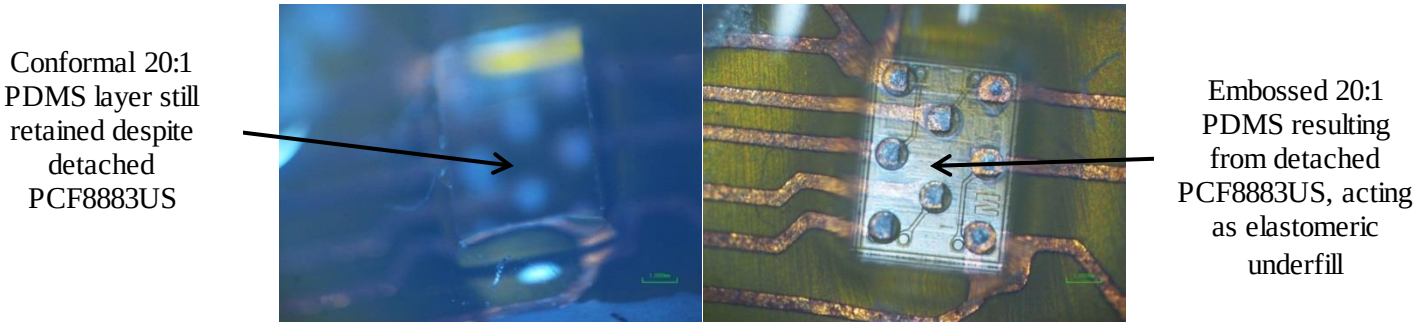

Figure 86 Microscope image capture of detached capacitive proximity and touch sensing chip due to mechanical forces of washing showing its conformal PDMS packaging (left) and the PDMS acting as an underfill (right)

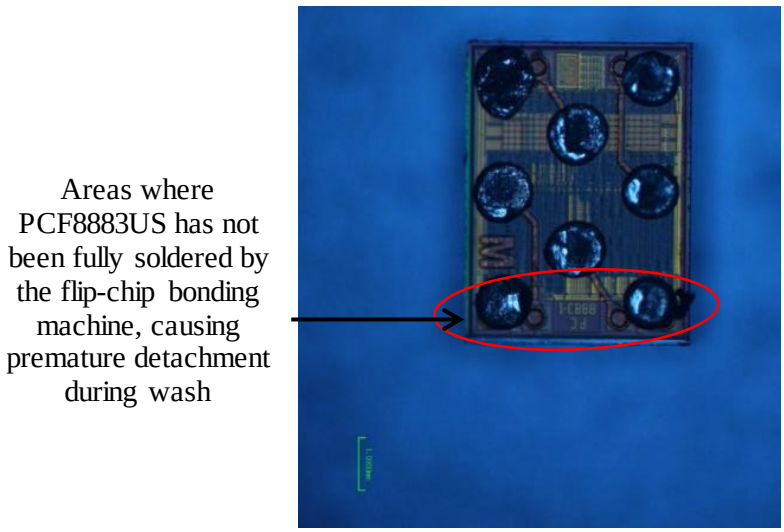

Figure 87 Detached capacitive proximity and touch sensing circuit with uneven soldering following 800 rpm 15 min machine wash, fully-cured solder bumps are highlighted

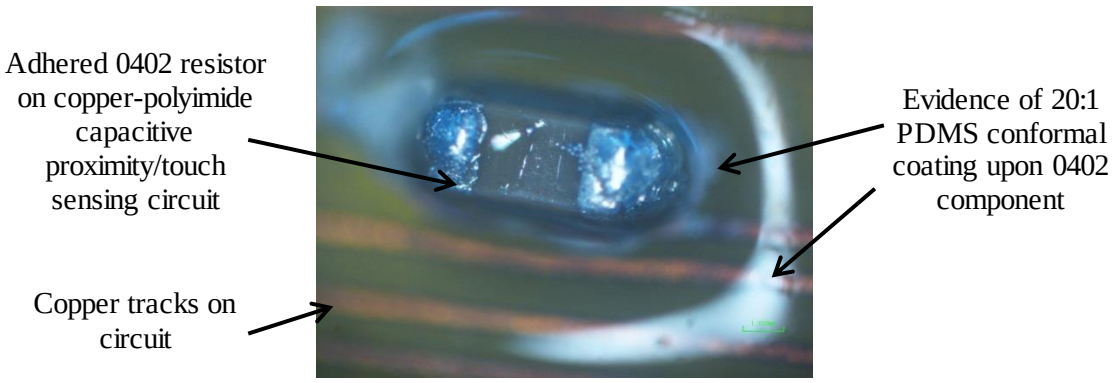

Figure 88 Successful PDMS conformal coating of other components on the circuit with no evidence of tears, rips, or fractures after washing

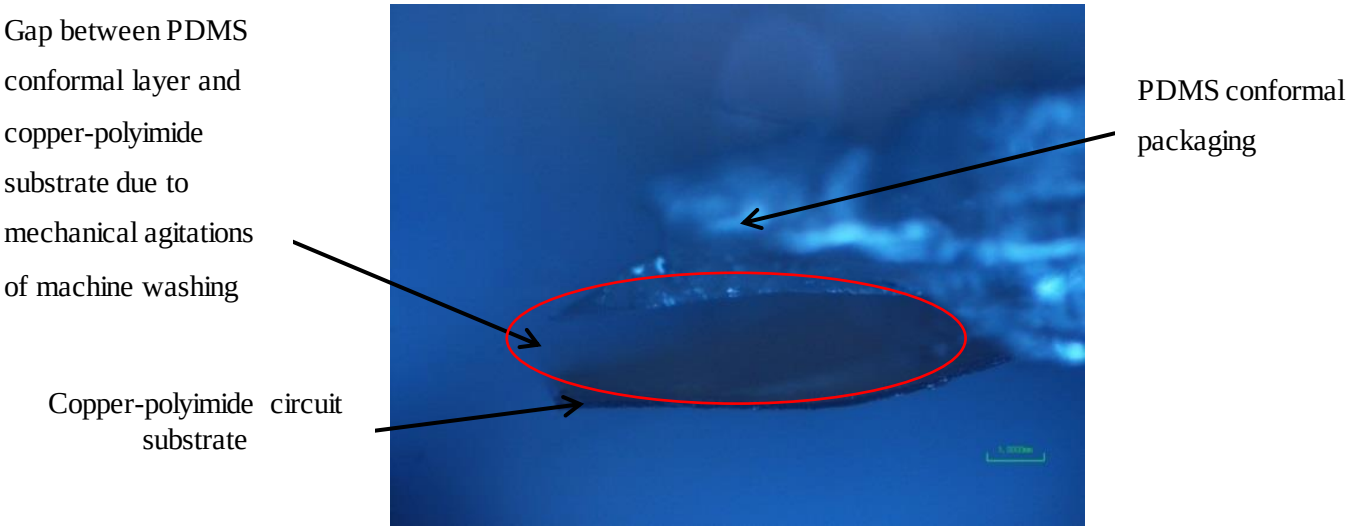

Figure 89 Gap between conformal PDMS packaging and copper-polyimide circuit due to mechanical abrasions of washing machine in an 800 rpm 15 min cycle

7.4.4.2 Silk Wash, 35 mins, 400 rpm

This e-textile sample failed due to PDMS tearing underneath circuit however PDMS on top of the circuit did not have a tear However, there was evidence of condensation/moisture surrounding the SMDs due to water entering the packaging due to the tear and reaching the components (Figure 90).

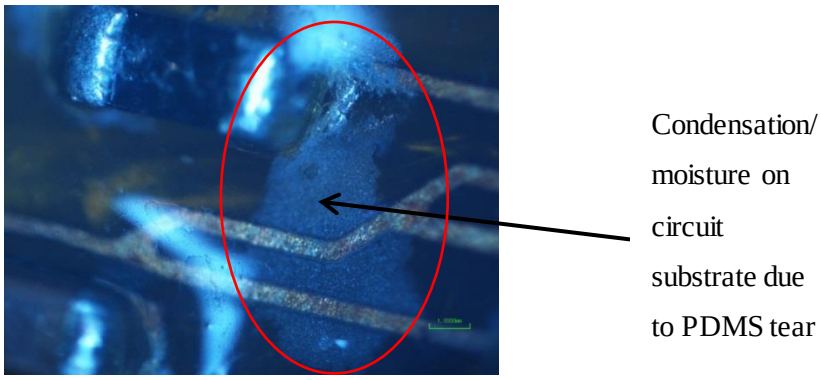

Figure 90 Evidence of moisture underneath PDMS packaging following a 400 rpm 37 min wash at 30 ºC

The tear was likely due to bending, twisting or friction of the e-textile. Yet, the PCF8883US was still on the circuit and not detached.

7.4.4.3 Wool wash 42 minutes at 400 rpm

This e-textile sample failed due to wire snapping off solder joint to ground. The wire ripped out of the encapsulation and as a result, there was evidence of condensation underneath PDMS due to water entering the packaging and reaching the components, Figure 91. Nonetheless, the central capacitive sensing chip still adhered to the circuit and all other components were still detached. This supports the

use of a 400 rpm spin speed to ensure the mounted SMD components survive washing by still adhering to their solder pads.

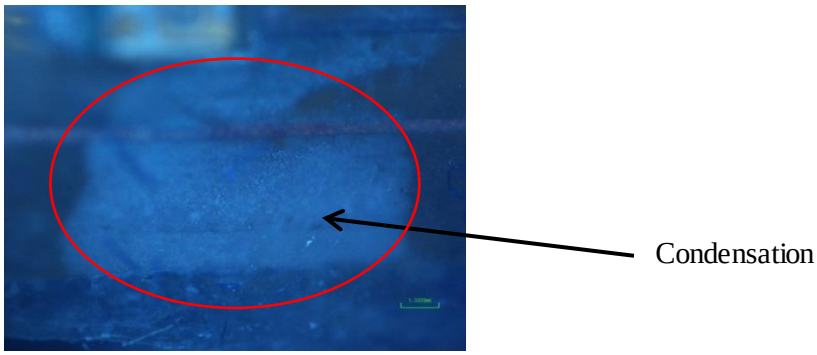

Figure 91 Condensation extending from LED to the etched copper tracks on the circuit

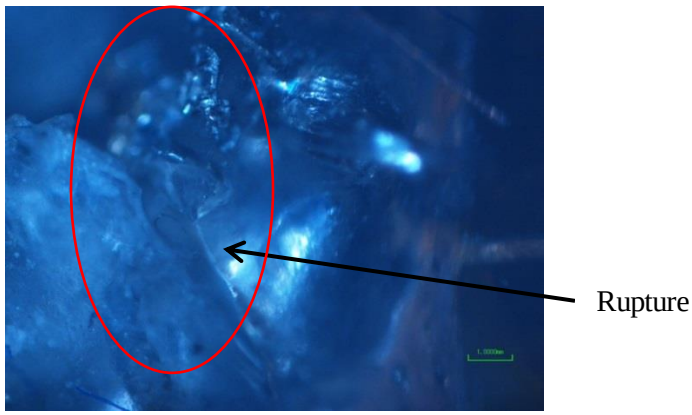

Figure 92 Fracture of conformal PDMS at power solder joint due to silk-copper wire being caught between textiles in 400 rpm, 42min 30ºC wash and resulted pulled out

This further supports the use of a reduced washing spin speed of 400 rpm, to ensure that all surface mount components adhere to the circuit. However, a circuit packaging which is more resistant to tearing is needed to prevent water, detergent, and fabric conditioner solution entering the circuit and causing malfunction. Given the benefits of PDMS shown in this thesis, this can be explored by having a PDMS that is more rigid at the wire solder joints or another substrate to ensure wires are secured onto the circuit. However, it has also revealed that improved soldering of the wires and potentially a need for underfill on the components are required for greater durability.

7.5 Conclusions

Experiments on the second prototype determined the final circuit design and component values on the third and final prototype. System design requirements were focused on developing a functional sensing circuit that can respond to a human hand when it is embedded into a textile. For this, the circuit had to be designed such that was thin (3.0 mm width or less) to fit inside the core of the yarn using the automated knitting machine and also to be handled by the hand looming weaving machine – the two e-textile demonstrator formats that would be made by this research. The PCF8883 IC chip by

NXP Semiconductor was chosen and used its SMD/ WLCSP form – the PCF8883US. This was because it had the smallest dimensions at time of research, its customisable sensing ability, and dual functionality operation.

Results from this chapter have shown that the optimum geometry of the sensing electrode is influenced by the C_{CLIN} and C_{CPC} values. For a strip-shaped sensing electrode to detect a human hand, electrode width is more influential than electrode length to enable proximity and touch detection using the PCF8883US. However, the electrode width needs to be as thin as possible to make the electrode as unobtrusive when woven or knitted into a textile swatch or yarn. Experiments showed that the minimum electrode width achievable for the PCF8883US for a strip-shaped geometry is 3.0 mm. The sampling response value for the PCF8883US will influence the electrode length needed to enable proximity detection for a desired distance range. Together with purposefully selecting an electrode length, the proximity detection distance of a flexible PCF8883US capacitive proximity and touch sensing circuit can be controlled for many applications and usages.

Moreover, when C_{CPC} is above 1.0 µF for a fixed 2.0 mm electrode width the circuit becomes too susceptible to static noise (Semiconductor, 2014) making the circuit unable to detect proximity. On the basis of usability, the most reliable circuit when embedded into a textile either at the core of the yarn or in a woven textile channel is C_{CLIN} = 82 pF and C_{CPC} = 2.2 µF for an electrode width is 3.0 mm allowing for shorter electrode lengths, such as 3.5 cm (35.0 mm), to allow the circuit to perform suitably.

Multiple electrode configurations arranged in parallel and series is a potential way to increase the surface area of the sensing electrode. A square-shaped single electrode of 121.0 cm^2 area gave a 12.0 cm nominal proximity detection distance whilst multiple electrodes arranged in the same area gave 4.8 cm - a 58.3 % difference. The desired 20 pF C_{SENS} capacitance value, formed by the sensing electrode and the human hand, was achieved with electrode dimensions – 35.0 mm x 3.0 mm and 105.0 mm x 3.0 mm. For the PCF8883US, both electrode sizes can be used within textiles to ensure the SMD performs at its optimum. Furthermore, two types of textile demonstrators were fabricated, a woven textile and a knitted yarn. The resulting circuit was fully integrated into the textiles. The 35.0 mm x 3.0 mm sized external electrode would offer the smallest strip-shaped electrode dimension to enable proximity and touch sensing for the PCF8883US for C_{CLIN} = 82 pF and C_{CPC} = 2.2 µF. The e-textile demonstrators could perform touch and proximity for short-range capacitive sensing.

COMSOL simulations revealed that electric potential is highest within the textile channel that the circuit and sensing electrode will be within. The electric field strength is also greatest within the textile channel, and regardless of where the trigger object is positioned beyond the textile this does not have any significant impact on the sensing electrode detection ability. Instead, the combination of the copper and PDMS forms a single-electrode triboelectric nanogenerator configuration, and when supplied a voltage creates a non-uniform electric field between the electrode and the human finger. As the electric field strength is strongest by the copper-PDMS electrode, COMSOL simulation indicates that the electrodes ability to attract charge on its surface increases. This would enhance the detection

capability of the circuit. Underwater tests featuring an averaged 40.3 µm conformal 20:1 PDMS packaging thin, flexible capacitive proximity and touch circuits were conducted. Experiments indicate that such circuits can still function after being submerged for over 6 months underwater, which has not been recorded in literature until now. The first underwater tests used copper wires to connect the sensory circuits to power and ground. However, copper wires snapped after the first week underwater which meant that some circuit readings could not be recorded. The copper wire snapped due to deterioration and erosion as a result of interfacing with water. Therefore, another circuit was put underwater with silk-cladded and multi-strand copper wire. These circuits have no signs of erosion and are still intact in time of writing.

Furthermore, washing tests with an average 40.3 µm-thick conformal 20:1 PDMS flexible sensory circuits were completed using the ISO 6330:2012 standard at different temperatures and durations. This was to evaluate PDMS' machine-washing durability when circuits are integrated into a textile. The washing test revealed that washing cycle rotary spin speed has a strong influence on the lifetime of the circuits. With an 800rpm washing spin speed at 30 °C for 15 mins, all circuits examined failed after one wash with detergent and fabric conditioner included. Therefore, the washing spin speed was reduced to its lowest setting at 400 rpm for two other washing speeds/cycle which survived between 10 to 15 cycles. The silk-encapsulated multi-strand copper wire used in the washing test snapped due to mechanical abrasions of the washing machine. 2 kg of cotton textile was included in the wash, which resulted in the circuits being folded, bent, and twisted during the washing cycle. This caused circuits to have their wires pulled from their solder joints. Subsequent washing with the torn hydrophobic PDMS packaging allowed aqueous washing solution to reach the components and caused the circuit to become non-functioning. Comparing the results from this thesis to that in literature (Linz, Kallmayer, Aschenbrenner, & Reichl, Embroidering electrical interconnects with conductive yarn for the integration of flexible electronic modules into fabric., 2005), (Merritt, Nagle, & Grant, 2009), (Varnaitė & Katunskis, 2009) , not all of these literatures test the functionality of a circuit with embedded electronic components. Linz et al. (Linz, Kallmayer, Aschenbrenner, & Reichl, Embroidering electrical interconnects with conductive yarn for the integration of flexible electronic modules into fabric., 2005) was most similar to this work, as it had a transponder electronic module but encapsulated with glob top and rigid packaging moulding. Yet, Merritt et al., (Merritt, Nagle, & Grant, 2009) was passive sensing electrodes, and Varnaitė et al had yarns acting as conductive wires respectively. As these literatures report survival of 5 washes and this work exceeds this amount PDMS as an encapsulation material for e-textile circuits should have further investigation. The work reported in this thesis presents washing test data specific to advanced e-textiles, whereby the electronics are fully integrated into the textile, achieving double the number of washes compared to other techniques. Literature that has reported high numbers of washing cycle survival such as 20 (Kazani, Hertleer, De Mey, Schwarz, Guxho, & Van Langenhove, 2012) and 50 (Kaappa, Joutsen, Cömert, & Vanhala, 2017) washing cycles did not feature electronic circuits in the washing machine but only printed conductive tracks and dry electrodes respectively. This thesis

therefore contributes to the state-of-the-art knowledge for washing cycle durability and robustness for e-textiles; where wires and electronic circuits are packaged and integrated into a textile for washing. This prompted mechanical experiments to be conducted on the 20:1, averaged 40.3 µm-thick PDMS encapsulated sensory circuits to identify which kind of mechanical strain resulted in the reduced functionality during the washing test. Hence, cyclic twisting and cyclic bending tests will be performed on these circuits with anticipation that they will reveal a similar change in TRC curve voltage drop to the washing tests.

Chapter 8: Cyclic Mechanical Experimentation of PDMS packaged E-Textile Sensory Circuits for Quantitative Durability

This chapter outlines mechanical robustness experiments that were completed at Nottingham Trent University's Advanced Textile Research Group. For each experiment, eight identically- made working proximity and touch sensing circuits, with conformal-coated 20:1 PDMS were subjected to twisting tests. The objective was to obtain quantitative data describing the mechanical robustness of the 20:1 PDMS as an encapsulating layer.

8.1 Preparation of PDMS-packaged Self-Capacitive Proximity and Touch Sensing Circuits for Mechanical Cyclic Twisting and Bending Experiments

Following results from the washing test, a Dymax 9001 resin that requires UV-cure was applied on solder joints opposite ends of the circuit. This was used by our team at Nottingham Trent University an encapsulation for individual SMD components. If the UV-curable resin was used on the entire copper-polyimide circuit, it would be completely rigid. Therefore, it would no longer drape nor meet the specifications of this Ph.D research the final circuit and e-textile needs to be flexible. Therefore, this resin was localised to the solder joints to offer mechanical robustness. This would prevent wire detaching, which microscopic analysis of the washing test predicted. To ensure the UV-resin was on top of the solder joints itself, the 20:1, average 40.3 µm conformal PDMS-coated circuit was not on the solder joint for the mechanical experiments.

UV-resin was deposited via syringe and was controlled with a positive pressure pump. With each dispense, 10 µL of resin was released onto soldering areas where the 36/0.04 mm silk covered stranded copper litz wire were located on the circuit to increase the likelihood of the circuit surviving the twisting test. Each solder joint had 4 pumps of resin applied. In addition to prevent wire detachment, the resin was also used to ensure all the wires were parallel and straight. This would represent how the circuits would be prepared to be handled by the knitting and weaving machines. This resin was applied to the solder connection on 15.0 cm x 3.0 mm electrode with a wire connected to the copper-polyimide. Furthermore, it was applied to connect power silk-copper wire to external electrode. At this time, silk copper wires were introduced as the next iteration of wire material for the FETT project, and therefore were used in subsequent circuit development for this research. The UV-resin was then cured by UV-light exposure of 30 s on each solder joint. The circuit is taped down to keep it straight and wires parallel. The plastic guard surrounding the circuit during the UV-exposure was to protect the eyes and body. It was advised by the team at Nottingham Trent University to apply another layer of UV-curable resin with Vectran to relieve strain upon the circuit when it passes

through the knitting machine. For this, the whole process was completed again after Vectran had been aligned above the already cured UV-curable resin on the solder joints for additional UV-resin coating. This made the resulting circuit system be identical to that within the textile yarn as part of the subsequent integration process. Figure 93 shows the outcome of these steps, the modified capacitive proximity and touch sensing circuit packaging system:

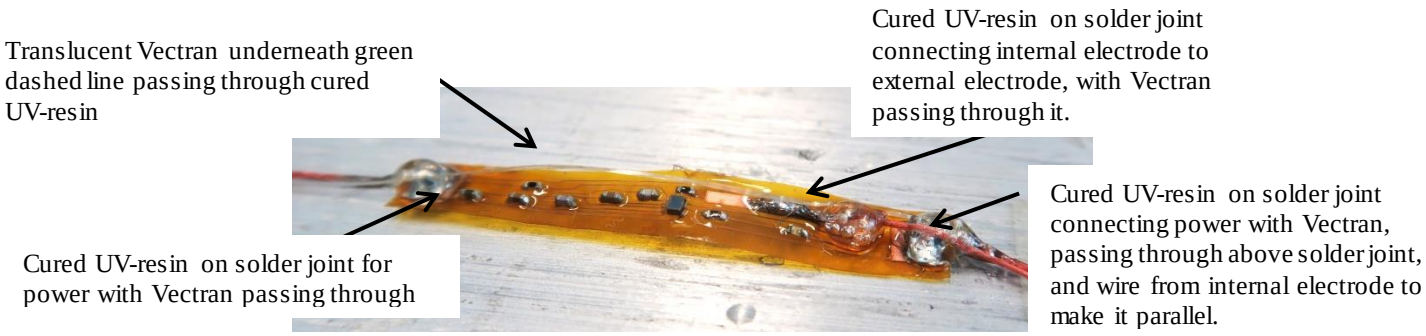

Figure 93 Improved packaging of capacitive proximity and touch sensing circuit for textile integration with conformal PDMS packaging and UV-resin at wire solder joints and Vectran

8.2 Cyclic Twisting Test of PDMS-packaged touch and proximity sensing circuit

The equipment used in this experiment was supplied by Nottingham Trent University and has been used to evaluate the mechanical durability of circuits in the FETT project. As this equipment was adjusted from its original manufacturing design by the team at Nottingham Trent University, there is no textile standard to comply the results to. This experimental setup has been verified by Nottingham Trent University as a measure that can be used to evaluate electronic yarns. Its methodology, used in this thesis, has been published and peer-reviewed.

8.2.1 Experiment Pre-Requisites due to FETT Project

To be consistent with other cyclic twisting tests completed in the FETT project, resistance was used to determine measure the degradation of the circuit due to this mechanical distortion. This measured has been used by our team at Nottingham Trent University with the Prowhite Twist Tester 1009 machine they edited to make a 180° rotary twist. When the conductive copper tracks on the copper-polyimide circuit are twisted periodically, its geometric profile is temporarily altered. Doing this continuously causes stress introducing cracks and weakening the copper. Twisting adds compressional strength to the copper tracks and causes work hardening. This causes the Young's modulus to change over time if this is completed successively. When this stress exceeds the copper's elastic limit this results in changes in permanent changes to its modulus of elasticity. As these tracks are connected by the SMDs and the central PCF8883US, measuring the resistance provides the total resistance of the copper tracks, internal resistance of the SMDs and PCF8883US on the circuit.

The resistance of the tracks would be negligible compared to the internal resistance of the PCF8883US. So, it was assumed that when resistance readings were no longer recordable, this would be the PCF8883US detaching from the circuit and this would be verified by microscopic inspection.

8.2.2 Experimental Setup

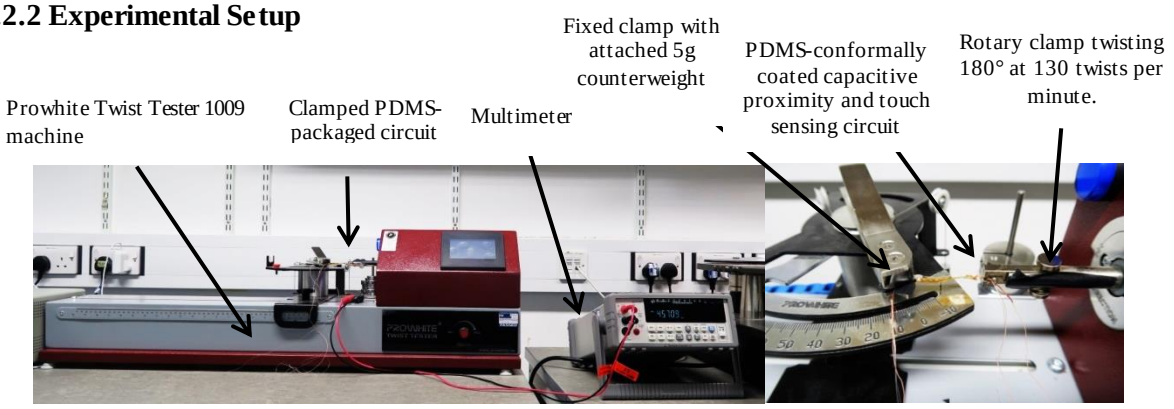

Figure 94 Cyclic Twisting test setup with twisting machine (left) and packaged circuit clamped onto twisting machine with counterweight (right)

The ends of the copper-polyimide circuit were attached to two clamps on the bespoke Prowhite Twist Tester 1009. It was made bespoke by one clamp end being fixed and the other having a motorised 180° rotary twist function. The twisting speed was adjusted to the lowest, approximately 130 twists per minute.

Measuring resistances of total capacitive proximity and touch sensing circuits tested on this machinery was also completed with other circuits in the FETT project (Li, Tudor, Liu, Torah, Komolafe, & Beeby, 2019). Wires for power and ground were connected to a multimeter in the resistance setting. The premise was that if all the component connections secured to the copper tracks on the circuit sustained despite the cyclic mechanical twists a total resistance reading of the circuit could be measured. During the experiment, if the multimeter returned an open-circuit reading it meant that a conductive connection had torn as a result of the repeated mechanical wear of the twisting motion. In addition to the clamps, the circuit was to start the experiment flat and taut. For this, a 5 g resistance counterweight acting on the fixed clamp end was applied. An initial experimental trial using a 10 g counterweight caused the UV-resin to tear off the circuit. This detachment occurred on where the ground wire is located, attached to the fixed clamp (non-rotary). Therefore, 5 g was chosen as the next weight down and the UV-resin no longer tore from the circuit.

Figure 95 Broken packaging with ground wire and cured UV-resin detaching off circuit due to 10g counterweight

8.2.3 Experimental Design

The experiment methodology was organised into a factor 10 set intervals of twists of increasing difficulty. This would measure the circuits' robustness against twisting with time. Hence, the twisting test was divided into 25-twist interval stages of 10, 50, 100, 500 and 1000, and 5000 until the maximum total number of twists was recorded. After each 25-twist interval set, the resistance of the circuit would be measured.

8.2.4 Results

The VHX-5000 microscope and accompanying software was used to inspect the circuits no longer producing a resistance reading as a result of the cyclic twisting test. Microscopic photos were captured of the circuits before and after mechanical twisting tests at their point of failure.

Microscope photos revealed that all of the surface-mount chips remain adhered onto the circuit. Table 18 shows how many cyclic twists each circuit survived.

Circuit Name	No. of survived cyclic twists
A	0 (had 10g counterweight)
B	2900
C	850
D	5100
E	500
F	20
G	10100

Table 18 Table of circuits in cyclic twisting tests and how many cyclic twists they endured

Figure 96 shows no microscopic signs of tear or detachment from the copper-polyimide circuit substrate. This figure also shows the circuit that experienced 10,100 twists and still showing a resistance reading.

Figure 96 Microscope image of circuit that survived 10,100 cyclic twists with all components adhered and no visible signs of tears to PDMS and UV-resin packaging

However, for other circuits that failed before 10,100 cyclic twists their causes of failure existed at the solder joints. This is shown in Figure 97, where the silk copper litz wires have connected to power and ground split, frayed, or torn off by the twisting machine.

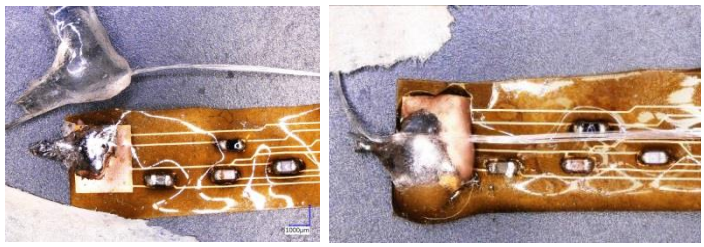

Figure 97 Broken UV-resin and torn silk-copper wire resulting from cyclic twisting test (left) compared to UV-resin still on circuit but frayed wire (right)

The failure was always on the side with the fixed, static clamp. This could be due to the increasing weakness of the wire at ground, as the rotary motion and not the twisted end of the circuit. This could be due to the temporary distance reduction between the clamps when the circuit was twisted via motor. It was observed during the experiment that the circuit experienced a momentum such that as it was twisted when it is twisted back causing a back and forth motion gradually causing the wire to fray. Nonetheless, all the SMD components were still on the circuit which show how mechanically-robust the PDMS conformal packaging is despite the cyclic mechanical deformation. Furthermore, closer inspection of the microscopic images showed signs of wear on twisted side of the circuit compared to the static side. This is observable in Figure 98 through the raised, localised translucent regions of the PDMS conformal packaging:

Figure 98 Side of twisted capacitive proximity and touch sensing circuit with evidence of worn PDMS packaging around surface mount resistors

8.2.5 Analysis

Functionality testing of the circuit after this twisting experiment revealed that 50% of the circuits could still sense touch and proximity. Comparing the circuits before and after the cyclic twisting test, the circuits before the twisting test performed very similarly. This is shown in Table 19 and Table 20. However, after the cyclic twisting tests superseded 2000 twists the circuits no longer performed sensing or became faulty. Faulty, such as the LED not illuminating as visual feedback but the oscilloscope showing the RC waveform responding to proximity and touch. This behaviour is evident by focusing on the maximum charging voltages of the circuits shown in graphs Figure 99 and Figure 100.

Circuit Label	**No Proximity/Touch**			**Proximity**			**Touch**		
	V_{MAX} (V)	Rise Time (s)	Fall Time (s)	V_{MAX} (V)	Rise Time (s)	Fall Time (s)	V_{MAX} (V)	Rise Time (s)	Fall Time (s)
A	4.26E+00	3.32E-07	2.48E-06	4.08E+00	3.22E-07	2.50E-06	3.95E+00	9.50E-07	5.39E-06
B	4.00E+00	3.38E-07	1.57E-06	4.00E+00	3.38E-07	1.56E-06	3.82E+00	1.57E-06	6.26E-06
C	3.47E+00	6.10E-07	2.13E-06	3.57E+00	5.66E-07	1.73E-06	3.59E+00	5.70E-07	1.57E-06
D	3.78E+00	4.04E-07	1.40E-06	3.76E+00	3.82E-07	1.36E-06	3.60E+00	4.14E-07	1.33E-06
E	3.89E+00	3.24E-07	1.48E-06	3.88E+00	3.28E-07	1.52E-06	3.75E+00	1.16E-06	5.27E-06
F	4.27E+00	4.82E-07	2.70E-06	4.12E+00	4.98E-07	2.24E-06	4.00E+00	5.06E-07	2.05E-06
G	4.04E+00	3.18E-07	5.11E-06	4.00E+00	3.24E-07	5.00E-06	3.85E+00	1.08E-06	1.27E-05

Table 19 Table of average maximum capacitor charging voltage (V_{MAX}), charging time (rise time) and discharging time (fall time) of six capacitive proximity and touch sensing circuits before cyclic twisting test

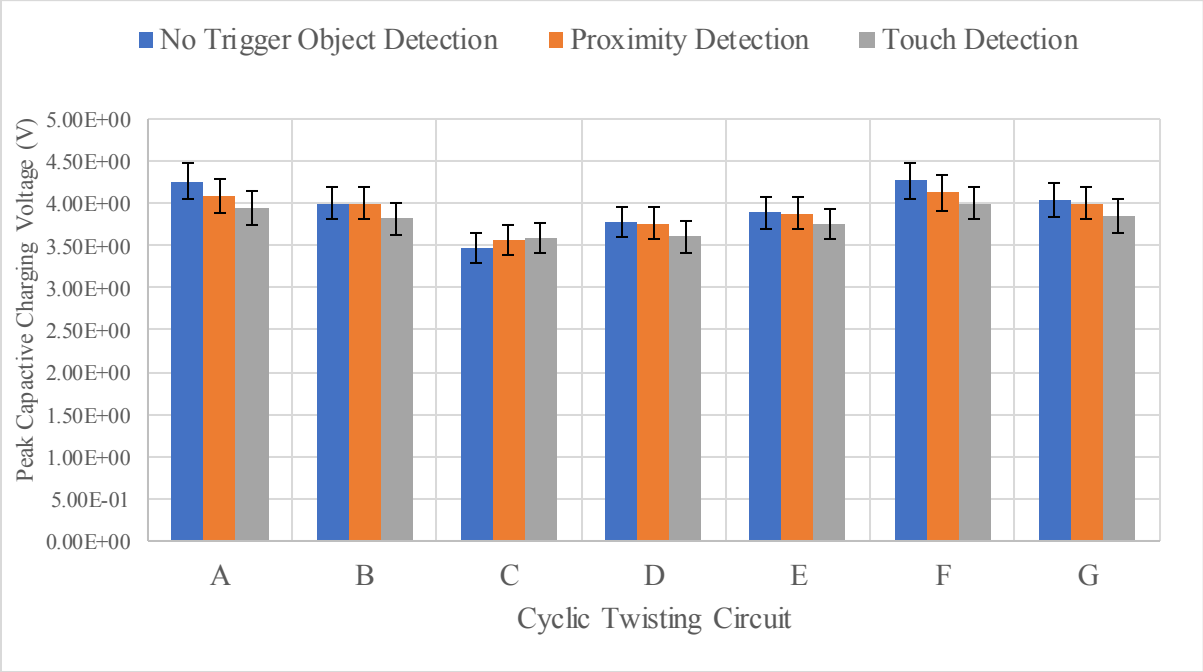

Figure 99 Graph comparison of Peak Capacitor Charging Voltage of Capacitive Proximity and Touch sensing before Cyclic Twisting Test

Circuit Label	No Proximity/Touch			Proximity			Touch		
	V_{MAX} (V)	Rise Time (s)	Fall Time (s)	V_{MAX} (V)	Rise Time (s)	Fall Time (s)	V_{MAX} (V)	Rise Time (s)	Fall Time (s)
A	4.39E+00	1.10E-06	4.26E-06	3.23E+00	5.96E-07	3.23E-06	3.70E+00	1.31E-06	1.05E-05
B	6.28E-01	9.60E-03	9.56E-03	6.28E-01	9.60E-03	9.60E-03	2.38E-06	9.56E-03	5.94E-03
C	4.40E-01	4.96E-03	6.16E-03	4.56E-01	8.61E-03	9.18E-03	2.21E+00	5.98E-03	6.38E-03
D	2.84E-01	6.04E-03	5.12E-03	3.84E-01	6.32E-03	5.12E-03	6.80E-01	2.65E-03	2.26E-03
F	2.52E-02	1.62E-01	1.58E-02	3.08E-02	1.61E-01	1.66E-06	9.36E-02	6.71E-02	4.08E-02
G	4.08E+00	8.06E-07	2.80E-06	4.13E+00	7.96E-07	2.80E-06	3.06E+00	1.44E-06	1.05E-05
H	3.92E+00	8.34E-07	2.16E-06	3.90E+00	1.08E-06	2.04E-06	3.42E+00	2.04E-06	8.61E-06

Table 20 Table of average maximum capacitor charging voltage **(V_{MAX}),** charging time (rise time) and discharging time (fall time) of six capacitive proximity and touch sensing circuits after cyclic twisting test

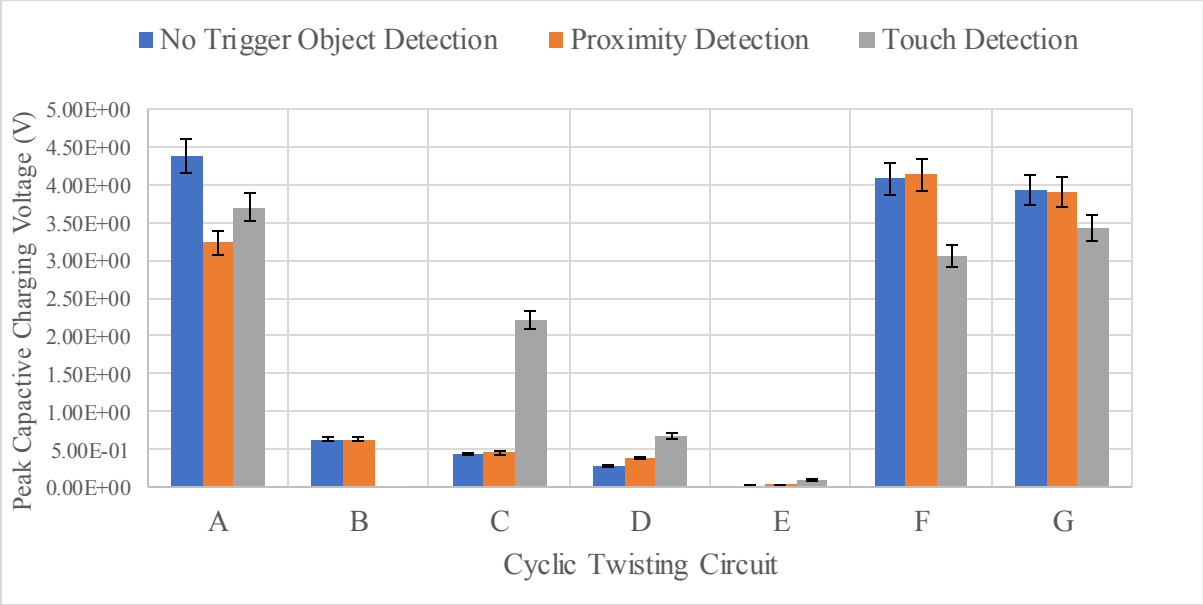

Figure 100 Graph comparison of Peak Capacitor Charging Voltage of Capacitive Proximity and Touch sensing after Cyclic Twisting Test

Circuit G survived 10,100 cyclic twists and was able to sense proximity and touch of a human hand afterwards. A compilation of all the real-time resistances changes for all circuits under investigation are displayed in Figure 101.

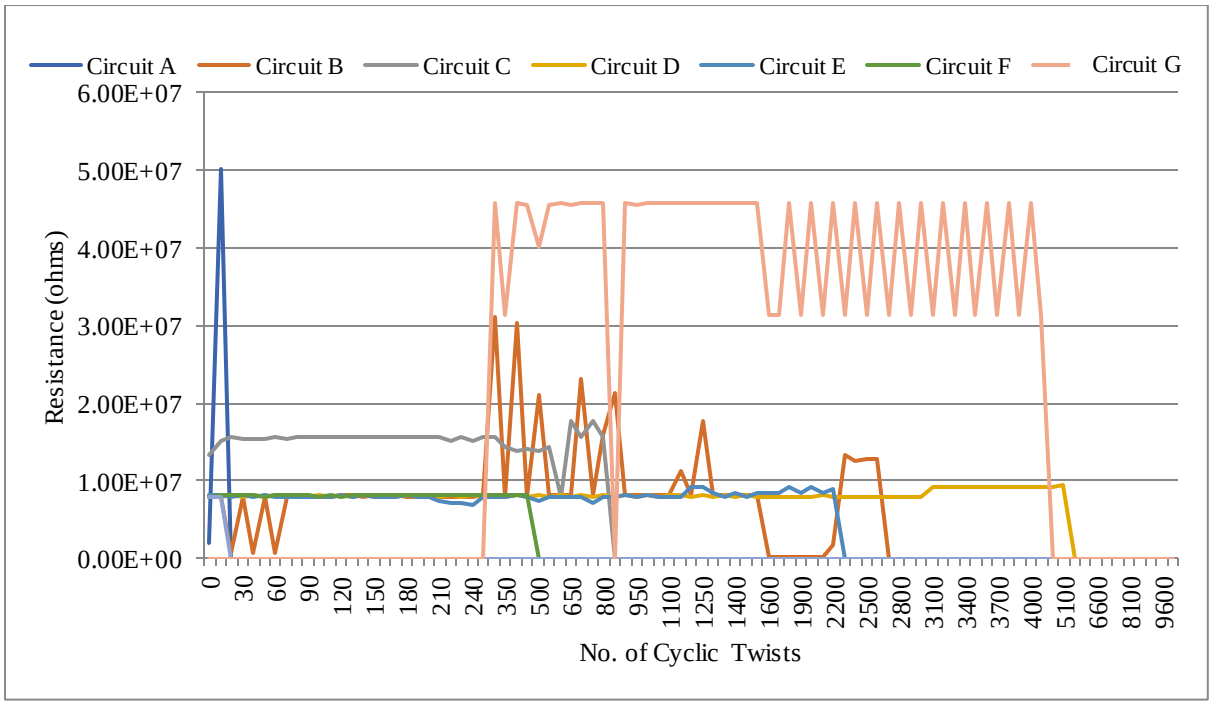

Figure 101 Graph of real-time resistance changes of capacitive proximity and touch sensing circuit during cyclic twisting test

As seen in the results tables and graphs, the high variability of the results is not associated with the functionality of the circuit but likely the human involvement of the soldering of the wires onto the

circuit. As this can never truly by identical it means that the robustness of the circuits will not be identical either. It seems the twisting experiments for the copper-polyimide circuits will in fact measure the robustness of how the copper-wires are secured onto the ends of the circuit. Although these results suggest that these wires can sustain 10,100 twists before tearing, the results also support a better soldering method to produce more consistency across the samples.

8.3 Cyclic Bending Test of E-Textile Yarn with integrated PDMS-packaged circuit

A bending rig apparatus, custom made by the FETT project was used for this research. All the circuits developed using the FETT platform technology would be subjected to tests using this apparatus. The bending rig comprises of two 3D-printed clamps attached to an L-shaped metal rail. As this rig was custom-made, it does not comply with an existing textile standard.

8.3.1 Experimental Design

Four identically made proximity and touch sensing circuits, with conformal-coated 20:1 PDMS were subjected to the cyclic bending test. The cycling bending test was to impose a back and forth bend across the length of the integrated sensory circuit. This would test the robustness and durability of the entire e-textile yarn system as of a result of the internal 20:1 PDMS packaging around the circuit.

8.3.2 Experimental Setup

This experiment followed the methodology already developed and followed by another member of the FETT project who developed this custom-made bending rig. This methodology was based on a circuit with LEDs in series and measured the voltage change as the circuit bent round a 10 mm radius in set intervals until the LEDs stopped functioning. In this experiment, the circuit would have its peak charging capacitive charging voltage, charging time, and discharging time measured in the same method in subchapter 4.5.2.

The top horizontal clamp of the bending rig is moved back and forth on the rail via a motorised conveyor belt, whilst the vertical clamp is attached to a 14 g counterweight. This counterweight amount was the default associated with this bending rig and could not be changed without disfiguring the bending rig completely. Therefore, it was used and considering that 10 g counterweight damaged the circuits in the twisting test this was taken into account when completing this experiment. The experiment was also pursued with its 14 g counterweight for it was used on other circuits developed in the FETT project that was tested on this bending rig. This 14 g counterweight was used pull the circuit over the rig tightly whilst keeping it flat against the 10.0 mm bending radii formed of a metal cylindrical bar. To ensure any damage to the circuit was minimised, the circuit was secured onto the bending rig with clamps. The knitted yarn with one circuit inside was positioned

between two screws found on each clamp before tightening. This ensured the yarn did not slip from the rig during the cyclic bending test. The clamp was positioned 5.0 cm away from the edge of the circuit, indicated with a marker on the knitted yarn. 5.0 cm was used as this was the distance used on other circuits tested on this bending rig.

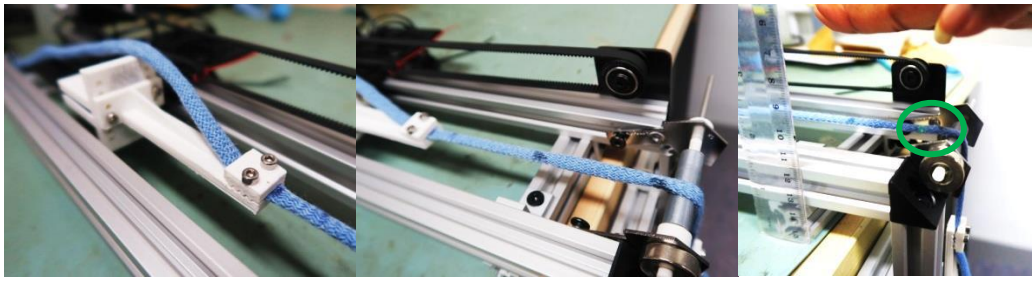

Figure 102 Clamped sensing yarn on cyclic bending rig attached to a motor and rotary belt (left), secured onto cyclic bending rig with 10 mm radii metal bar (middle), and working proximity sensing (right)

The black markings in Figure 102 show where the circuit is located inside the yarn. The starting position of the cyclic bending test was with the circuit flat. When powered, the cyclic bending rig would complete 10 back-and-forth motorised cyclic bends before stopping and the circuit will cyclically bend over the bending radius. During each cyclic period, the oscilloscope would measure the changing in peak charging voltage of the circuit. The proximity and touch sensing yarns were checked for functionality via oscilloscope, outlined in subchapter 4.5.2 Functionality Test after each 10 cyclic bends by touching and putting a human hand above the circuit located at the core of a yarn. The sampling rate of the oscilloscope, 20 seconds per division and 5 sample readings per second, was such to match the time taken for the bending rig to complete 10 cycles. This was the maximum settings for the oscilloscope. This enabled the oscilloscope to monitor the functionality of the circuit whilst cyclically bent in real time. Real-time monitoring was outputted via the oscilloscope by observing the circuit's voltage over time. The circuit was allowed to rest 5 seconds between each set of 10 cyclic bends and it was ensured that the circuit was at the same starting position before the next cyclic bending cycle began.

8.3.3 Results

Five circuits were tested in this experiment, it was noted that when a counterweight was applied to the yarn before the experiment began caused the outer knitted sleeve to stretch by 4.0 cm. Hence, there was more strain on one side of the circuit compared to the other. This was accounted for when collecting the results and analysing its data. The greatest number of cyclic bends the circuit could survive despite the uneven strain was 50. Unlike circuits completed prior to using this bending test, the capacitive proximity and touch sensing circuits had the PDMS and UV-curable packaging in

addition to the textile outer layer. Figure 103 shows the results for the circuit that survived 50 cycles before proximity and touch sensing of a human hand until they could no longer be detected.

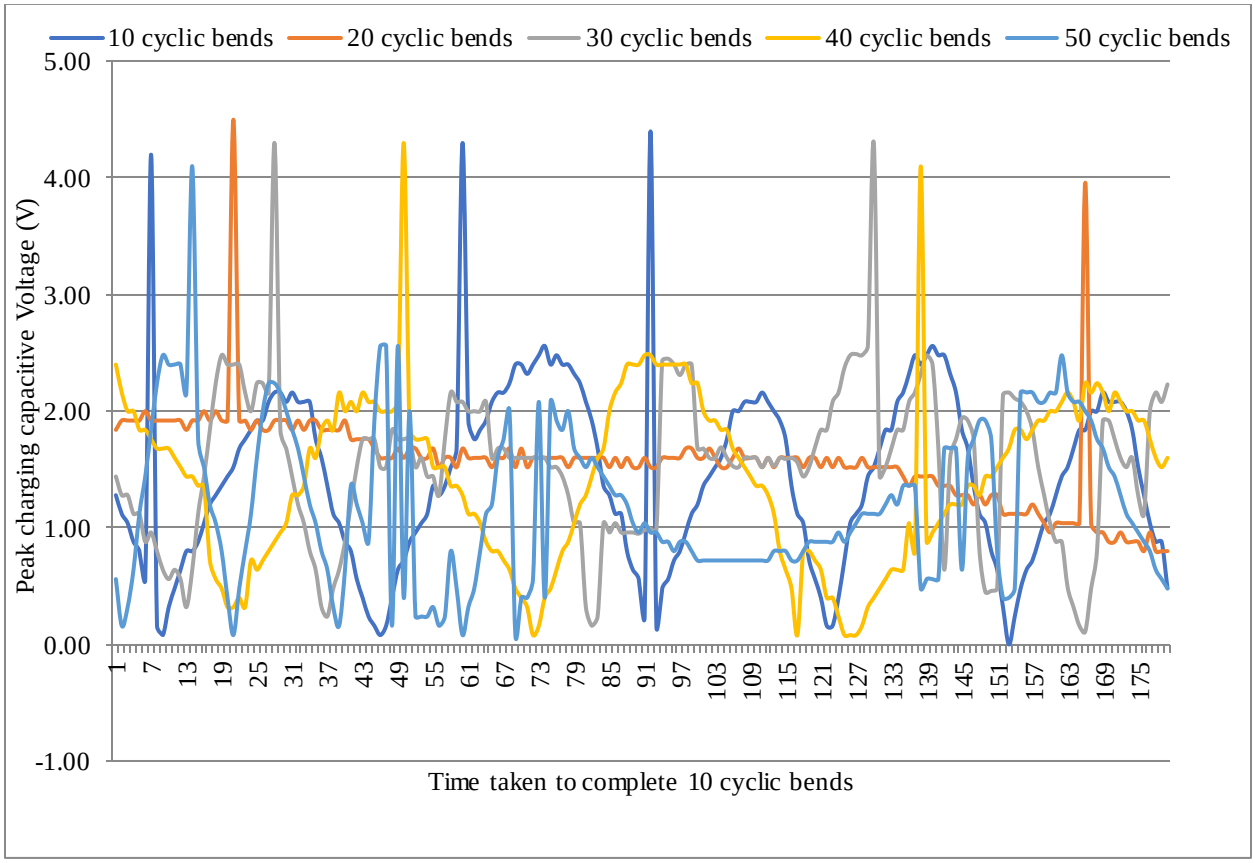

Figure 103 Cyclic Bending Test results showing maximum capacitive charging voltage with time for Circuit 1 that survived 50 cycles

The time duration for 10 cycles is 3 minutes, and the graph above and those that follow show the change in maximum charging voltage in volts of the capacitive proximity and touch sensing circuit before the experiment and on every 10th cyclic bend. As shown in Figure 103, the voltage value is oscillating like the sawtooth waveform characterised by the circuit when it is functioning. The general trend is that the peak charging capacitor voltage of the circuit drops from maximum 4.3 V to an average 2.0 V following each 10 cyclic bending period. There are noticeable spikes towards throughout each trace which reduces as the number of complete cycles increase. The sawtooth waveforms in the graph have significant spikes, as seen in Figure 104 and Figure 105 .

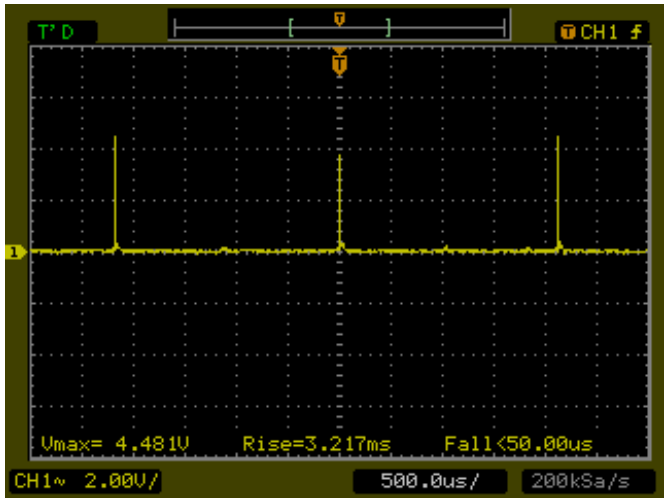

Figure 104 Initial oscilloscope waveform generated when circuit is given power, showing three periodic outputs.

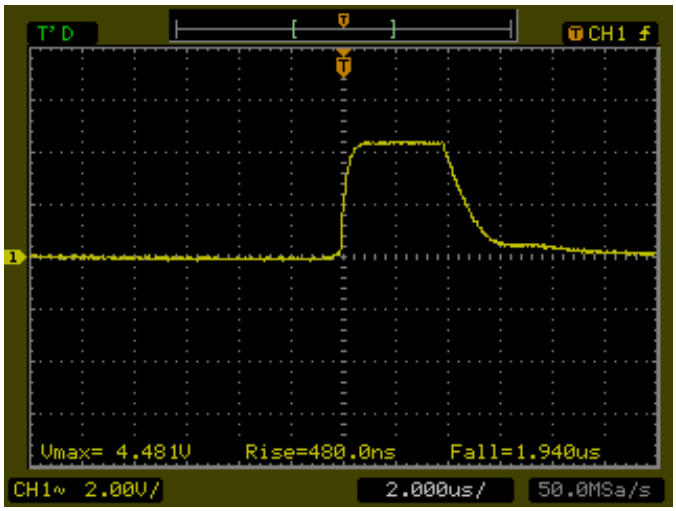

Figure 105 Zooming into one of the outputs in the initial oscilloscope waveform shows the RC curve response showing the peak capacitive charging voltage (V_{MAX}), the capacitor charging time (rise time), and capacitor discharging time (fall time) of capacitive circuit

Selecting these spikes individually reveal RC curves that have been recorded in other experiments in this thesis. As the circuit was able to sense proximity and touch sensing at following the reading with the LED illuminating, these spikes are the LED turning on – indicating functionality. This behaviour was evident with other circuits in this experiment.

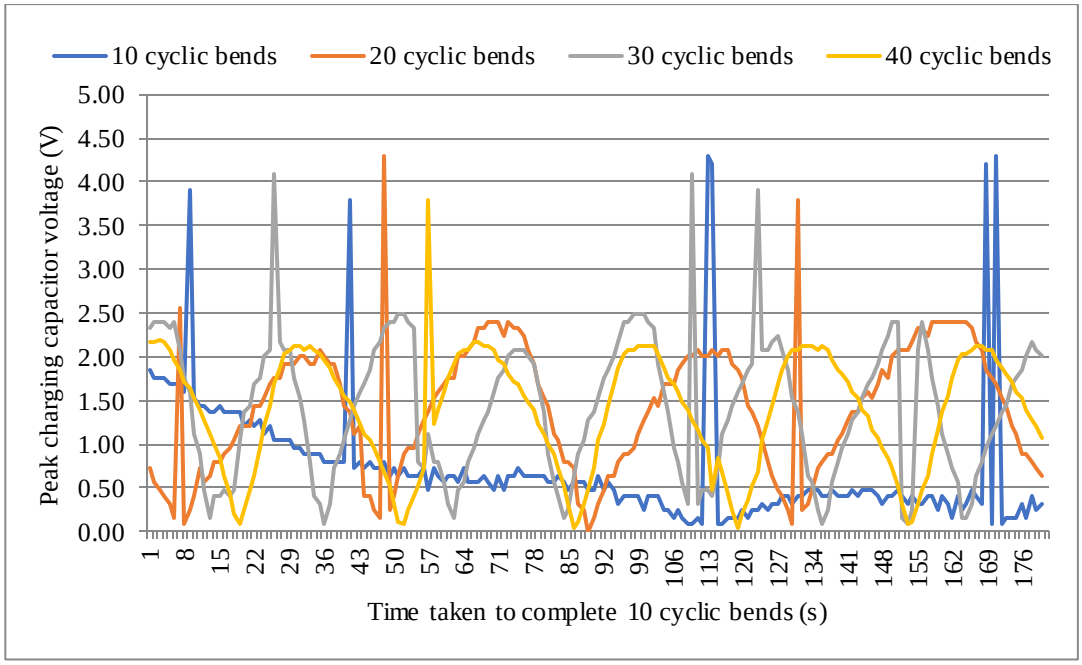

Figure 106 Cyclic Bending Test results showing maximum capacitive charging voltage with time for Circuit 2 that survived 40 cycles

Circuit 2 survived the second highest number of cyclic bends in this experiment as shown in Figure 106. Similarly, to Figure 103, graph showing data for circuit 2 also shows the expected sawtooth waveform with spikes between 4.0 V and 5.0 V to denote functionality. After the circuit has undergone some cyclic bending, the spikes which otherwise occurred periodically are not as visible in the subsequent traces despite proximity and touch sensing of a human hand still being evident. It was initially thought this was caused by the damaging effect the cyclic bending has upon the circuit. By the 40th cyclic bending cycle, the voltage oscillates at a slower rate compared to the 10th cyclic bending cycle, shown by the reduced frequency of waveform peaks. Again, the same behaviour to Figure 103 is evident with circuit 2 that the number of spikes per waveform reduces as the number of cyclic bends increase. Furthermore, on the cycle that the circuit is about to fail, the spike occurs before 5 cycles. This behaviour is consistent with circuit 1 and circuit 2 which prompted a prediction as to when the circuit would lose functionality.

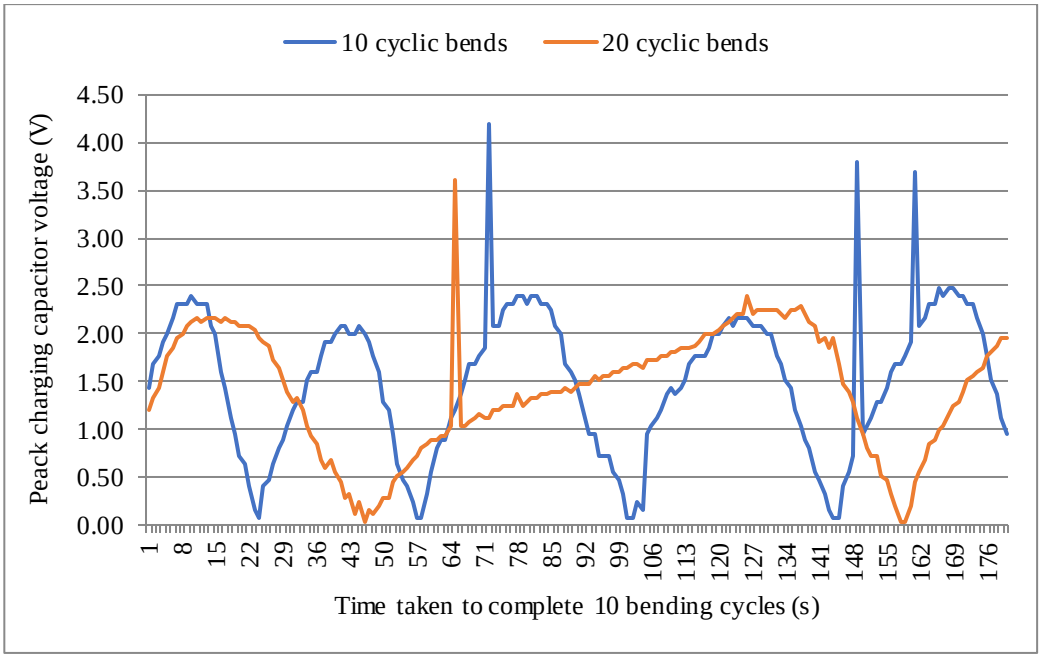

Figure 107 Cyclic Bending Test results showing maximum capacitive charging voltage with time for Circuit 3 that survived 20 cycles

The analysis regarding the evidence of the RC curve same can be said for circuit 3 in Figure 107. However, in this graph it is clearer when the circuit begins to fail. The period of the sawtooth shape for the 20th cycle is greater compared to the 10th cycle. Additionally, as the circuit begins to fail the period of the sawtooth trace for the 10th cycle becomes increasingly greater. The same behaviour is displayed by data from circuit 1 and 2 are evident in circuit 3, the presence of spikes in the sawtooth waveform. Compare this to the 20th cycle, where the characteristic oscillatory waveform changes into a linear trace. From 64 seconds to 141 seconds, the voltage values increase overall until it peaks approximately at 2.0 V. The circuit during this period is beginning to malfunction as the impact of the mechanical deformity is weakening the central PCF8883US or SMD component on the circuit. This had not occurred for other circuits under experimentation, and therefore indicated that the mechanical cause of failure would differ from circuits 1 and 2 following microscope inspection.

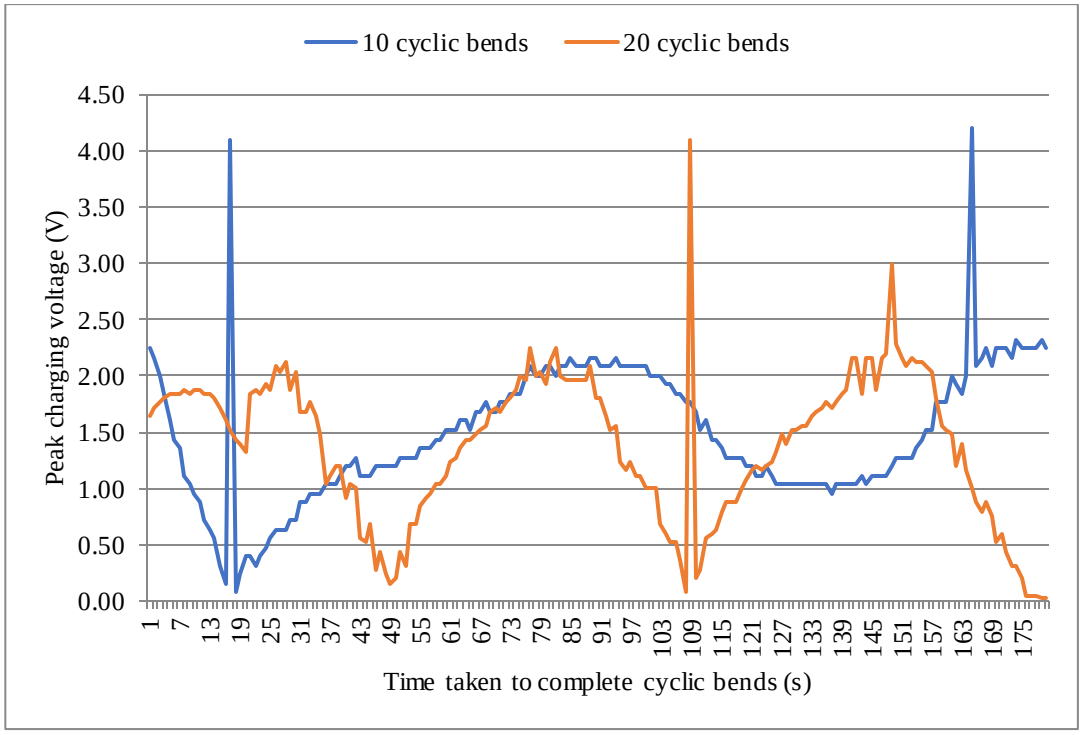

Figure 108 Cyclic Bending Test results showing maximum capacitive charging voltage with time for Circuit 4 that survived 20 cycles

In comparison to circuit 3, circuit 4's behaviour during 10 cyclic bends feature more spikes than during the 20 cyclic bending period. Although, the linear section of the reading from 19 seconds to 91 seconds is similar to the circuit 3's 20 bending cycle results at 64 seconds to 141 seconds. However, circuit 4 can recover, with a notable peak charging voltage value of 4.2 V at 165 seconds indicating a functioning PCF8883US circuit. The waveform during the 10^{th} to 20^{th} cyclic bending duration demonstrates the PCF8883US circuit failing before the experimental period was over. As the decline is sharp at 151 seconds to 180 seconds, this indicates the failure period due to a gradual mechanical fault. Similar to the sharp incline in the last 20 seconds of circuit 3, this characteristic part of the waveform appeared to represent a similar type of fault. As this was a gradual failure, it could not be a detachment of the SMD components or the PCF8883US as any break in the circuit would cause the circuit waveform to flat line instantly. Therefore, the source of failure must have been gradual such as the power or ground wires interfacing with the solder pads either ends of the circuit tearing away. The counterweight was attached to the yarn where the power wire, however there were two UV-curable resin glob top regions in series to each other – the internal electrode sensor solder pad and the power solder pad. The Vectran fibre passed through these glob top regions and also the glob top on the ground solder pad. As there was less glob top UV-resin on the end of the circuit where the ground solder pad was located, it was predicted that this side was where the mechanical damage would be found.

8.3.4 Analysis

All of the circuits were removed from the yarns and inspected individually by Nikon Eclipse LV100 microscope. This was to determine the mechanical fatigue locations of the circuit which caused it to no longer function as a capacitive proximity and touch sensing e-textile. The yarn was split open and cut along the length with scissors, until the circuit was located. To ensure the circuit was not damaged, the scissors was used to make short-lengths cuts of 1.0 cm and the knitted yarn was pulled apart by hand. The location of the circuit was marked with pen on the knitted yarn to avoid cutting the circuit. The circuit was then placed on the viewing stage and flattened before analysing the circuit with the microscope. Circuit 1, that survived 50 cyclic bends, had all its SMD components and wires intact – Figure 109.

Figure 109 Photo of circuit 1 used in cyclic bending test that survived 50 cycles with intact packaging, components, and wires

Under the microscope, it was observed that no tears, ruptures, or scratches were evident on the PDMS layers both above and underneath the substrate between the components. As in Figure 110, the central PCF8883US was still adhered to the circuit and the microscope verified that all solder bumps were attached to their associated solder pads on the copper-polyimide circuit substrate.

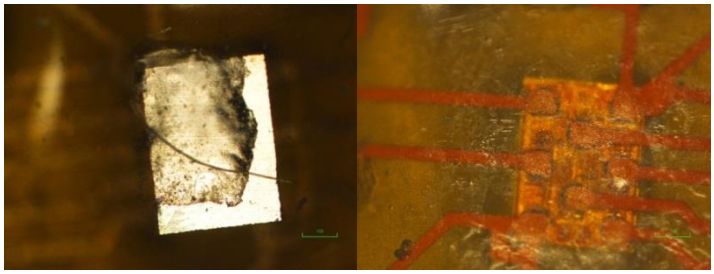

Figure 110 Photo of PDMS rupture in conformal region of PCF8883US for circuit 1 of cyclic bending test but no damage underneath chip

The likely cause of failure of this circuit was a bend which occurred very abruptly. It was thought that this had caused the puncture of the PDMS on region above the central PCF8883US. All other SMDs did not feature this rupture or any other signs of damage with an example shown in Figure 111. The Vectran, used to take a portion of strain from the circuit during the knitting process was still intact. Also, the microscope did not reveal any micro-cracks in the copper tracks, which concludes that the failure of this circuit was due to going over the 10.0 mm bending radii on the 50th trial.

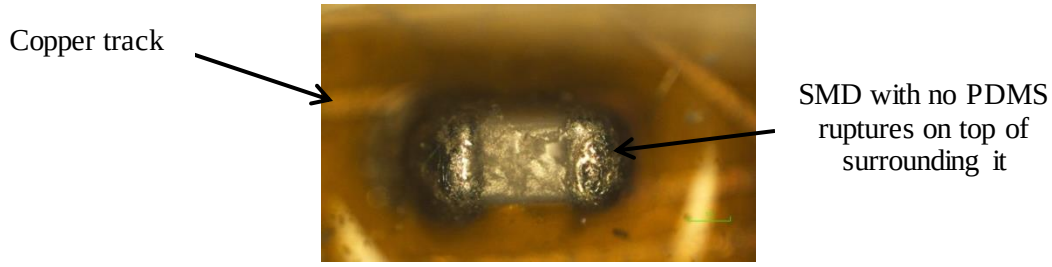

Figure 111 Microscope image of one SMD component on circuit 1 after 50 cyclic bends with textile fibres on the PDMS surface

As predicted, circuit 2 failed by the ground wire snapping out of the UV-curable resin and hence detached from the solder joint on the copper-polyimide circuit substrate. This is visible on the left side of the circuit in Figure 122. The same behaviour was observed with the washing test as a cause of failure when the washing speed was 800 rpm.

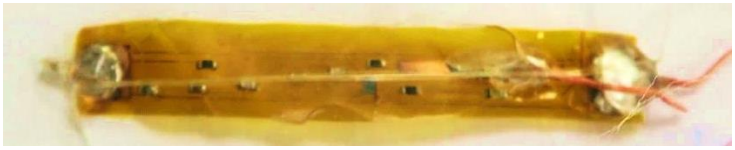

Figure 112 Photo of circuit 2 of cyclic bending test removed from its yarn below whereby the ground wire on the left has snapped off due to mechanical strain of counterweight

The microscope revealed the extent of this detachment. The left image of Figure 113 shows that the wire detached from the narrow end of the UV-curable resin on the edge of the ground solder pad. The wire did not detach at the thickest portion which was above the solder joint.

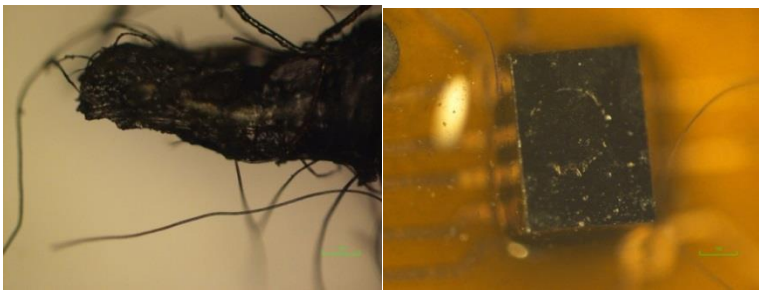

Figure 113 Photo of microscope images of broken UV-curable resin (left) and intact PCF8883US and PDMS conformal layer of cyclic bending test circuit 2 (right)

This effectively reveals a weak point of the circuit and suggests that the resin should be applied more evenly on the solder joints and/or covering a greater surface area on the edges of the circuit, or underneath to make a stronger joint. All the SMD components including the PCF8883US showed no signs of damage or the PDMS packaging above or surrounding these components. The UV-curable resin detached completely from circuit 3 also on the ground side, as predicted; only shown in Figure 114. This is where the counterweight was also clamped during the cyclic bending test.

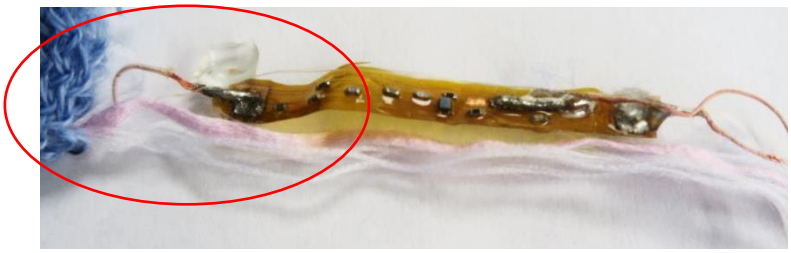

Figure 114 Photo of circuit 3 used in cyclic bending test that survived 20 cycles with detached UV-curable resin on ground solder pad

Circuit 3 only survived 20 cyclic bends, and the microscope images in Figure 115 suggested no other signs of failure as all the other components were adhered onto the circuit and there was no damage to the PDMS conformal layer above and underneath.

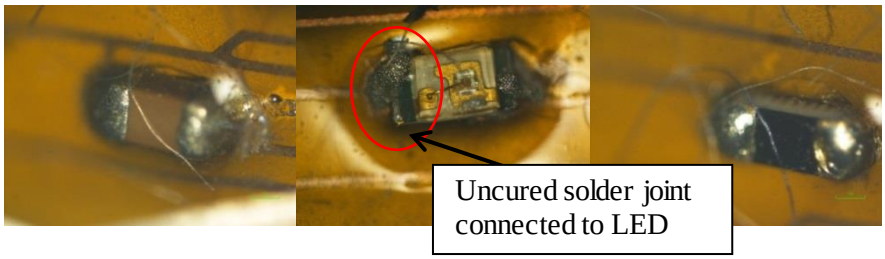

Figure 115 Microscope images of circuit 3 showing undamaged SMD components and PDMS packaging following 20 cyclic bends

The LED in Figure 115 has insufficient soldering curing. Its detachment would have caused the circuit to stop functioning but the LED circuit was still attached to the circuit. As a result, this circuit needed further inspection in case the PDMS had held detached components in place.

Circuit 4 failed due to the ground wire snapping out of the UV-curable resin, as predicted, but also the Vectran snapping. In Figure 116, the ground wire is detached through the UV-curable resin as seen on the left-side of its image.

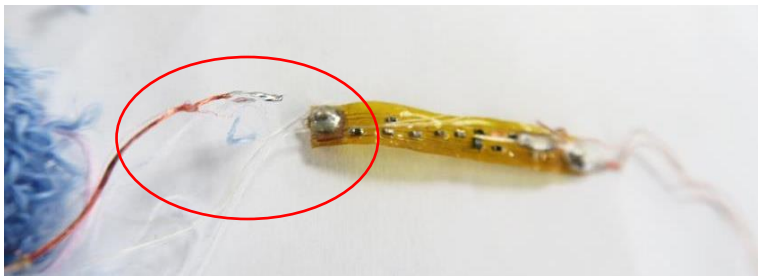

Figure 116 Photo of circuit 4 with wire detached from solder joint where it survived 20 cyclic bends

Circuit 4 also survived only 20 cyclic bends, like circuit 3. The wire detached from the UV-curable resin in the same way as circuit 3, whereby the resin broke at its most narrow section (Figure 117).

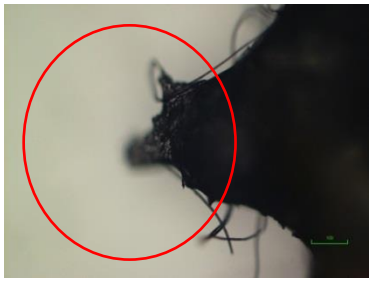

Figure 117 Microscopic image of circuit 4 with more severe damage to the UV-curable resin where ground wire has detached

Inspecting the damage of circuit 4, it is clear in Figure 117 that the portion of UV-curable resin on the wire had completely detached unlike in circuit 2. Furthermore, the damage is more severe on circuit 4. On circuit 2, having the portion of UV-resin that would be on the wire seems to have caused the circuit to survive for longer as more of the UV-resin is present to hold the wire in place. However, circuit 4 had its UV-curable resin cracked nearest to the edge of the circuit on the ground wire. This suggests that the circuit failed more quickly which is supported by the graphs and data collected.

To find the reason for circuit 3's failure, a scalpel was used to remove the PDMS conformal coating – evidenced in Figure 118. To avoid damaging the circuit, it was angled at the side of the copper-polyimide substrate and the tip of the scalpel was used make an incision at the substrate's corner. Tweezers was then used to lift the PDMS conformal layer gradually and slowly. This was to check if any of the SMD components underneath were loose and therefore be its cause of failure.

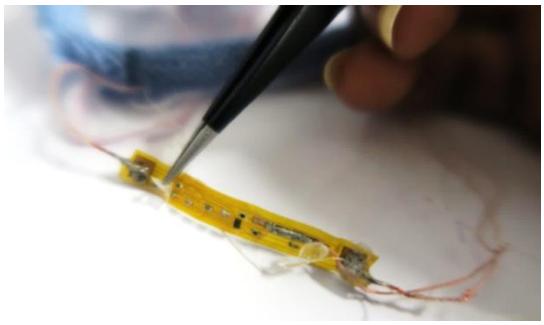

Figure 118 The PDMS conformal coating was torn from the copper-polyimide circuit substrate with tweezers

Upon removing the PDMS conformal layer from circuit 3, all the SMDs and the PCF8883US were checked for detachment and evidence of cracks. All of the components were adhered onto the circuit. Therefore, it is suspected that there were internal cracks in the solder that cannot be seen by the microscope on the ground wire solder pad to cause the circuit failure. Such a result has been noted in literature (Mattana, 2013) to cause a circuit to stop functioning following fatigue from a cyclic mechanical bending test. Therefore, nano-cracks was suspected in solder pads or copper etched tracks nearest to the ground solder pads as a result of the force which detached the UV-curable resin from

the ground wire. Without this UV-resin layer, the solder joint's resistance to stress increased causing a vulnerable weak point along the copper-etched tracks as opposed to the solder itself.

8.4 Conclusions

The experimental results from the cyclic twisting test and cyclic bending tests have provided insight to the extent cyclic washing machine motion can damage the e-textile systems developed in this thesis – PDMS-packaged, flexible, capacitive proximity and touch sensing in knitted yarn and woven fabric format. The cyclic twisting test had the circuits twisted between 180°. The machine with a 5 g counterweight attached to a fixed clamp and a motorised rotating clamp. The experiment showed circuits surviving maximum 10,100 twists with others a not displaying resistance reading prematurely. Microscope inspection of the twisted circuit showed no signs of rips, ruptures, tears, or openings in the PDMS as a result of cyclic twisting. All the UV-curable resin regions were intact and all the SMD components were adhered onto the copper-polyimide circuit. 50% of circuits tested could display proximity and touch sensing after the cyclic twisting test. Importantly, the circuit which still showed conductivity at 10,100 cyclic twists still could sense proximity and touch of a human hand. The cause of failure for the other 4 circuits occurred on the same side – where the ground wire is located and the clamp is fixed. Therefore, this highlighted whether resistance was the only measure that could have been evaluated for this machine for sensory circuits.

The washing machine result and microscopic inspections, showed damage that was more reminiscent of those in the cyclic bending test. The circuits in the cyclic bending test had a survival range of 20 to 50 cyclic bends. Microscopic inspection revealed that circuit failure was due to the ground wire, connected to the 14 g counterweight to detach from the circuit through the UV-curable resin by the wire tearing but solder joint staying intact. Additionally, the UV-curable resin localised on the solder joint would detach from the circuit as a result from the cyclic bending. The solder joint still adhered onto the circuit. In one case, for circuit 3, the Vectran fibre running above the circuit snapped completely which is indication of high strain across the circuit due to the cyclic bending rig setup and/or the counterweight. Unlike the washing test conducted at 800 rpm, all the PCF8883US components were adhered onto the circuit. Comparable to the washing machine test, the ground wire detached from the circuit whereas the power wire and external electrode wire did not detach. Therefore, this indicates that the bonding strength of the wires either side of the circuit were uneven and could be improved by controlled/automated resin deposition and curing. For all these cyclic bending tests, it is suspected that the counterweight was too heavy for the yarn and therefore caused strain on one side of the circuit which damaged it before it began. As the number of cyclic bending increased the impact of the damage also increased. Therefore, the construction of the bending rig would need to be changed such that the counterweight was located somewhere else on the circuit or the strain on either side of the circuit was equal to make it a fair experiment.

Chapter 9: Conclusions, Discussion, and Recommended Future Research

This final thesis chapter summarises the research completed in this Ph.D and reviews its success and contribution to the field. It then recommends future work that can expand this research. Part of the 9.3 subchapter was published in (Ojuroye O., 2017), and (Ojuroye O., 2016).

9.1 Conclusions

Electronic textiles (e-textiles) are an emerging technology comprised of electronic circuit systems embedded into the fabric using traditional textile techniques such as knitting and weaving. Such systems can be formed using off-the-shelf passive components and integrated circuits (ICs) available commercially. An e-textile switching mechanism can be provided by proximity and touch sensing input behaviour from a human hand to switch circuits, for example, turning on an LED for visual verification of successful switching. Challenges to be overcome to achieve reliable e-textile detection systems include optimised circuit sampling rate, detection sensitivity, and sensing electrode dimensions when operating among textile fibres.

This thesis' research goal to develop a completely unobtrusive, functional, washable, and flexible sensing circuit that can be integrated into textiles was achieved. The result is a state-of-the-art capacitive proximity and touch sensing e-textile made using today's textile construction methods. System design requirements were focused on developing a functional sensing circuit that can respond to a human hand after surviving the textile manufacturing process. For this, the circuit had to be designed such that was thin – 3.0 mm wide or less to fit inside the core of the yarn using the automated knitting machine and 5.0 mm wide or less to be handled by the hand-loom weaving machine – the two e-textile demonstrator formats that would be made by this research. *The final circuit has 3.5 cm (L) x 3.0 mm (W) circuit dimension with a 40.3 µm (H) 20:1 PDMS conformal thickness and, 150 µm-width copper tracks on a polyimide substrate.* This capacitive circuit can complete proximity and touch sensing of a human hand that can actuate LED illumination. The selection of the IC chip that could perform capacitive and proximity section was outlined in this thesis, comparing different IC chips available at the time for their technical specifications, dimensions, and sensing capabilities. *The PCF8883 IC chip by NXP Semiconductor was chosen and used its WLCSP form.* This was because it had the smallest dimensions at time of research, its customisable sensing ability, and dual functionality operation. This circuit has an external copper-polyimide electrode attached to the input pin of the PCF8883US IC used to enable this dual-functionality. The surface-mount components are 0402 metric size with a WLSPC-packaged proximity and touch sensing chip at its centre. The circuit was entirely packaged in an averaged 40.3 µm conformal PDMS packaging layer, with 0.04 mm diameter silk covered stranded copper litz wire

connecting to the power and ground connection. Components values for this circuit were experimentally determined by calibrating its detection sensitivity and sampling rate to tailor its performance with the smallest dimensions possible. *The external electrode lengths, for a fixed 3.0 mm width, were also experimentally verified to be 3.5 cm and 10.5 cm* for optimum PCF8883US functionality and short-range 2.5 cm proximity distance to reduce false triggering of the circuit.

When in aqueous environments, another research objective was the circuit had to be hydrophobic and be chemical-resistant to be cleaned like traditional textiles i.e. using a consumer washing machine or hand-washed. Mechanically, the sensory e-textiles had to be robust, flexible, and twistable enough to survive the industrial process and to become commercially viable. This Ph.D addressed this by selecting PDMS as a hydrophobic packaging substrate and experimentally verified how its fabrication method can be tailored for improved resistance to water, detergent, and fabric conditioner so that the sensing circuit within the textile can be protected whilst washed. *An averaged 40.3µm conformal coating was achieved using a suspension method developed in this research. Underwater tests evaluated the durability of the PDMS packaging, resulting with PDMS being able to preserve circuit functionality for 6 months submerge time*. By creating demonstrators for this Ph.D research – knitted yarn and woven fabric swatch – this Ph.D developed a new e-textile system comprising of:

- Capacitive proximity and touch sensing circuits fabricated using the FETT project methodology, validating the process
- A PDMS conformal-packaged capacitive proximity and touch sensing circuits, whereby the PDMS mixing ratio is tailored for e-textile application
- Circuits that are hydrophobic, and experiments showed the PDMS-packaged circuits were robust enough to function after long-term underwater submerge and machine wash
- Circuits that can still function after being handled by automated and non-automated knitting and weaving machines used in industry, demonstrating scalability
- Circuits that are mechanically flexible, hydrophobic to water - in addition to aqueous detergent and fabric conditioner solutions – and can be disguised within textiles

Electrode size and component experiments determined the necessary sensitivity and sampling rate values for this chip to detect through fabric for its optimum capacitance performance value of 20 pF. Experiments revealed that when an electrode is strip-shaped for e-textile applications, its width is more influential than electrode length in enabling capacitive dual-functionality proximity and touch sensing. *A square-shaped electrode offers a 58.3 r% increase in nominal proximity detection distance compared to multiple electrodes arranged in the same area.* The resulting circuit from these experiments confirmed a strip-shaped 35.0 mm x 3.0 mm copper sensing electrode would be its smallest size - whilst keeping the PCF8883US in optimum functionality. *This sensing electrode dimension, with sampling frequency and sensitivity component values C_{CLIN} = 82 pF and C_{CPC} = 2.2*

µF respectively, would to enable proximity and touch sensing for short-range capacitive sensing for e-textile applications.

This new e-textile system was tested for durability, resilience, and robustness through washing tests and mechanical tests. The durability, resilience, and robustness of the PDMS packaging layer was investigated via contact angle, aqueous permeation, underwater, washing machine test, cyclic twisting, and cyclic bending tests against textile standards. *The PDMS-packaged circuit remains functional after 6 months underwater and have helped contribute towards future washing standards for e-textiles with experiments determining a 400 rpm spin speed for 30^{O}C washing cycles at 15 mins, ~30 mins, and ~45 mins for increased functionality. Washing tests showed survival for maximum 10 washes and revealed that washing settings such as washing spin speed is a primary factor in determining its survival rate.* Additionally, mechanical tests were completed to investigate the 20:1 PDMS robustness as a circuit packaging material but also to verify which mechanical deformity (experienced by the e-textile whilst in the washing machine) is most detrimental. *The 20:1 PDMS-packaged circuit could survive a maximum 10,100 cyclic twisting cycles at 180-270° rotation, 50 cyclic bending cycles at 90° bend and 10 mm radius. Bending, not twisting motion, was determined to be the most harmful mechanical deformation for the circuit. This was evident by the type of failure, similar to those in the washing test i.e. wires ripped out of solder joint through the PDMS packaging causing aqueous solution to reach the electronics.*

Simulation of this work was used to predict the changing electric field when the sensing electrode was integrated into a textile and triggered by a human finger by touch and proximity. *The simulation confirmed that the highest electric potential of the generated electric field will be localised within the textile and dispersed outwards. This is due to the combination of PDMS and copper as it acts as a single-electrode TENG, increases the electric field strength and therefore increasing the circuit sensitivity. Hence, the PDMS-copper electrode benefited the circuit. Optimising the component values for sensitivity and sampling rate when detecting through fabric would further increase circuit operation.*

Applications of this work can vary by changing the actuator (the LED) on the touch and proximity sensing e-textile circuit's output. Demonstrators of this work in form of dual-functionality proximity and touch sensing textile yarns and a woven fabric were developed as a result of this thesis. In this light, the novelty of this research is not necessarily producing a novel proximity and touch sensing circuit for e-textiles. Rather, a systematic approach and construction of PDMS-packaged flexible strip-shaped circuits that can be integrated to form e-textiles. It extends the FETT project, which can convert existing rigid, PCB electronic circuit designs to strip-shaped and flexible circuits that can be integrated into the core of a knitted yarn and woven into fabric. With this research's contribution, complex sensory circuits can survive machine washing and cyclic mechanical deformations.

The conclusions presented here achieve the aims originally set by this Ph.D thesis and has demonstrated its novelty through a range of experiments and e-textile demonstrators. A series of

publications have shown this Ph.D has contributed to the state-of-the-art and outlining how e-textiles can benefit society. It is hoped this P.hD reserach will be a source of knowledge and evidence in creating standards for e-textiles for consumer usage for wearables and beyond – such as furniture, automotive interiors, and decor.

9.2 Discussion

9.2.1 Motivations

This Ph.D research investigated whether it was feasible to fabricate a new method of designing and creating flexible capacitive proximity and touch sensing circuits. Such circuits had to be integrated into textiles, cleaned, and mechanically deform like traditional textiles for wearable and other applications. The circuits produced would need to be flexible to mimic the drape of fabric when fully integrated, would have sensors and actuators to create 'active' smart textiles, and lastly would be manufactured using industrially-feasible and scalable techniques. Overall, the design and mechanics of the e-textile had to be adaptable to be located at or be interfaced with different parts of the body. Hence, it was dependent on its application i.e. how it would be incorporated within different textile products. This research consulted these motivations by creating two types of e-textile demonstrators – capacitive touch and proximity sensing knitted yarns and woven fabric - which can sense and be used to interact with its environment and owner.

Overall, this thesis showed that the FETT project platform technology, their fabrication method to create flexible copper-polyimide circuits, can be used to create capacitive sensing circuits. This circuit had a final dimension of 3.0 mm in width and 3.5 cm (35.0 mm) length. It conducted experiments determining the component values that should be on a circuit featuring the dual-functioning proximity and touch sensing PCF8883US chip such that it can sense through fabric. Experiments established how PDMS can be applied to the e-textile field when its fabrication can be tailored for improved hydrophobicity, minimised swelling, and chemical resistance to detergent and fabric conditioner solutions used in commercial washing machines. Unlike previous attempts in the FETT project, the solder paste was successfully cured in a thermal reflow oven which utilised thermal convection to achieve an even cure to adhere the SMD components onto the substrate. The circuit was then successfully made into two types of interactive demonstrators – yarns and fabric – through knitting and weaving techniques respectively. As such circuits were to sense through fabric after being integrated by textile integrating machinery; this added a series of research questions to be answered by this thesis.

9.2.2 Answered Research Questions

This Ph.D research and its results have allowed these research questions to be consulted. This has been addressed by certain chapters of this thesis:

Question 1: How can IC-based sensors function and be interacted with when integrated into a textile among fibres?

Chapter 2, the Literature Review, examined the different approaches proximity and touch sensing e-textile systems have been pursued in literature and compared their effectiveness. The e-textile system setup produced in this Ph.D - whereby a ≤ 5 mm thin sensory circuit would be expected to function beneath textile, hydrophobic, and elastomeric layers - meant that some sensing approaches were unsuitable. This was especially the case for magnetic approaches whereby components were too large to fit within the dimensions of the circuit, infrared could not be used as it would sense the fabric layer and introduce unreliable detection, and camera-based systems would require external equipment for the system to operate. Capacitive sensing was selected as the best option to sense proximity and touch sensing through fabric and detect human interaction. Chapter 3 defined the research's e-textile system design requirements and specifications that dictated which sensory integrated circuit (IC) chip could be chosen to sense proximity and touch through capacitance. Factors such as package size, power consumption and pin layout underneath the chips were important to ensure the resulting circuit size was small enough to be handled by the knitting and weaving machines. PCF8883US was selected as the IC chip that met the most design requirements for this research. In chapter 4, the circuit fabrication methodology was outlined. Chapter 6 detailed how the e-textile system was developed by integrating the PDMS-packaged sensing circuit into textiles so it could still function – and demonstrated the circuit can survive the textile integration process. With knitting, the sensory circuit is integrated at the core of a knitted yarn and surrounded by insulating packing yarns to make the resulting e-yarn have uniform diameter and softness to touch. It did not affect the operation of the circuit significantly but in theory does add another dielectric layer that the IC's sensitivity had to be adjusted to compensate. Chapter 7 then presented a series of experiments adjusting the PCF8883US operation and detection efficiency to textile environments – as part of this P.hD's novelty. It had a limited width and had to sense the touch and proximity of a human hand, so it had its sensitivity and detection sampling rate tailored to function when embedded into fabric. It was found that $C_{CPC} = 2.2$ µF and $C_{CLIN} = 82$ pF were values needed for the PCF8883US to calibrate it to a sensing electrode that was 3.0 mm width and 3.5 cm to 10.5 cm in length. Such dimensions could be handled by the knitting and weaving machines used in this research. This resulting circuit could achieve the required 20 pF capacitance value as specified by the IC manufacturer as the optimum value for C_{SENS} for the PCF8883US circuit. This work was published in IEEE Sensors (Ojuroye, Torah, & & Beeby, 2019).

Question 2: Can the proximity and touch sensing circuits still function with an encapsulation layer when integrated into a textile?

This question addresses part of the novelty of this P.hD research, and is its main contribution to the e-textiles field. Through this P.hD research, it reports the first time in the literature that a capacitive proximity and touch sensor fabricated to be integrated into textiles with a 20:1 PDMS encapsulation – with demonstrated durability and robustness to aqueous solution recorded. Chapter 5 detailed the process of tailoring polydimethylsiloxane as electronic packaging for e-textile circuits and the results were published in journal papers IEEE Sensors (Ojuroye, Torah, & Beeby, 2018) and Microsystem Technologies (Ojuroye, Torah, & Beeby, 2019). Chapter 5 specifically revealed that a 20:1 PDMS base to curing agent ratio overall achieved the greatest contact angle values and hence the most hydrophobic. It could also exhibit approximately 45-48% less swelling in tap and distilled water respectively than the manufacturer-recommended mixing ratio of 10:1. The degree of swelling of all the mixing ratios investigated in detergent and fabric conditioner was relatively less compared to samples in distilled and tap water. This was due to the lubricating layer produced by detergent and fabric conditioner which seemed to prevent water entering the PDMS during the submersion time. An average 40.3 μm PDMS conformal thickness upon the circuit was achieved by the suspension method applied in this research. This thickness was then tested for aqueous robustness and durability through underwater experiments. Underwater tests showed that the capacitive proximity and touch sensing circuit packaged with 20:1 PDMS layer can only function when packaged. If completely packaged with no degradation, tears, or holes the circuits can survive underwater for approximately 6 months. Once the PDMS had been fabricated, to increase its hydrophobicity and minimise its swelling due to washing, it was then used to package the sensory circuit. This thesis has not only shown that the circuit can still function with a PDMS layer, but that such a layer is uniform, and can protect the circuit such that it can operate underwater for 6 months.

Question 3: Can the circuits still survive and function after being integrated into fabric using industrial weaving and knitting machinery?

This was answered by Chapter 6: E-Textile System Construction Featuring of PDMS-Packaged Flexible Capacitive Proximity and Touch Circuit, 7.4 Washing Experiment Evaluating Robustness of Integrated Conformal PDMS Packaged Capacitive Proximity and Touch Sensing E-Textile Circuit , and Chapter 8: Cyclic Mechanical Experimentation of PDMS packaged E-Textile Sensory Circuits for Quantitative Durability. The knitting and weaving techniques utilised in this Ph.D research are traditionally used to form textiles without any circuity. This was important, as it was anticipated that the capacitive proximity and touch sensing circuit could be handled by knitting and weaving machines. This was the case whereby the 20:1 PDMS packaged capacitive proximity and touch sensing circuits were integrated into the core of a yarn by knitting techniques – whereby the circuit was enwrapped in a knitted sheath and woven into a fabric by a hand loom. With both textile integration techniques, the circuit displayed functionality. However, in order to increase the likelihood

of survival, the solder pads for power, ground, and the external electrode has rigid Dymax 9001 UV-cured resin applied. Furthermore, a Vectran fibre was attached to the circuit by UV-resin in such a way to make the wires parallel and offer strain relief upon the circuit when it handled by the knitting and weaving machinery - reducing the likelihood of the wires being pulled off the copper-polyimide circuit substrate.

Question 4: Can the proximity and touch sensing circuit still display functionality after being washed with a commercial washing machine?

Yes, and this was directly answered by 7.4 Washing Experiment Evaluating Robustness of Integrated Conformal PDMS Packaged Capacitive Proximity and Touch Sensing E-Textile Circuit . These experiments were conducted with detergent and fabric conditioner, with a methodology compliant with textile washing standard 6300:2012. Proximity and touch detection were still observable from the e-textiles once washed. The results showed that circuits survived maximum 10 washes with a 400 rpm washing spin speed which was an improvement from 1 cycle survival with a washing speed of 800 rpm. Therefore, the washing speed is a critical factor to minimise abrasion and mechanical damage during the washing process. Additionally, the washing test used different washing settings SuperQuick (15 mins, 30°C), Silk/Delicates (37 mins, 30°C), and Wool/handwash (42 mins, 30°C). The circuit in the Wool settings survived the most washing cycles, showing that washing speed is more influential than washing cycle duration in maintaining circuit functionality. The PDMS hydrophobic packaging can protect the circuit from water for a long period of time, as shown in the underwater tests in 7.3 Underwater Experiment Evaluating Durability of PDMS Packaged Self-Capacitive Proximity and Touch Sensing Circuits. Causes of failure was found via microscope, that mechanical abrasions due to the spinning can cause wires to detach out of the solder joint and introduce gaps in the PDMS encapsulations. This allowed water to enter the packaging and the circuit to stop functioning.

Question 5: Can the proximity and touch sensing circuit still display functionality after being mechanically deformed like a traditional textile?

Content in Chapter 8: Cyclic Mechanical Experimentation of PDMS packaged E-Textile Sensory Circuits for Quantitative Durability was used to consult this research question. The best result for the cyclic twisting test was a circuit showing functionality until 10,100 cyclic 180° twists and for the cyclic bending tests up to 50 bends at 10.0 mm bending radius. These circuits had the PDMS encapsulation and integrated into textiles prior testing. In this case, the experiments showed that cyclic bending is more detrimental than cyclic twisting as a mechanical deformation for e-textiles in a washing machine. Although these are some of the best recorded in literature and in the FETT project, it was found that successive bending can make the circuit lose all functionality whilst successive twisting can still show touch detection. Successive twisting did not tear, rupture, or detach the PDMS conformal layer of the circuit for the cyclic twisting and cyclic bending tests. The causes of failure

were due to wires detaching out of the solder joint for both the cyclic twisting test and the bending test. The wire that detached was always the side with the counterweight attached. Therefore, the problem was the experimental setup and not the circuit. Broken circuits had their PDMS layer removed once detached from its textile encapsulation.

9.3 Recommendations for Future Research

For future research, further reduction of the circuit dimensions should be explored. The size of components is reduced each year due to minaturisation of the phone industry and industrial pick and place equipment is getting faster and more accurate. So, the advancement of nano-technology could enable nanosensors to feature on copper-polyimide flexible circuits to reduce the width further. A resulting system would need to function beyond prototype but its fabrication method must be compatible with large-scale manufacturing so the resultant e-textiles can be industrially feasible and scalable.

This thesis has produced publications on the future applications of the flexible, washable, and touch and proximity interactive e-textile system produced in complex environments. This includes in an internet-of-things (IoTs) network (Ojuroye O. , Torah, Komolafe, & and Beeby, 2019), when textiles become intelligent due to the use of machine learning computation (Ojuroye O. , Torah, Beeby, & Wilde, 2016), and in specific uses such as in educational settings (Ojuroye & Wilde, 2018) , (Wilde & Ojuroye, 2018). The state-of-the-art in electronic textile (e-textile) research are not currently commercially viable/industrially feasible due to technical challenges around the architecture (reliability of exposed electronics, lack of flexibility), data security and production equipment. Hence, it is important for engineers, computer scientists, and textile designers in this field to have a universal understanding whilst collaborating to develop e-textile products. As e-textiles is part of a very hybrid field, it is imperative moving forward to ensure terminologies are unified. This would aid those working in the field to talks across disciplinary boundaries which could hinder collaboration if not consulted. To simplify this, this thesis published (Ojuroye, Torah, & Beeby, 2017) a design of a novel categorisation chart that measures the extent of electronic integration within textiles. This chart can indicate how textiles' level of electronic integration impacts its degree of computational intelligence, necessary security, commercial viability and industrial compatibility. Concepts of this chart were used to envision applications of electronic textiles, such as the system developed in this thesis. When changing the actuator or other components, this could be performing wireless communication, measuring biological data, and utilising artificial intelligence to build contextual data of its environment.

More washing tests on e-textiles could also examine whether these circuits can survive when ironed or steamed. This is especially needed, if the textile is expected to be wearable and integrated into textiles such as cottons and linens that are typically ironed or steamed to remove wrinkles. PDMS has a high melting point, so experiments can be conducted to discover the minimum conformal

thickness of PDMS to protect the circuitry from heat. Simulations can also be conducted beforehand to verify this. Following the simulations, another washing test whereby the different temperatures are also considered should be explored.

The capacitive proximity and touch sensing circuit fabricated in this Ph.D research currently had its operation optimised to sense a human hand to actuate the illumination of an LED for visible feedback. The circuit is being used as a switch to activate the LED at the PCF8883US output pin but another component or circuit could replace the circuit to demonstrate the many use-cases for this system. Use-cases such as interfacing with connected systems such as vehicles and smart home appliances through replacing the LED at the output with a RFID transponder tag utilising wireless communication. Technologies such as the GLONASS-GPS and RAIN RFID will enable more integration of such SMDs and processors so they can function within e-textiles, allowing e-textiles to communicate with each other at further distances and – if intelligent – can form a unified knowledge about its environment. This would contribute towards tailored e-textiles to its user, which would follow on from work by (Ziefle, 2014) who has considered the idea of e-textile in smart home settings exhibiting personalised behaviour to its user. GPS technology demonstrated by an e-textile microstrip patch antenna has been tested in literature (Elliot, 2012) . Overall, wireless technology triggered by touch/proximity sensing e-textiles to explore personalised interaction should be looked in further. Furthermore, the e-textile system developed in this Ph.D should be applied to other flexible copper-polyimide sensory circuits in the FETT project using the same platform technology manufacturing method outlined in Table 3. Trials of PDMS packaging on other circuits in the FETT project has already been conducted and currently being compared to other substrates utilised by other team members. The dual accelerometer-gyroscope can still function with PDMS packaging and can communicate with a computer whilst submerged in water and flexed due to PDMS' hydrophobicity and elastomeric characteristics. PDMS should be applied to other circuits in development in the FETT project to determine if they can become underwater technologies.

Mechanical experiments revealed that the Dymax 9001 UV-curable resin could detach with high mechanical strain, especially when imposed by bending. As the PDMS layer remained unscathed for the cyclic twisting test, and its aqueous durability was supported by the 6-month underwater test survival result, more investigation should be on different mixing ratios. Investigating a PDMS mixing ratio with a higher Young's modulus than 20:1, such as 5:1 or 7:1, on the solder joints or even to act as underfill could be done. Although, with these particular mixing ratios the flexibility of the overall circuit could be reduced – as 5:1 and 7:1 produce less flexible PDMS substrates – it would not be completely rigid unlike the Dymax 9001 and it will still be chemically-resistant, hydrophobic, along with all other beneficial properties this Ph.D thesis have found suitable for e-textile applications. Nevertheless, this Ph.D thesis has found that as a result of using mixing ratios 5:1 and 7:1 hydrophobicity and degrees of swelling in aqueous solution will change. Therefore, this could become an area of scientific enquiry for e-textiles research.

Appendices

Appendix A: Table Comparison of Circuit Packaging Substrates for Ph.D System Design Specifications

Typical Properties	POLYIMIDE (KAPTON)	POLYDIMETHYLSILOXANE (PDMS)	POLYETHERETHERKETONE (PEEK)
***Colour**	Translucent	Clear	Black
Dielectric Constant at 1 kHz	= 3.4 (Dupont)	= 2.68 @100 kHz	= 3.1 (Victrex)
Dielectric Strength	= 0.33 kilovolts per mil v/mil (Dupont)	= 0.5 kilovolts per mil v/mil	= 190 kilovolts per mil v/mil (Plastics P.)
Dissipation Factor at 1 kHz	0.0018 (Dupont)	< 0.00133 (@100 kHz)	N/A (Plastics P.)
Young's Modulus	2.48 GPa (Ochoa, 2013)	0.36 – 1.24 GPa (Ochoa, 2013)	6.2 – 32.2 GPa (Services)
Flowable	Yes @ 420ºC (Stenzenberger, 1990)	Yes @ Room Temperature	Yes @ 320ºC (Victrex)
Gel Hardness	N/A	N/A	N/A
***Curing Conditions**	2 hours @150ºC 3 hours @ 160ºC 4 hours @ 170ºC (Hubbard, 2004)	10 minutes @ 150ºC 20 minutes @ 125ºC 35 minutes @ 100ºC	90 s
***Hydrophobic**	No	Yes	No (Fellow, Polyetheretherketone)
Mix Ratio	N/A	10:1 Base to Catalyst/Curing agent 87-RC, recommended	N/A
Room Temperature Cure – Hours	N/A	= 48 hours	N/A
Self-Levelling	N/A	Yes	N/A
Temperature Range	-269ºC to 400ºC (Dupont)	-45ºC to 200ºC	Max 250ºC (Fellow, Polyetheretherketone)
Thermal Conductivity	N/A	= 0.27 Watts per meter K	= 0.22 – 0.94 Watts per meter K (Services)

Viscosity	N/A	N/A	N/A
Volume Resistivity	= 1.5e+017 ohm-centimeters	= 2.9e+014 ohm-centimeters	= +016 ohm-centimeters (Victrex)
***Water Resistant**	No (Dupont)	Yes	No (Fellow, Polyetheretherketone)
***Compatibility -> Plastics**	Yes (Dupont)	Yes	N/A
***Compatibility -> Solvents**	Yes (Dupont)	Yes	Yes (Fellow, Polyetheretherketone)
Cure Properties -> Addition Cure	Yes (Dupont)	Yes	Yes (Jama, 1992) To achieve flexibility (Weiss & Muenstedt, 2002)
***Resistance -> Oxidation Resistance**	No (Zhang X. M., 2014)	Yes	Yes (Weiss & Muenstedt, 2002)
Resistance -> Ozone Resistance	Yes (Components)	Yes	Yes (Applications)
Resistance -> Thermal Resistance	Yes (Dupont)	Yes	Yes (Weiss & Muenstedt, 2002)
Resistance -> UV Resistance	Yes (Dupont)	Yes	N/A
***Resistance -> Water Resistance**	No (Dupont)	Yes	No
Thermal Properties -> High Temperature Stable	Yes (Dupont)	Yes	Yes (Fellow, Polyetheretherketone)
Thermal Properties -> Low Temperature Stable	Yes (Dupont)	Yes	N/A
***Flexible when cured**	Yes (Dupont)	Yes	No (Weiss & Muenstedt, 2002)
***Elastomeric**	No	Yes	No
***Tensile Strength**	69 MPa (Dupont)	1.5 – 1.9 MPa (Services)	98 MPa (Victrex)
***Refractive index**	1.70 (Dupont)	1.38 – 1.43 (Services)	N/A (Services)
***Poisson's Ratio**	0.34 (Dupont)	0.5 (Services)	0.4 (Services)

Table 21 Comparison of polymer characteristics for Polyimide, Polydimethylsiloxane, and Polyetheretherketone

Typical Properties	POLYETHERSULPHONE (PES)	POLYETHERIMIDE (PEI)	PARYLENE
***Colour**	Clear Amber	Translucent Amber	Clear
Dielectric Constant at 1 kHz	N/A	3.1 (Plastics P.)	3.1 (MIT)
Dielectric Strength	= 16 kilovolts per mil v/mil (Plastics P.)	= 30 kilovolts per mil v/mil (Plastics P.)	= 5.5 to 7 kilovolts per mil v/mil (Parylene)
Dissipation Factor at 1 kHz	N/A (Plastics P.)	N/A (Plastics P.)	0.0002 to 0.019 (Parylene)
Young's Modulus	2.48 GPa (Services)	3.4 – 5.6 GPa (From)	0.4 GPa (MIT)
Flowable	Yes @ 141ºC or 219ºC depending on crystalline structure (Corporation M.)	No	N/A
Gel Hardness	N/A	N/A	N/A
***Curing Conditions**	N/A	1hr @ 270ºC 2hrs @ 200ºC (Sasaki, 1988)	5 hrs
***Hydrophobic**	No	No (Sen, 2007)	Yes (Parylene)
Mix Ratio	N/A	N/A	N/A
Room Temperature Cure – Hours	N/A	N/A	N/A
Self-Levelling	N/A	N/A	N/A
Temperature Range	-110ºC to 220ºC (Fellow, Polyethersulphone)	Max temperatures 290ºC to 410ºC (Parylene)	
Thermal Conductivity	= 0.18 Watts per meter K (From)	= 0.18 – 0.23 Watts per meter K (From)	= $2.0x10^{-4}$ (MIT)
Viscosity	N/A	N/A	N/A
Volume Resistivity	= +016 ohm-centimeters (Plastics P.)	7.10e (Plastics P.)	= 1e+017 ohm-centimeters to = 6e+016 ohm-centimeters (Parylene)
***Water Resistant**	No	No (Sen, 2007)	Yes (MIT)

***Compatibility -> Plastics**	N/A	N/A	N/A
***Compatibility -> Solvents**	Fair (Spec)	N/A	Yes (Engineering)
Cure Properties -> Addition Cure	N/A	N/A	N/A
***Resistance -> Oxidation Resistance**	Yes (Database)	Yes (Johnson R. O., 1983)	N/A
Resistance -> Ozone Resistance	N/A	N/A	N/A
Resistance -> Thermal Resistance	Yes (Database)	Yes (Johnson R. O., 1983)	N/A
Resistance -> UV Resistance	Fair (Fellow, Polyethersulphone)	N/A	N/A
***Resistance -> Water Resistance**	No	No (Sen, 2007)	Yes (Parylene)
Thermal Properties -> High Temperature Stable	Yes (Database)	N/A	N/A
Thermal Properties -> Low Temperature Stable	N/A	N/A	N/A
***Flexible when cured**	No (Database)	No (CORP.)	Yes (Engineering)
***Elastomeric**	No	No	No (Engineering)
***Tensile Strength**	50- 70.3MPa (Services)	83.4 – 178.5 (Services)	45MPa – 76MPa (Parylene)
***Refractive index**	1.59 – 1.64 (Services)	1.67 (Services)	1.661 – 1.669 (Parylene)
***Poisson's Ratio**	0.37 (Services)	0.36 (Services)	0.4 (MIT)

Table 22 Comparison of polymer characteristics for Polyethersulphone, Polyetherimide, and Parylene

Typical Properties	POLYETHYLENE NAPHTHALATE (PEN)	POLYETHYLENE TEREPHTHALATE (PET)	POLY(METHYLMETHACRYLATE) (PMMA)
***Colour**	Clear	Clear but becomes opaque with thickness (Fellow, Polyethylene Terephthalate)	Clear

Dielectric Constant at 1 kHz	3 (Vishay)	3.2 (Members)	3.5 (Members)
Dielectric Strength	=160 kilovolts per mil v/mil (Zhai, 2014)	= 17 kilovolts per mil v/mil (Fellow, Polyethylene Terephthalate)	=15 kilovolts per mil v/mil (Plastics P.)
Dissipation Factor at 1 kHz	0.005 (Zhai, 2014)	0.002 (Fellow, Polyethylene Terephthalate)	0.040 (Members)
Young's Modulus	5 to 5.5 GPa (Zhai, 2014)	3.5 to 11 GPa (From)	1.1 (Services) – 3.3 GPa (Fellow, Polymethylmethacrylate)
Flowable	N/A	No	Yes
Gel Hardness	N/A	M94-101	N/A
***Curing Conditions**	N/A	N/A	N/A
***Hydrophobic**	N/A	Yes (Fellow, Polyethylene Terephthalate)	Yes and No – Can be cured to be hydrophobic or hydrophilic (Li Y. W., 2013)
Mix Ratio	N/A	N/A	N/A
Room Temperature Cure – Hours	N/A	N/A	N/A
Self-Levelling	N/A	N/A	N/A
Temperature Range	To 155ºC (Zhai, 2014)	-40ºC to 170ºC (Fellow, Polyethylene Terephthalate)	-40ºC to 90ºC (Fellow, Polymethylmethacrylate)
Thermal Conductivity	= 0.15 Watts per meter K (Zhai, 2014)	= 0.26 – 0.42 Watts per meter K (Services)	= 0.19 Watts per meter K (From)
Viscosity	N/A	N/A	N/A
Volume Resistivity	= +015 ohm-centimeter	< +014 ohm-centimeter (Fellow, Polyethylene Terephthalate)	= 2.14 +015 ohm-centimeter (Fellow, Polymethylmethacrylate)
***Water Resistant**	N/A	Yes (Fellow, Polyethylene Terephthalate)	Yes, but a 500 $x10^{-13}$ cm^3. cm cm^{-2} s^{-1} Pa^{-1} permeability to water at 25ºC (Fellow, Polymethylmethacrylate)

***Compatibility -> Plastics**	N/A	N/A	N/A
***Compatibility -> Solvents**	N/A	Yes except from alkalis (Fellow, Polyethylene Terephthalate)	No (Fellow, Polymethylmethacrylate)
Cure Properties -> Addition Cure	N/A	N/A	N/A
***Resistance -> Oxidation Resistance**	No (Zhai, 2014)	N/A	Yes -moderate (Fellow, Polymethylmethacrylate)
Resistance -> Ozone Resistance	N/A	N/A	Yes -moderate (Fellow, Polymethylmethacrylate)
Resistance -> Thermal Resistance	N/A	N/A	Low -flammable (Fellow, Polymethylmethacrylate)
Resistance -> UV Resistance	Yes (moderate) (Zhai, 2014)	N/A	Yes - moderate (Fellow, Polymethylmethacrylate)
***Resistance -> Water Resistance**	N/A	N/A	N/A
Thermal Properties -> High Temperature Stable	N/A	N/A	N/A
Thermal Properties -> Low Temperature Stable	N/A	N/A	N/A
***Flexible when cured**	N/A	No (Plastics C.)	Yes, but brittle (Fellow, Polymethylmethacrylate)
***Elastomeric**	N/A	No (Fellow, Polyethylene Terephthalate)	No (Fellow, Polymethylmethacrylate)
***Tensile Strength**	= 200 MPa (Zhai, 2014)	7.2 – 40.2 MPa (Services)	4.8 – 88.3 (Services)
***Refractive index**	1.62 (Polymer)	1.5 – 1.52 (Services)	1.49 – 1.51 (Services)
***Poisson's Ratio**	N/A	0.35 – 0.45 (Services)	0.35 – 0.4 (Services)

Table 23 Comparison of polymer characteristics for Polyethylene Naphthalate, Polyethylene Terephthalate, and Poly(methylmethacrylate)

Typical Properties	POLY(ETHYLENE GLYCOL) DIACRYLATE (PEG)	POLYTETRAFLUOROETHYLENE (PTFE)
***Colour**	Clear	Translucent (Fellow, Polytetrafluoroethylene)
Dielectric Constant at 1 kHz	N/A	2.0 (Members)
Dielectric Strength	N/A	= 50-70 kilovolts per mil v/mil (Plastics P.)
Dissipation Factor at 1 kHz	N/A	<0.0001 (Members)
Young's Modulus	N/A	0.3 to 0.8 GPa (Fellow, Polytetrafluoroethylene)
Flowable	N/A	Yes
Gel Hardness	N/A	D50-55 - Shore
***Curing Conditions**	N/A	No (Fellow, Polytetrafluoroethylene)
***Hydrophobic**	N/A	Yes
Mix Ratio	N/A	N/A
Room Temperature Cure – Hours	N/A	N/A
Self-Levelling	N/A	N/A
Temperature Range	N/A	N/A
Thermal Conductivity	N/A	= 0.24 to 0.65 Watts per meter K (From)
Viscosity	N/A	N/A
Volume Resistivity	N/A	= +018 ohm-centimeter to +019 ohm-centimeter (Fellow, Polytetrafluoroethylene)
***Water**	No (Polysciences)	Yes

Resistant		
***Compatibility -> Plastics**	N/A	N/A
***Compatibility -> Solvents**	Yes (Alfa, 46801 Polyethylene glycol diacrylate)	Yes (Fellow, Polytetrafluoroethylene)
Cure Properties -> Addition Cure	N/A	N/A
***Resistance -> Oxidation Resistance**	N/A	Yes (Fellow, Polytetrafluoroethylene)
Resistance -> Ozone Resistance	N/A	Yes (Applications)
Resistance -> Thermal Resistance	N/A	Yes (Fellow, Polytetrafluoroethylene)
Resistance -> UV Resistance	No (Kim P. J., 2006)	No (Fellow, Polytetrafluoroethylene)
***Resistance -> Water Resistance**	N/A	N/A
Thermal Properties -> High Temperature Stable	N/A	Yes (Fellow, Polytetrafluoroethylene)
Thermal Properties -> Low Temperature Stable	N/A	N/A
***Flexible when cured**	Yes (Alfa, 46497 Polyethylene glycol diacrylate, M.W. 3,400)	No
***Elastomeric**	Yes (Alfa, 46497 Polyethylene glycol diacrylate, M.W. 3,400)	No
***Tensile Strength**	N/A	= 10 to 40 MPa (Fellow, Polytetrafluoroethylene)

***Refractive index**	1.46 (Polymer)	1.35 (Polymer)
***Poisson's Ratio**	0.499 (Chan, 2012)	0.46 (Fellow, Polytetrafluoroethylene)

Table 24 Comparison of polymer characteristics for Poly(ethylene glycol) Diacrylate and Polytetrafluroethylene

Appendix B: Table Comparison of Polydimethylsiloxane Products for Ph.D System Design Specifications

Typical Properties	SYLGARD™ 186 SILICONE ELASTOMER KIT	SYLGARD™ 184 SILICONE ELASTOMER KIT	SYLGARD™ 182 SILICONE ELASTOMER KIT
Colour	Translucent	Clear	Clear
Dielectric Constant at 100 Hz	N/A	= 2.72	N/A
Dielectric Constant at 100 kHz	N/A	= 2.68	N/A
Dielectric Strength	N/A	= 500 volts per mil v/mil	= 475 volts per mil v/mil
Dissipation Factor at 100 Hz	N/A	= 0.00257	N/A
Dissipation Factor at 100 kHz	N/A	< 0.00133	N/A
Durometer - Shore 00	N/A	N/A	N/A
Durometer - Shore A	= 24 Shore A	= 43 Shore A	= 51 Shore A
Dynamic Viscosity	= 66700 Centipoise	= 3500 Centipoise	N/A
Flowable	N/A	Yes	N/A
Gel Hardness	N/A	N/A	N/A
Heat Cure	15 Minutes @ 150 ºC 25 Minutes @ 100 ºC	10 Minutes @ 150 ºC 20 Minutes @ 125 ºC 35 Minutes @ 100 ºC	N/A
Hydrophobic	N/A	Yes	N/A
Linear CTE	N/A	N/A	N/A
Mix Ratio	N/A	10:1 Base to Catalyst 87-RC	N/A
Room Temperature Cure - Hours	N/A	= 48 hours	N/A
Self-Levelling	N/A	Yes	N/A
Shelf Life	N/A	= 720 Days	N/A
Specific Gravity @ 25ºC	= 1.12	= 1.03	= 1.03
Temperature Range	-45ºC to 200ºC	-45ºC to 200ºC	-45ºC to 200ºC
Thermal Conductivity	N/A	= 0.27 Watts per meter K	= 0.16 Watts per meter K
UL 94 V-0 @ 8.4 mm thickness	N/A	Yes	N/A

UL 94 V-1 @ 6.0 mm thickness	N/A	Yes	N/A
Viscosity	N/A	N/A	N/A
Volume Resistivity	N/A	= 2.9e+014 ohm-centimeters	= 1.61e+015 ohm-centimeters
Water Resistant	N/A	Yes	N/A
Working Time	N/A	> 90 Minutes	> 480 Minutes
Compatibility -> Ceramics	N/A	Yes	N/A
Compatibility -> Plastics	N/A	Yes	N/A
Compatibility -> Polyesters	N/A	Yes	N/A
Cure Properties -> Addition Cure	Yes	Yes	Yes
General Properties -> Low Odor	N/A	Yes	N/A
General Properties -> Soft Gel	N/A	N/A	N/A
General Properties -> Solventless	N/A	Yes	Yes
General Properties -> Thermosetting	N/A	Yes	N/A
Product-Use Properties -> Parts Supplied -> Two-Part	Yes	Yes	Yes
Resistance -> Oxidation Resistance	N/A	Yes	N/A
Resistance -> Ozone Resistance	N/A	Yes	N/A
Resistance -> Thermal Resistance	Yes	Yes	Yes
Resistance -> UV Resistance	N/A	Yes	N/A
Resistance -> Water Resistance	N/A	Yes	N/A
Thermal Properties -> High Temperature Stable	Yes	Yes	Yes

Table 25 Comparison of PDMS characteristics for Dow Corning's SYLGARD ™ 186, 184 and 182

Typical Properties	SYLGARD™ 527 A&B SILICONE DIELECTRIC GEL	SYLGARD™ 1-4128 CONFORMAL COATING KIT	SYLGARD™ 577 PRIMERLESS SILICONE ADHESIVE
Colour	Clear Red	N/A	Grey
Dielectric Constant at 100 Hz	= 2.85	N/A	= 2.83
Dielectric Constant at 100 kHz	= 2.85	N/A	= 2.78
Dielectric Strength	= 425 volts per mil v/mil	N/A	= 500 volts per mil v/mil
Dissipation Factor at 100 Hz	= 0.002	N/A	N/A
Dissipation Factor at 100 kHz	= 0.0001	N/A	= 0.00065
Durometer - Shore 00	N/A	= 64 Shore 00	< 0.0004
Durometer - Shore A	N/A	N/A	= 60 Shore A
Dynamic Viscosity	N/A	N/A	N/A
Flowable	N/A	N/A	= 224 %
Gel Hardness	= 113 Grams/Penetration (1	N/A	Yes
Heat Cure	210 minutes @ 100 ºC 35 minutes @ 150 ºC 75 minutes @ 125 ºC	N/A	N/A
Hydrophobic	N/A	N/A	60 minutes @ 125 ºC
Linear CTE	= 335 µm/m/ºC	N/A	N/A
Mix Ratio	N/A	N/A	N/A
Room Temperature Cure - Hours	N/A	N/A	N/A
Self Leveling	N/A	N/A	N/A
Shelf Life	= 365 Days	= 720 Days	Yes
Specific Gravity @ 25ºC	N/A	N/A	N/A
Temperature Range	-45ºC to 200ºC	N/A	N/A
Thermal Conductivity	N/A	N/A	N/A
UL 94 V-0 @ 8.4 mm thickness	N/A	N/A	N/A
UL 94 V-1 @ 6.0 mm thickness	N/A	N/A	N/A
Viscosity	N/A	= 475 mPa.s	= 988 psi
Volume Resistivity	= 2.75e+015 ohm-centimeters	N/A	N/A
Water Resistant	N/A	N/A	N/A

Working Time	N/A	N/A	N/A
Compatibility -> Ceramics	N/A	N/A	N/A
Compatibility -> Plastics	N/A	N/A	N/A
Compatibility -> Polyesters	N/A	N/A	N/A
Cure Properties -> Addition Cure	Yes	N/A	N/A
General Properties -> Low Odor	N/A	N/A	N/A
General Properties -> Soft Gel	Yes	N/A	N/A
General Properties -> Solventless	N/A	Yes	N/A
General Properties -> Thermosetting	N/A	N/A	N/A
Product-Use Properties -> Parts Supplied -> Two-Part	Yes	N/A	Yes
Resistance -> Oxidation Resistance	N/A	N/A	N/A
Resistance -> Ozone Resistance	N/A	N/A	N/A
Resistance -> Thermal Resistance	N/A	N/A	N/A
Resistance -> UV Resistance	N/A	N/A	N/A
Resistance -> Water Resistance	N/A	N/A	N/A
Thermal Properties -> High Temperature Stable	N/A	N/A	N/A

Table 26 Comparison of PDMS characteristics for Dow Corning's SYLGARD ™ 527 A &B, 1-4-128, and 577 polymers

Typical Properties	**SYLGARD™ 527 A&B SILICONE DIELECTRIC GEL**	**SYLGARD™ 3-6636 SILICONE DIELECTRIC GEL KIT**	**SYLGARD™ 517 DIELECTRIC GEL PARTS A AND B**
Colour	Clear	Clear	N/A
Dielectric Constant at 100 Hz	= 2.85	N/A	N/A
Dielectric Constant at 100 kHz	= 2.85	N/A	N/A
Dielectric Strength	= 425 volts per mil v/mil	= 425 volts per mil v/mil	N/A
Dissipation Factor at 100 Hz	= 17 kV/mm	N/A	N/A

Dissipation Factor at 100 kHz	= 0.002	N/A	N/A
Durometer - Shore 00	= 0.0001	N/A	N/A
Durometer - Shore A	N/A	N/A	N/A
Dynamic Viscosity	N/A	N/A	N/A
Flowable	N/A	N/A	N/A
Gel Hardness	N/A	N/A	N/A
Heat Cure	= 113 Grams/Penetration (1	= 110 Grams/Penetration (1	N/A
Hydrophobic	210 minutes @ 100 ºC 35 minutes @ 150 ºC 75 minutes @ 125 ºC	180 minutes @ 70 ºC 45 minutes @ 100 ºC	N/A
Linear CTE	N/A	N/A	N/A
Mix Ratio	= 335 µm/m/ºC	N/A	N/A
Room Temperature Cure - Hours	A/B 1:1	N/A	N/A
Self-Levelling	= 465 Centipoise	N/A	N/A
Shelf Life	N/A	N/A	N/A
Specific Gravity @ 25ºC	N/A	N/A	N/A
Temperature Range	N/A	= 365 Days	N/A
Thermal Conductivity	= 0.95	N/A	N/A
UL 94 V-0 @ 8.4 mm thickness	N/A	N/A	N/A
UL 94 V-1 @ 6.0 mm thickness	N/A	-45ºC to 200ºC	N/A
Viscosity	N/A	N/A	N/A
Volume Resistivity	N/A	N/A	N/A
Water Resistant	= 470 mPa.s	N/A	N/A
Working Time	= 454 mPa.s	N/A	N/A
Compatibility -> Ceramics	N/A	N/A	N/A
Compatibility -> Plastics	N/A	N/A	N/A
Compatibility -> Polyesters	N/A	N/A	N/A
Cure Properties -> Addition Cure	N/A	Yes	N/A
General Properties -> Low Odor	N/A	N/A	N/A

General Properties -> Soft Gel	N/A	Yes	N/A
General Properties -> Solventless	N/A	N/A	N/A
General Properties -> Thermosetting	N/A	N/A	N/A
Product-Use Properties -> Parts Supplied -> Two-Part	Yes	Yes	N/A
Resistance -> Oxidation Resistance	N/A	N/A	N/A
Resistance -> Ozone Resistance	N/A	N/A	N/A
Resistance -> Thermal Resistance	N/A	N/A	N/A
Resistance -> UV Resistance	N/A	N/A	N/A
Resistance -> Water Resistance	N/A	N/A	N/A
Thermal Properties -> High Temperature Stable	N/A	Yes	N/A

Table 27 Comparison of Dow Corning's SYLGARD ™ 527 A&B, 3-6636, and 517 polymer products

Typical Properties	**SYLGARD™ 567 PRIMERLESS SILICONE ENCAPSULANT KIT**
Colour	Black
Dielectric Constant at 100 Hz	= 2.85
Dielectric Constant at 100 kHz	= 2.79
Dielectric Strength	= 405 volts per mil v/mil
Dissipation Factor at 100 Hz	= 16 kV/mm
Dissipation Factor at 100 kHz	N/A
Durometer - Shore 00	N/A
Durometer - Shore A	= 40 Shore A
Dynamic Viscosity	= 1500 Centipoise
Flowable	N/A
Gel Hardness	Yes

Heat Cure	N/A
Hydrophobic	120 Minutes @ 100ºC 180 Minutes @ 70ºC
Linear CTE	Yes
Mix Ratio	= 300 µm/m/ºC
Room Temperature Cure - Hours	1:1 Base to Catalyst
Self-Levelling	N/A
Shelf Life	Yes
Specific Gravity @ 25℃	= 140 psi
Temperature Range	= 720 Days
Thermal Conductivity	N/A
UL 94 V-0 @ 8.4 mm thickness	= 1.24
UL 94 V-1 @ 6.0 mm thickness	-45ºC to 200ºC
Viscosity	N/A
Volume Resistivity	= 0.29 Watts per meter K
Water Resistant	N/A
Working Time	N/A
Compatibility -> Ceramics	Yes
Compatibility -> Plastics	Yes
Compatibility -> Polyesters	Yes
Cure Properties -> Addition Cure	Yes
General Properties -> Low Odor	Yes
General Properties -> Soft Gel	N/A
General Properties -> Solventless	Yes
General Properties -> Thermosetting	Yes
Product-Use Properties -> Parts Supplied -> Two-Part	Yes
Resistance -> Oxidation Resistance	Yes
Resistance -> Ozone Resistance	Yes
Resistance -> Thermal Resistance	Yes
Resistance -> UV Resistance	Yes
Resistance -> Water Resistance	Yes
Thermal Properties -> High Temperature Stable	Yes

Table 28 Characteristics of Dow Corning's SYLGARD TM 567

Appendix C: Table of Comparison for Touch and Proximity Sensing Surface Mount Components for E-Textile Circuitry

Name	Manufacturer	Dimensions	Typical Detection Distance	Energy Consumption	Sensitivity
FDC2114	Texas Instruments	4.0 mm x 4.0 mm	Depends on distance between the shield and sensing plate, and the sampling rate. Experiments showed target distance detection up to 100.0 mm	• Supply Voltage: 2.7 V to 3.6 V • Power Consumption: Active: 2.1 mA	• Resolution: up to 28 bits • System Noise Floor: 0.3 fF at 100sps
VL6180X	ST Microelectronics	4.8 mm x 2.8 mm x 1.0 mm	Up to 100.0 mm	• 2.6 V – 3.0 V Supply Voltage	• Hardware standby (GPIO0 = 0): < 1 μA • Software standby: < 1 μA • ALS: 300 μA Ranging: 1.7 mA (typical average
*CY8C201A0-LDX2I Capacitive Button	Cypress Semiconductor Corporation	3.0 mm x 3.0 mm x 0.6 mm	-	• Active current: continuous sensor scan: 1.5 mA	Wide range of operating voltages: • 2.4 V to 2.9 V • 3.10 V to 3.6 V • 4.75 V to 5.25 V
VCNL4020X01	Vishay Semiconductors	4.90 mm x 2.90 mm x 0.83 mm	1 mm to 200 mm	• Supply voltage range V_{DD} : 2.5 V to 3.6 V Current: 1.5 - 2μA	• 16 bit dynamic range from 0.25 lx to 16 klx
TIDA-00244	Texas Instruments	4.0 mm x 3.5 mm	Not stated	• SN65HVD101 : 9 V to 36 V Supply Range • MSP430FR5738: 2 V to 3.6 V	Not stated
PCF8883T//PCF8883US	NXP Semiconductor	5 mm x 3.99 mm x 1.48 mm (PCF8883T)	2.0 cm, 5.0 cm with a 5 x 10 cm electrode plate		Not defined by influenced by CPC, CLIN, and electrode size –sensitivity can be configured for the chip environment

		1.16 mm x 0.86 mm x 0.44 mm (PCF8883US)			
LT-1PA01		3.05 mm x 2.1 mm x .01 mm	70 mm	• Supply Voltage: 2.7 V to 3.6 V • Supply Current: 80µA	•Sensitive enough to detect black ESD foam which reflects only 1% of IR. Blonde hair typically reflects more than brown hair and skin tissue is more reflective than human hair.
APDS-9960	SparkFun	3.94 mm x 2.36 mm x 1.35 mm	100mm	• Supply Voltage: 2.4 V to 3.6 V • LED Supply Voltage: 3.0 V to 4.5 V	• If operating from a single supply, use a 22-Ω resistor in series with the VDD supply line and a 1-µF low ESR capacitor to filter any power supply noise. • The key goal is to reduce the power supply noise coupled back into the device during the LED pulses. • Power consumption and noise are minimized with adjustable IR LED timing.
GP2AP002 S30F	Sharp	4.0 mm x 2.0 mm x 1.25 mm	• Maximum detection distance: 65.0 mm	• Supply Voltage: 2.4 V to 3.6 V • Operating Current: 240 µA • LED Peak Current: 170 mA	• SD-sensitive Because it is fabricated by sub-micron CMOS process • However, GP2AP002S30F starts to exhibit false detection with external light noise beyond this level.

GP2AP020 A00F	Sharp	4.0 mm x 2.0 mm x 1.2 mm	60.0 mm	• Supply Voltage: 1.7 V to 3.6 V • Operating Current: 240 µA • LED Peak Current: 170 mA	• Minimum Detection sensitivity (light sensor) 0.02 lx
ISL29028I ROZ-T7	Renesas Electronics	2.0 mm x 2.1 mm x 0.7 mm	1.0 mm to 200.0 mm	• DC Typical Supply Current for ALS/Prox Sensing: 138 µA • 110 µA for Sensors and Internal Circuitry • 1.7 V to 3.63 V Supply for I^2C Interface • 2.25 V to 3.63 V Sensor Power Supply	• Ambient Light Sensor: 50 Hz/60 Hz Flicker Noise and IR Rejection • Proximity Sensor: Ambient IR Noise Cancellation (Including Sunlight)
LMP91300	PCF8883T/PCF8883US by NXP Semiconductor	2.05 mm x 2.67 mm	The LMP91300 detects the presence of a metal object based On the RP change of an LC oscillator, depending on the distance of the metal object	Typical Current: 3mA	Using a lower response time will shorten the settling time of the digital filter and give faster readings from the RP to digital converter but will increase the noise in the reading. A higher setting gives the digital filter more time to settle and will decrease the noise in the reading.
MTCH102	Microchip Technology	3.0 mm x 3.0 mm x 1.1 mm (SOIC) 3.0 mm x 3.0 mm x 0.5 mm (DFN)	The device will sample the voltage on the MTSA (sensitivity) pin after every 32nd scan, so it does not only support setting a fixed sensitivity by a resistor ladder, but it also allows adjusting the sensitivity dynamically while the device is running.	Total Power dissipation: 800 mW	The MTSA pin is an input that determines the sensitivity of touch/proximity sensors. Applying VDD will give the lowest sensitivity while applying VSS will give the highest.

MTCH112	Microchip Technology	4.90 mm x 3.90 mm x 1.75 mm (SOIC) 3.0 mm x 3.0 mm x 0.90 mm	For a rounded diameter sensor (1-3 inches) the detection distance range is (2.25 to 4.5 inches). The maximum proximity distance will be highly dependent on the level of noise in the environment.	Total Power dissipation: 800 mW	Proximity Threshold Register (PROX_THRESH) is identical to the Press Threshold register, except that it relates to the proximity detection. Increase this value to decrease the sensitivity of the sensor in low-noise environments. • 13 bits signal resolution

Table 29 Technical specifications for touch and proximity detection chip

Appendix D: FETT Fabrication Methodology of Strip-Shaped Flexible Circuits for Textile Integration

The fabrication method used in this research was the same as that already devised and used in the FETT project by all other circuits in development.

Starting with deposition, the spin coating process during lithography is the means to evenly coat a wafer with a chemically resistant polymer. Additive materials are used in the deposition stage, which are either sputtered or spin-coated on a substrate such as polyimide or silicon. Another name for this polymer is a 'resist' or 'photoresist', to which is exposed to UV light through a quartz mask to either break or link the polymer chains.

A silicon wafer is used for supporting the copper-coated polyimide which acts as the circuit substrate. The silicon wafer was then to be inserted into the Brewer Resist Spinner E4109 and a positive photoresist called 81813 was used. The selected recipe from this stage was AZ183YW which had a max speed of 2000 rpm (50 s). The silicon wafer was placed on stage panel within resist spanner and centered using the "calibrating lever". If centered correctly, the wafer will turn on its axis without translating in the x and y directions. Centering is important to ensure even coating of photoresist. The photoresist acts as an adhesive layer between the silicon wafer and the copper plated polyimide instead of glue or tape to prevent the copper polyimide from ripping or tearing during the removal process. The first spinning process resulted in less than 1µm thickness of photoresist on the silicon wafer, just enough to cover its surface.

The copper-plated polyimide was prepared for spin-coating by cutting it into the same shape as a silicon wafer. The pre-cut copper polyimide is aligned, pressed, and laid on top of the photoresist covered silicon wafer. Again, this structure was spun for the same time duration, speed, and thermally cured at the same settings.

The objective of the thermal curing step was to provide an adhesion for the copper-plated polyimide to secure on top of the silicon wafer. After two spin coating process has completed, this created a silicon wafer which has a thin layer of copper polyimide sandwiched between layers of photoresist either side. This silicon wafer structure undergoes a thermal cure for 3 minutes at $100^{O}C$ in the Thermo Scientific Heraeus Oven. This thermal cure process is done to bake the photoresist and thicken it. The thermal cure process solidifies the photoresist to produce a cured layer suitable for the photoresist process. Following the deposition, spin coating, and thermal curing processes, the secured copper-plated polyimide silicon wafer was placed inside a UV Photolithography aligner machine. Photolithography involves exposing ultraviolet (UV) light onto deposited resist on the circuit substrate through a mask. A filter is removed from machinery to make it UV photolithography. EVG Mask Aligner software was used to control the photolithography machinery.
This photolithography machinery process to transfer circuit design onto copper-polyimide surface:

- Insert frame for initial mask aligner.

- Take out frame and insert thermal cured copper polyimide silicon wafer.
- Align camera to focus acetate circuit design onto thermal cured copper polyimide silicon wafer.
- Start UV exposure.
- Take out thermal cured copper polyimide silicon wafer.

The AK2070_AK recipe is used, having a UV exposure time of 10s that has been calibrated to the photoresist used. UV exposure crosslinks the photoresist – areas where the resist is exposed the resist becomes weak whilst areas where it is covered by the circuit acetate stencil the resist becomes cross-linked and strong. Due to the print of the circuit artwork on the acetate mask, the acetate mask was placed underneath the glass tile that was used for UV exposure. After the UV exposure, the UV-cured, copper-plated polyimide silicon wafer was placed into a 4:1 ratio of water to developer solution in a shallow flask. To remove the photoresist that have been weakened by UV exposure a developer solution is used. The AZ 400K Developer is mixed in 1 part to 4 parts water. 100ml of developer was used to 400 ml water and placed in a glass beaker. The UV exposed, thermal cured copper polyimide silicon wafer is placed in beaker of developer solution and swirled for 30 s. Then the wafer was removed and swirled in water for 20s.The wafer was dried with nitrogen gas to remove the water and any residue. Using the dufilier, it confirmed a 2.0 mm thickness of photoresist on the silicon wafer.

To remove the copper regions on the UV-exposed wafer, copper etching is completed. Copper etching removes copper that has weakened due to UV exposure, to reveal the circuit design. Etching the 18μm-thick copper layer from the 25μm-thick polyimide substrate requires chemical removal. 1.1kg of Fine Etch Crystals, made by Universal Etch, were saturated with 4.5 litres of room-temperature water (approx. 20°C) and mixed until all the crystals had dissolved. This turned the mixture into a translucent liquid. The solution was poured into a Mega Electronics PA104 etch tank. This 5 L capacity etch tank is free-standing, and typically used for the rapid production of PCBs (Mega Electronics PCB Bubble Etch Tank). The temperature was set at its maximum before wafers - with the lithography-treated copper-plated polyimide (i.e. with photolithography tracks) - were inserted into the etch tank holding reservoir and lowered into the solution.

Air is forced through two pumps in the etch tank to produce a bubbling agitation on the wafer surface PCBs (Mega Electronics PCB Bubble Etch Tank). The etch tank bubbles the solution for an even removal of the UV treated copper regions of the copper-plated polyimide. The result it the removal of the polyimide that was UV cured, such that the copper interconnects and solder pads remained on the polyimide substrate. It was timed that 8-15 minutes was the required etch duration to remove the surplus copper of the polyimide substrate whilst retaining the copper on the tracks and solder pads. After the copper etch, the wafer is swirled in water and dried with nitrogen gas. Residue photoresist and copper etch is removed with acetone which otherwise makes circuit non-conductive.

Appendix E: Woven Capacitive Touch and Proximity Sensing E–Textile Demonstrator Methodology

The circuit was treated as a weft yarn in this process to insert the circuit and its wires within the fabric as it is woven. Different colours of yarns could be strategically controlled to disguise the circuit even further. This was to fulfil the objective to make the circuit unobtrusive when integrated into a woven textile. To start the weaving process, warp yarns were prepared on a warping mill.

Figure 119 (Left) Warp yarns wrapped around warping mill for weaving process, (right) Separation of the warp yarn using a cross stick on the loom

The warp yarns were then wound on the back beams of the loom and a cross stick was used to separate the warp yarns. Then, each warp yarn was threaded by a heddle where they are arranged vertically through the loom.

Figure 120 (Left) Warp yarns are put through heddles and threaded vertically in loom, (right) Attaching warp yarn to front beam such that weaving can take place

The threaded warp yarns are rested on a dent on the reed of the loom, and this stage is called reeding. The reed is used to control how tightly the weave will be. The read was placed on the beater of the loom so that a tight weave could occur and keep the circuit secured in the fabric. The warp yarn is then tied to the front beam of the loom before the weaving of the weft yarn and the circuits began. The warp yarn was set up in double cloth so that a horizontal pocket/channel could be created whilst the capacitive proximity and touch sensing circuit was being woven simultaneously.

Appendix F: Additional Experiment Result Tables for Chapter 7

F.1 Data Collection for Nominal Proximity Detection Distance with Tailored Electrode Surface Area and Strip-layout

Additional Electrode Size area (cm^2)	Max. Proximity Detection Distance (cm)
16	3
16	2.6
16	2.5
16	2.8
16	3.2
Average	**2.82**
25	3.5
25	4.5
25	4.6
25	4.8
25	4.7
Average	**4.42**
36	4
36	4.5
36	5.4
36	5.4
36	6
Average	**5.06**
49	5
49	5.3
49	5.7
49	6.2
49	6
Average	**5.64**
64	4.4
64	6.7
64	7
64	7.5
64	7.5
Average	**6.62**
81	9.5
81	10
81	10.2
81	10.5
81	6
Average	**9.24**
100	7.5
100	10

100	11
100	12
100	13
Average	**10.7**
121	10.5
121	12
121	12.5
121	13
121	14
Average	**12.4**
144	14
144	1
144	20
144	5
144	17
Average	**11.4**
169	5
169	10
169	11
169	9
169	15
Average	**10**
196	6
196	17
196	18
196	17
196	17
Average	**15**
225	1
225	2
225	4
225	4.5
225	6
Average	**3.5**
256	4
256	4.5
256	7
256	8.5
256	6
Average	**6**

Table 30 Experimental data of electrode surface area and corresponding nominal proximity distance

F.2 Data Collection for smallest single electrode dimension to enable proximity and touch sensing for optimum circuit performance, C_{SENS} value

Number of Electrodes in 121 cm^2 strip-square area	Max. Proximity Detection Distance (cm)
2	1.5
2	1.4
2	1.7
2	1.5
2	1.6
Average	**1.54**
3	3.9
3	4.1
3	4.2
3	3.9
3	4
Average	**4.02**
4	3.9
4	3.8
4	4.4
4	3.9
4	4.2
Average	**4.04**
5	4.3
5	4.6
5	4.3
5	4.6
5	4.6
Average	**4.48**
6	4.6
6	4.9
6	4.6
6	4.5
6	4.8
Average	**4.68**
7	4.8
7	4.9
7	4.6
7	4.9
7	4.8
Average	**4.80**
8	4.8
8	4.9
8	4.8
8	4.7

8	4.8
Average	**4.80**
9	4.8
9	4.8
9	4.9
9	4.7
9	4.8
Average	**4.80**

Table 31 Experimental data of number of strip-shaped electrodes with a 121 cm^2 area and the corresponding nominal proximity distance

F.3 Data Collection for external electrode length, with a fixed 3 mm width to enable proximity and touch sensing for optimum C_{SENS} value = 20 pF

External Electrode Length (cm)	**3.5**	**7.0**	**10.5**	**14.0**	**17.5**
Capacitance value C_{SENS} (F)	4.11	12.17	10.91	11.29	19.63
	4.28	8.04	5.90	13.17	10.99
	4.18	6.37	8.04	4.78	14.43
	3.06	8.81	3.26	5.77	10.91
	15.09	8.15	14.46	20.77	35.40
No trigger object detection C_{SENS} Average (F)	**3.91**	**7.84**	**8.51**	**11.16**	**13.99**
Capacitance value C_{SENS} (F)	17.22	10.61	16.06	18.33	32.52
	35.40	11.04	10.38	7.18	10.12
	16.68	9.02	8.39	12.77	53.40
	10.55	18.09	10.98	9.43	2.59
	26.79	26.92	23.29	25.62	19.44
Proximity detection C_{SENS} Average (F)	**20.23**	**15.14**	**13.82**	**14.66**	**14.78**
Capacitance value C_{SENS} (F)	13.37	16.12	25.84	19.60	10.46
	24.08	12.82	15.33	13.45	11.60
	25.60	13.67	21.78	13.43	12.64
	15.61	17.63	22.88	13.56	22.38
	26.39	21.77	14.24	37.60	10.07
Touch detection C_{SENS} Average (F)	**25.35**	**16.40**	**20.01**	**15.01**	**11.19**

Table 32 Experimental data of external electrodes with varying length and fixed a 3 mm width and the corresponding C_{SENS} value

Numbers in red text were considered as outliers and therefore not used to calculate the average readings.

Appendix G: COMSOL Simulation Methodology

In order to design and simulate an e-textile capacitive sensor in COMSOL, a series of steps need to be followed:

A. Model Navigator

1. Start by opening the Model Navigator after running COMSOL 5.3. Select the Electrostatics Module.
2. Then select Stationary Physics as the type of Study as shown in the following figure:

B. Geometry Modelling

1. To draw a 3D geometry, right-click on Component 1 in the Model Builder and select Block. This block will act as a layer that forms the electrode within the e-textile.
2. Set the width and depth of the block to 0.003 m and 0.035 m respectively. Additionally, set the position to 'Centre' and click **Build**.
3. Make another block the same way with the same dimensions. With the two blocks, label other first block 'Polyimide' and the second block 'Copper'.
4. For the Polyimide Layer, set the height to 2.5*10^-5 and for the Copper Layer set its height to 1.8*10^-5. Click **Build All**.
5. To ensure the copper layer is located on top of the of the polyimide layer, set its z-coordinate in the Position section to 2.15*10^-5:

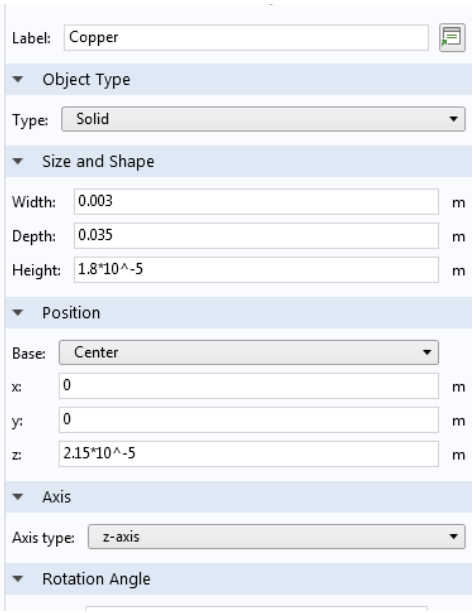

Figure 121 Positioning solid shape representing copper on top of solid shape representing polyimide to represent copper-polyimide circuit

6. Right-click 'Component 1' again and select cylinder. This will act as the yarn portion of the system. Rename the cylinder 'Textile Yarn', and set its radius and height to 0.0025 m and 0.04 m

respectively. Set its position on the y-coordinate to -0.02 m to make the internal copper and polyimide blocks in the middle of the yarn. Finally, set the cylinder in the y-direction by selecting y-axis:

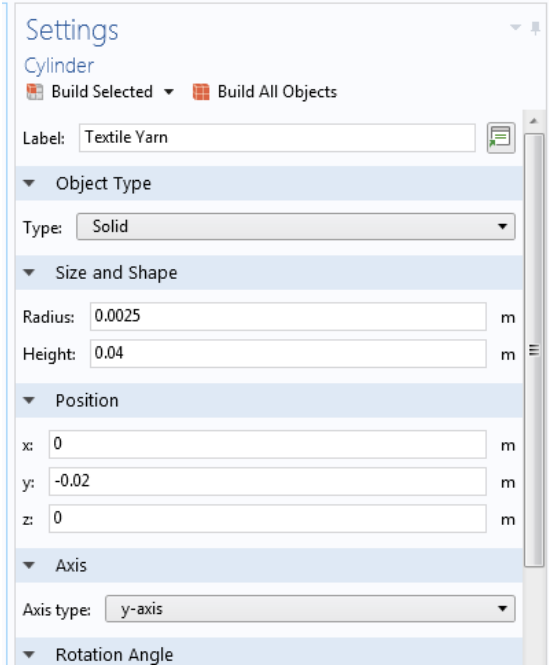

Figure 122 Defining size dimensions of textile yarn in COMSOL

This results in the following figure:

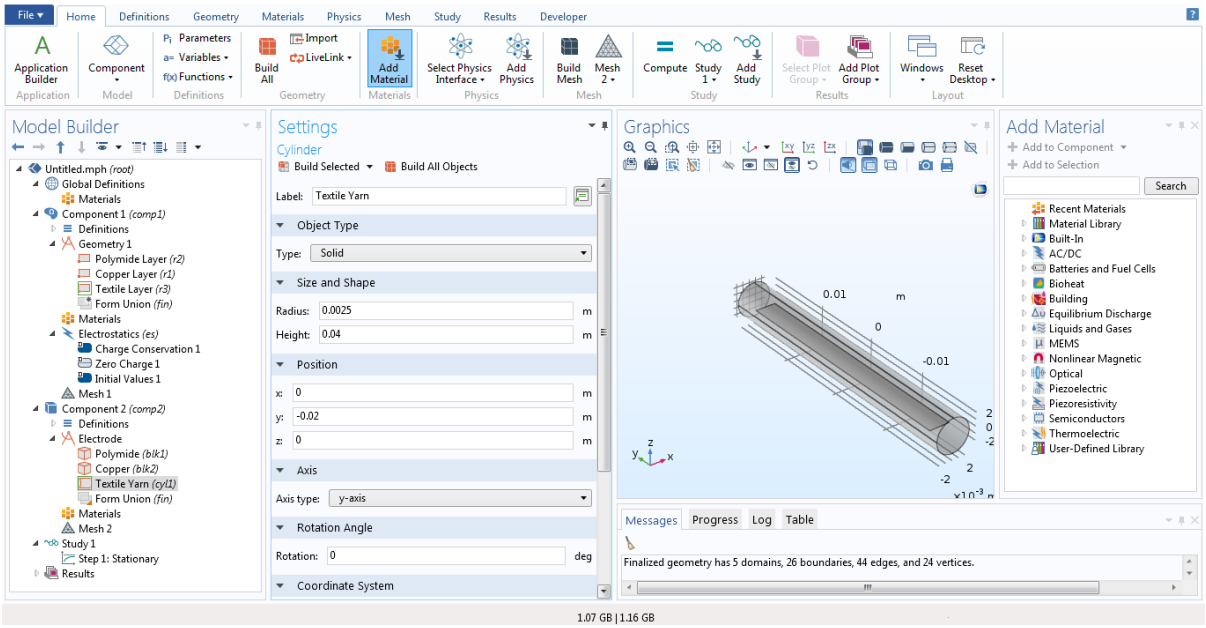

Figure 123 COMSOL generation of copper-polyimide substrate in core of textile yarn

7. The human finger can be represented with a cylinder. An adult size finger has an average radius of 2.5 mm (reference) and average index finger length of 2.0 cm (reference), so this became the value of

its radius and height respectively. The cylinder was then centred and since its starting position for the finger would be touching the yarn, so its z-coordinate became 0.0025.

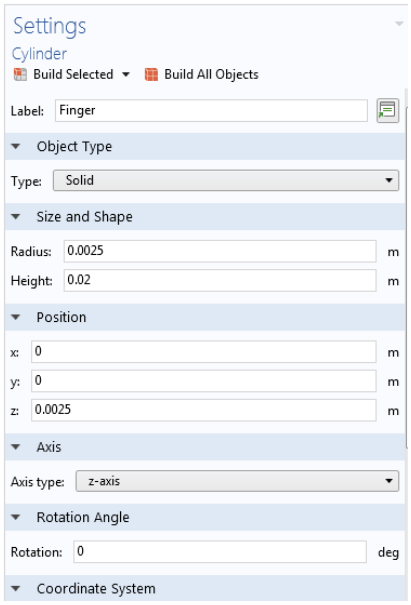

Figure 124 Defining dimensions of solid shape that will represent a human finger as second electrode

7. Finally, the whole simulation setup was to be encased in a region of air. For this, right-click the E-Textile Setup Geometry and select *Block*. Label this block 'air' and apply a 0.05m value to width, height, and depth. Then, set its base to 'Centre'.

C. Applying Materials

1. Select the Materials Tab and Select Add Material.

2. For the Copper block, select Materials –> MEMS –> Metals –> Cu –Copper, and apply it to domain 5. Apply a Poisson's Ratio value of 3.4.

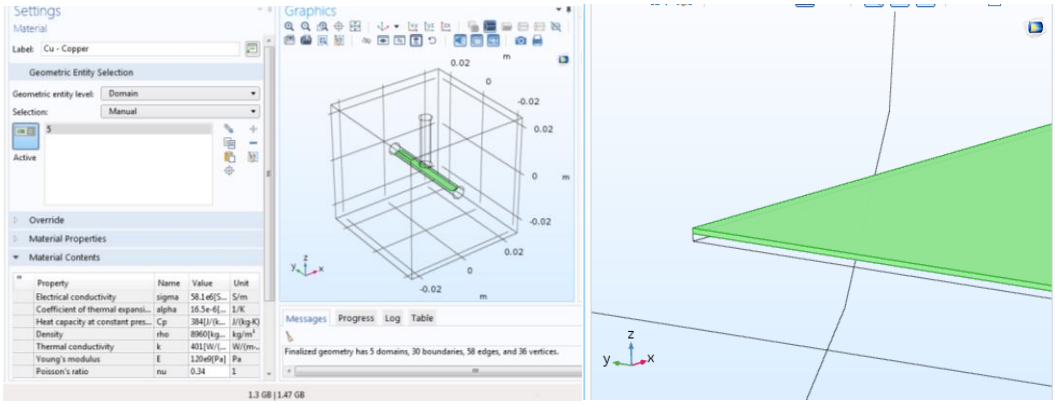

Figure 125 Applying material type and contents details to solid representing copper layer on copper-polyimide substrate in COMSOL

3. For the Polyimide block, select Materials –> MEMS –> Polymers –> Polyimide, and apply it to domain 4.

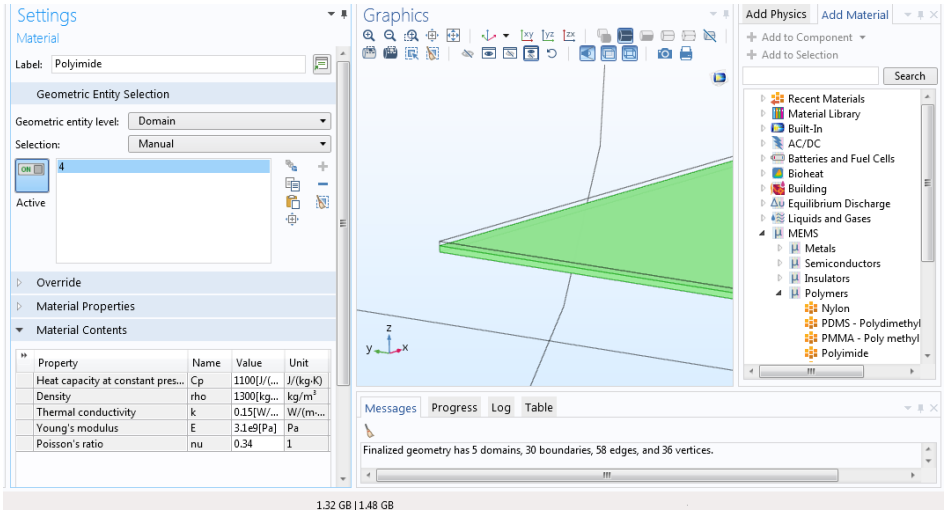

Figure 126 Close-up of applying material type and contents details to solid representing polyimide layer on copper-polyimide substrate

4. For the Textile Yarn block, select Materials –> MEMS –> Polymers –> Nylon, and apply it to domain 2.

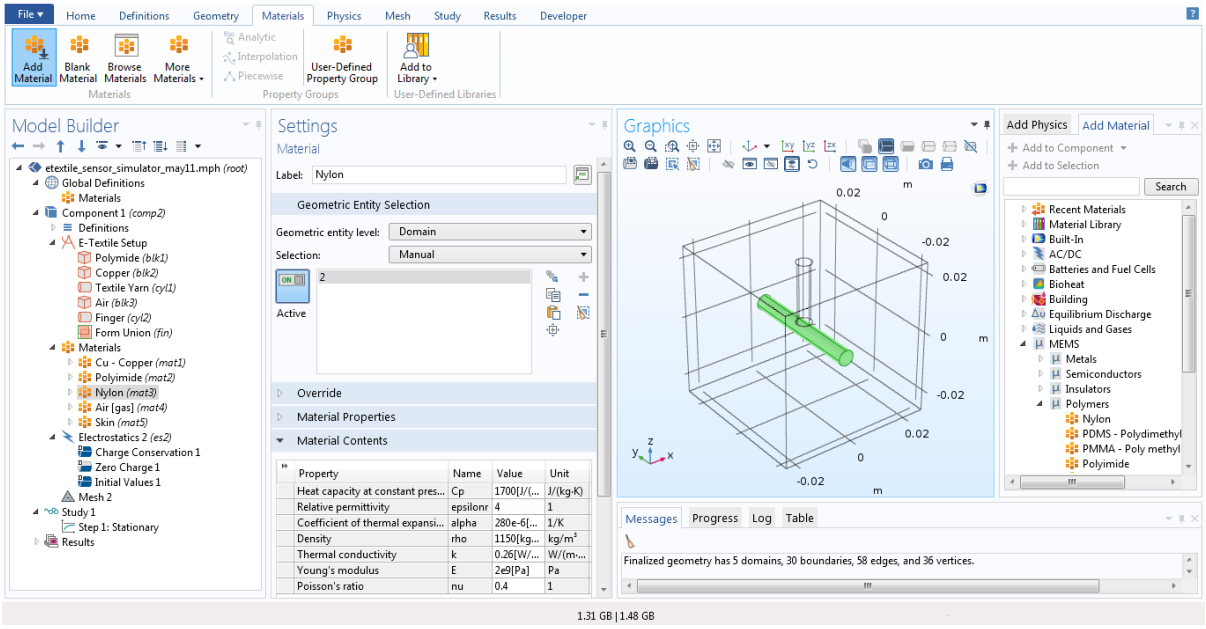

Figure 127 Applying material type and contents details to solid representing textile yarn

5. For the Air block, select Materials –> Liquids and Gases –> Gases –> Air, and apply it to domain 1.

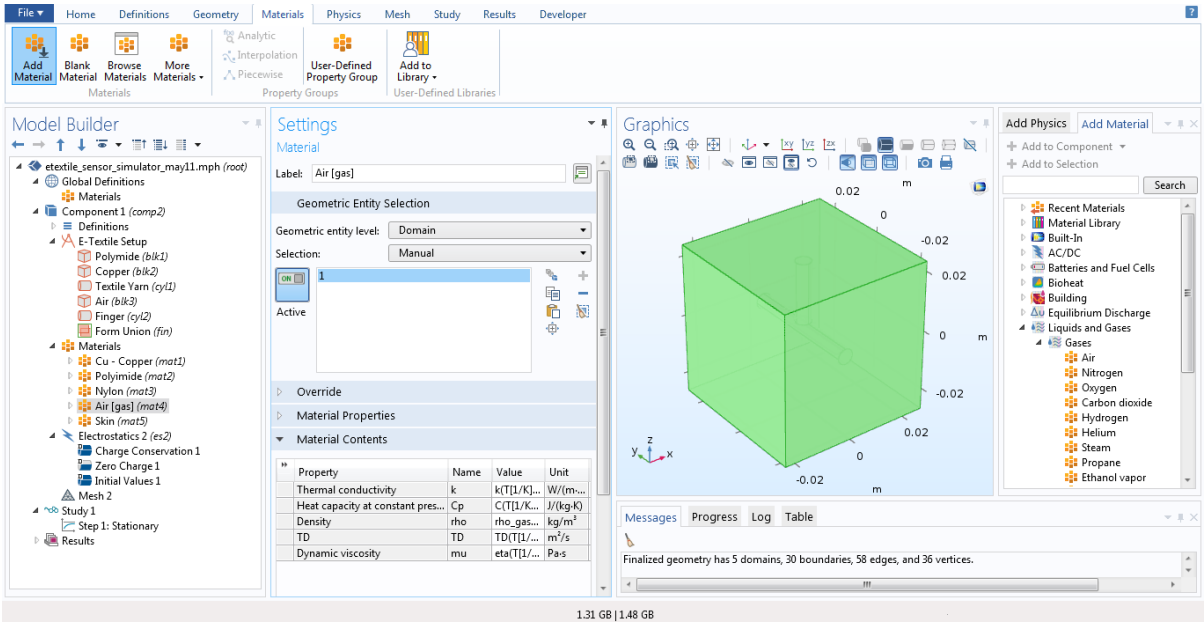

Figure 128 Applying material type and contents details to solid representing block of air

8. For the finger block, select Materials –> Bioheat –> Skin, and apply it to domain 3.

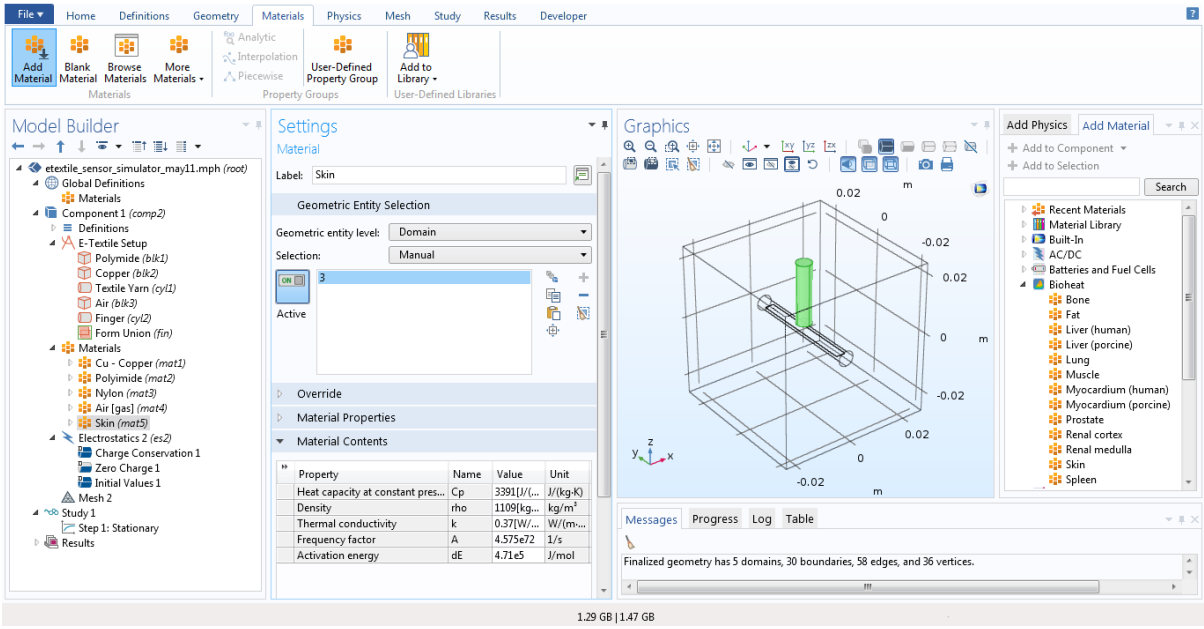

Figure 129 Applying material type and contents details to solid representing human finger

D. Physics Settings

1. Subdomain Settings: Select the Electrostatics Physics in Model view and right-click to add Ground and Electric Potential.

2. Boundary Conditions: There are three boundary conditions that need to be defined. First is the ground, second is the electric potential (voltage) and third is the zero charge condition. To access boundary conditions, select Boundary Settings under the Physics menu.

Domain number	**5**	**4**	**2**	**1**	**3**
Layer	Polyimide	Copper	Textile Yarn	Air	Finger
Boundary Condition	Symmetry/Zero charge	Electric Potential (4.12 voltage)	Symmetry/Zero charge	Zero charge	Ground

Table 33 COMSOL Simulation Boundary Conditions

An initial value of zero was set to all domains.

E. Mesh Analysis

1. In order to do a Mesh Analysis, click on Mesh → Size -> Fine -> Initialize Mesh:

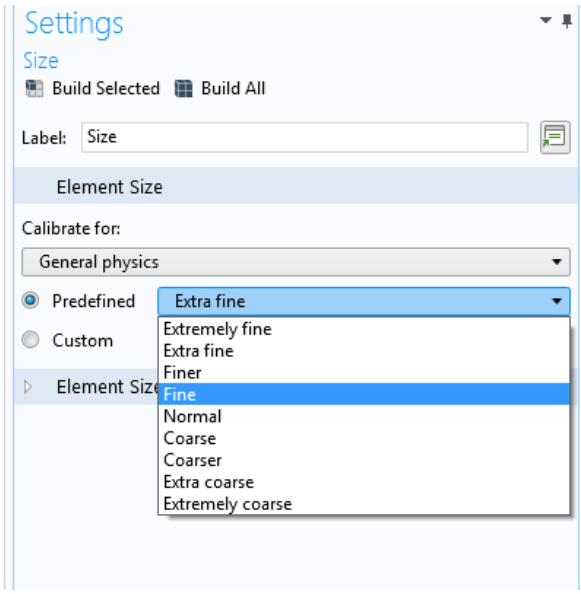

Figure 130 Initialising mesh in COMSOL to Fine

2. Once the Create Mesh Analysis is complete, the e-yarn structure will look like the following figure:

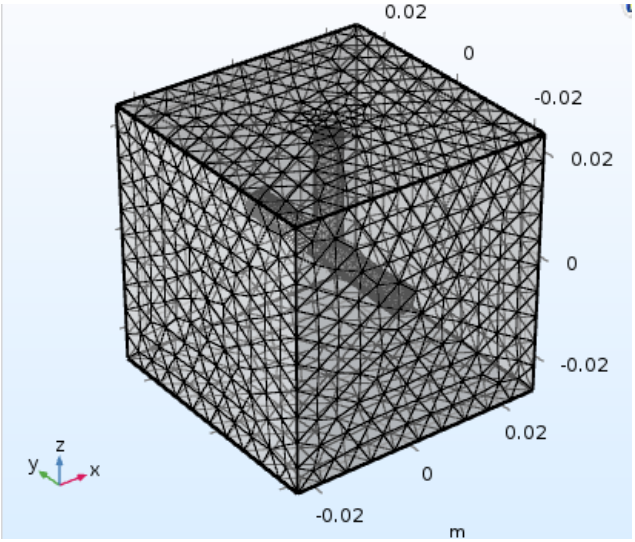

Figure 131 Completed mesh analysis of copper-polyimide circuit in core of textile yarn in COMSOL

F. Solve Problem

1. In order to get a solution to the problem by quantifying the electric field, click on Study → Solve Compute

2. Once the Solve Problem Analysis is complete, the final capacitive sensor structure appears with its electric field as follows:

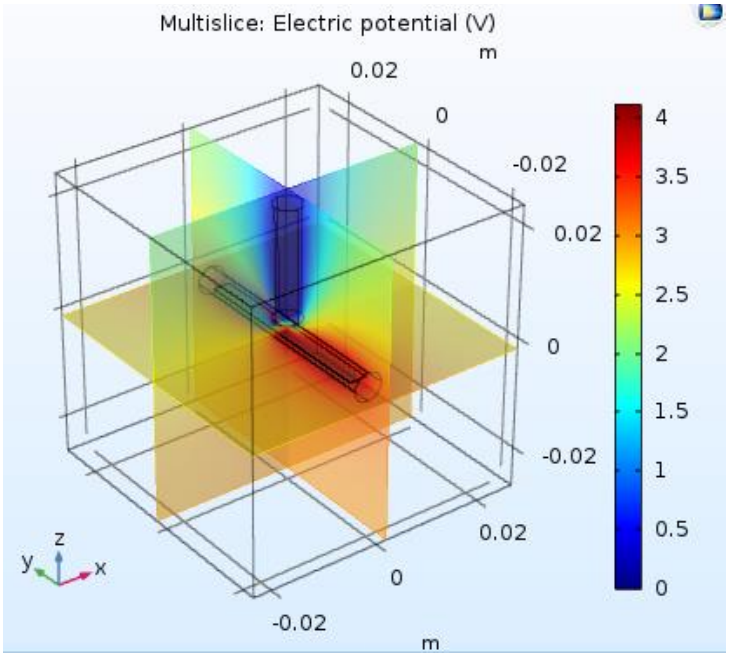

Figure 132 COMSOL simulation generation of electric potential of electric field from copper-polyimide circuit at core of textile yarn

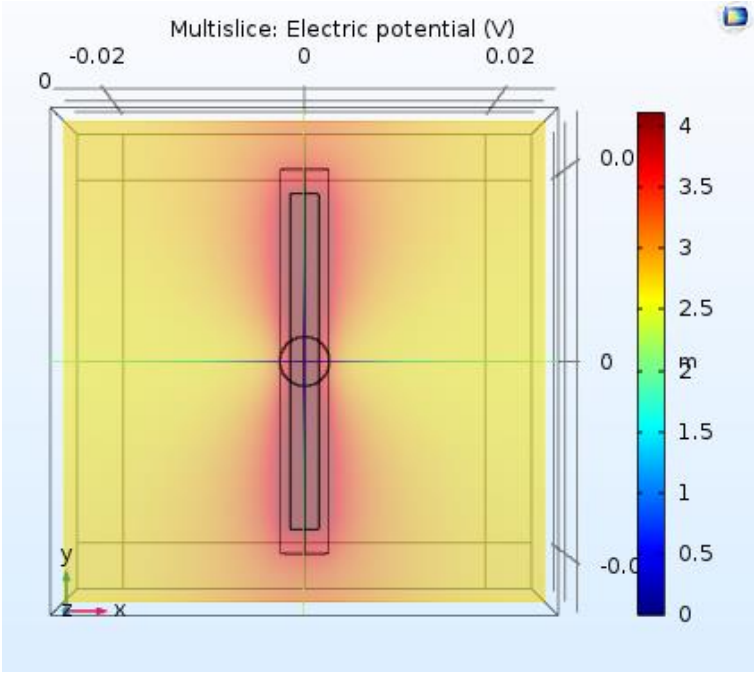

Figure 133 Z-axis view of COMSOL simulation generating electric potential of electric field from copper-polyimide circuit at core of textile yarn

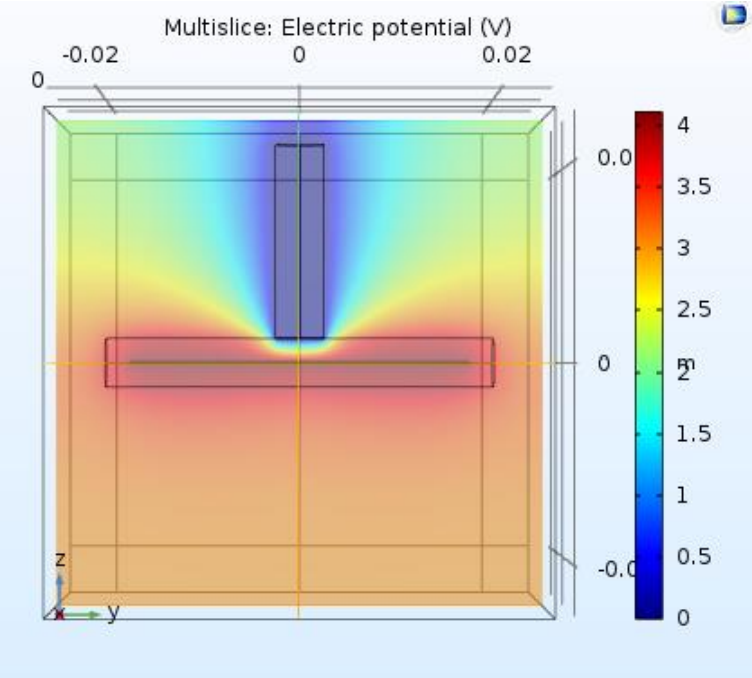

Figure 134 X-axis view of COMSOL simulation generating electric potential of electric field from copper-polyimide circuit at core of textile yarn

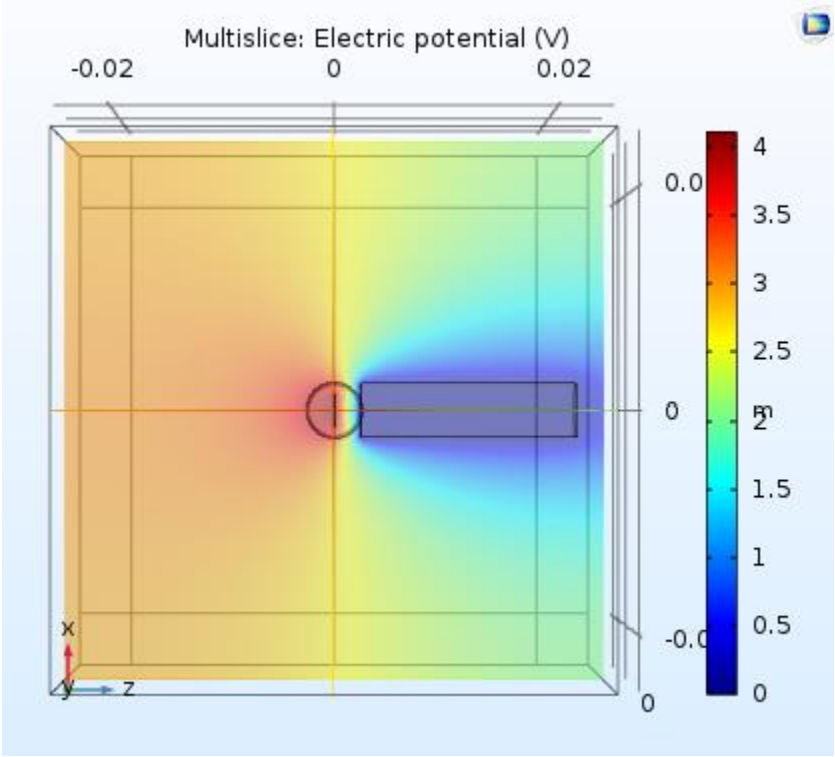

Figure 135 Y-axis view of COMSOL simulation generating electric potential of electric field from copper-polyimide circuit at core of textile yarn

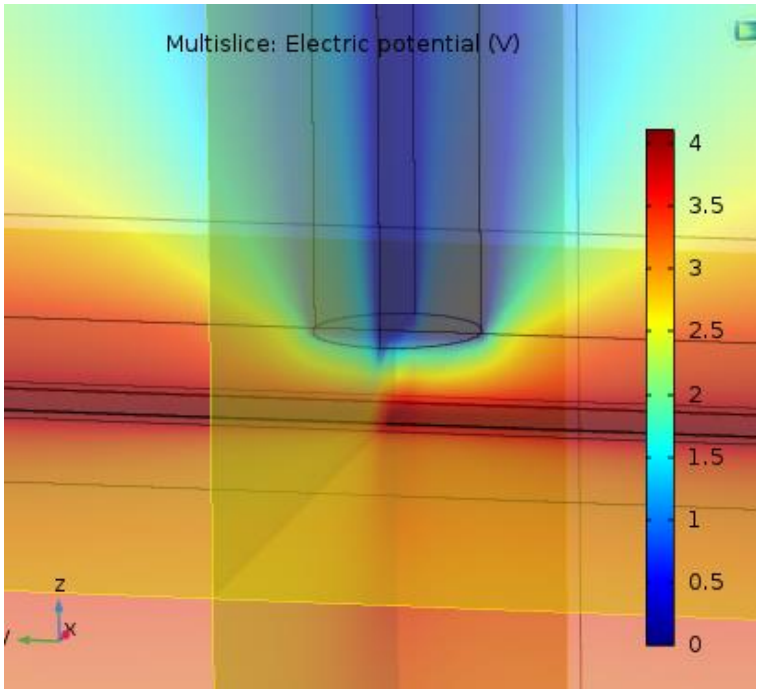

Figure 136 Close up view of COMSOL simulation generating electric potential of electric field from copper-polyimide circuit at core of textile yarn

G. Compute Changing Electric Field with Time

1. In order to calculate the change in electric field with a changing variable, right-click Study and select **Parametric Sweep**.

2. Then right-click Global Definitions and select **Parameters**. Create a parameter called 'F' and give it the existing value of 0.0025 [m] and describe it has 'Finger height'. This value is the finger touching the e-yarn.

3. Select Parametric Sweep and click the 'Parameter name' drop-down menu to select 'F'. Then give the values of 'F' such that the finger distance from the e-yarn will increase 5mm with each sweep:

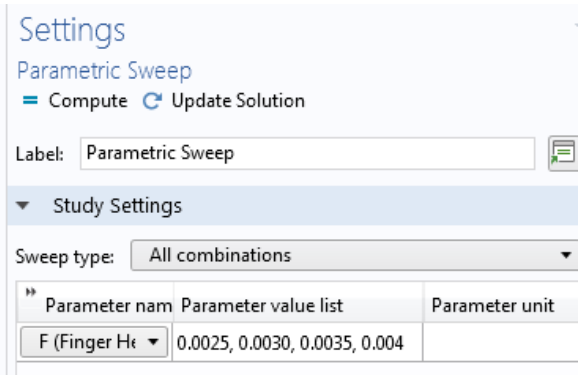

Figure 137 Defining proximity distance of human finger in COMSOL for parametric sweep computation

4. Then solve this solution by selecting **Compute**. This results in a series of solutions which shows how the electric field changes as a human finger touches the e-yarn to have a decreasing proximity distance:

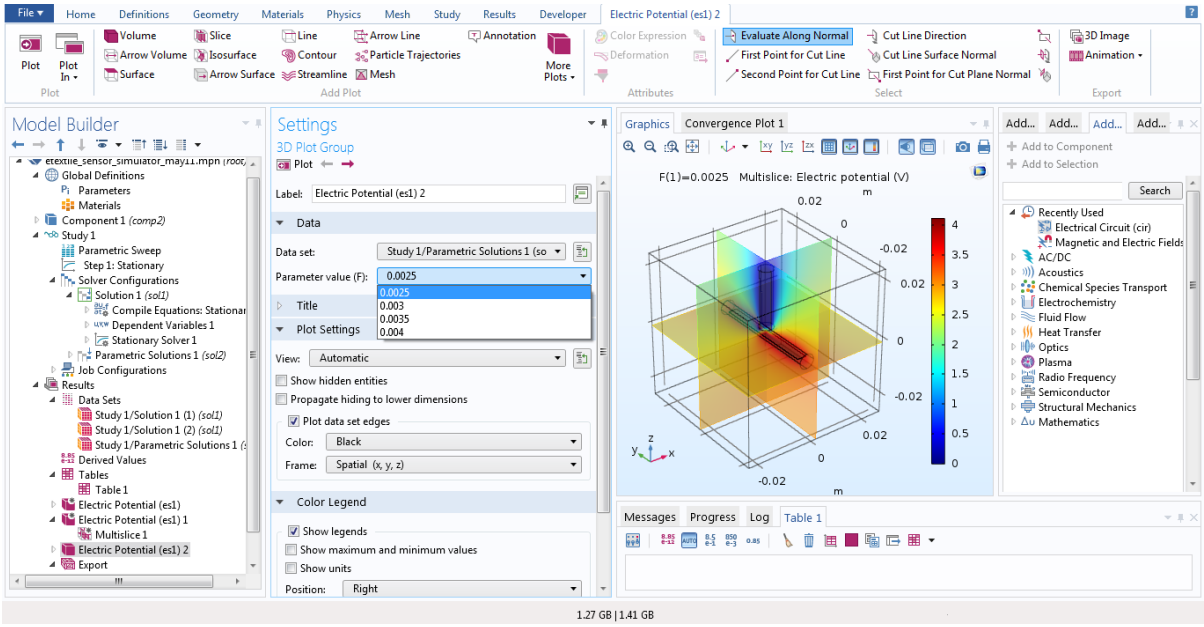

Figure 138 Selecting proximity detection distance of human hand from copper-polyimide textile yarn

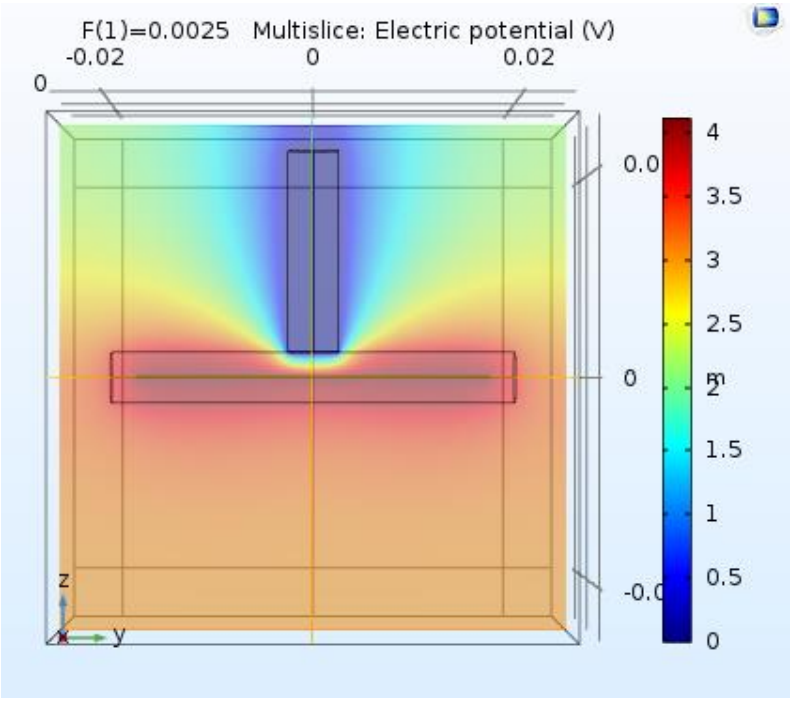

Figure 139 Selecting touch detection distance of human hand from copper-polyimide textile yarn

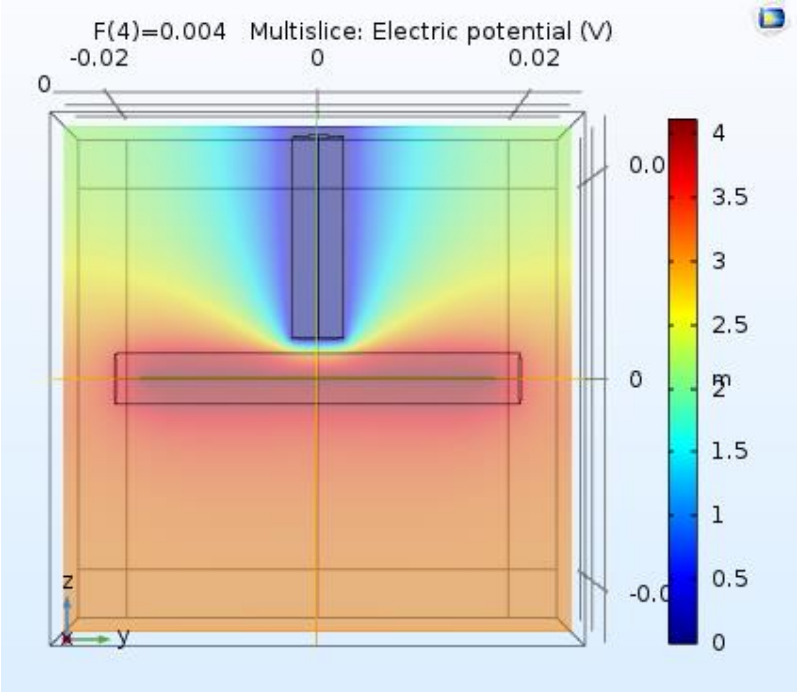

Figure 140 Selecting 1.5 cm proximity detection distance of human hand from copper-polyimide textile yarn

5. To change the finger from touch to proximity, the z-coordinate of the finger can be increased. The PCF8883US as a nominal detection distance of 5.0 cm. The capacitance value can be calculated based on the changing distance the finger has to the e-yarn.

3. Other variables can be changed, such as putting a PDMS layer on top of the copper-polyimide and also changing the cylindrical textile yarn into a planar woven textile.

Glossary of Terms

Capacitive coupling/decoupling – Transfer of energy from one circuit/electrical system to another due to mutual capacitance between the circuits/systems.

Durable – Being able to withstand damage and wear.

Electrode – A conductive interactive region through which an electric current can pass through it to a power source, electronic components, or a living body.

Fabric - Natural or manmade yarns can be assembled into fabrics, which in turn can be produced using different methods. Such methods include be knitting, weaving, felting, bonding, and tufting. Conversely, fabrics can be made from fibres directly, called non-woven fabrics.

Freeform manufacturing – An additive manufacturing process where solid objects are made from net-shape-parts, requiring less material and build time.

Knitting - Yarns are interloped to make elastic and flexible fabric (Spencer, 2001) in a knot-like manner. Yarns are shaped into loops and interlaced together to form fabric.

Micromolecules – Molecules or relatively lower molecular weight.

Nominal detection distance – Maximum proximity detection distance from sensing electrode.

Polymer – A substance consisting of a chain of large molecules with high molecular mass, which themselves are made from identical molecules of lower molecular mass.

Stretchability – Describes the degree an entity can be stretched.

Substrate – A base layer to which materials are printed or coated onto.

Robust – Strong and insensitive damaging impact.

Unobtrusive – discreet and not disruptive impression of an object as part of a larger system.

Washability – Describes the degree an entity can be washed.

Weaving - Woven fabrics are produced by interlacing a warp yarn and weft yarn perpendicularly. The warp yarn runs along the length and the weft yarn along the width (Lord & Mohamed, 1982). The sequence of interlacing, called the weave design (Robinson & Marks, 1973), can affect the aesthetic and degree of mechanical deformity with the resultant fabric.

Yarns - An assembly of fibres or filaments that are substantial in length and have a small cross-section made with or without twisting (Denton, 2002).

Bibliography

(ISO), I. d. (n.d.). ISO 6330:2012(en) Textiles — Domestic washing and drying procedures for textile testing. Retrieved July 2018, from ISO: https://www.iso.org/obp/ui/#iso:std:iso:6330:ed-3:v1:en

Alfa. (n.d.). 46497 Polyethylene glycol diacrylate, M.W. 3,400. Retrieved August 2017, from https://www.alfa.com/en/catalog/046497/

Alfa. (n.d.). 46801 Polyethylene glycol diacrylate. Retrieved August 2017, from https://www.alfa.com/en/catalog/046801/

Andersson, O. (2012). Experiment!: planning, implementing and interpreting. John Wiley & Sons.

Ankhili, A., Tao, X., Cochrane, C., Coulon, D., & Koncar, V. (2018). Washable and Reliable Textile Electrodes Embedded into Underwear Fabric for Electrocardiography (ECG) Monitoring. Materials 11(2).

Applications, O. (n.d.). Ozone Compatible Materials. Retrieved August 2017, from http://www.ozoneapplications.com/info/ozone_compatible_materials.htm

Armani, D., Liu, C., & Aluru, N. (1999). Re-configurable fluid circuits by PDMS elastomer micromachining. Twelfth IEEE International Conference on Micro Electro Mechanical Systems (pp. 222-227). IEEE International MEMS 99 Conference.

Arshad, A., Khan, S., Alam, A. Z., Tasnim, R., Gunawan, T. S., Ahmad, R., et al. (2016). An activity monitoring system for senior citizens living independently using capacitive sensing technique. In Instrumentation and Measurement Technology Conference Proceedings (I2MTC) (pp. 1-6). IEEE.

Ascari, L., Corradi, P., Beccai, L., & & Laschi, C. (2007). A miniaturized and flexible optoelectronic sensing system for tactile skin. Journal of Micromechanics and Microengineering, 17(11), 2288.

Aud, M., Abbott, C., Tyrer, H., Neelgund, R., Shriniwar, U., A.Mohammed, et al. (2010). Smart Carpet: Developing a Sensor System to Detect Falls and Summon Assistance . Gerontological Nursing, vol.36, Issue 7, 8-12.

Baker, J. H. (1996). Direct measurement of the electrical impedance of narrow gap radio frequency gas discharges in the 100 MHz region. Measurement Science and Technology, 7(11), 1631.

Baribina, N., Baltina, I., & Oks, A. (2018). Application of Additional Coating for Conductive Yarns Protection against Washing. In Key Engineering Materials Vol. 762 (pp. 396-401). Trans Tech Publications.

Bartolozzi, C., Natale, L., Nori, F., & Metta, G. (2016). Robots with a sense of touch. Nature Materials 15(9), 921.

Berzowska, J. (2005). Electronic textiles: Wearable computers, reactive fashion, and soft computation. Textile 3.1, 58-75.

Brandstein, M. S., & Silverman, H. F. (1997). A practical methodology for speech source localization with microphone arrays. Computer Speech & Language, 11(2), 91-126.

Braun, A., Wichert, R., Kuijper, A., & Fellner, D. W. (2015). Capacitive proximity sensing in smart environments. Journal of Ambient Intelligence and Smart Environments, 7(4), 483-510.

Braun, T., Becker, K. F., Koch, M., Bader, V., Aschenbrenner, R., & Reichl, H. (2005). Reliability potential of epoxy based encapsulants for automotive applications. Microelectronics reliability, 45(9-11), 1672-1675.

Brauner, P. v. (2017). Towards Accepted Smart Interactive Textiles. In International Conference on HCI in Business, Government, and Organizations (pp. 279-298). Springer.

Briand, D., Molina-Lopez, F., Quintero, A. V., Ataman, C., Courbat, J., & de Rooij, N. F. (2011). Why going towards plastic and flexible sensors? Procedia engineering, 25, 8-15.

Brook, M. A. (2000). Polymer Chemistry. New York: Wiley.

Brooks, J., Das, U., & Smith, L. (1989). Effect of lubrication on tensile, frictional, and weaving properties of sirospun wool yarn. Textile Research Journal, 59(7), 382-388.

Buechley, L., Eisenberg, M., Catchen, J., & Crockett, A. (2008). The LilyPad Arduino: using computational textiles to investigate engagement, aesthetics, and diversity in computer science education. In Proceedings of the SIGCHI conference on Human factors in computing systems (pp. 423-432). ACM.

Bürgi, L., Pfeiffer, R., Mücklich, M., Metzler, P., Kiy, M., & Winnewisser, C. (2006). Optical proximity and touch sensors based on monolithically integrated polymer photodiodes and polymer LEDs. Organic Electronics, 7(2), 114-120.
Chan, V. J. (2012). Multi-material bio-fabrication of hydrogel cantilevers and actuators with stereolithography. Lab on a Chip, 12(1), 88-98.
Chang, J. H., Liu, Y., Kang, D., & Tai, Y. C. (2013). Reliable-packaging for parylene-based flexible retina implant. Transducers & Eurosensors XXVII: The 17th International Conference on Solid-State Sensors, Actuators and Microsystems (TRANSDUCERS & EUROSENSORS XXVII) (pp. 2612-2615). IEEE.
Cheng, J., Amft, O., & Lukowicz, P. (2010). Active capacitive sensing: Exploring a new wearable sensing modality for activity recognition. In International Conference on Pervasive Computing (pp. 319-336). Heidelberg: Springer.
Cherenack, K., & van Pieterson, L. (2012). Smart textiles: challenges and opportunities. Journal of Applied Physics 112.9.
Cherenack, K., Zysset, C., Kinkeldei, T., Münzenrieder, N., & Tröster, G. (2010). Woven electronic fibers with sensing and display functions for smart textiles. Advanced materials, 22(45), 5178-5182.
Christiaens, W., Loeher, T., Pahl, B., Feil, M., Vandevelde, B., & Vanfleteren, J. (2008). Embedding and assembly of ultrathin chips in multilayer flex boards. Circuit World, 34(3), 3-8.
Components, H. (n.d.). Kapton Insulated Heaters Holroyd Technical Datasheet . Retrieved August 2017, from http://www.holroydcomponents.com/assets/uploads/documents/kapton_tech.pdf
Controls, F. (2016, February 22). Operating Principles for Magnetic Sensors. Retrieved from Fargo Controls: http://www.fargocontrols.com/sensors/magnetic_op.html
CORP., A. P. (n.d.). Ultem® / PEI (Polyetherimide). Retrieved August 2017, from https://www.aetnaplastics.com/products/d/Ultem
Corporation, E. R. (n.d.). Chemical Resistance - Research Plus. Retrieved 2017, from Eppendorf Research: https://online-shop.eppendorf.com/OC-en/Manual-Liquid-Handling-44563/Pipettes-44564/Eppendorf-Research-plus-PF-222159.html
Corporation, M. (n.d.). Materials. Retrieved August 2017, from http://www.microspecorporation.com/materials.php?id=20
Coyle, S. &. (2010). Smart nanotextiles: materials and their application.
Dam, R. M. (2006). Solvent-resistant elastomeric microfluidic devices and applications . (Doctoral dissertation, California Institute of Technology). California, United States of America: California Institute of Technology.
Database, P. (n.d.). Polysulfone. Retrieved August 2017, from http://polymerdatabase.com/polymer%20classes/Polysulfone%20type.html
Davison, A. J. (2003). Real-time simultaneous localisation and mapping with a single camera. Proceedings Ninth IEEE International Conference on Computer Vision (p. 1403). Nice: IEEE.
Dementyev, A. (2016). Towards self-aware materials. In Proceedings of the TEI'16: Tenth International Conference on Tangible, Embedded, and Embodied Interaction (pp. 685-688). ACM.
Dementyev, A., Kao, H. L., & Paradiso, J. A. (2015). Sensortape: Modular and programmable 3d-aware dense sensor network on a tape. In Proceedings of the 28th Annual ACM Symposium on User Interface Software & Technology (pp. 649-658). ACM.
Denton, M. J. (2002). Textile Terms and Definitions. Manchester.
Dobbelstein, D., Winkler, C., Haas, G., & Rukzio, E. (2017). PocketThumb: a Wearable Dual-Sided Touch Interface for Cursor-based Control of Smart-Eyewear. Proceedings of the ACM on Interactive, Mobile, Wearable and Ubiquitous Technologies, 1(2), 9.
Dupont. (n.d.). Dupont Summary Properties for Kapton Polyimide Films. Retrieved August 2017, from http://www.dupont.com/products-and-services/membranes-films/polyimide-films/brands/kapton-polyimide-film.html/
Electronics, N. (2014). PCF8883 Capacitive touch/proximity switch with auto-calibration, large voltage operating range, and very low power consumption.
Elliot, P. G. (2012). E-textile microstrip patch antennas for GPS. . In Proceedings of the Location and Navigation Symposium (pp. 66-73). IEEE.
Engineering, P. (n.d.). Why Use Parylene. Retrieved August 2017, from http://www.paryleneengineering.com/why_use_parylene.htm

Essö, C. (2007). Modifying Polydimethylsiloxane (PDMS) surfaces.
Falconnet, D. B. (2002). Fracture toughness of weft-knitted fabric composites. Composites Part B: Engineering, 33(8), 579-588.
Feili, D., Schuettler, M., Doerge, T., Kammer, S., Hoffmann, K., & Stieglitz, T. (2006). Flexible organic field effect transistors for biomedical microimplants using polyimide and parylene C as substrate and insulator layers. Journal of micromechanics and microengineering 16, no. 8, 1555.
Fellow, G. (n.d.). Polyetheretherketone. Retrieved August 2017, from http://www.goodfellow.com/E/Polyetheretherketone.html
Fellow, G. (n.d.). Polyethersulphone. Retrieved August 2017, from http://www.goodfellow.com/E/Polyethersulphone.html
Fellow, G. (n.d.). Polyethylene Naphthalate. Retrieved August 2017, from http://www.goodfellow.com/E/Polyethylene-naphthalate.html
Fellow, G. (n.d.). Polyethylene Terephthalate. Retrieved August 2017, from http://www.goodfellow.com/E/Polyethylene-terephthalate.html
Fellow, G. (n.d.). Polymethylmethacrylate. Retrieved August 2017, from http://www.goodfellow.com/E/Polymethylmethacrylate.html
Fellow, G. (n.d.). Polytetrafluoroethylene. Retrieved August 2017, from http://www.goodfellow.com/E/Polytetrafluoroethylene.html
Fericean, S. (2007). New Noncontacting Inductive Analog Proximity and Inductive Linear Displacement Sensors for Industrial Automation. IEEE SENSORS, 7(11), 1538-1545.
Fericean, S., Dorneich, A., Droxler, R., & Krater, D. (2009). Development of a microwave proximity sensor for industrial applications. IEEE Sensors Journal, 9(7), 870-876.
Ferri, J. L.-R.-B. (2017). A Wearable Textile 2D Touchpad Sensor Based on Screen-Printing Technology. . Materials, 10(12).
Frank, S., & Kuijper, A. (2017). AuthentiCap-A Touchless Vehicle Authentication and Personalization System. In European Conference on Ambient Intelligence. (pp. 46-63). Springer.
Frequency of fabric conditioner usage in the United Kingdom (UK) 2015-2017. (n.d.). Retrieved 2018, from Statista.com: https://www.statista.com/statistics/302322/fabric-conditioner-usage-frequency-in-the-uk/
Frequency of liquid detergents for fabrics usage in the United Kingdom (2015-2017). (n.d.). Retrieved 2018, from Stastista.com: https://www.statista.com/statistics/302319/liquid-detergents-for-fabrics-usage-frequency-in-the-uk/
From, M. I. (n.d.). Polytetrafluoroethylene-PTFE. Retrieved August 2017, from http://www.makeitfrom.com/material-properties/Polytetrafluoroethylene-PTFE
Fu, Y., Chan, Y., Yang, M., Chan, Y., Virkki, J., Björninen, T., et al. (2015). Experimental study on the washing durability of electro-textile UHF RFID tags. IEEE Antennas and Wireless Propagation Letters 14, 466-469.
Fujii, T. (2002). PDMS-based microfluidic devices for biomedical applications. Microelectronic Engineering, 61, 907-914.
George, B., Zangl, H., Bretterklieber, T., & Brasseur, G. (2010). A combined inductive–capacitive proximity sensor for seat occupancy detection. IEEE transactions on instrumentation and measurement, 59(5), 1463-1470.
Ghosh, A. K. (2012). Introduction to measurements and instrumentation. PHI Learning Pvt. Ltd.
Gomes, D., de Souza, N., & Silva, J. (2013). Using a monocular optical microscope to assemble a wetting contact angle analyser. Measurement, 46(9), 3623-3627.
Gradl, S., Cibis, T., Lauber, J., Richer, R., Rybalko, R., Pfeiffer, N., et al. (2017). Wearable Current-Based ECG Monitoring System with Non-Insulated Electrodes for Underwater Application. Applied Sciences, 7(12), 1277.
Grosse-Puppendahl, T. B. (2013). OpenCapSense: A rapid prototyping toolkit for pervasive interaction using capacitive sensing. International Conference on Pervasive Computing and Communications (PerCom). IEEE.
Grosse-Puppendahl, T., Holz, C., Cohn, G., Wimmer, R., Bechtold, O., Hodges, S., et al. (2017). Finding common ground: A survey of capacitive sensing in human-computer interaction. In Proceedings of the 2017 CHI Conference on Human Factors in Computing Systems (pp. 3293-3315). ACM.

Guo, X., Huang, Y., Cai, X., Liu, C., & Liu, P. (2016). Capacitive wearable tactile sensor based on smart textile substrate with carbon black/silicone rubber composite dielectric. Measurement Science and Technology, 27(4).
Hagan, M. (2017). Inductive proximity sensors network in intelligent clothes. In E-Health and Bioengineering Conference (EHB) (pp. 225-228). IEEE.
Hamedi, M., Forchheimer, R., & Inganäs, O. (2007). Towards woven logic from organic fibres. Nature Materials, 357-362.
Han, J. Y. (2005). Low-cost multi-touch sensing through frustrated total internal reflection. In Proceedings of the 18th annual ACM symposium on User interface software and technology (pp. 115-118). ACM.
Hardy, D., Anastasopoulos, I., Nashed, M., Oliveira, C., Hughes-Riley, T., Komolafe, A., et al. (2018). An automated process for inclusion of package dies and circuitry within a textile yarn. Symposium on Design, Test, Integration & Packaging. Rome: IEEE.
Hassler, C., von Metzen, R., Ruther, P., & Stieglitz, T. (2010). Characterization of parylene C as an encapsulation material for implanted neural prostheses. Journal of Biomedical Materials Research Part B: Applied Biomaterials 93, no. 1, 266-274.
Hénault, I. B., & Elms, R. A. (2004). Fundamental Properties of Silicones Related to Fabric Care Benefits. Belgium: Dow Corning.
Hirai, S., & Naraki, K. (2016). Fabric interface with proximity and tactile sensation for human-robot interaction. IEEE/RSJ International Conference on Intelligent Robots and Systems (IROS) (pp. 238-245). IEEE.
Hodges, S., Izadi, S., Butler, A., Rrustemi, A., & & Buxton, B. (2007). ThinSight: versatile multi-touch sensing for thin form-factor displays. In Proceedings of the 20th annual ACM symposium on User interface software and technology (pp. 259-268). ACM.
Holleis, P., Schmidt, A., Paasovaara, S., Puikkonen, A., & Häkkilä, J. (2008). Evaluating capacitive touch input on clothes. in Proceedings of the 10th international conference on Human computer interaction with mobile devices and services (pp. 81-90). ACM.
Honda, T., Miyazaki, M., Nakamura, H., & Maeda, H. (2005). Controllable polymerization of N-carboxy anhydrides in a microreaction system. Lab on a Chip, 5(8), 812-818.
Hoogerwerf, A. C., & Wise, K. D. (1994). A three-dimensional microelectrode array for chronic neural recording. IEEE Transactions on Biomedical Engineering 41, no. 12, 1136-1146.
Horrocks, A. R., & Anand, S. C. (2000). Handbook of technical textiles. Elsevier.
Hu, Y., Zhao, T., Zhu, P., Zhu, Y., Shuai, X., Liang, X., et al. (2016). Low cost and highly conductive elastic composites for flexible and printable electronics. Journal of Materials Chemistry C, 4(24), 5839-5848.
Hubbard, R. L. (2004). Low temperature curing of polyimide wafer coatings. IEEE/CPMT/SEMI 29th International Conference in Electronics Manufacturing Technology Symposium (pp. 149-151). IEEE.
Inoue, M., Tada, Y., Itabashi, Y., Kimura, R., & Taya, S. (2016). Variation in electrical conductivity of stretchable printed wires and electrodes due to fatigue damage in several situations. International Conference on Electronics Packaging (ICEP) (pp. 137-140). IEEE.
Jagiella, M., Fericean, S., & Dorneich, A. (2006). Progress and recent realizations of miniaturized inductive proximity sensors for automation. IEEE Sensors journal, 6(6), 1734-1741.
Jama, C. D. (1992). Treatment of poly (ether ether ketone)(PEEK) surfaces by remote plasma discharge. XPS investigation of the ageing of plasma-treated PEEK. . Surface and interface analysis, 18(11), 751-756.
Jamone, L., Natale, L., Metta, G., & Sandini, G. (2015). Highly sensitive soft tactile sensors for an anthropomorphic robotic hand. IEEE Sensors Journal, 15(8), 4226-4233.
Jeong, J., McCall, J., Shin, G., Zhang, Y., Al-Hasani, R., Kim, M., et al. (2015). Wireless optofluidic systems for programmable in vivo pharmacology and optogenetics. Cell, 162(3), 662-674.
Jeong, O. C., & Konishi, S. (2006). All PDMS pneumatic microfinger with bidirectional motion and its application. Journal of Microelectromechanical Systems, 15(4), 896-903.
Jindal, S. (n.d.). Proximity Sensing Slideshow,. Retrieved February 22, 2016, from Slideshare: http://www.slideshare.net/shwetajindal5/proximity-sensor-41316668
Jingcheng Li, J. C. (2012). A shell-based magnetic field model for magnetic proximity detection systems. Saf Sci , 50(3), 463-471.
Johnson, A., & Wise, D. K. (2015). Patent No. 8,927,876. US.

Johnson, R. O. (1983). Polyetherimide: A new high-performance thermoplastic resin. . Journal of Polymer Science: Polymer Symposia (Vol. 70, No. 1), 129-143.
Jost, K. D. (2014). Textile energy storage in perspective. Journal of Materials Chemistry A, 2(28), 10776-10787.
Kaappa, E., Joutsen, A., Cömert, A., & Vanhala, J. (2017). The electrical impedance measurements of dry electrode materials for the ECG measuring after repeated washing. Research Journal of Textile and Apparel 21(1), 59-71.
Kallmayer, C., Pisarek, R., Cichos, S., Neudeck, A., & Gimpel, S. (2003). New assembly technologies for textile transponder systems. Electronic Components and Technology Conference (pp. 1123-1126). IEEE.
Kan, W., Huang, Y., Zeng, X., Guo, X., & Liu, P. (2018). A dual-mode proximity sensor with combination of inductive and capacitive sensing units. Sensor Review.
Kang, D., Matsuki, S., & Tai, Y. C. (2015). Study of The Hybrid Parylene/PDMS Material. 28th IEEE International Conference on Micro Electro Mechanical Systems (MEMS) (pp. 397-400). IEEE.
Kang, T., & Kim, M. (2001). Effects of silicone treatments on the dimensional properties of wool fabric. Textile Research Journal, 71(4), 295-300.
Karnfelt, C., Tegnander, C., Rudnicki, J., Starski, J., & Emrich, A. (2006). Investigation of Parylene-C on the performance of millimeter-wave circuits. IEEE transactions on microwave theory and techniques 54, no. 8, 3417-3425.
Kazani, I., Hertleer, C., De Mey, G., Schwarz, A., Guxho, G., & Van Langenhove, L. (2012). Electrical conductive textiles obtained by screen printing. Fibres & Textiles in Eastern Europe 20(1), 57-63.
Kim, D., Lu, N., Ma, R., Kim, Y., Kim, R., Wang, S., et al. (2011). Epidermal electronics. Science 333(6044), 838-843.
Kim, H., & Jeong, O. (2011). PDMS surface modification using atmospheric pressure plasma. Microelectronic Engineering, 88(8), 2281-2285.
Kim, P. J. (2006). Fabrication of non-biofouling polyethylene glycol micro-and nanochannels by ultraviolet-assisted irreversible sealing. Lab on a Chip, 6(11), 1432-1437.
Kim, Y., Cho, S., Shin, D., Lee, J., & Baek, K. (2013). Single Chip Dual Plate Capacitive Proximity Sensor With High Noise Immunity. IEEE Sensors Journal, 14(2), 309-310.
Kinkeldei, T., Munzenrieder, N., Zysset, C., Cherenack, K., & Tröster, G. (2011). Encapsulation for flexible electronic devices. IEEE Electron Device Letters 32(12), 1743-1745.
Köhler, A. R. (2013). Challenges for eco-design of emerging technologies: The case of electronic textiles. Materials & Design 51, 51-60.
Lakdawala, N., Pham, J., Shah, M., & Holton, J. (2011). Effectiveness of low-temperature domestic laundry on the decontamination of healthcare workers' uniforms. Infection Control & Hospital Epidemiology, 32(11), 1103-1108.
Leading fabric conditioner brands of Comfort in the UK 2014-2017, by number of users. (n.d.). Retrieved 2018, from Statista.com: https://www.statista.com/statistics/304532/leading-fabric-conditioner-brands-in-the-uk/
Leading fabric conditioners in the United Kingdom (UK) 2017, by number of users. (n.d.). Retrieved 2018, from Statista.com: https://www.statista.com/statistics/303982/leading-fabric-conditioner-brands-in-the-uk/
Leading liquid detergent brands of Ariel in the UK 2013-2017, by number of users. (n.d.). Retrieved 2018, from Statista.com: https://www.statista.com/statistics/304512/leading-brands-liquid-detergent-for-fabrics-in-the-uk/
Lee, H., & Cho, J. (2005). Development of conformal PDMS and parylene coatings for microelectronics and MEMS packaging. In ASME International Mechanical Engineering Congress and Exposition (pp. 279-283.). American Society of Mechanical Engineers.
Lee, J., Park, C., & Whitesides, G. (2003). Solvent compatibility of poly (dimethylsiloxane)-based microfluidic devices. Analytical chemistry, 75(23), 6544-6554.
Li, M., Tudor, J., Liu, J., Torah, R., Komolafe, A., & Beeby, S. (2019). Novel electronic packaging method for functional electronic textiles. IEEE Transactions on Components, Packaging and Manufacturing Technology.

Li, X., Lin, Z., Cheng, G., Wen, X., Liu, Y., Niu, S., et al. (2014). 3D fiber-based hybrid nanogenerator for energy harvesting and as a self-powered pressure sensor. ACS nano, 8(10), 10674-10681.
Li, Y. W. (2013). Effect of hydrophobic acrylic versus hydrophilic acrylic intraocular lens on posterior capsule opacification: meta-analysis. . PloS one, 8(11), 77864.
Lin, Z. I. (2017). Conductive fabrics made of polypropylene/multi-walled carbon nanotube coated polyester yarns: Mechanical properties and electromagnetic interference shielding effectiveness. Composites Science and Technology, 141, 74-82.
Linz, T., Kallmayer, C., Aschenbrenner, R., & Reichl, H. (2005). Embroidering electrical interconnects with conductive yarn for the integration of flexible electronic modules into fabric. Ninth IEEE International Symposium on Wearable Computers (pp. 86-89). IEEE.
Lord, P. R., & Mohamed, M. H. (1982). Weaving: Conversion of yarn to fabric. Elsevier.
Lowe, D., & Rezkallah, K. (1999). A capacitance sensor for the characterization of microgravity two-phase liquid-gas flows. Measurement Science and Technology, 10(10), 965.
Lu, B., Lin, J., Liu, Z., Lee, Y., & Tai, Y. (2011). Highly flexible, transparent and patternable parylene-C superhydrophobic films with high and low adhesion. 24th International Conference on Micro Electro Mechanical Systems (MEMS) (pp. 1143-1146). IEEE.
Lu, B., Liu, Z., & Tai, Y. (2011). Ultrathin parylene-C semipermeable membranes for biomedical applications. IEEE 24th International Conference on n Micro Electro Mechanical Systems (MEMS) (pp. 505-508). IEEE.
Lu, N. L. (2012). Highly sensitive skin-mountable strain gauges based entirely on elastomers. Advanced Functional Materials 22(19), 4044-4050.
Lukas Bürgi, R. P. (2006). Optical proximity and touch sensors based on monolithically integrated polymer photodiodes and polymer LEDs. Organic Electronics, 7(2), 114-120.
Lymberis, A., & Paradiso, R. (2008). Smart fabrics and interactive textile enabling wearable personal applications: R&D state of the art and future challenges. 30th Annual International Conference EMBS. Engineering in Medicine and Biology Society.
Mao, Y., Geng, D., Liang, E., & Wang, X. (2015). Single-electrode triboelectric nanogenerator for scavenging friction energy from rolling tires. . Nano Energy, 227-234.
Mark, J., & Pan, S. J. (1982). Reinforcement of polydimethylsiloxane networks by in-situ precipitation of silica: A new method for preparation of filled elastomers. Macromolecular Rapid Communications, 3(10), 681-685.
Mathur, K. &. (2011). Color and weave relationship in woven fabrics. In Advances in Modern Woven Fabrics Technology. InTech.
Matsuda, A., Kotani, Y., Kogure, T., Tatsumisago, M., & Minami, T. (2000). Transparent anatase nanocomposite films by the sol–gel process at low temperatures. Journal of the American Ceramic Society, 83(1), 229-231.
Matsuhisa, N., Kaltenbrunner, M., Yokota, T., Jinno, H., Kuribara, K., Sekitani, T., et al. (2015). Printable elastic conductors with a high conductivity for electronic textile applications. Nature communications, 6, 7461.
Mattana, G. K.-L. (2013). Woven temperature and humidity sensors on flexible plastic substrates for e-textile applications. . IEEE Sensors Journal 13(10), 3901-3909.
Mattmann, C., Clemens, F., & Tröster, G. (2008). Sensor for measuring strain in textile. Sensors 8(6), 3719-3732.
Matveev, M. Y., Long, A., & Jones, A. (2012). Mechanical properties of textile composites with variability in micromechanical properties. 15th European conference on composite materials. Venice.
Mega Electronics PCB Bubble Etch Tank. (n.d.). Retrieved 2016, from Rapidonline.com: https://www.rapidonline.com/mega-electronics-pcb-bubble-etch-tank-29472
Members, T. (n.d.). Electrical Properties of Plastics. Retrieved August 2017, from http://members.tm.net/lapointe/Plastics.htm
Meng, B., Tang, W., Too, Z. H., Zhang, X., Han, M., Liu, W., et al. (2013). A transparent single-friction-surface triboelectric generator and self-powered touch sensor. Energy & Environmental Science, 6(11), 3235-3240.
Merchant, S. (2011). Negotiating underwater space: The sensorium, the body and the practice of scuba-diving. Tourist Studies, 11(3), 215-234.

Merritt, C. R., Nagle, H. T., & Grant, E. (2009). Fabric-based active electrode design and fabrication for health monitoring clothing. IEEE Transactions on information technology in biomedicine, 274-280.
MIT. (n.d.). Parylene. Retrieved August 2017, from http://www.mit.edu/~6.777/matprops/parylene.htm
Morent, R., Geyter, D., N., A. F., De Smet, N., Gengembre, L., De Leersnyder, E., et al. (2007). Adhesion enhancement by a dielectric barrier discharge of PDMS used for flexible and stretchable electronics. Journal of Physics D: Applied Physics, 40(23), p.7392.
Nano-Tera. (n.d.). Technology Integration into Textiles: Empowering Health and Security (TecInTex) Project. Retrieved February 16, 2016, from http://www.nano-tera.ch/projects/69.php
Nano-Tera. (n.d.). Textiles With Integrated Gas Sensors (TWIGS) project. Retrieved February 16, 2016, from http://www.nano-tera.ch/projects/308.php
Nelson, G. (2001). Microencapsulation in textile finishing. Review of Progress in Coloration and related Topics, 31(1), 57-64.
Nelson, G. (2002). Application of microencapsulation in textiles. International Journal of Pharmaceutics, 242(1-2), 55-62.
Neumann, M. (1985). The dielectric constant of water. Computer simulations with the MCY potential. . The Journal of Chemical Physics, 82(12), , 5663-5672.
Nonaka, H., & & Da-te, T. (1995). Ultrasonic position measurement and its applications to human interface. IEEE transactions on Instrumentation and Measurement, 44(3), 771-774.
Noordegraaf, J. (1996). Conformal coating using parylene polymers. Medical device technology 8, no. 1 , 14-20.
Normann, M., Kyosev, Y., Ehrmann, A., & Schwarz-Pfeiffer, A. (2016). Multilayer textile-based woven batteries. In Recent Developments in Braiding and Narrow Weaving (pp. 129-136). Springer International Publishing.
Ochoa, M. W. (2013). A hybrid PDMS-Parylene subdural multi-electrode array. Biomedical microdevices 15, no. 3 , 437-443.
Ojuroye, O., & Wilde, A. (2018). On the feasibility of using electronic textiles to support embodied learning. In R. K. I. Buchem, Perspectives on Wearable Enhanced Learning (WELL): Current Trends, Research, and Practice. Springer.
Ojuroye, O., Torah, R., & Beeby, S. (2017). Levels of Electronic Integration within Textiles Chart. WomENcourage Computer Science Conference 2017. Barcelona: ACM.
Ojuroye, O., Torah, R., & Beeby, S. (2018). Improving the integration of e-textile microsystems' encapsulation by modifying PDMS formulation. In 2018 Symposium on Design, Test, Integration & Packaging of MEMS and MOEMS (DTIP) (pp. 1-6). Rome, IEEE.
Ojuroye, O., Torah, R., & Beeby, S. (2019). Modified PDMS packaging of sensory e-textile circuit microsystems for improved robustness with washing. Journal of Microsystem Technologies, 1-16.
Ojuroye, O., Torah, R., Beeby, S., & Wilde, A. (2016). Autonomy is the key: from smart towards intelligent textiles. WomENcourage Computer Science Conference. Linz, ACM.
Ojuroye, O., Torah, R., Beeby, S., & Wilde, A. (2016). Autonomy is the key: from smart towards intelligent textiles. In, Workshop on Autonomous Everyday Objects: Exploring Actuation in Ubiquitous Devices. Heidelberg: Ubiquitous Computing and International Symposium on Wearable Computers.
Ojuroye, O., Torah, R., Beeby, S., & Wilde, A. G. (2016). Smart textiles for smart home control and enriching future wireless sensor network data. In In Sensors for Everyday Life (pp. 159-183). Springer.
Ojuroye, O., Torah, R., Komolafe, A., & and Beeby, S. (2019). Embedded Capacitive Proximity and Touch Sensing Flexible Circuit System for Electronic Textile and Wearable Systems. IEEE Sensors, 1- 11.
Orr, R. J., & Abowd, G. D. (2000). The smart floor: A mechanism for natural user identification and tracking. In CHI'00 extended abstracts on Human factors in computing systems (pp. 275-276). ACM.
Palchesko, R., Zhang, L., Sun, Y., & Feinberg, A. (2012). Development of polydimethylsiloxane substrates with tunable elastic modulus to study cell mechanobiology in muscle and nerve. PloS one, 7(12).

Pan, X., Wang, Z., Cao, Z., Zhang, S., He, Y., Zhang, Y., et al. (2016). A self-powered vibration sensor based on electrospun poly (vinylidene fluoride) nanofibres with enhanced piezoelectric response. Smart Materials and Structures 25.10.

Pang, C., Lee, G. Y., Kim, T. I., Kim, S. M., Kim, H. N., Ahn, S. H., et al. (2012). A flexible and highly sensitive strain-gauge sensor using reversible interlocking of nanofibres. Nature materials 11.9, 795.

Paradiso, R., & De Rossi, D. (2006). Advances in textile technologies for unobtrusive monitoring of vital parameters and movements. In Engineering in Medicine and Biology Society, 28th Annual International Conference of the IEEE (pp. 392-395). IEEE Engineering in Medicine and Biology Society.

Park, C., Moon, Y., Seong, H., Jung, S., Oh, J., Na, B., et al. (2016). Photolithography-Based Patterning of Liquid Metal Interconnects for Monolithically Integrated Stretchable Circuits. ACS applied materials & interfaces 8, no. 24, 15459-15465.

Park, J. Y., Yoo, S. J., Lee, E. J., Lee, D. H., Kim, J. Y., & Lee, S. H. (2010). Increased poly (dimethylsiloxane) stiffness improves viability and morphology of mouse fibroblast cells. BioChip Journal, 4(3), 230-236.

Park, S., Mackenzie, K., & Jayaraman, S. (2002). The wearable motherboard: a framework for personalized mobile information processing (PMIP). Proceedings of the 39th Annual Design Automation Conference. ACM.

Parylene. (n.d.). Parylene Properties Chart for Parylene N, C, D . Retrieved August 2017, from http://www.parylene.com/pdfs/PTC-Parylene_Properties_Chart.pdf

Paul, G. T. (2014). The development of screen printed conductive networks on textiles for biopotential monitoring applications. Sensors and Actuators A: Physical, 206, 35-41.

Pichal, J., Koller, J., Aubrecht, L., Vatuňa, T., Špatenka, P., & Wiener, J. (2004). Application of atmospheric corona discharge for PES fabric modification. Czechoslovak Journal of Physics, 54(3), 828.

Pickering, K. L., & Murray, T. L. (1999). Weak link scaling analysis of high-strength carbon fibre. Composites Part A: Applied Science and Manufacturing 30.8, 1017-1021.

Plastics, C. (n.d.). PET. Retrieved August 2017, from https://www.curbellplastics.com/Research-Solutions/Materials/PET

Plastics, P. (n.d.). Electrical Properties of Plastic Materials - Professional Plastics. Retrieved August 2017, from http://www.professionalplastics.com/professionalplastics/ElectricalPropertiesofPlastics.pdf

Polymer, S. (n.d.). Refractive Index of Polymers by Index. Retrieved August 2017, from http://scientificpolymer.com/technical-library/refractive-index-of-polymers-by-index/

Polysciences. (n.d.). Polyethylene glycol diacrylate (PEGDA 400). Retrieved August 2017, from http://www.polysciences.com/default/catalog-products/peg400da/

Poupyrev, I., Gong, N. W., Fukuhara, S., Karagozler, M. E., Schwesig, C., & Robinson, K. E. (2016). Project Jacquard: interactive digital textiles at scale. In Proceedings of the 2016 CHI Conference on Human Factors in Computing Systems (pp. 4216-4227). ACM.

Pu, X., Li, L., Song, H., Du, C., Zhao, Z., Jiang, C., et al. (2015). A self-charging power unit by integration of a textile triboelectric nanogenerator and a flexible lithium-ion battery for wearable electronics. Advanced Materials 27(15), 2472-2478.

Qadir, M. B. (2018). Development of Multifunctional Yarns and Fabrics for Interactive Textiles. International Journal of Fashion and Textile Engineering, 5(5).

Ramaratnam, K., Tsyalkovsky, V., Klep, V., & Luzinov, I. (2007). Ultrahydrophobic textile surface via decorating fibers with monolayer of reactive nanoparticles and non-fluorinated polymer. Chemical Communications, (43), 4510-4512.

Rantanen, J., Impiö, J., Karinsalo, T., Malmivaara, M., Reho, A., Tasanen, M., et al. (2002). Smart clothing prototype for the arctic environment. Personal and Ubiquitous Computing 6(1), 3-16.

Rao, J., Liu, K., & Qiu, J. (2013). A novel all solid-state sub-microsecond pulse generator for dielectric barrier discharges. IEEE Transactions on Plasma Science, 41(3), 564-569.

Rekimoto, J. (2001). Gesturewrist and gesturepad: Unobtrusive wearable interaction devices. Proceedings. Fifth International Symposium on Wearable Computers (pp. 21-27). Zurich: IEEE.

Ren, X., Lu, H., Zhou, J., Chong, P., Yuan, W., & Noh, M. (2017). Porous Polydimethylsiloxane as a Gas–Liquid Interface for Microfluidic Applications. Journal of Microelectromechanical Systems, 26(1), 120-126.
Reverter, F., Li, X., & Meijer, G. C. (2006). Stability and accuracy of active shielding for grounded capacitive sensors. Measurement Science and Technology, 17(11).
Robinson, A. T., & Marks, R. (1973). Woven cloth construction.
Robotics, I. (2016, February 22). Disadvantages of Hall Effect Sensors. Retrieved from http://www.intorobotics.com/types-sensors-target-detection-tracking/
Rodger, D. C., Li, W., Weiland, J. D., Humayun, M. S., & Tai, Y. C. (2013). Flexible Circuit Technologies for Biomedical Applications. Advances in Micro/Nano Electromechanical Systems and Fabrication Technologies.
Rodger, D., Weiland, J., Humayun, M., & Tai, Y. (2005). Scalable flexible chip-level parylene package for high lead count retinal prostheses. The 13th International Conference on Solid-State Sensors, Actuators and Microsystems, vol. 2 (pp. 1973-1976). IEEE.
Rossmeisl, J., Qu, Z.W., Zhu, H., Kroes, G.J. and Nørskov, J.K. (2007). Electrolysis of water on oxide surfaces. *Journal of Electroanalytical Chemistry*, *607*(1-2), pp.83-89.
Rus, S., Braun, A., & Kuijper, A. (2017). E-Textile Couch: Towards Smart Garments Integrated Furniture. In European Conference on Ambient Intelligence (pp. 214-224). Springer.
Rus, S., Sahbaz, M., Braun, A., & Kuijper, A. (2015). Design factors for flexible capacitive sensors in ambient intelligence. In European Conference on Ambient Intelligence (pp. 77-92). Springer.
Salem, E., Wilson, S., Neeb, A., Delk, J., & Cleves, M. (2009). Mechanical reliability of AMS 700 CX improved by parylene coating. The journal of sexual medicine 6, no. 9, 2615-2620.
Salim, A. & Lim, S. (2017). Review of recent inkjet-printed capacitive tactile sensors. Sensors, 17(11).
Salvado, R., Loss, C., Gonçalves, R., & Pinho, P. (2012). Textile materials for the design of wearable antennas: a survey. Sensors 12.11, 15841-15857.
SAPICH, O. (2013). Trends in man made fiber and textile industry.
Saponas, T. S., Harrison, C., & Benko, H. (2011). PocketTouch: through-fabric capacitive touch input. In Proceedings of the 24th annual ACM symposium on User interface software and technology (pp. 303-308). ACM.
Sasaki, S., & Hasuda, Y. (1988). Polyetherimide Adhesive. The Journal of Adhesion 25.2, 159-160.
Satharasinghe, A., Hughes-Riley, T., & Dias, T. (2018). Photodiodes embedded within electronic textiles. Scientific reports, 8(1), 16205.
Schmitz, A., Maggiali, M., Natale, L., & Metta, G. (2010). Touch sensors for humanoid hands. In RO-MAN IEEE, 691-697.
Schwarz, A., Van Langenhove, L., Guermonprez, P., & Deguillemont, D. (2010). A roadmap on smart textiles. Textile progress, 42(2), 99-180.
Seghir, R., & Arscott, S. (2015). Extended PDMS stiffness range for flexible systems. Sensors and Actuators A: Physical, 230, 33-39.
Semiconductor, N. (2009). UM10370 User Manual for the PCF8883 Evaluation Kit OM11055. NXP Semiconductor.
Semiconductor, N. (2014). PCF8883 Capacitive touch/proximity switch with auto-calibration, large voltage operating range, and very low power consumption.
Semiconductor, N. (2017). AN12082 Capacitive Touch Sensor Design. NXP Semiconductor.
Sen, A. K. (2007). Coated textiles: principles and applications. . Crc Press.
Services, C. P. (n.d.). Life Sciences Materials PDMS. Retrieved August 2017, from http://www.cidraprecisionservices.com/life-sciences-materials-pdms.html
Shimonomura, K., & & Nakashima, H. (2013). A combined tactile and proximity sensing employing a compound-eye camera. SENSORS, 1-2.
Singh, G., Nelson, A., Robucci, R., Patel, C., & Banerjee, N. (2015). Inviz: Low-power personalized gesture recognition using wearable textile capacitive sensor arrays. International Conference on Pervasive Computing and Communications (PerCom) (pp. 198-206). IEEE.
Smith, J. R. (1999). Electric field imaging. Massachusetts Institute of Technology.
Spec, I. (n.d.). Polysulfone Chemical Compatibility Chart from ISM . Retrieved August 2017, from https://www.industrialspec.com/images/editor/polysulfone-chemical_compatibility-chart-2016-from-ism.pdf
Spencer, D. J. (2001). Knitting technology: a comprehensive handbook and practical guide (Vol. 16). CRC press.

Statistica. (n.d.). Leading liquid detergent brands in the United Kingdom (UK) 2017, by number of users. Retrieved 2018, from Statista.com: https://www.statista.com/statistics/303966/leading-brands-liquid-detergent-for-fabrics-in-the-uk/

Stenzenberger, H. D. (1990). Polyimides. In D. Wilson. Glasgow: Blackie.

Stieglitz, T., Haberer, W., Lau, C., & Goertz, M. (2004). Development of an inductively coupled epiretinal vision prosthesis. Engineering in Medicine and Biology Society (pp. 4178-4181). IEEE.

Stieglitz, T., Kammer, S., Koch, K., Wien, S., & Robitzki, A. (2002). Encapsulation of flexible biomedical microimplants with parylene C. In IFESS.

Sung, W. L., Cheng, C., & Fang, W. (2015). Micro devices integration with stretchable spring embedded in long PDMS-fiber for flexible electronics. 28th IEEE International Conference on Micro Electro Mechanical Systems (MEMS) (p. 42). IEEE.

Takamatsu, S., Yamashita, T., & Itoh, T. (2014). Meter-Scale LED-embedded light fabric for the application of fabric ceilings in rooms. Microsystem Technologies, 21(6), 1209-1217.

Takamatsu, S., Yamashita, T., Murakami, T., Masuda, A., & Itoh, T. (2015). Fabrication and evaluation of LED-embedded ribbons for highly flexible lighting applications in rooms. Microsystem Technologies, 1-9.

Tao, X., Huang, T., Shen, C., Ko, Y., Jou, G., & Koncar, V. (2018). Bluetooth Low Energy-Based Washable Wearable Activity Motion and Electrocardiogram Textronic Monitoring and Communicating System. Advanced Materials Technologies, 1700309.

Tao, X., Koncar, V., Huang, T. H., Shen, C. L., Ko, Y. C., & Jou, G. T. (2017). How to Make Reliable, Washable, and Wearable Textronic Devices. Sensors 17(4), 673.

Toepke, M., & Beebe, D. (2006). PDMS absorption of small molecules and consequences in microfluidic applications. Lab on a Chip, 6(12), 1484-1486.

Torah, R., Komolafe, A., Li, M., Ojuroye, O., & Beeby, S. (2017). Novel Manufacturing Methods for Functional Electronic Textiles. Printed and Stretchable Congress. London.

Tybrandt, K., & Vörös, J. (2016). Fast and efficient fabrication of intrinsically stretchable multilayer circuit boards by wax pattern assisted filtration. small, 12(2), 180-184.

Tybrandt, K., Stauffer, F., & Vörös, J. (2016). Multilayer Patterning of High Resolution Intrinsically Stretchable Electronics. Scientific reports, 6.

Using a washing machine: how to use detergent in your washing machine. (n.d.). Retrieved February 9, 2018, from Cleanpedia.com: goo.gl/X9RfyW

Vallett, R., Young, R., Knittel, C., Kim, Y., & Dion, G. (2016). Development of a Carbon Fiber Knitted Capacitive Touch Sensor. MRS Advances 1(38), 2641-2651.

Varnaitė, S., & Katunskis, J. (2009). Influence of washing on the electric charge decay of fabrics with conductive yarns. Fibres & Textiles in Eastern Europe 17(5), 69-75.

Velderrain, M., & Lipps, N. (2011). Guidelines for choosing a silicone based on water vapor transmission rates for barrier applications. Moisture Permeability of Silicone Systems, 1-8.

Victrex. (n.d.). VICTREX PEEK 450G Datasheet. Retrieved August 2017, from https://www.victrex.com/~/media/datasheets/victrex_tds_450g.pdf

Vishay. (n.d.). Retrieved August 2015, from Introduction Characteristics and Definitions used for Film Plastics: https://www.vishay.com/docs/28147/intro.pdf

Wack, H., & Bertling, J. (2007). Water-Swellable Materials–Application in Self-Healing Sealing Systems. . In Proceedings of the First International Conference on Self Healing Materials (pp. 18-20). Dordrecht, The Netherlands: Springer.

Wainwright, H. L. (2016). Design, evaluation, and applications of elecronic textiles. In Performance Testing of Textiles , 193-213.

Walker, C. R., & Anderson, I. (2017). Monitoring diver kinematics with dielectric elastomer sensors. In Electroactive Polymer Actuators and Devices (EAPAD) Vol. 10163 (p. 1016307). International Society for Optics and Photonics.

Wang, E. J., Garrison, J., Whitmire, E., Goel, M., & Patel, S. (2017). Carpacio: Repurposing Capacitive Sensors to Distinguish Driver and Passenger Touches on In-Vehicle Screens. In Proceedings of the 30th Annual ACM Symposium on User Interface Softwar and Technology (pp. 49-55). ACM.

Wang, G., Babaahmadi, V., He, N., Liu, Y., Pan, Q., Montazer, M., et al. (2017). Wearable supercapacitors on polyethylene terephthalate fabrics with good wash fastness and high flexibility. Journal of Power Sources, 367, 34-41.

Wang, Y., & Jing, X. (2005). Intrinsically conducting polymers for electromagnetic interference shielding. Polymers for advanced technologies, 16(4), 344-351.
Wei, H., Chueh, B., Wu, H., Hall, E., Li, C., Schirhagl, R., et al. (2011). Particle sorting using a porous membrane in a microfluidic device. Lab on a chip, 11(2), 238-245.
Wei, Y., Torah, R., Li, Y., & Tudor, J. (2015). Dispenser printed proximity sensor on fabric for creative smart fabric applications. In Design, Test, Integration and Packaging of MEMS/MOEMS (DTIP) (pp. 1-4). IEEE.
Weiss, C., & Muenstedt, H. (2002). Surface modification of polyether ether ketone (peek) films for flexible printed circuit boards. The Journal of adhesion, 78(6), 507-519.
Westerhoff, P., Prapaipong, P., Shock, E., & Hillaireau, A. (2008). Antimony leaching from polyethylene terephthalate (PET) plastic used for bottled drinking water. Water Research, 42(3), 551-556.
Where do I put fabric conditioner, washing powder, or liquid detergent in my washing machine? (n.d.). Retrieved February 9, 2018, from Cleanpedia.com: goo.gl/hixVBW
Wijesiriwardana, R., Mitcham, K., Hurley, W., & Dias, T. (2005). Capacitive fiber-meshed transducers for touch and proximity-sensing applications. IEEE Sensors Journal, 5(5), 989-994.
Wilde, A., & Ojuroye, O. (2018). Ubiquitous Embodied Learning with E-Textiles Electronic Textiles. (pp. Mobile, Wearable, Ubiquitous Systems Research Symposium). Cambridge: University of Cambridge.
Wimmer, R., & Baudisch, P. (2011). Modular and deformable touch-sensitive surfaces based on time domain reflectometry. In Proceedings of the 24th annual ACM symposium on User interface software and technology (pp. 517-526). ACM.
WTEC. (n.d.). Advantages of Optical Sensing. Retrieved February 22, 2016, from WTEC: http://www.wtec.org/loyola/opto/c6_s3.htm
Xingxiang, Z., & Xiaoming, T. (2001). Smart textiles: Passive smart. Textile Asia 32.6, 45-49.
Yao, S., & Zhu, Y. (2015). Nanomaterial-enabled stretchable conductors: strategies, materials and devices. Advanced Materials 27(9), 1480-1511.
Yong, S. O. (2018). Solid-State Supercapacitor Fabricated in a Single Woven Textile Layer for E-Textiles Applications. Advanced Engineering Materials.
Yoon, Y., Park, H., Lim, Y., Choi, K., Lee, K., Park, G., et al. (2006). Effects of parylene buffer layer on flexible substrate in organic light emitting diode. Thin Solid Films 513, no. 1, 258-263.
Yu, K., & Han, Y. (2006). A stable PEO-tethered PDMS surface having controllable wetting property by a swelling–deswelling process. Soft Matter, 2(8), 705-709.
Zappi, P., Farella, E., & Benini, L. (2008). Pyroelectric infrared sensors based distance estimation. IEEE Sensors, 716-719.
Zeng, W., Shu, L., Li, Q., Chen, S., Wang, F., & Tao, X. M. (2014). Fiber-based wearable electronics: a review of materials, fabrication, devices, and applications. Advanced Materials 26.31, 5310-5336.
Zhai, W. C. (2014). Fabrication of lightweight, flexible polyetherimide/nickel composite foam with electromagnetic interference shielding effectiveness reaching 103 dB. Journal of Cellular Plastics, 50(6), 537-550.
Zhang, X. M. (2014). Atomic oxygen erosion resistance of sol–gel oxide films on Kapton. . Journal of sol-gel science and technology, 69(3), 498-503.
Zhang, Z. P., Song, X. F., Cui, L. Y., & Qi, Y. H. (2018). Synthesis of Polydimethylsiloxane-Modified Polyurethane and the Structure and Properties of Its Antifouling Coatings. Coatings, 8(5), 157.
Ziefle, M. B. (2014). Understanding requirements for textile input devices individually tailored interfaces within home environments. . International Conference on Universal Access in Human-Computer Interaction (pp. 587-598). Springer.
Zimmerman, T. G., Smith, J. R., Paradiso, J. A., Allport, D., & Gershenfeld, N. (1995). Applying electric field sensing to human-computer interfaces. In Proceedings of the SIGCHI conference on Human factors in computing systems (pp. 280-287). ACM.
Zurich, E. (n.d.). Electronic Sensor Fibres. Retrieved February 16, 2016, from http://www.ife.ee.ethz.ch/research/groups/PlasticElectronics/groups/PlasticElectronics/Smarttextiles/ElectroSensorFibers

Zysset, C., Kinkeldei, T. W., Munzenrieder, N., Cherenack, K., & Troster, G. (2012). Integration Method for Electronics in Woven Textiles. IEEE Transactions on Components, Packaging and Manufacturing Technology. 2, pp. 1107-1117. IEEE.

Zysset, C., Kinkeldei, T., Cherenack, K., & Tröster, G. (2010). Woven Electronic Textiles: An Enabling Technology for Health-care Monitoring. Proceedings of the UbiComp (pp. 26–29). Copenhagen: UbiComp.

Zysset, C., Kinkeldei, T., Münzenrieder, N., Petti, L., Salvatore, G., & Tröster, G. (2013). Combining electronics on flexible plastic strips with textiles. Textile research journal 83(11), 1130-1142.